N73-11005

NASA TECHNICAL MEMORANDUM

NASA TM X-2603

NASA TM X-2603

CASE FILE COPY

EXPERIMENTAL AERODYNAMIC CHARACTERISTICS OF 120°-INCLUDED-ANGLE CONE WITH ATTACHED AND SEPARATED 20°-INCLUDED-ANGLE CONE AT MACH NUMBERS OF 2.36 AND 2.70

by Clarence A. Brown, Jr., Charles D. Trescot, Jr., and Celia S. Richardson

Langley Research Center
Hampton, Va. 23365

NATIONAL AERONAUTICS AND SPACE ADMINISTRATION • WASHINGTON, D. C. • OCTOBER 1972

1. Report No.	2. Government Accession No.	3. Recipient's Catalog No.
NASA TM X-2603		
4. Title and Subtitle EXPERIMENTAL AERODYNAMIC CHARACTERISTICS OF 120°-INCLUDED-ANGLE CONE WITH ATTACHED AND SEPARATED 20°-INCLUDED-ANGLE CONE AT MACH NUMBERS OF 2.36 AND 2.70		5. Report Date October 1972
		6. Performing Organization Code
7. Author(s) Clarence A. Brown, Jr., Charles D. Trescot, Jr., and Celia S. Richardson		8. Performing Organization Report No. L-8427
9. Performing Organization Name and Address NASA Langley Research Center Hampton, Va. 23365		10. Work Unit No. 117-07-04-01
		11. Contract or Grant No.
		13. Type of Report and Period Covered Technical Memorandum
12. Sponsoring Agency Name and Address National Aeronautics and Space Administration Washington, D.C. 20546		14. Sponsoring Agency Code
15. Supplementary Notes		

16. Abstract

An investigation has been conducted in the Langley Unitary Plan wind tunnel to determine the aerodynamic characteristics of two different size blunt 120°-included-angle cones behind a 20°-included-angle cone. Forces and moments were measured at Mach numbers of 2.36 and 2.70, longitudinal separation distances from 0 to 3.5 body diameters, lateral (side) distances from 0 to 0.50 body diameter, angles of attack of the 120°-included-angle cone from 0.5° to 22°, angles of attack of the 20°-included-angle cone from 0° to 180°, and a Reynolds number of 3.280×10^6 per meter (1.0×10^6 per foot).

These tests indicated that large variations in pitching-moment, normal-force, and axial-force coefficients were noted for both Mach numbers and all longitudinal distances for the 120° cones in the wake of a 20° cone.

17. Key Words (Suggested by Author(s))		18. Distribution Statement	
Blunt cones Separation Aerodynamic characteristics		Unclassified – Unlimited	
19. Security Classif. (of this report)	20. Security Classif. (of this page)	21. No. of Pages	22. Price*
Unclassified	Unclassified	145	$3.00

*For sale by the National Technical Information Service, Springfield, Virginia 22151

EXPERIMENTAL AERODYNAMIC CHARACTERISTICS OF 120°-INCLUDED-ANGLE CONE WITH ATTACHED AND SEPARATED 20°-INCLUDED-ANGLE CONE AT MACH NUMBERS OF 2.36 AND 2.70

By Clarence A. Brown, Jr., Charles D. Trescot, Jr.,
and Celia S. Richardson
Langley Research Center

SUMMARY

An investigation has been conducted in the Langley Unitary Plan wind tunnel to determine the aerodynamic characteristics of two different size blunt 120°-included-angle cones behind a 20°-included-angle cone. Forces and moments were measured at Mach numbers of 2.36 and 2.70, longitudinal separation distances from 0 to 3.5 body diameters, lateral (side) distances from 0 to 0.50 body diameter, angles of attack of the 120°-included-angle cone from 0.5° to 22°, angles of attack of the 20°-included-angle cone from 0° to 180°, and a Reynolds number of 3.280×10^6 per meter (1.0×10^6 per foot).

These tests indicated that the base pressure coefficients were greater (less negative) for the 120°-included-angle cone with the separated 20°-included-angle cone than with the attached 20°-included-angle cone. The 120°-included-angle cone with the attached 20°-included-angle cone produced larger pitching moments and normal forces and less axial force than the 120°-included-angle cone with the 20°-included-angle cone separated.

Large variations in pitching-moment and normal-force coefficients are noted for both Mach numbers and all longitudinal distances for the 120°-included-angle cone in the wake of the 20°-included-angle cone. This effect decreases as the longitudinal distance between the two cones is increased.

INTRODUCTION

The Mars planetary entry program being considered by NASA utilizes a vehicle capable of landing a scientific payload in a low-density atmosphere. Vehicle designs for such types of missions have resulted in entry configurations with low ballistics coefficients (refs. 1 to 3) and a decelerator parachute system operating in the wake of the forebody. The flow field produced by the entry body is a very complex structure (refs. 4, 5, and 6) and the behavior of decelerator devices, such as parachutes, are questionable and of major concern.

In an effort to understand the operation and behavior of decelerator parachutes operating in the wake of entry configurations, NASA has developed a vehicle to test parachutes at earth altitudes simulating the low-density Martian atmosphere. The test vehicle (ref. 7) is an expandable 120°-included-angle cone propelled to altitude in a folded configuration (similar to an umbrella) with a 20°-included-angle cone attached to the nose of the folded 120°-included-angle cone to house the control and erection systems, serve as a heat shield, and reduce the ascent vehicle drag. During reentry above the parachute test altitude, the 120°-included-angle cone was erected and the 20°-included-angle cone was separated. The erected 120°-included-angle cone was then used as a test vehicle for parachute deployment and stability tests in the wake of a large-diameter blunt body.

Recently, a vehicle utilizing the 120°-included-angle large-diameter blunt body was flown to test a disk-gap-band parachute. Upon separation of the 20°-included-angle cone from the 120°-included-angle cone, the 120°-included-angle cone experienced oscillations in pitch and yaw. Some oscillation of the 120°-included-angle cone had been expected but the magnitude was large enough to cause severe compromise to the test objectives.

In order to analyze the motions of the 120°-included-angle cone in the wake of a 20°-included-angle cone, a wind-tunnel program was initiated to determine the aerodynamic characteristics of two different size blunt 120°-included-angle cones with a 20°-included-angle cone attached and separated at various longitudinal and lateral stations.

This paper presents the static-force and moment data obtained at Mach numbers of 2.36 and 2.70, longitudinal separation distances from 0 to 3.5 body diameters, lateral (side) distances from 0 to 0.50 body diameter, angles of attack of the 120°-included-angle cones from 0.5° to 22°, angles of attack of the 20°-included-angle cone from 0° to 180°, and a Reynolds number of 3.280×10^{6} per meter $(1.0 \times 10^{6}$ per foot).

SYMBOLS

Values are given in both SI and U.S. Customary Units. Measurements and calculations were made in the U.S. Customary Units.

The results of the tests are presented in coefficient form for the body-axis system.

The pitching-moment reference center is located at the base of the 120°-included-angle cone on the geometric center line.

C_A axial-force coefficient, $\dfrac{\text{Axial force}}{q_{\infty}S}$

C_N	normal-force coefficient, $\frac{\text{Normal force}}{q_\infty S}$
C_Y	side-force coefficient, $\frac{\text{Side force}}{q_\infty S}$
C_l	rolling-moment coefficient, $\frac{\text{Rolling moment}}{q_\infty SD}$
C_m	pitching-moment coefficient, $\frac{\text{Pitching moment}}{q_\infty SD}$
$\frac{C_m}{C_N}, \frac{C_n}{C_Y}$	center-of-pressure location, body diameters
C_n	yawing-moment coefficient, $\frac{\text{Yawing moment}}{q_\infty SD}$
$(C_{p,b})_{av}$	average base pressure coefficient, $\frac{(p_{st,b})_{av} - p_{st,\infty}}{q_\infty}$
D	reference diameter of 120^o-included-angle cone
M_∞	free-stream Mach number
$p_{st,\infty}$	free-stream static pressure
$(p_{st,b})_{av}$	average static pressure at model base
$p_{t,\infty}$	tunnel stagnation pressure
q_∞	free-stream dynamic pressure, $\frac{\gamma}{2} p_{st,\infty} M_\infty{}^2$
R	Reynolds number based on free-stream conditions
S	reference area (base area of 120^o-included-angle cone), $\pi D^2/4$
T_∞	total tunnel temperature
x	longitudinal coordinate (see fig. 1(f))
y	lateral coordinate (see fig. 1(f))
α	angle of attack

γ ratio of specific heats

Subscripts:

20° 20°-included-angle cone

120° 120°-included-angle cone

APPARATUS AND TESTS

Models

Details of the models used in the investigation are shown in figure 1. Typical photographs of the models mounted in the wind tunnel are shown as figure 2. Two 120°-included-angle cones and two 20°-included-angle cones (hereafter referred to as 120° cones and 20° cones, respectively), constructed of polished aluminum, were used in the investigation.

One of the 120° cones (fig. 1(a)) had a base diameter of 12.268 cm (4.83 in.) with a nose radius of 2.535 cm (0.998 in.). The second 120° cone (fig. 1(b)) had a base diameter of 16.002 cm (6.30 in.) and was constructed in a manner similar to the 12.268-cm-diameter (4.83 in.), 120° cone. Provisions were made so that a portion of the model at the nose could be removed in order to mount the 20° cone.

The two 20° cones were also constructed of polished aluminum. The 20° cone (fig. 1(c)) had a base diameter of 2.756 cm (1.085 in.) and had a nose radius of 0.089 cm (0.035 in.). The 20° cone shown in figure 1(c) was mounted on both 120° cones as shown in figure 1(d). The 20° cone used during the separation tests is shown in figure 1(e). The 20° cone was supported in the tunnel test section by a horizontal cantilevered rod having a diameter of 2.54 cm (1.00 in.) at the tunnel wall and 0.511 cm (0.201 in.) at the cone (fig. 1(e)). The use of the horizontal cantilevered strut necessitated the use of a solid door in the wind tunnel in place of the glass door normally used. The solid steel door eliminated the possibility of obtaining schlieren photographs during the tests.

Tunnel

Tests were conducted in the low Mach number test section of the Langley Unitary Plan wind tunnel (refs. 8 and 9). The wind tunnel is a continuous-flow system having variable-pressure capability. The test section is approximately 1.2 m (4 ft) square and 2.1 m (7 ft) long. The nozzle leading to the test section is an asymmetric sliding-block type, which permits a continuous variation in Mach number from 1.5 to 2.9 in the low Mach number section.

Test Conditions and Measurements

The tests conducted with the nonseparated configurations were performed through an angle-of-attack range of -4° to 22° and at Mach numbers of 2.36 and 2.70. For tests of the separated configurations the angle-of-attack ranges varied from 0.5° to 22° for the 120° cone and 0° to 180° for the 20° cone. For all tests, the Reynolds number was 3.280×10^6 per meter (1.0×10^6 per foot).

The stagnation dewpoint was maintained at 239 K (-30° F) in order to avoid condensation effects. The test conditions for each configuration were as follows:

M_∞	T_∞		$p_{t,\infty}$		q_∞		R	
	K	$^\circ$F	N/m^2	lb/ft^2	N/m^2	lb/ft^2	Per meter	Per foot
2.36	339	150	37 825.41	790	10 738.63	224	3.28×10^6	1.0×10^6
2.70	339	150	45 198.96	944	9 907.38	207	3.28×10^6	1.0×10^6

Aerodynamic forces and moments of the 120° cones were measured by means of a six-component electrical strain-gage balance connected to the base of the cone. The balance, in turn, was rigidly fastened to a sting-support system. The forces and moments were measured on the 120° cones with the 20° cone attached and separated. During the separation tests of the 12.268-cm-diameter (4.83 in.), 120° and 20° cones, the two cones were separated in the longitudinal (x) direction 0, 0.621, 1.242, 2.070, and 3.520 body diameters. Separation of the two cones in the lateral (y) direction was 0, 0.25, and 0.50 body diameters. The locations of the cones during the separation tests is shown by the dots in figure 1(f). During the separation tests of the 16.002-cm-diameter (6.30 in.), 120° and 20° cones, the two cones were separated in the longitudinal (x) direction 0, 0.476, 0.952, and 1.587 body diameters. Separation of the two cones in the lateral (y) direction was 0 and 0.25 body diameters.

For the attached configurations, angles of attack were corrected for average tunnel-flow angularity and for deflection of model and sting support as a result of aerodynamic loads. For the separated configurations, corrections were made for the average tunnel flow when the two cones were on the same geometric center line with respect to the tunnel. This correction was then used for the remaining tests at a given x/D location.

Photographs of several test configurations mounted in the wind tunnel are shown as figure 2. Balance chamber and base pressures were measured on the 120° cones alone and with the 20° cone attached. Two base-pressure tubes were located 180° apart midpoint from the model center line and outer edge of the 120° cone and the third base-pressure tube was located in the balance cavity. No base or balance cavity measurements were made during the separation tests.

Accuracy

The accuracy of the individual measured quantities, based on instrumentation, calibration, and balance loads, is estimated to be within the following limits:

	$M_\infty = 2.36$		$M_\infty = 2.70$	
	12.268-cm-diameter (4.83 in.) cone	16.002-cm-diameter (6.30 in.) cone	12.268-cm-diameter (4.83 in.) cone	16.002-cm-diameter (6.30 in.) cone
ΔC_N	±0.0053	±0.0031	±0.0057	±0.0033
ΔC_A	±.0270	±.0159	±.0292	±.0172
ΔC_m	±.0006	±.0003	±.0006	±.0003
ΔC_l	±.0003	±.0002	±.0004	±.0002
ΔC_n	±.0012	±.0005	±.0013	±.0006
ΔC_Y	±.0114	±.0067	±.0123	±.0072

PRESENTATION OF RESULTS

The results of the investigation are presented in the following figures:

DISCUSSION OF RESULTS

Base Pressure of 120°-Included-Angle Cone

The base pressure coefficients measured are greater (less negative) for the 120° cone with the separated 20° cone than with the attached 20° cone for both size models (fig. 3). For both Mach numbers and size models, there is a larger difference in the base pressure between attached cone and separated cone at angles of attack below 6° than above 6°. For both size models, there is generally a greater difference in base pressure for the lower Mach number ($M_\infty = 2.36$) than for the higher Mach number ($M_\infty = 2.70$).

Longitudinal Aerodynamic Characteristics of 120°-Included-Angle Cone With Attached and Separated 20°-Included-Angle Cone

For both size models (figs. 4 and 7), the pitching-moment and normal-force coefficients are considerably greater for the 120° cone with the attached 20° cone than with the separated 20° cone at angles of attack up to about 8°. At angles of attack above 8°, a change in the slope of the normal force and pitching moment can be seen for the configurations with nose cone attached. Comparisons of the normal-force and pitching-moment curves with the 20° cone attached for the two sizes of 120° cones (figs. 4 and 7) show larger coefficients for the smaller 120° cone than for the larger cone. As expected, adding the 20° cone to the 120° cone reduces the axial-force coefficient about 34 percent (fig. 4) near zero angle of attack for the smaller cone and about 20 percent (fig. 7) for the larger 120° cone for both Mach numbers. Near zero angle of attack, the effect of adding the same size 20° cone to the 120° cones is to increase the axial-force coefficient from 1.03 (fig. 4) for the smaller diameter 120° cone to 1.22 (fig. 7) for the larger diameter 120° cone. As the angle of attack is increased, the axial force for the attached 20° cone approaches the same value as with the separated 20° cone for both Mach numbers.

Longitudinal Aerodynamic Characteristics of 12.268-cm-Diameter (4.83 in.) Cone for Various Angles of Attack and x/D and y/D Locations

Figures 5 and 6 show the effects of angle of attack and x/D and y/D locations on the longitudinal aerodynamic characteristic of the 120° cone. When the two cones are at y/D = 0, large variations in pitching-moment and normal-force coefficients are noted for both Mach numbers and all x/D locations. However, this effect is less pronounced at the larger x/D locations.

For $\alpha_{120^\circ} \approx 0^\circ$ and x/D = 0.621, the pitching-moment coefficient becomes more negative with increases in α_{20° until α_{20° reaches 15° then increases as α_{20° increases. As x/D is increased, the pitching moment becomes more positive as α_{20°

increases. This result is probably due to the influence of the recompression shock of the forebody on the 120° cone. When the two bodies are in line, the pitching-moment and normal-force coefficients are nonlinear at all x/D locations except one. This exception is at the lowest Mach number and largest x/D location.

The presence of the forebody on the 120° cone tends to reduce the axial-force coefficient. The axial-force coefficient decreases as the two bodies were separated up to a distance of 2.07 body diameters then increases at 3.52 body diameters.

As would be expected, moving the forebody cone laterally (y-direction) did not affect the longitudinal aerodynamic characteristics as much as moving the forebody cone longitudinally (x-direction). However, abrupt changes were noted at some lateral separations. These abrupt changes are probably due to the interaction of the recompression shock of the forebody cone and the bow wave generated by the aft body cone on the 120° cone.

Longitudinal Aerodynamic Characteristics of 16.002-cm-Diameter (6.30 in.) Cone for Various Angles of Attack and x/D and y/D Locations

Limited data were obtained with a larger diameter 120° cone and the same 20° forebody cone. The pretest plans stated that data would be taken at selected points to determine if similar trends were obtainable for a larger diameter cone and the same 20° forebody cone. These tests utilized the same model balance as did the smaller model and some overloading was experienced where reflected shocks interacted with the trailing 120° cone. To prevent damage to the tunnel balance, data were taken for points that did not overload the balance.

Although the x/D values differ for the two 120° cones, examining figures 8 and 9 and comparing these with figures 5 and 6 show similar changes in pitching-moment, normal-force, and axial-force coefficients for both Mach numbers.

Lateral Aerodynamic Characteristics of 120°-Included-Angle Cones With Attached and Separated 20°-Included-Angle Cone for Various x/D and y/D Locations

Figures 10 and 13 show little effect on the yawing-moment, rolling-moment, or side-force coefficient for the 120° cone with the attached or separated 20° cone.

For the 12.268-cm-diameter (4.83 in.), 120° cone, separating the 120° cone and 20° cone in the longitudinal direction (X-axis) did not produce sharp changes in lateral aerodynamic characteristics (figs. 11 and 12). However, when the 20° cone is moved in the lateral direction (Y-axis), some changes are noted in the lateral aerodynamic characteristics. These changes in lateral aerodynamic characteristics do not appear to be as pronounced as those changes in the longitudinal aerodynamic characteristics.

Center-of-Pressure Location

Figures 16 to 20 are plots of longitudinal and lateral center-of-pressure location for the two 120° cones with the attached and separated 20° cone at both Mach numbers and each of the 120° cones for various angles of attack and x/D and y/D locations. As previously mentioned, the pitching-moment reference center is located at the base of the 120° cone on the geometric center line.

For the 120° cone (fig. 16), the spike effect of the attached 20° cone increased the center-of-pressure location behind the body at low angles of attack then decreased the center-of-pressure location behind the body at angles of attack greater than 10°. The effect of the 20° cone on the larger diameter body (16.002 cm (6.30 in.)) is not as great as for the smaller body (12.268 cm (4.83 in.)).

Figures 17 to 20 show the variations in the longitudinal and lateral center-of-pressure locations for the 12.268-cm- and the 16.002-cm-diameter, 120° cones as a function of angle of attack of the 120° cone. Examination of these plots shows that at certain combinations of α_{120°, α_{20°, x/D, y/D, and Mach number, the center-of-pressure location moves in front of and behind the base of the 120° cone. In part, this is due to the interaction of the recompression wave generated by the forebody and bow wave generated by the afterbody.

CONCLUDING REMARKS

An investigation has been conducted in the Langley Unitary Plan wind tunnel to determine the aerodynamic characteristics of two different size blunt 120°-included-angle cones behind a 20°-included-angle cone. Forces and moments were measured at Mach numbers of 2.36 and 2.70, longitudinal separation distances from 0 to 3.5 body diameters, lateral (side) distances from 0 to 0.5 body diameter, angles of attack of the 120°-included-angle cone from 0.5° to 22°, angles of attack of the 20°-included-angle cone from 0° to 180°, and a Reynolds number of 3.280×10^6 per meter (1.0×10^6 per foot).

The investigation indicated that the base pressure coefficient was greater (less negative) for the 120°-included-angle cone with the separated 20°-included-angle cone than with the attached 20°-included-angle cone. The pitching-moment and normal-force coefficients were considerably greater for the 120°-included-angle cone with the attached 20°-included-angle cone than with the separated 20°-included-angle cone at angles of attack up to about 8°. At angles of attack above 8°, nonlinearities are present for the 120°-included-angle cone with the attached 20°-included-angle cone. Attaching the 20°-included-angle cone to the 120°-included-angle cone reduced the axial-force coefficient 34 percent and 20 percent near zero angle of attack for the small and large cones, respectively.

Large variations in pitching-moment and normal-force coefficients are noted for both Mach numbers and all x/D locations for the 120°-included-angle cone in the wake of the 20°-included-angle cone. This effect decreases as the longitudinal distance between the two cones is increased.

The results presented in this paper indicate that when a blunt body is within the wake of a forebody, the forces and moments are affected by the wake of the forebody. Rapid and abrupt changes in forces and moments are probably due to the interaction of the forebody recompression wave and the afterbody bow wave and can cause large oscillatory motions of the afterbody. (See NASA TN D-6910.)

Langley Research Center,
National Aeronautics and Space Administration,
Hampton, Va., July 27, 1972.

REFERENCES

1. Campbell, James F.; and Howell, Dorothy T.: Supersonic Aerodynamics of Large-Angle Cones. NASA TN D-4719, 1968.
2. Stallings, Robert L., Jr.; and Tudor, Dorothy H.: Experimental Pressure Distributions on a 120° Cone at Mach Numbers From 2.96 to 4.63 and Angles of Attack From 0° to 20°. NASA TN D-5054, 1969.
3. Campbell, James F.; and Howell, Dorothy T.: Supersonic Lifting Capabilities of Large-Angle Cones. NASA TN D-5499, 1969.
4. McShera, John T., Jr.: Wind-Tunnel Pressure Measurements in the Wake of a Cone-Cylinder Model at Mach Numbers of 2.30 and 4.65. NASA TN D-2928, 1965.
5. Campbell, James F.; and Grow, Josephine W.: Experimental Flow Properties in the Wake of a 120° Cone at Mach Number 2.20. NASA TN D-5365, 1969.
6. Brown, Clarence A., Jr.; Campbell, James F.; and Tudor, Dorothy H.: Experimental Wake Survey Behind a 120°-Included-Angle Cone at Angles of Attack of 0° and 5°, Mach Numbers From 1.60 to 3.95, and Longitudinal Stations Varying From 1.0 to 8.39 Body Diameters. NASA TM X-2139, 1971.
7. Henning, Allen B.; and Lundstrom, Reginald R. (With appendix A by James C. Young): Flight Test of an Erectable Spacecraft Used for Decelerator Testing at Simulated Mars Entry Conditions. NASA TN D-6910, 1972.
8. Anon.: Manual for Users of the Unitary Plan Wind Tunnel Facilities of the National Advisory Committee for Aeronautics. NACA, 1956.
9. Schaefer, William T., Jr.: Characteristics of Major Active Wind Tunnels at the Langley Research Center. NASA TM X-1130, 1965.

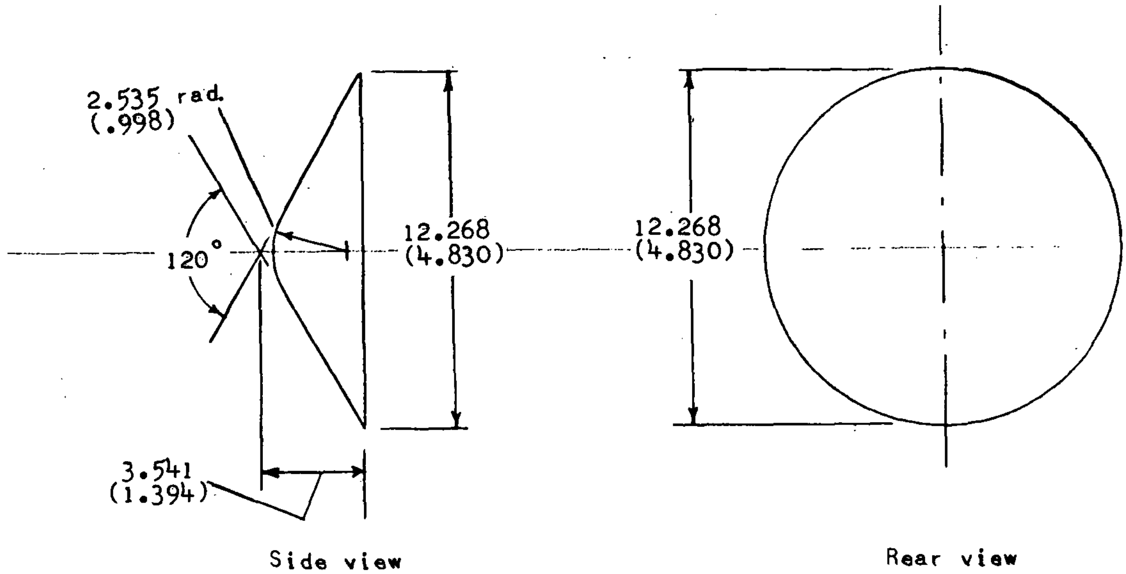

(a) 12.268-cm-diameter (4.83 in.), 120°-included-angle cone.

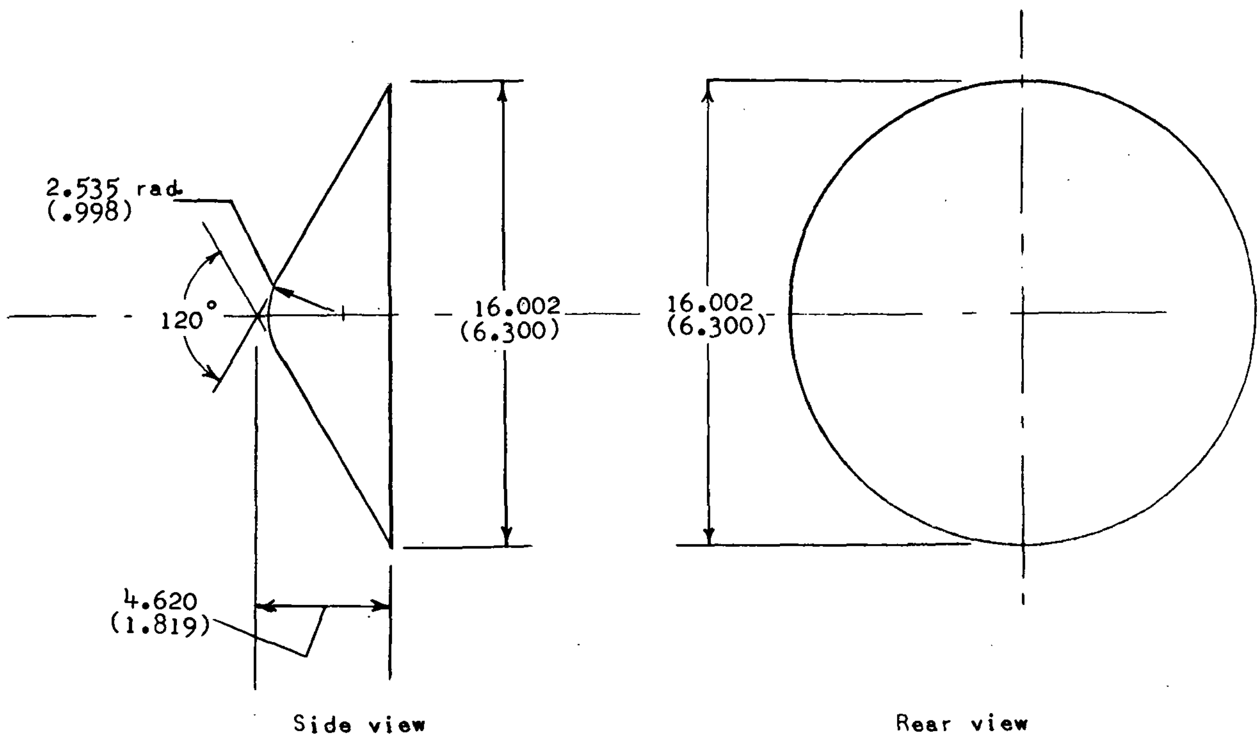

(b) 16.002-cm-diameter (6.30 in.), 120°-included-angle cone.

Figure 1.- Details of models used in investigation. Linear dimensions are in cm (in.).

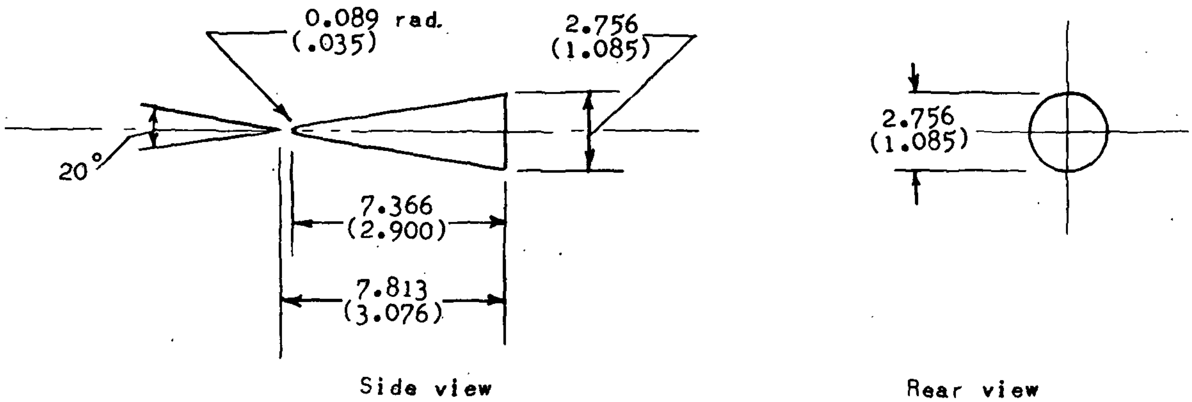

(c) 20°-included-angle cone.

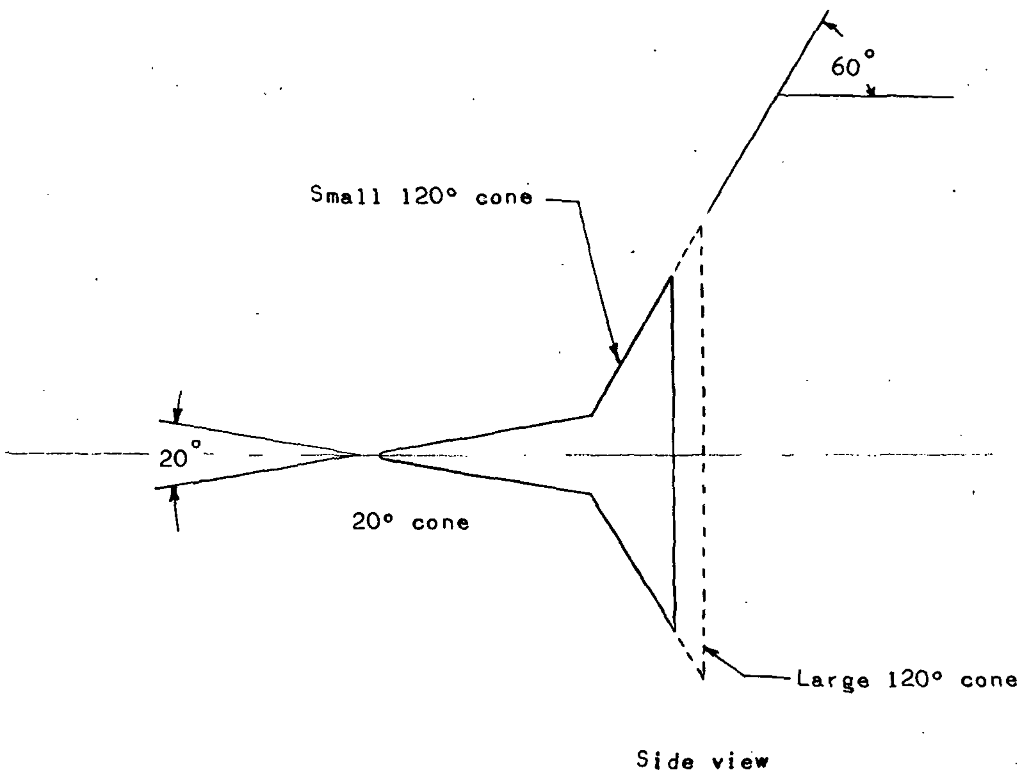

(d) 20°-included-angle cone mounted on 120°-included-angle cone.

Figure 1.- Continued.

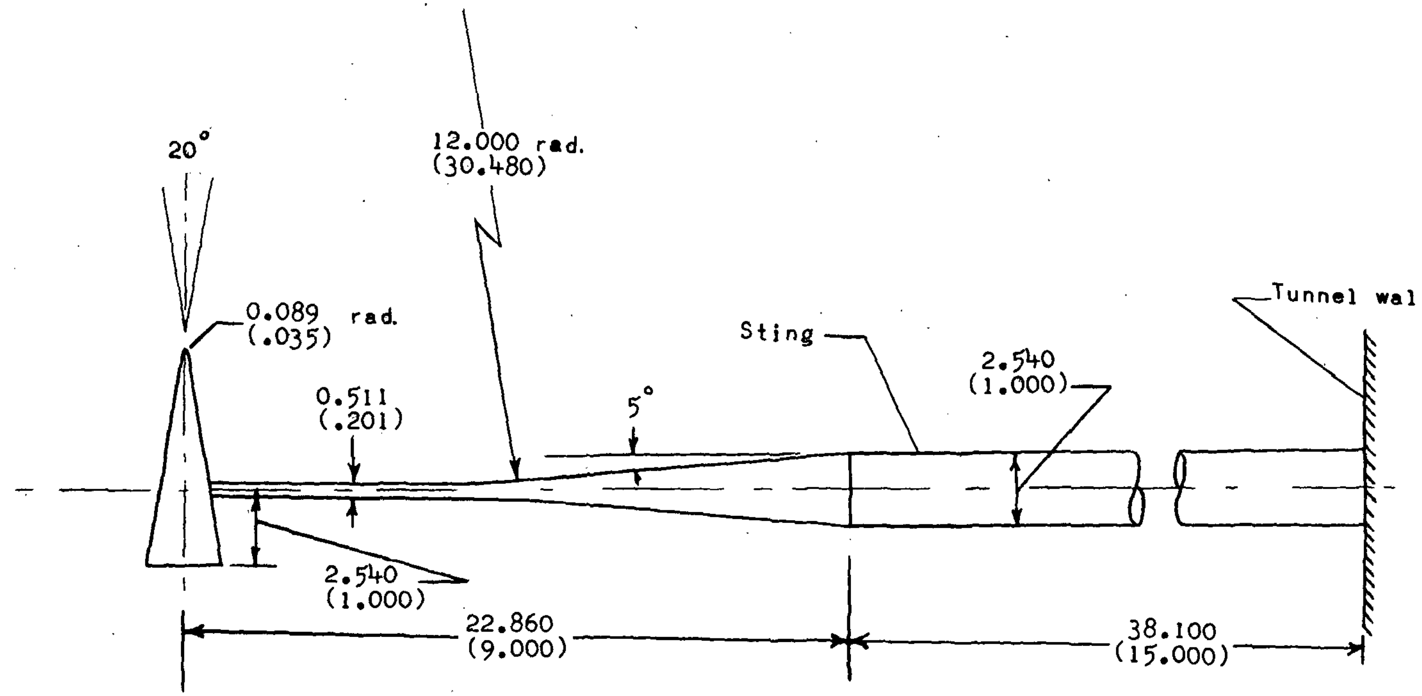

(e) 20°-included-angle cone mounted on tunnel wall.

Figure 1.- Continued.

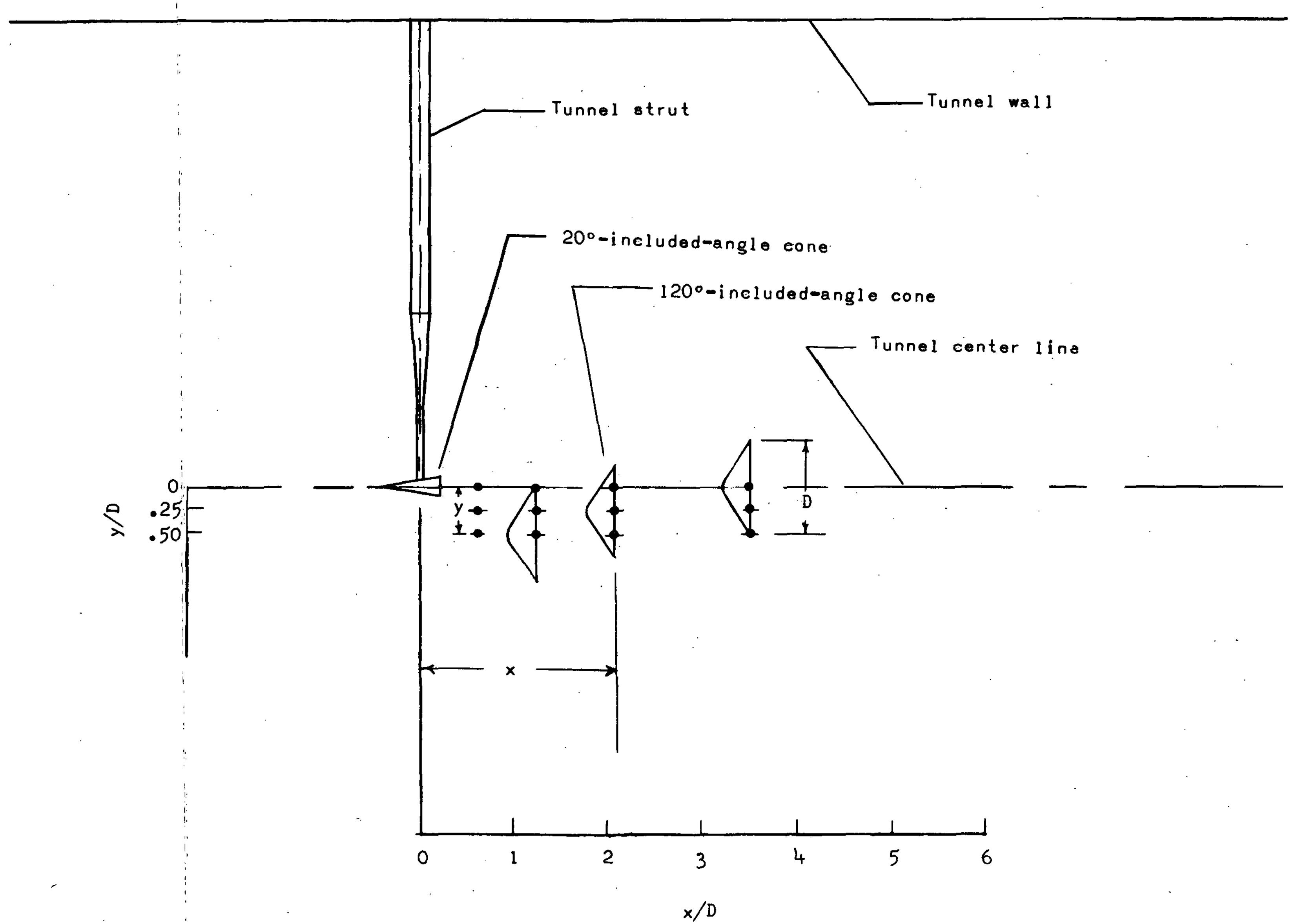

(f) Sketch showing locations of cones during tests of 12.268-cm-diameter (4.83 in.), 120°-included-angle cone.

Figure 1.- Concluded.

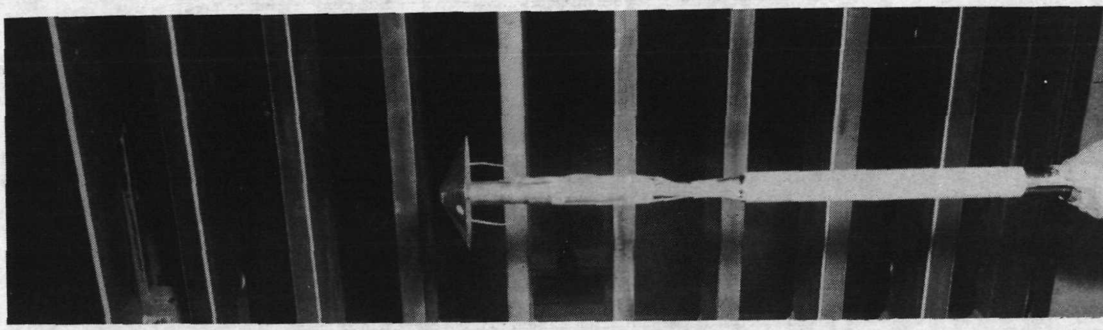

L-72-2478

(a) 12.268-cm-diameter (4.83 in.), 120°-included-angle cone alone.

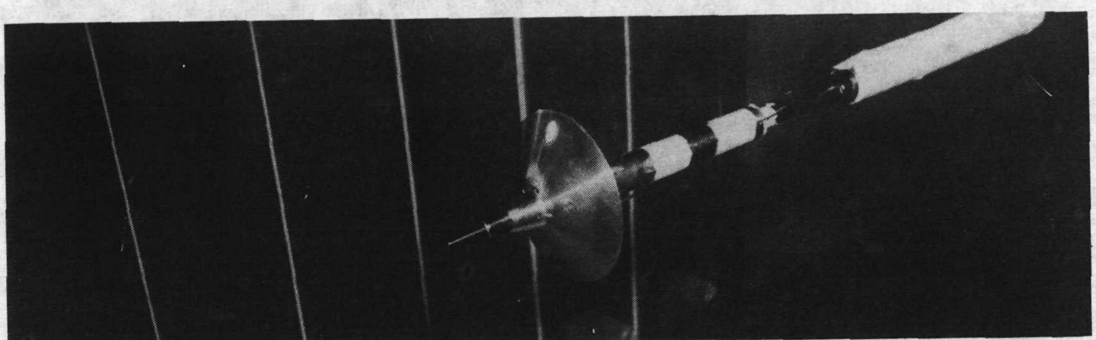

L-72-2479

(b) 12.268-cm-diameter (4.83 in.), 120°-included-angle cone with attached 20°-included-angle cone.

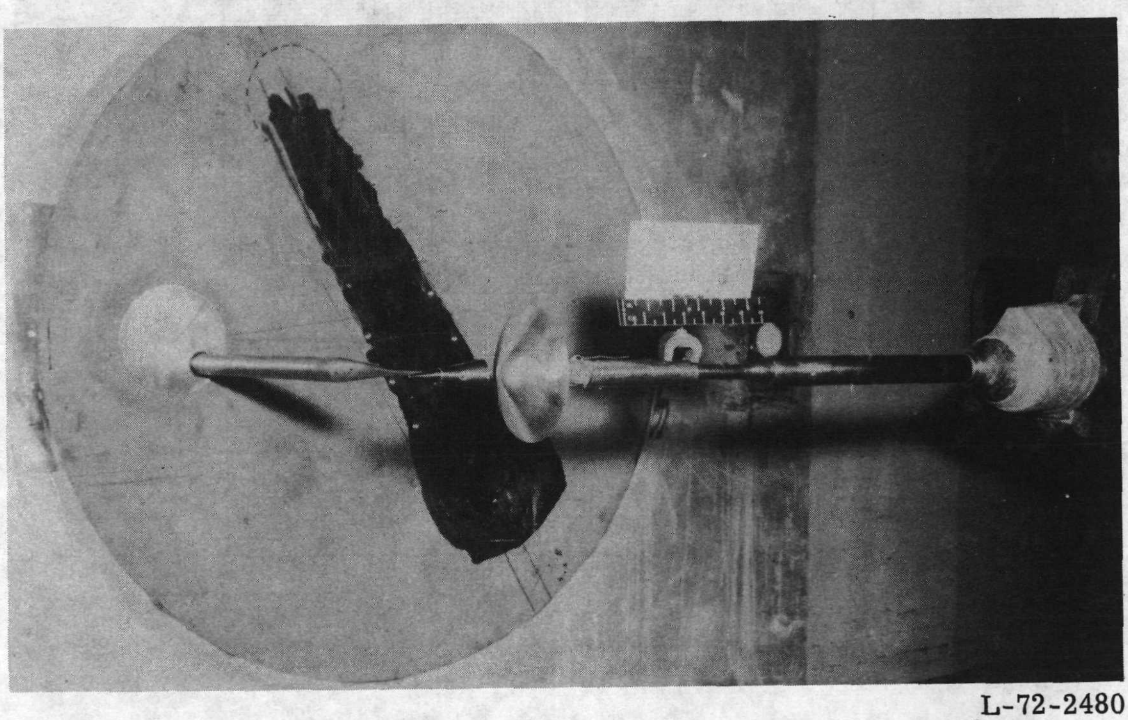

L-72-2480

(c) 12.268-cm-diameter (4.83 in.), 120°-included-angle cone with 20°-included-angle cone mounted on tunnel wall.

Figure 2.- Configurations used in investigation.

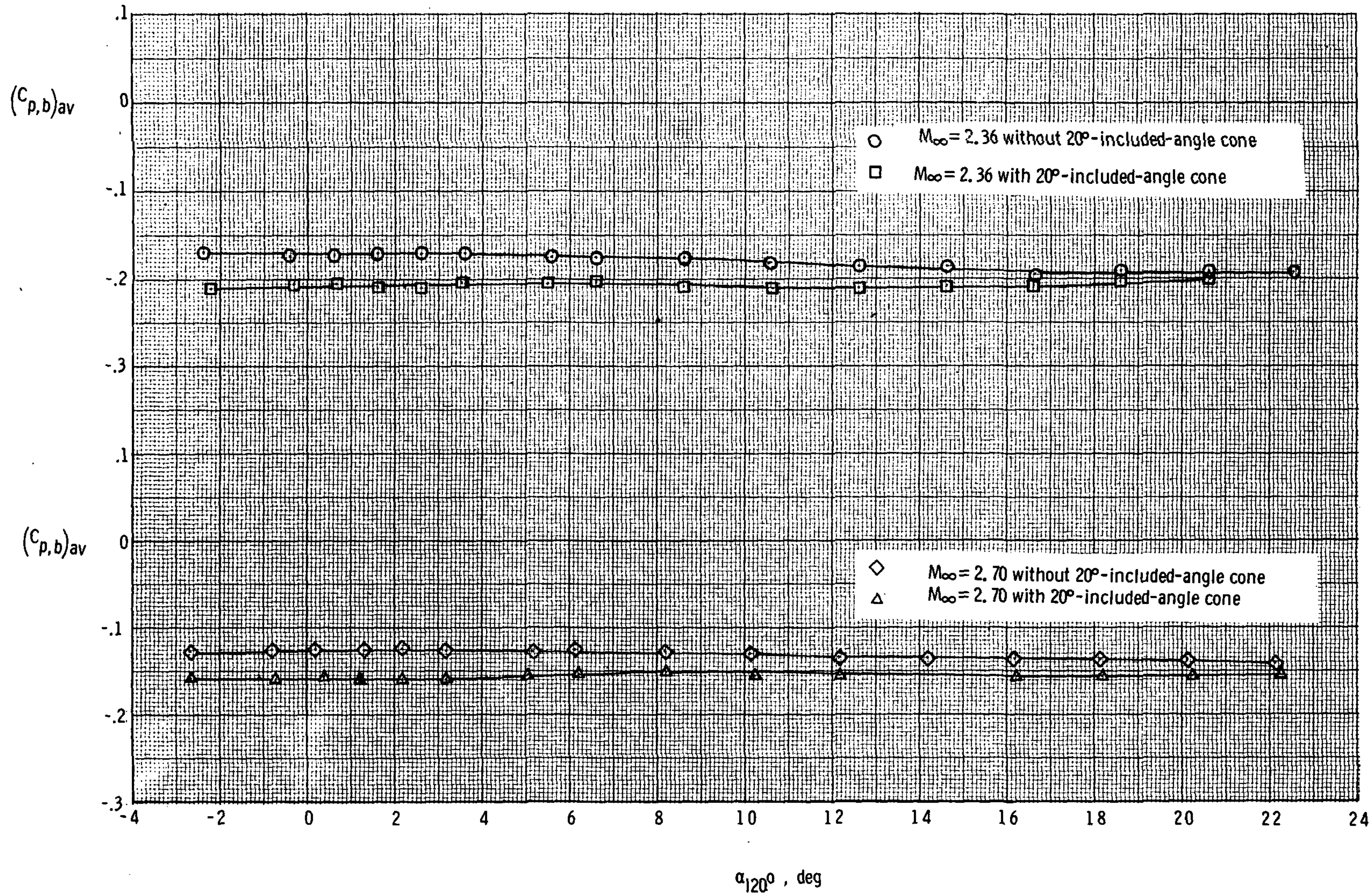

(a) 12.268-cm-diameter (4.83 in.), 120°-included-angle cone.

Figure 3.- Variation of average base pressure coefficient with angle of attack of 120°-included-angle cones with attached and separated 20°-included-angle cone.

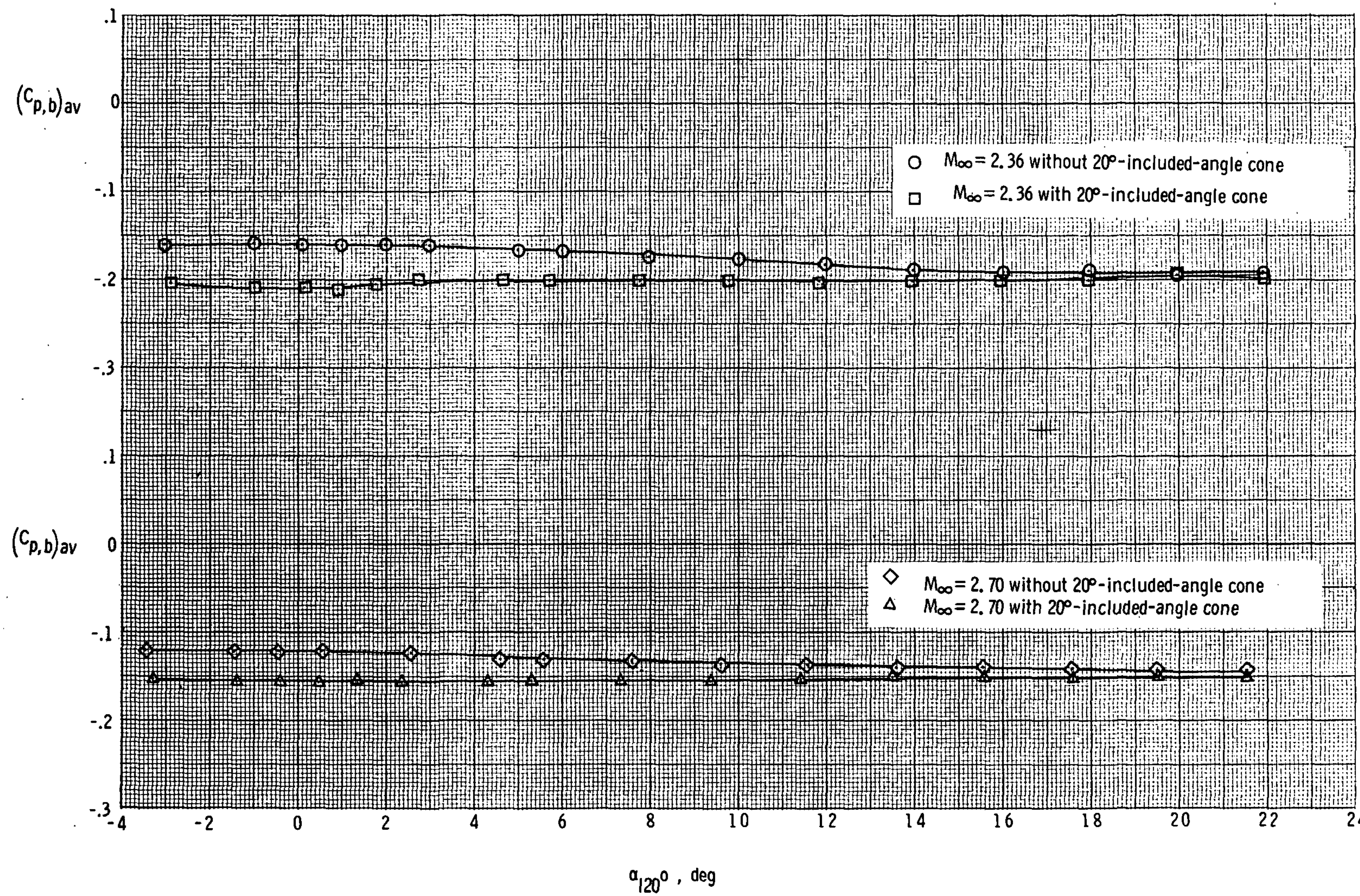

(b) 16.002-cm-diameter (6.30 in.), 120°-included-angle cone.

Figure 3.- Concluded.

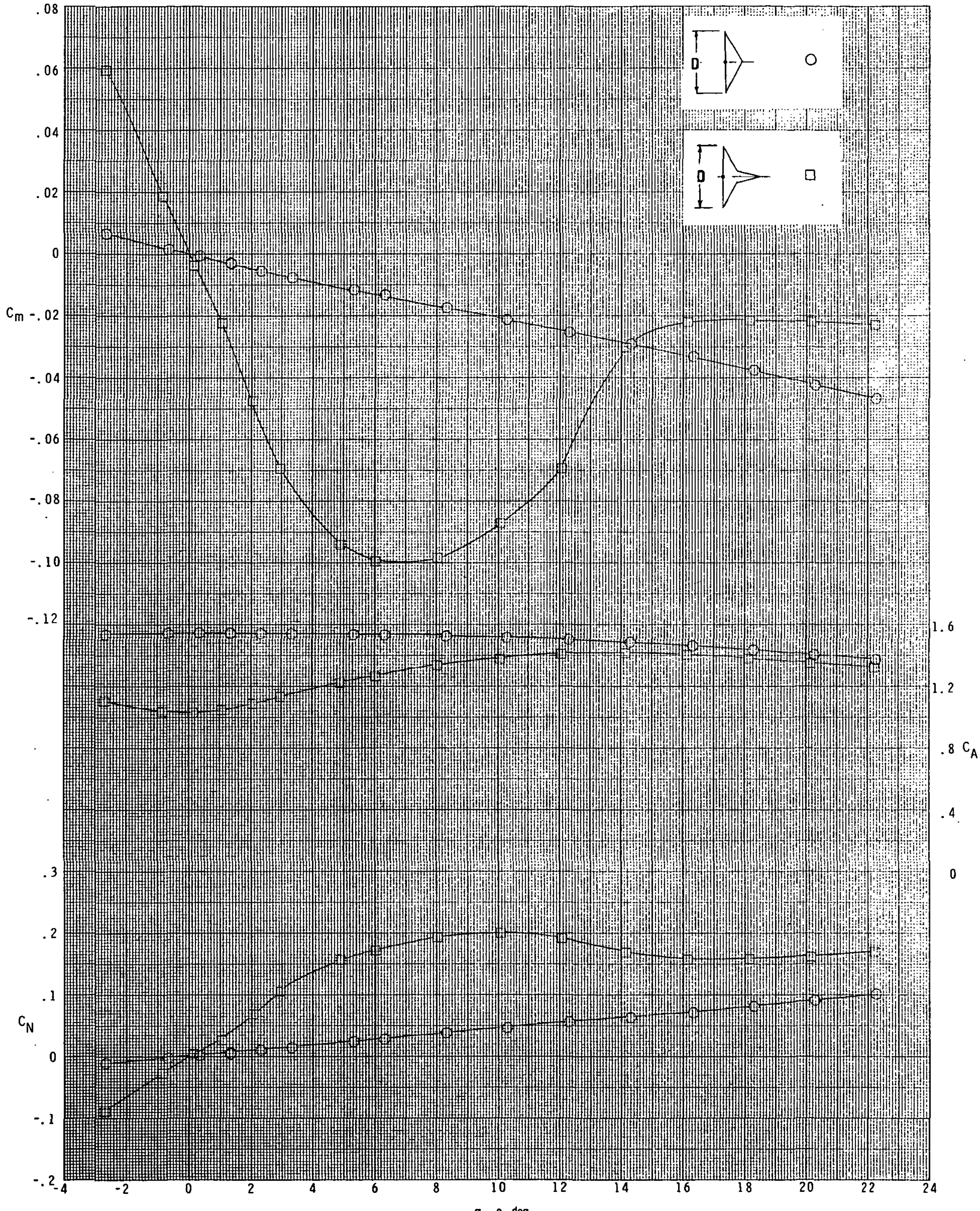

(a) $M_\infty = 2.36$.

Figure 4.- Variation of pitching-moment, axial-force, and normal-force coefficients with angle of attack for 12.268-cm-diameter (4.83 in.), 120°-included-angle cone with attached and separated 20°-included-angle cone.

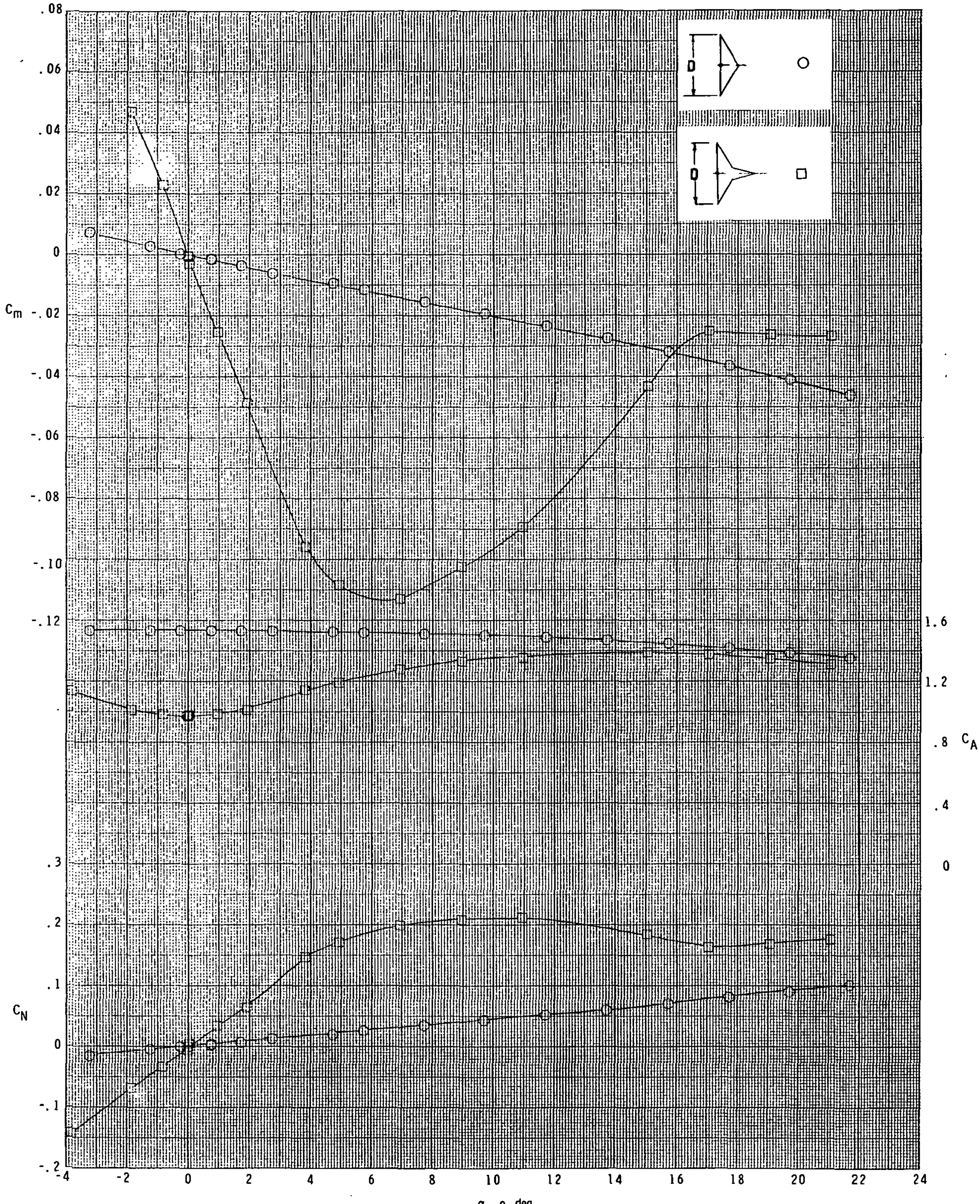

(b) $M_\infty = 2.70$.

Figure 4.- Concluded.

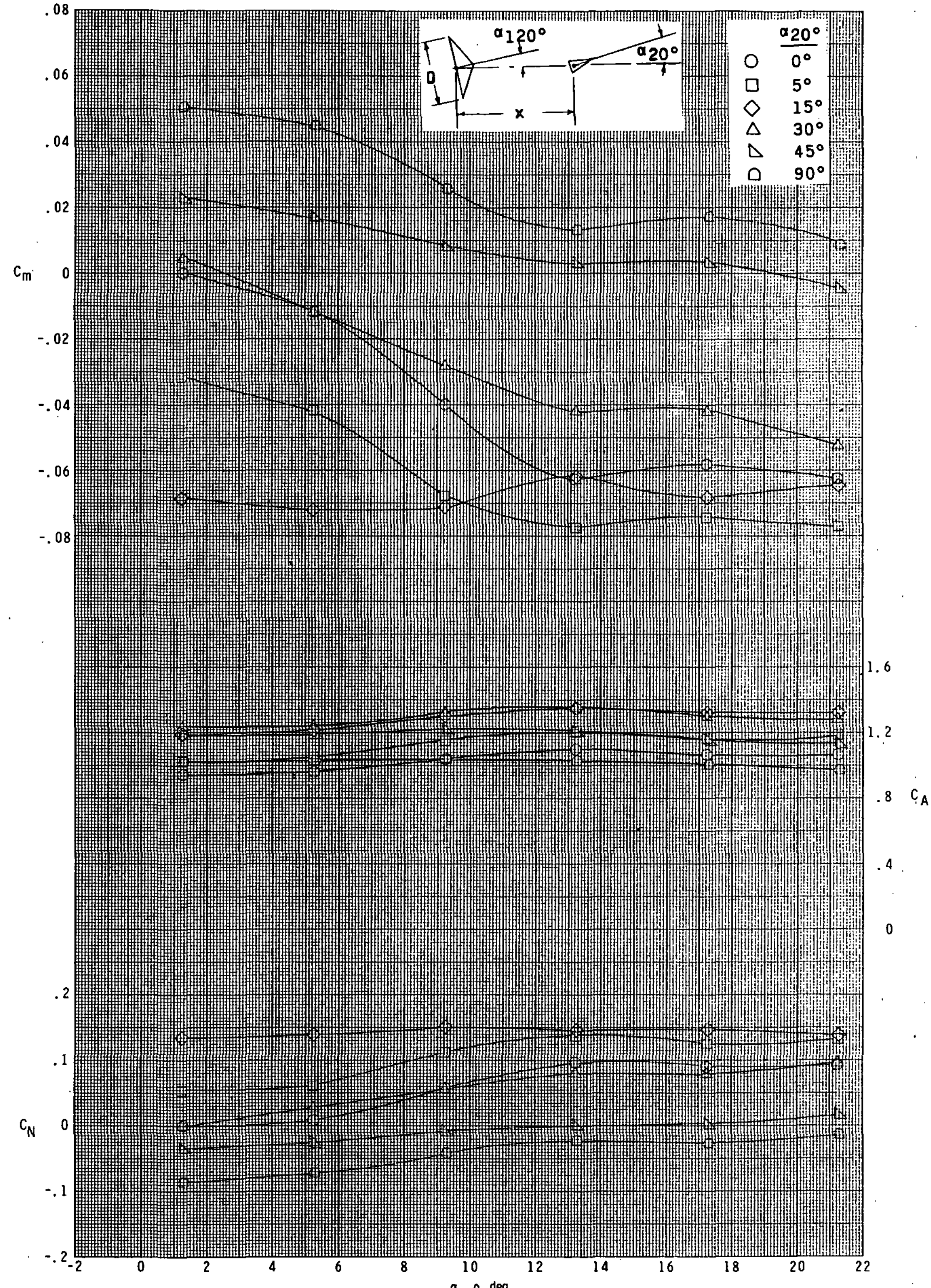

(a) x/D = 0.621; y/D = 0.

Figure 5.- Variation of pitching-moment, axial-force, and normal-force coefficients with angle of attack of 12.268-cm-diameter (4.83 in.), 120°-included-angle cone for various angles of attack of 20°-included-angle cone at $M_\infty = 2.36$.

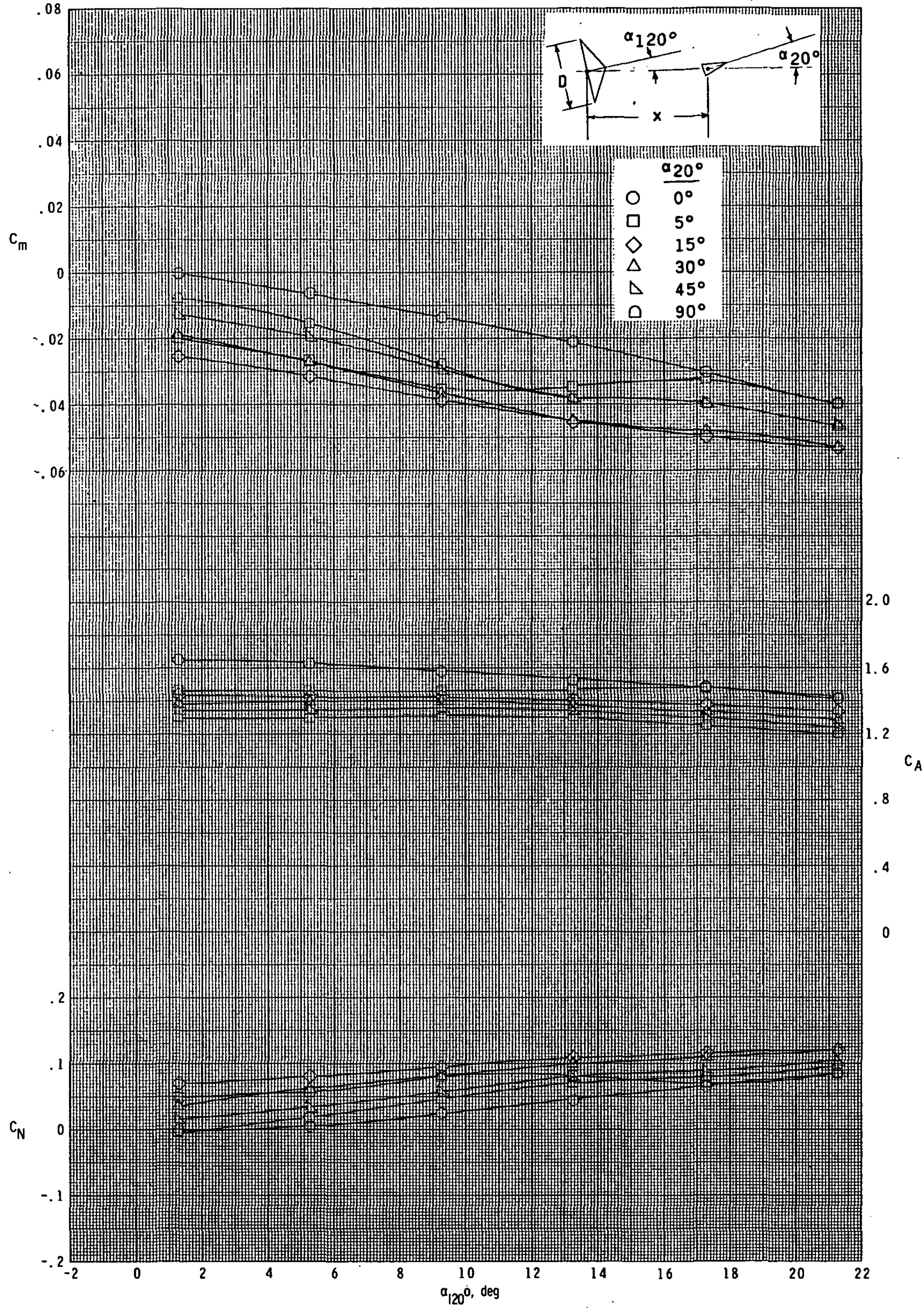

(b) x/D = 0.621; y/D = 0.25.

Figure 5.- Continued.

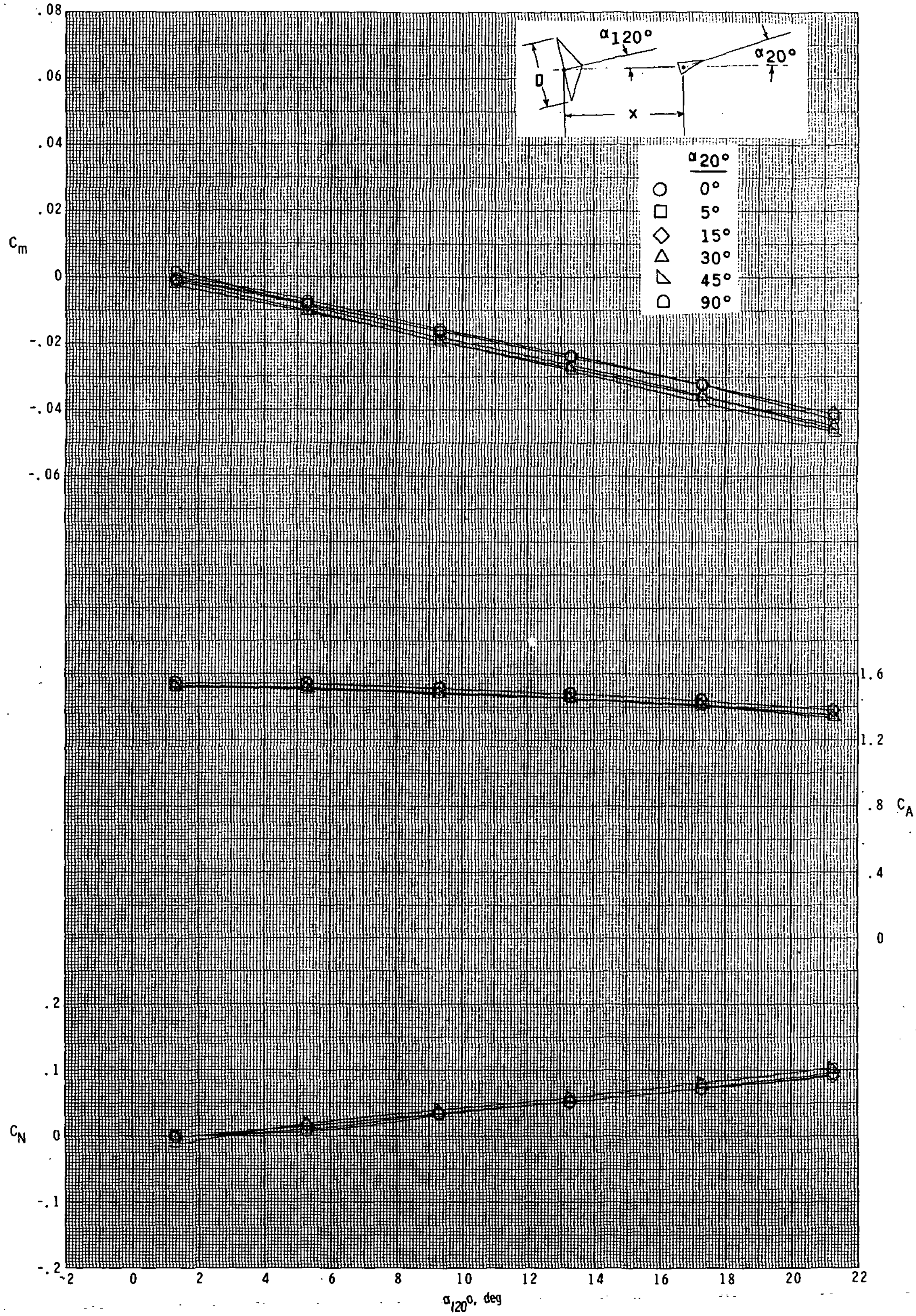

(c) $x/D = 0.621$; $y/D = 0.50$.

Figure 5.- Continued.

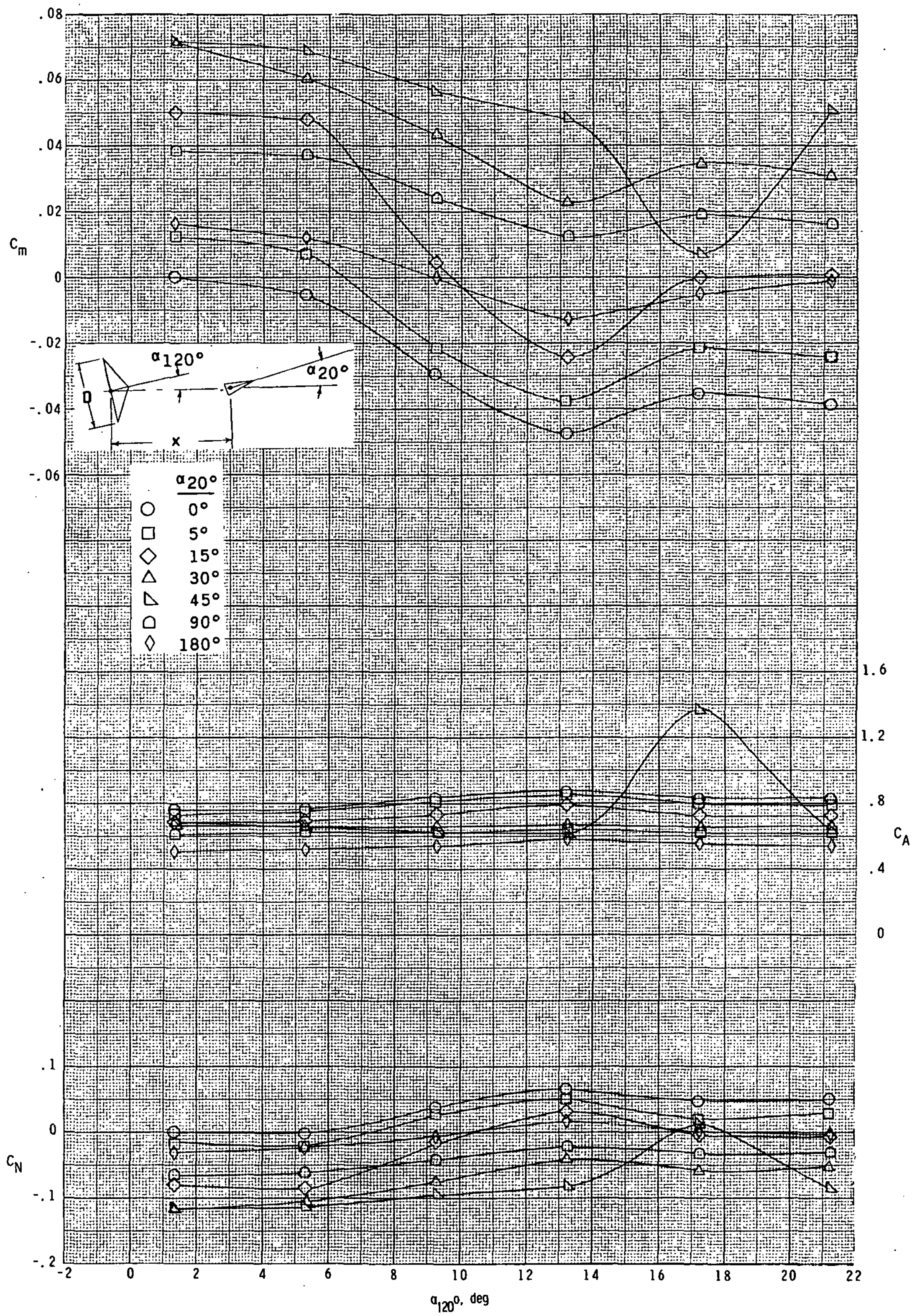

(d) x/D = 1.242; y/D = 0.

Figure 5.- Continued.

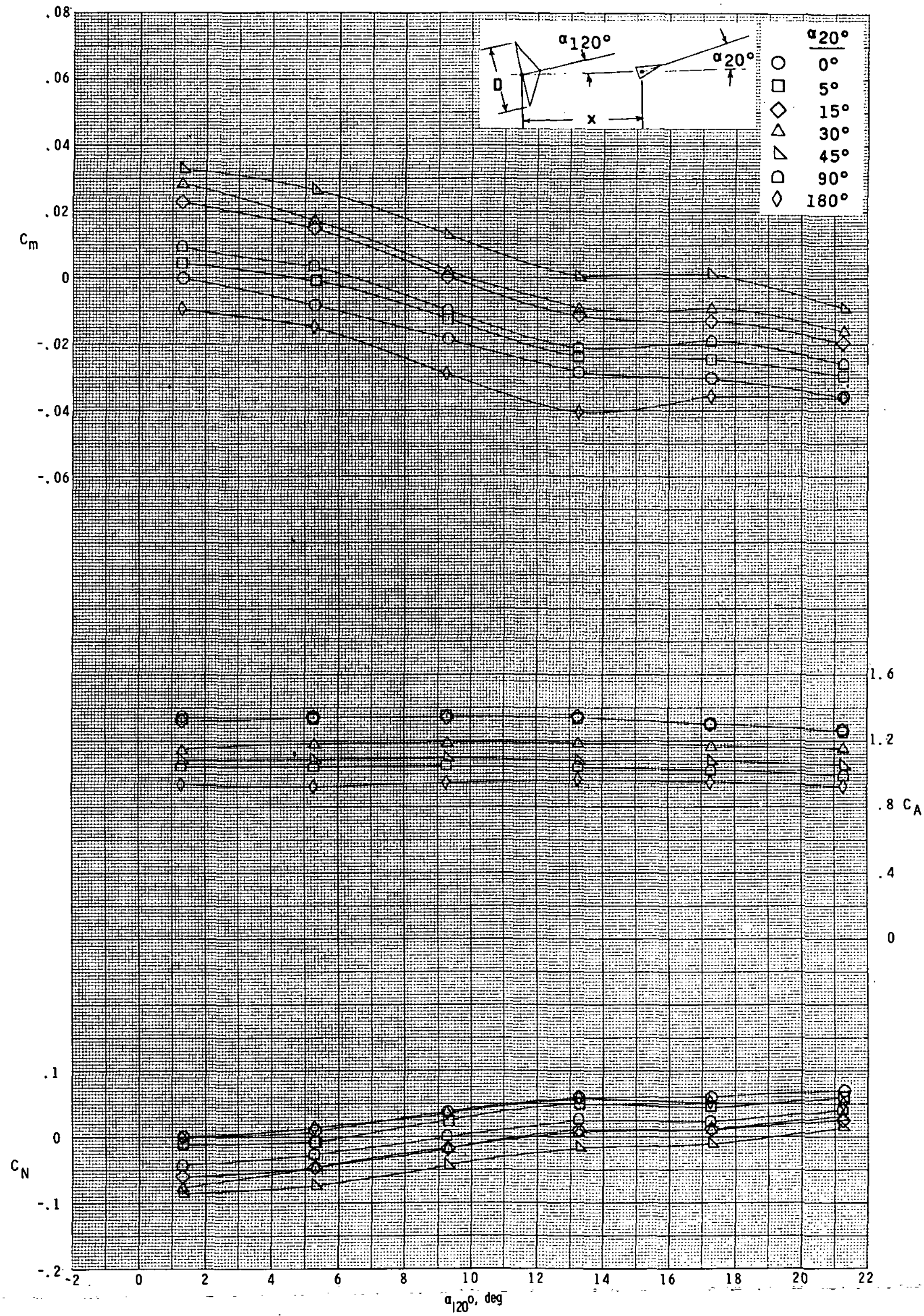

(e) x/D = 1.242; y/D = 0.25.

Figure 5.- Continued.

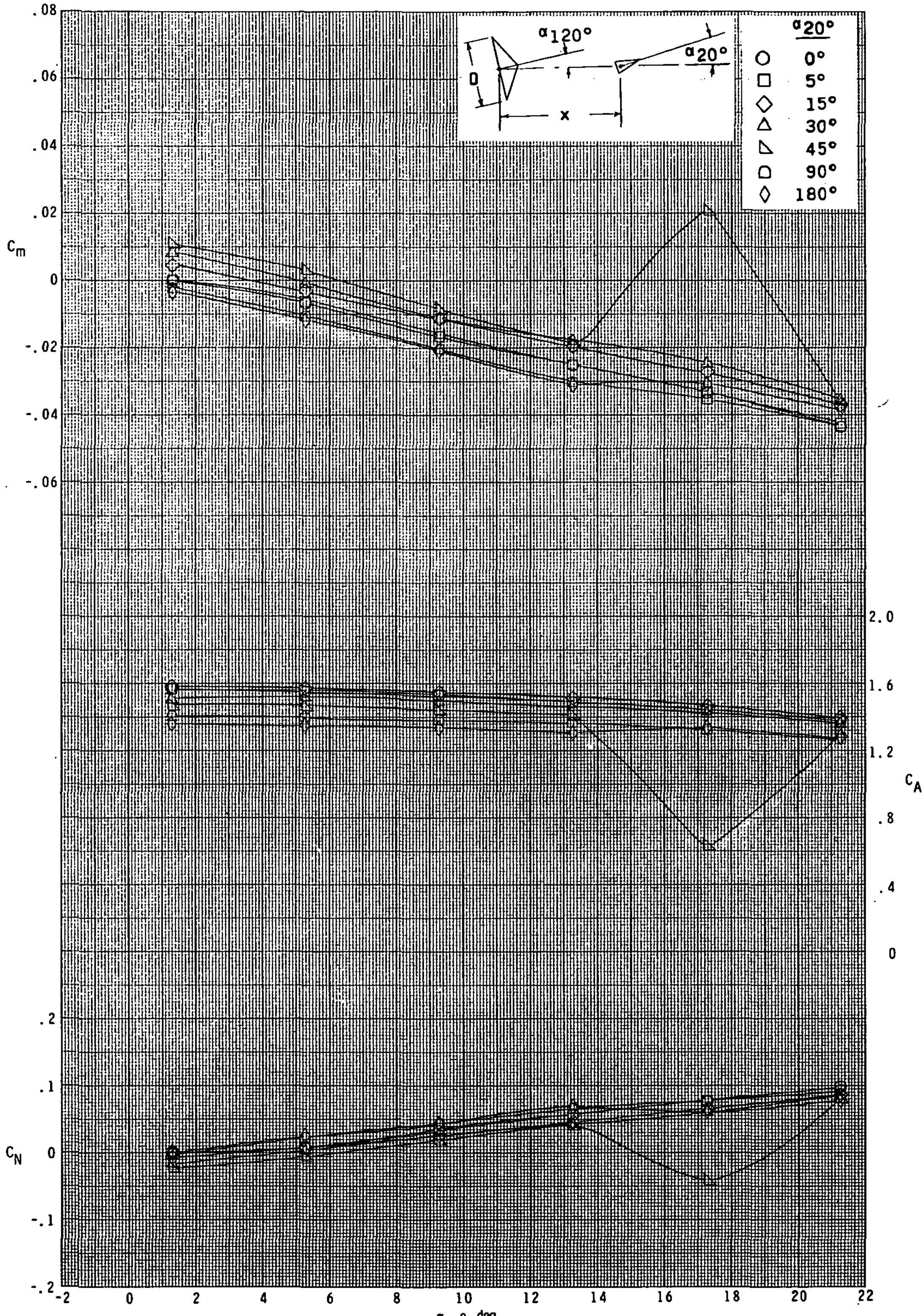

(f) x/D = 1.242; y/D = 0.50.

Figure 5.- Continued.

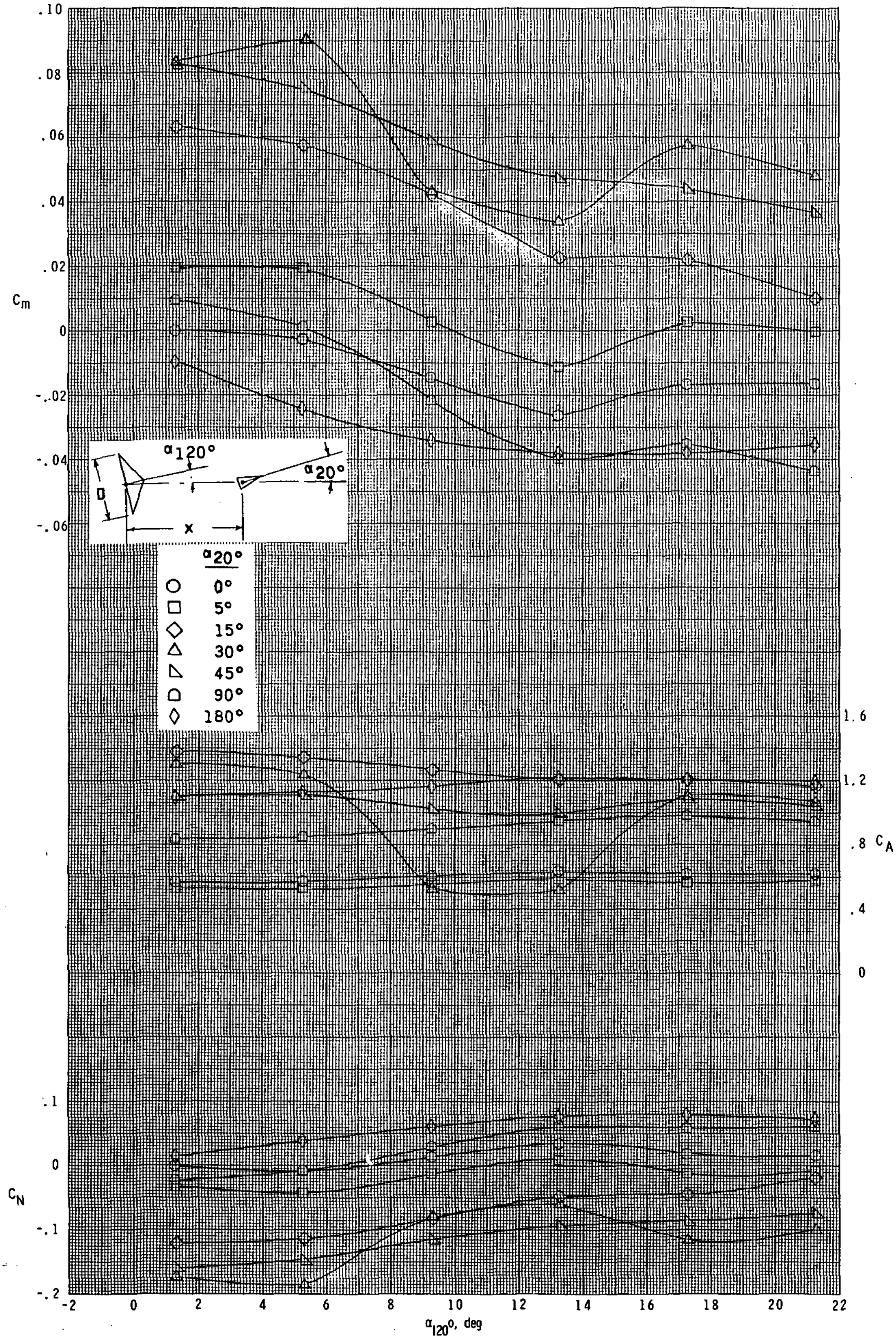

(g) x/D = 2.070; y/D = 0.

Figure 5.- Continued.

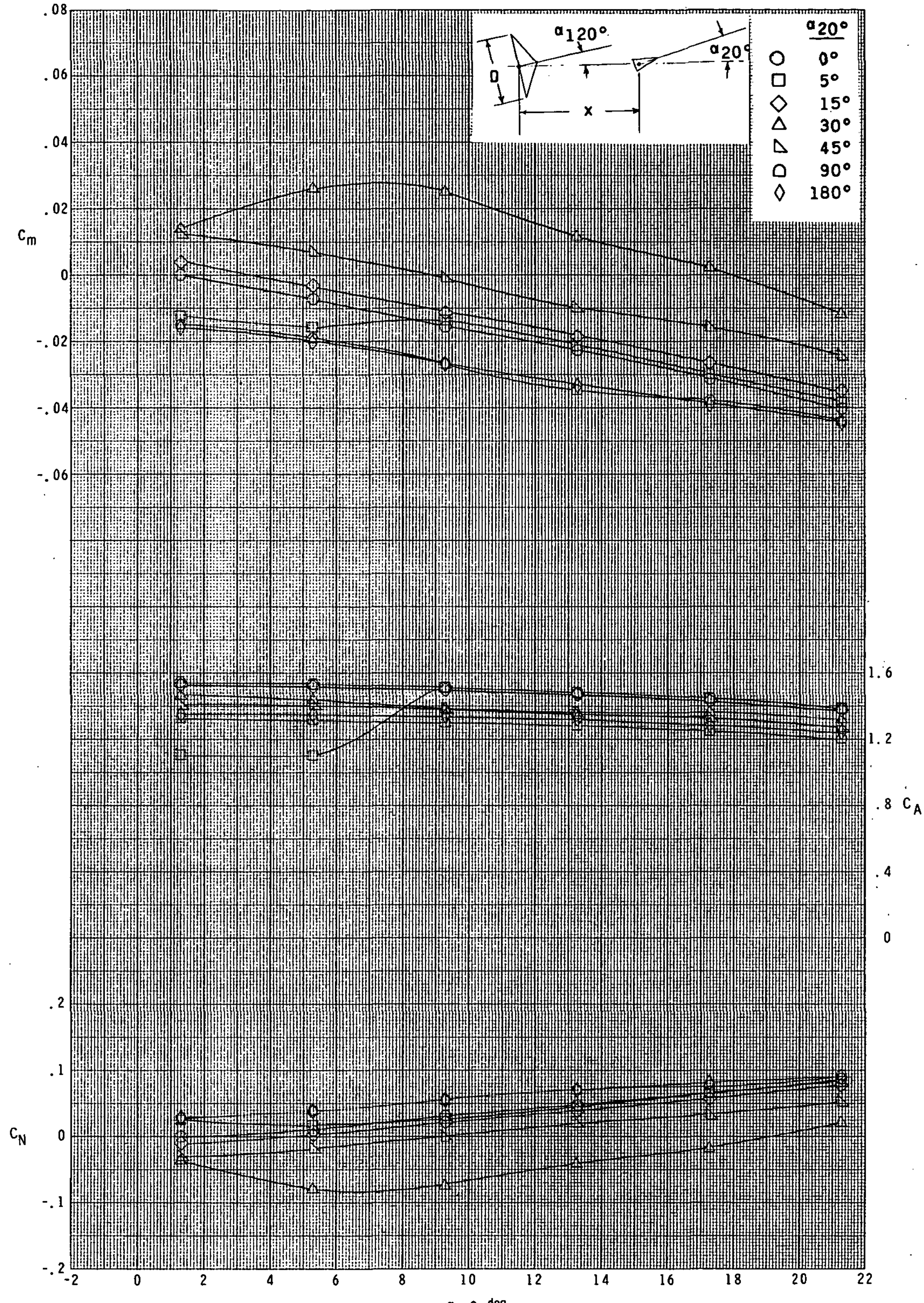

(h) x/D = 2.070; y/D = 0.25.

Figure 5.- Continued.

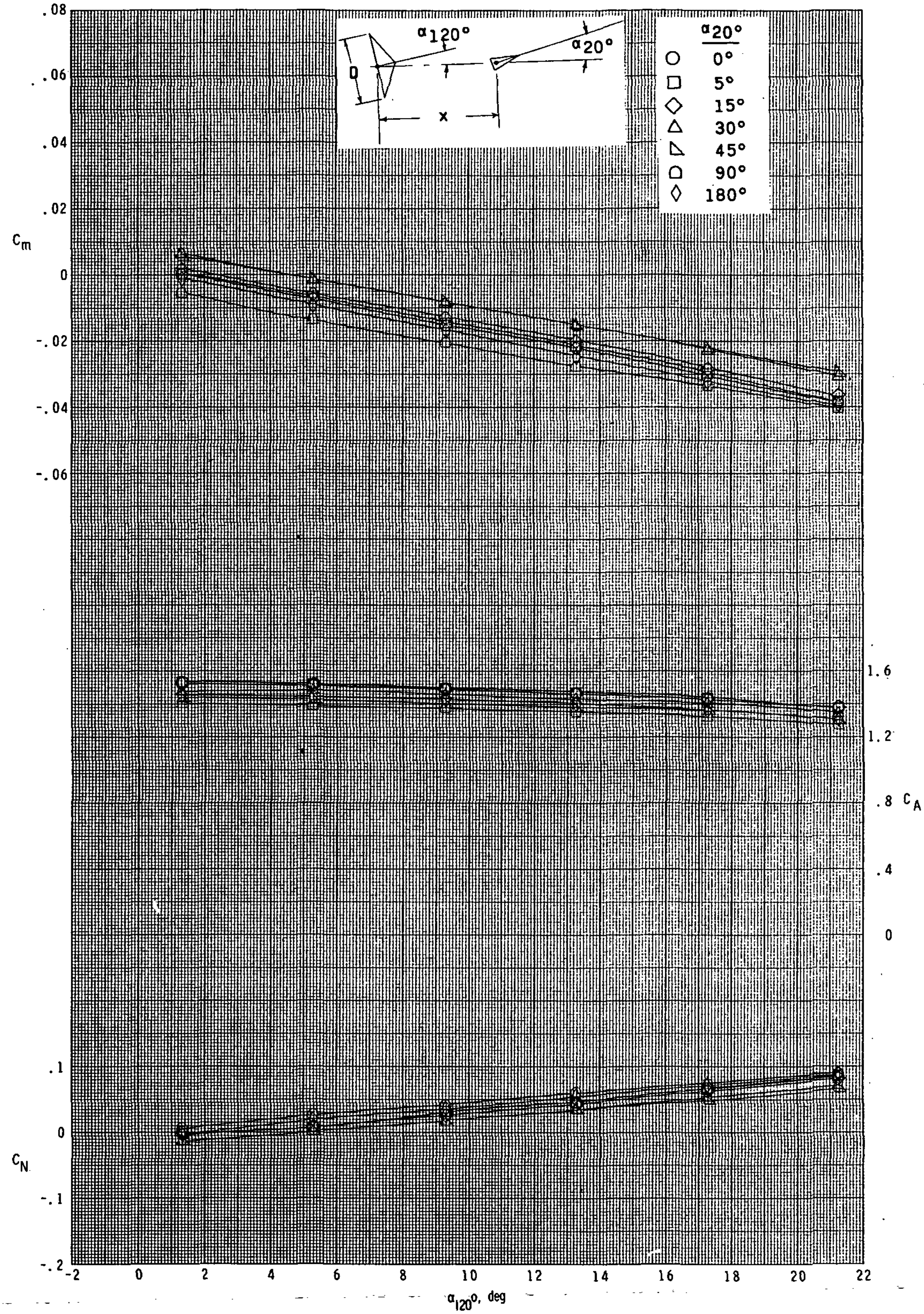

(i) x/D = 2.070; y/D = 0.50.

Figure 5.- Continued.

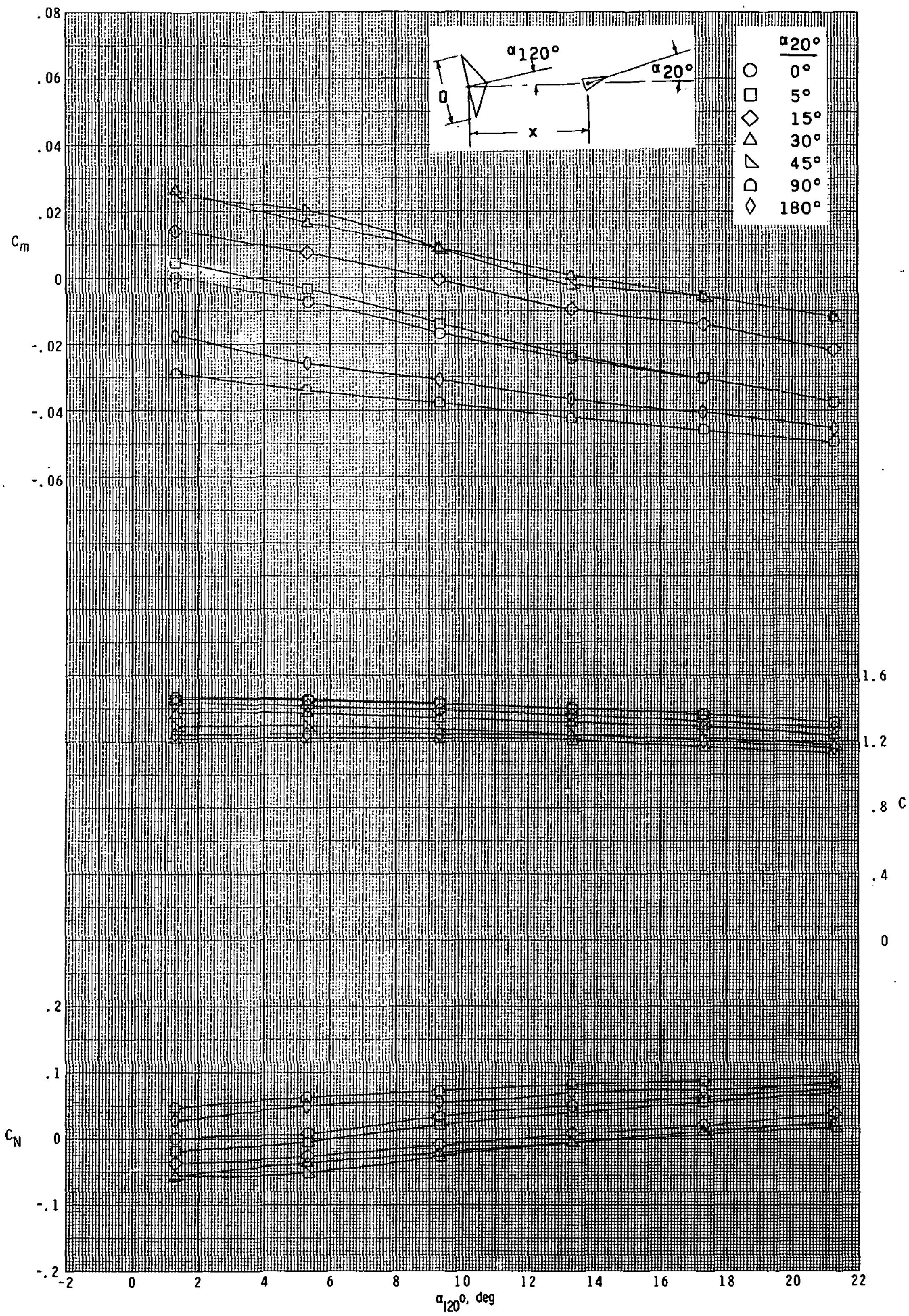

(j) x/D = 3.520; y/D = 0.

Figure 5.- Continued.

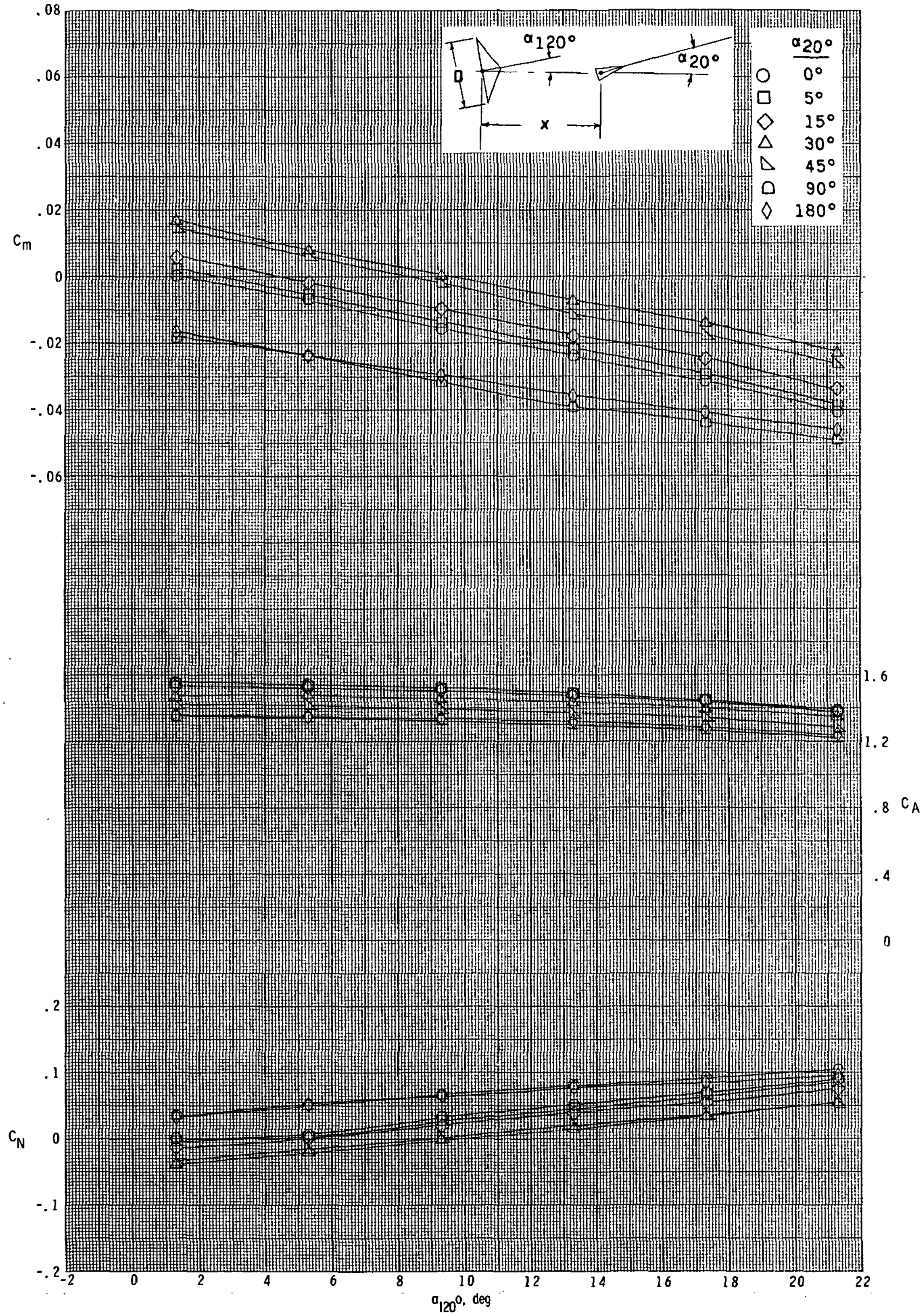

(k) x/D = 3.520; y/D = 0.25.

Figure 5.- Continued.

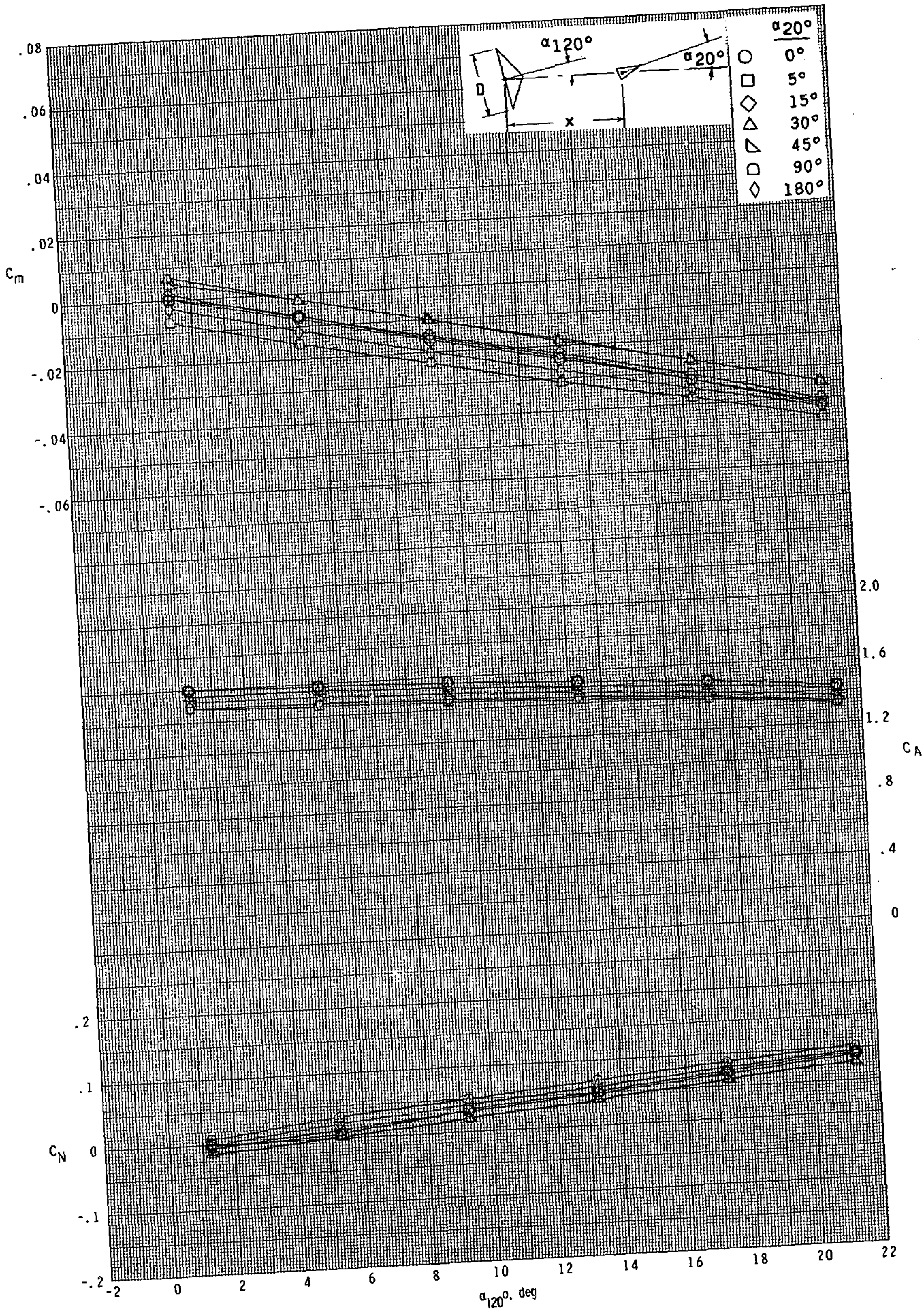

(l) x/D = 3.520; y/D = 0.50.

Figure 5.- Concluded.

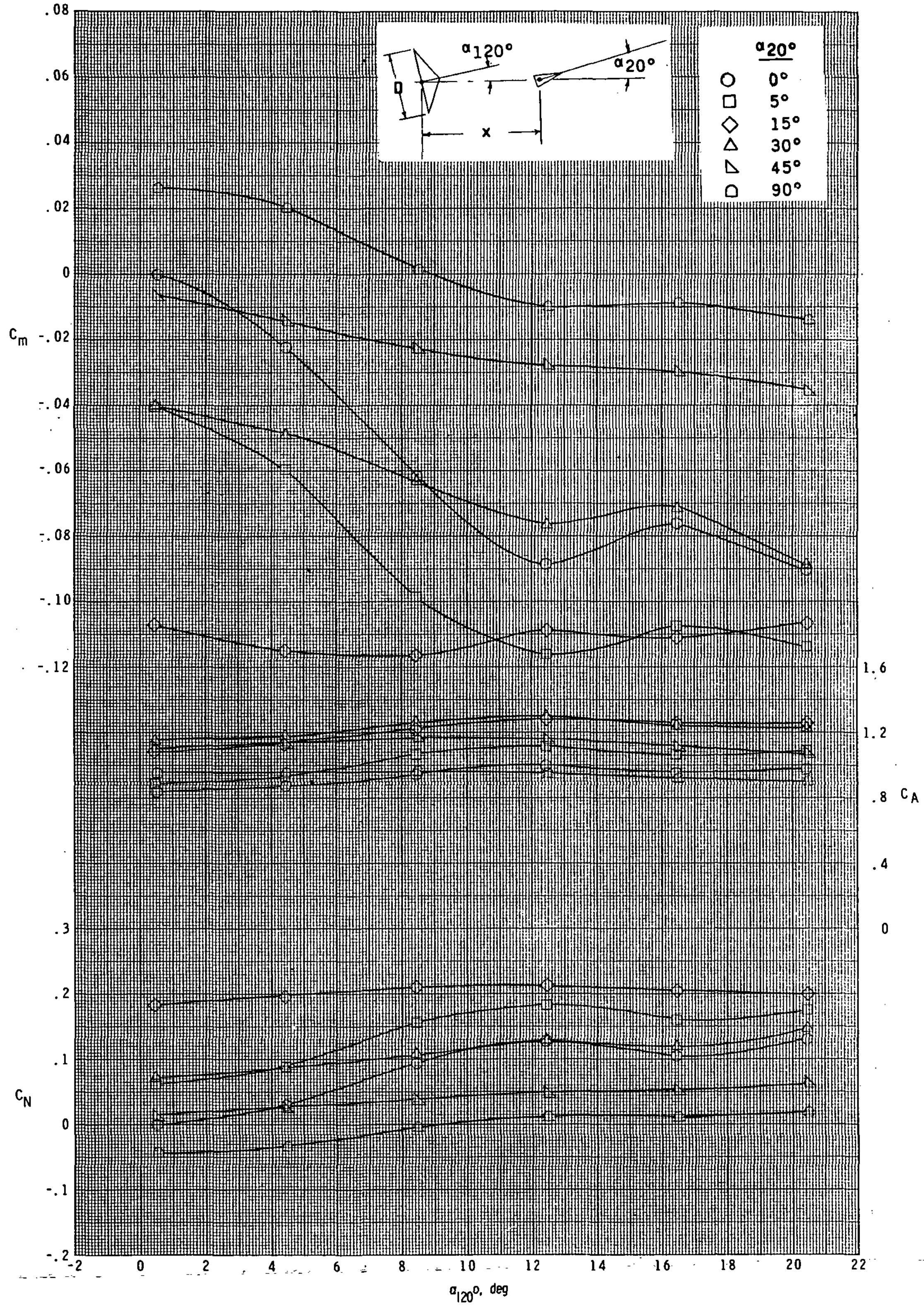

(a) $x/D = 0.621$; $y/D = 0$.

Figure 6.- Variation of pitching-moment, axial-force, and normal-force coefficients with angle of attack of 12.268-cm-diameter (4.83 in.), 120°-included-angle cone for various angles of attack of 20°-included-angle cone at $M_\infty = 2.70$.

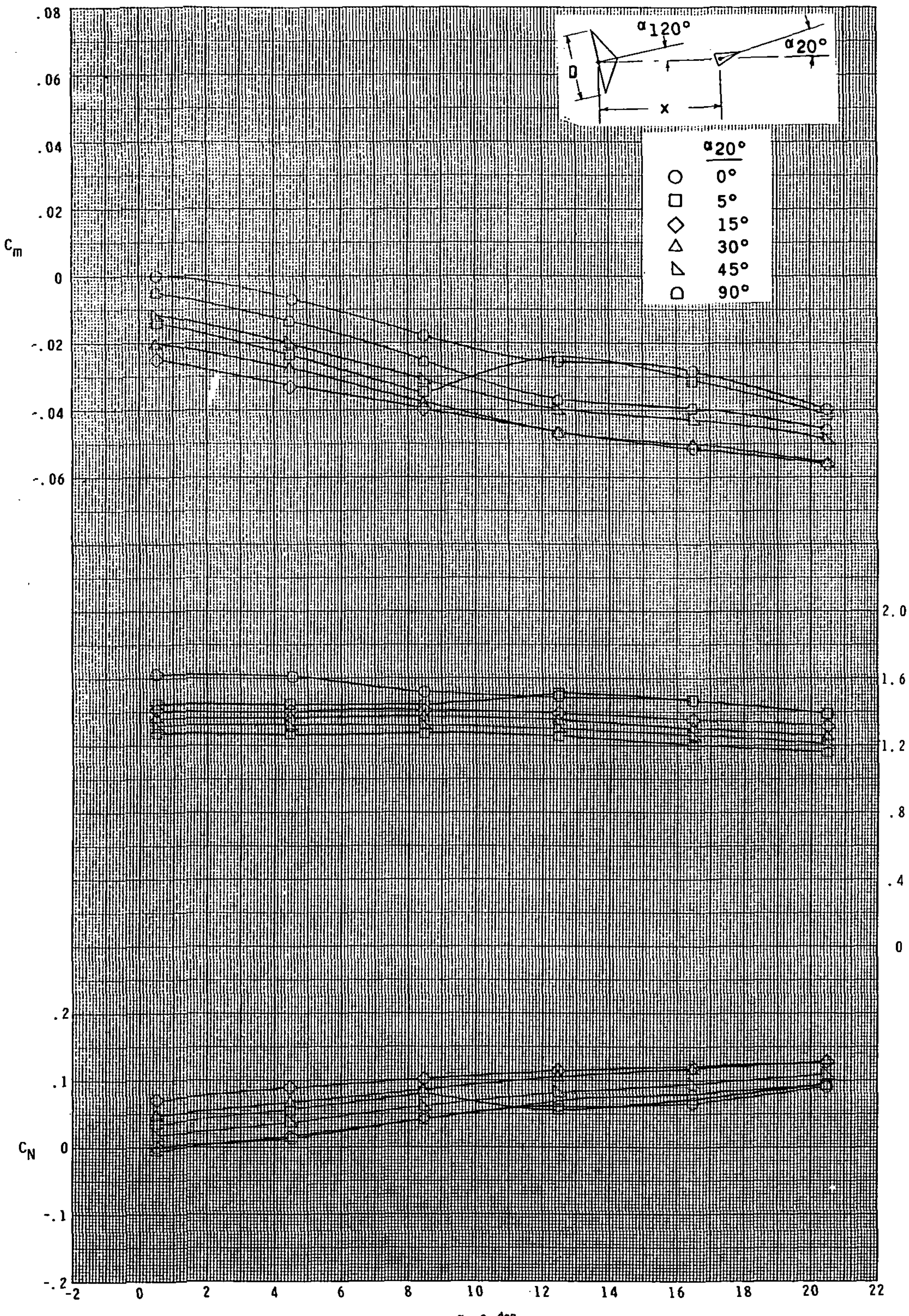

(b) $x/D = 0.621$; $y/D = 0.25$.

Figure 6.- Continued.

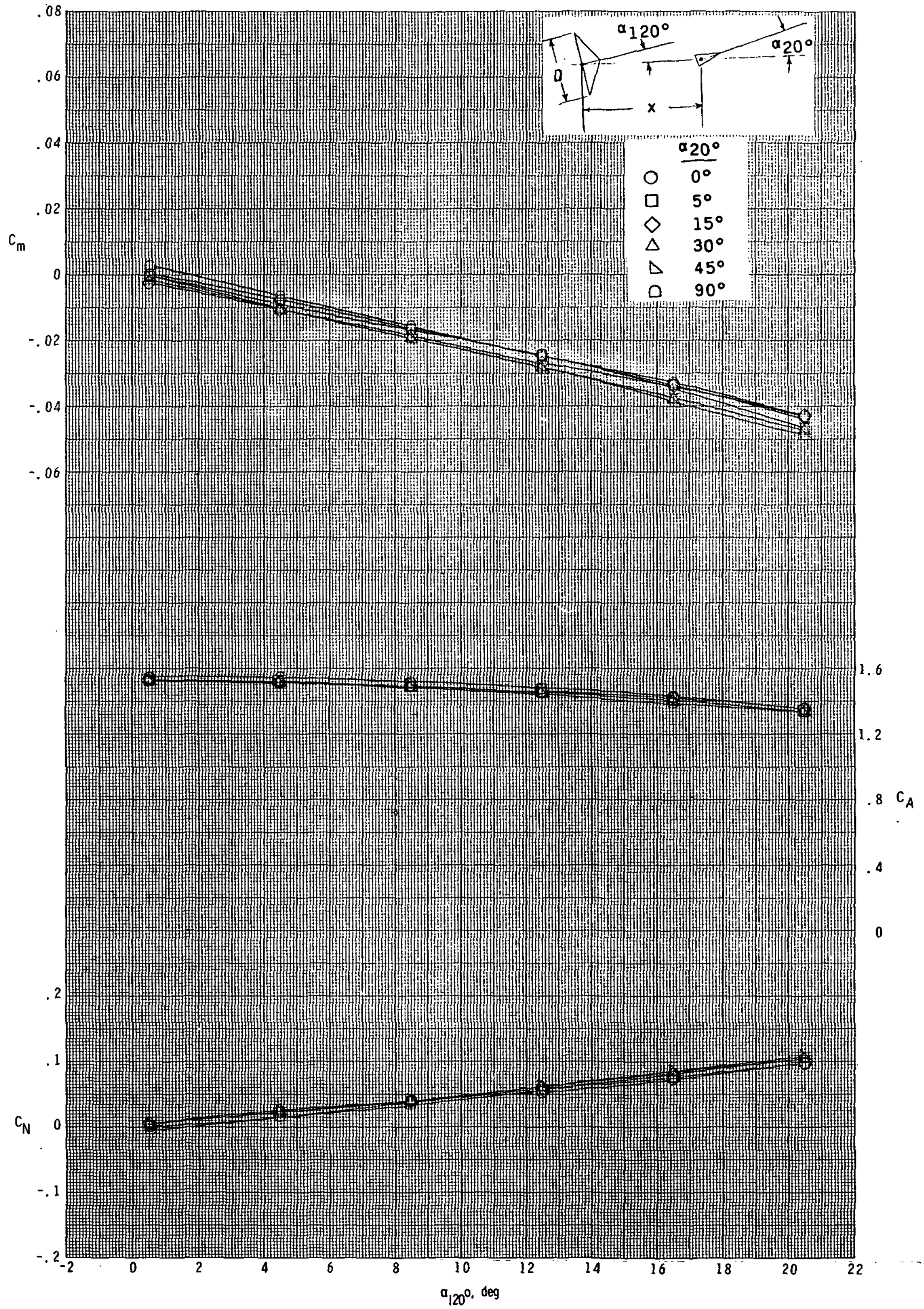

(c) x/D = 0.621; y/D = 0.50.
Figure 6.- Continued.

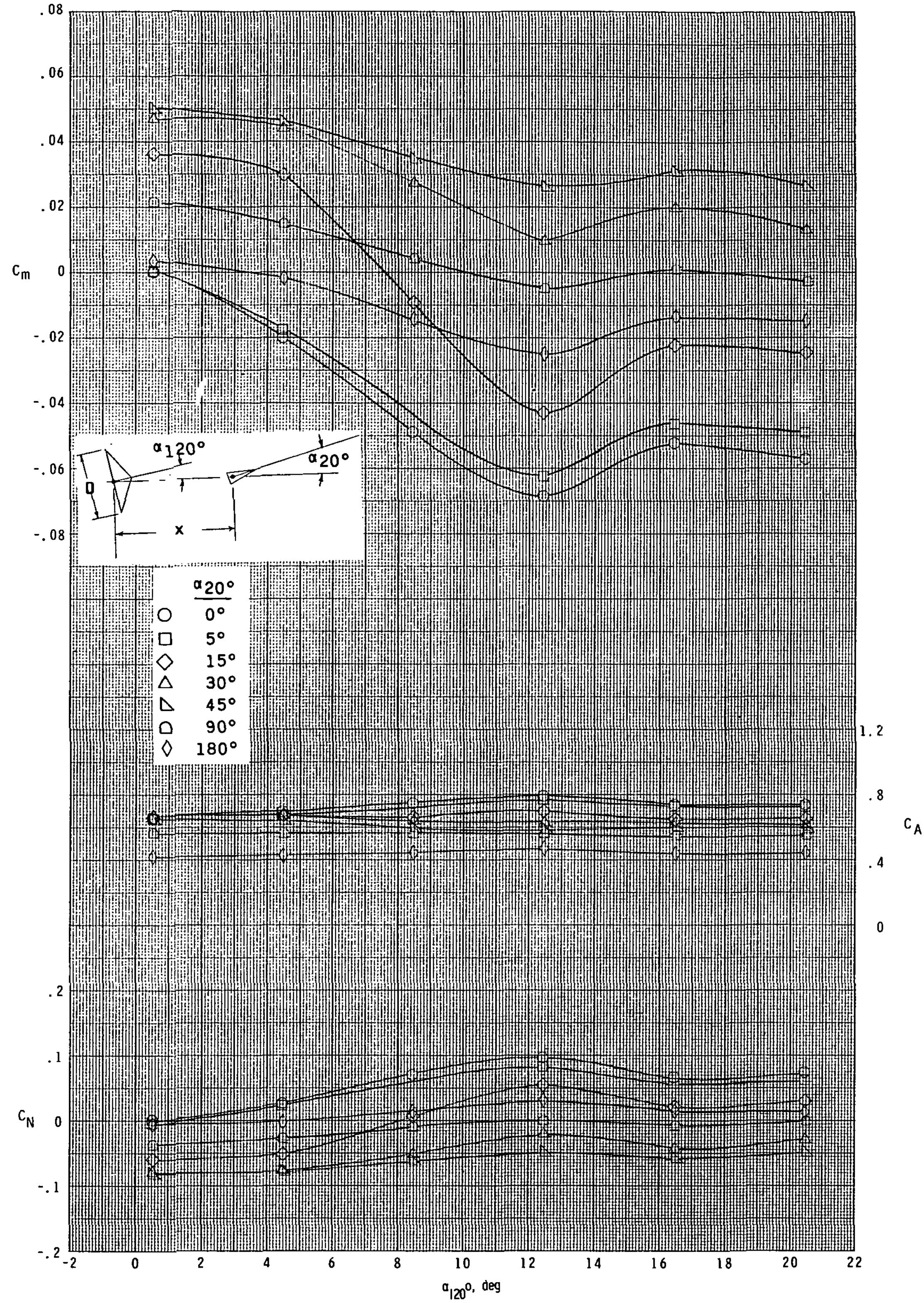

(d) x/D = 1.242; y/D = 0.

Figure 6.- Continued.

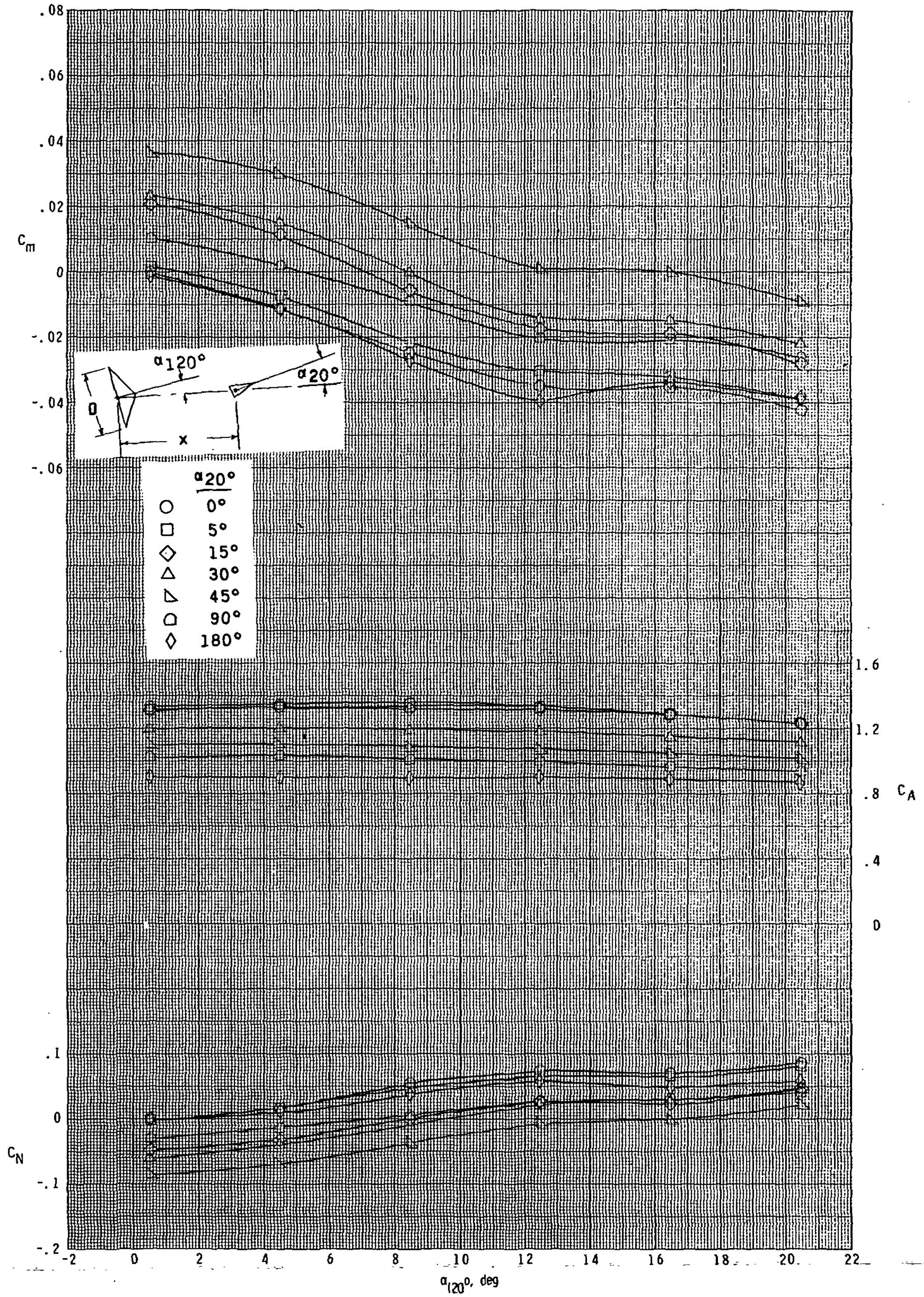

(e) x/D = 1.242; y/D = 0.25.

Figure 6.- Continued.

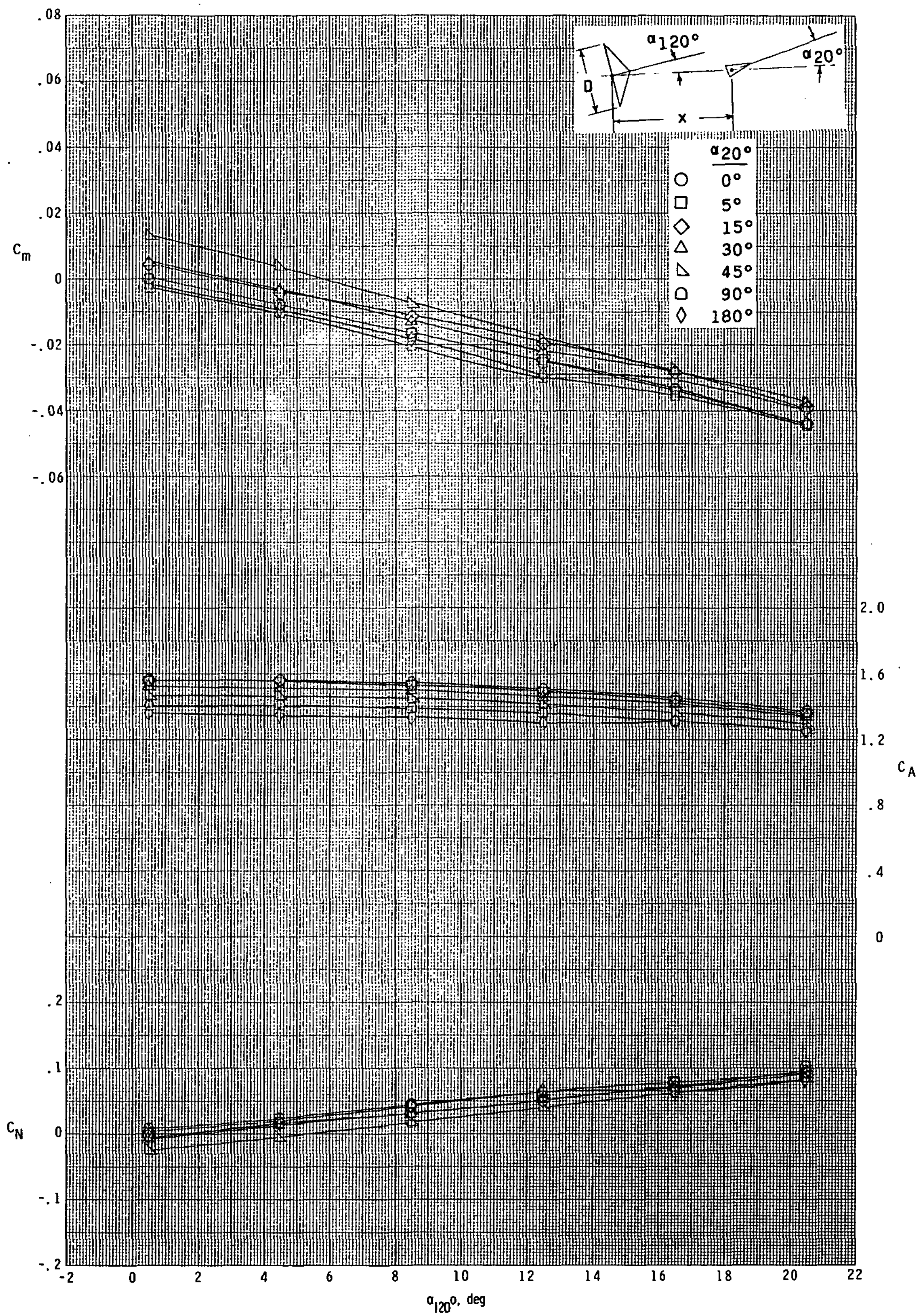

(f) x/D = 1.242; y/D = 0.50.

Figure 6.- Continued.

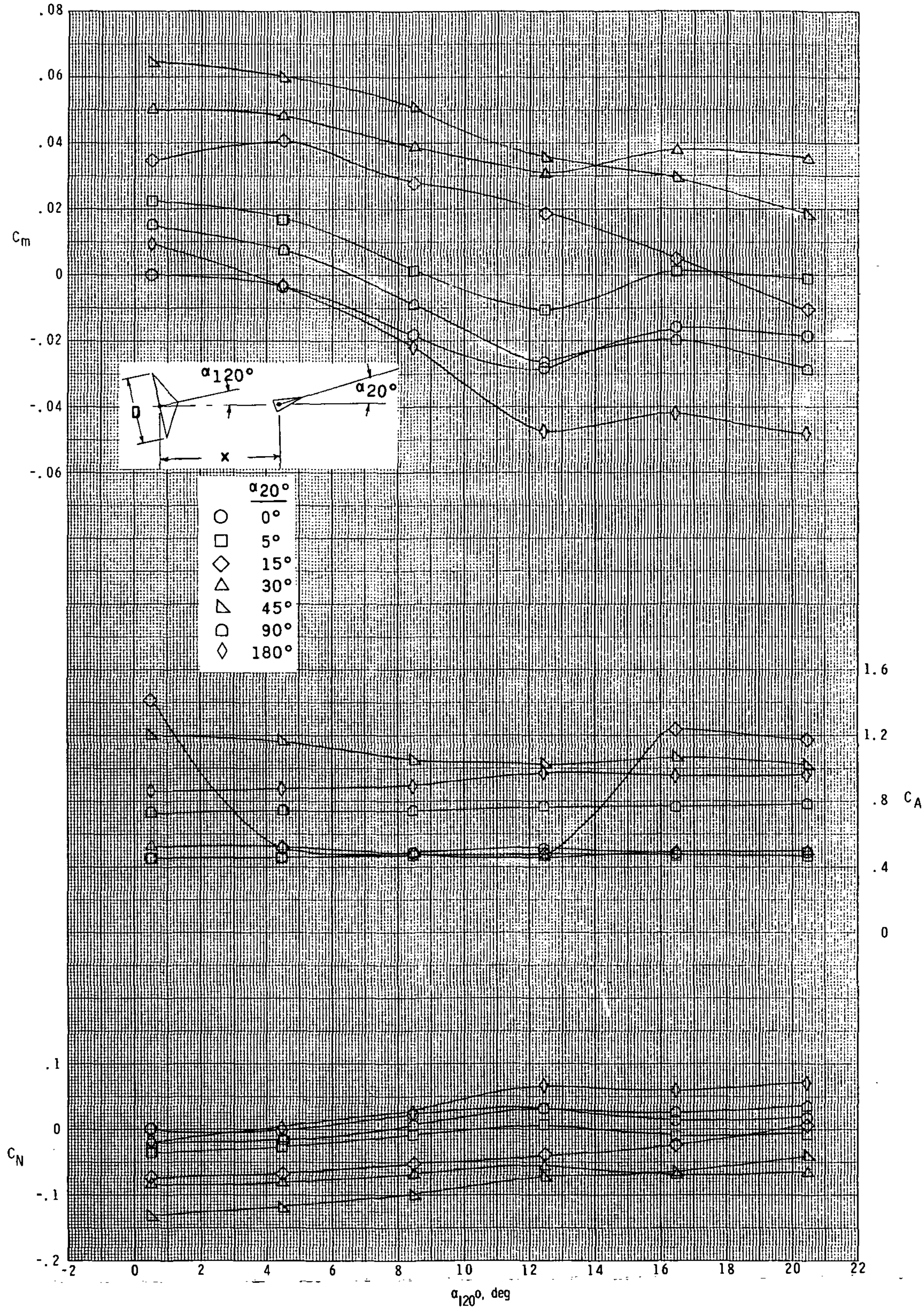

(g) x/D = 2.070; y/D = 0.

Figure 6.- Continued.

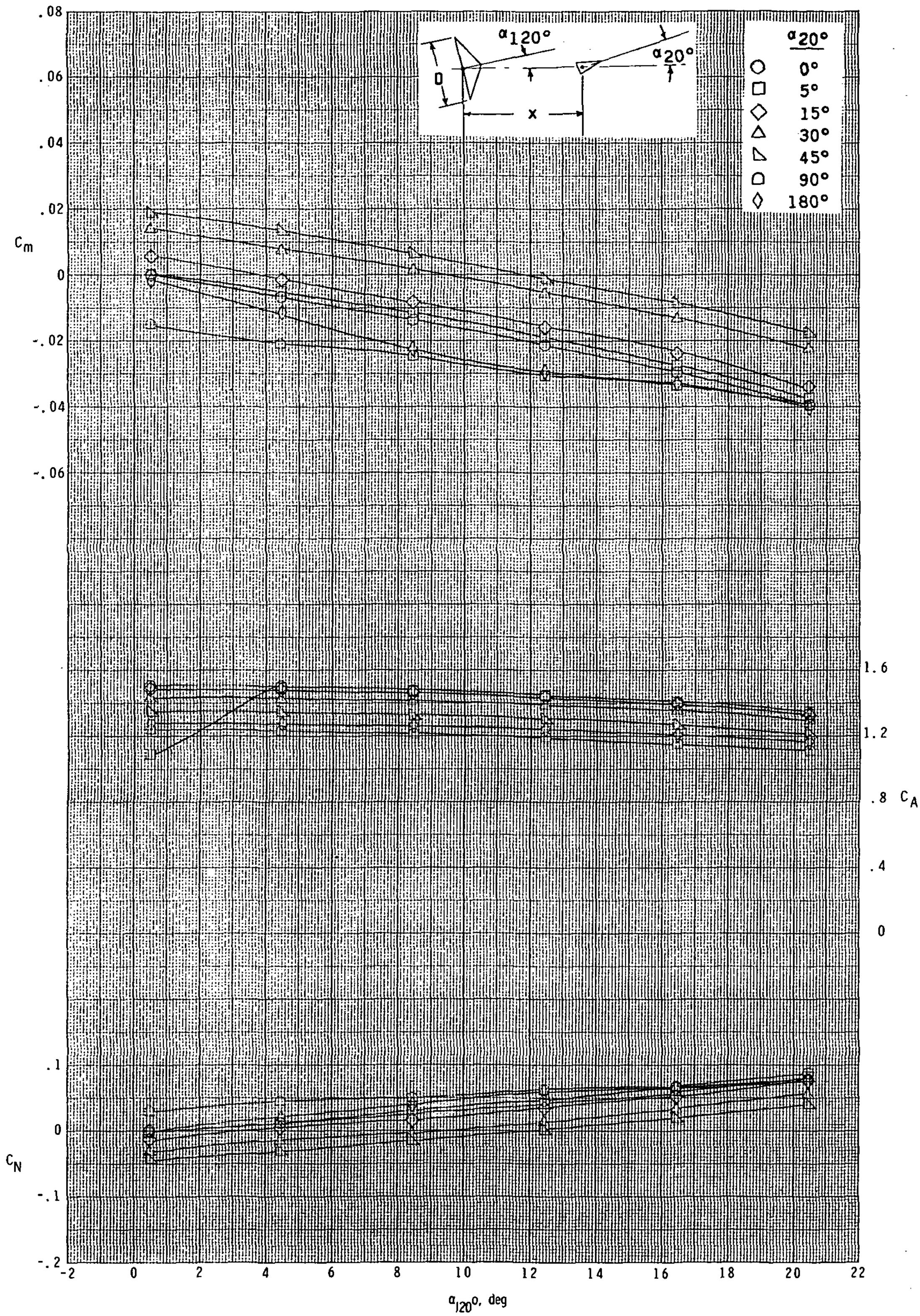

(h) x/D = 2.070; y/D = 0.25.

Figure 6.- Continued.

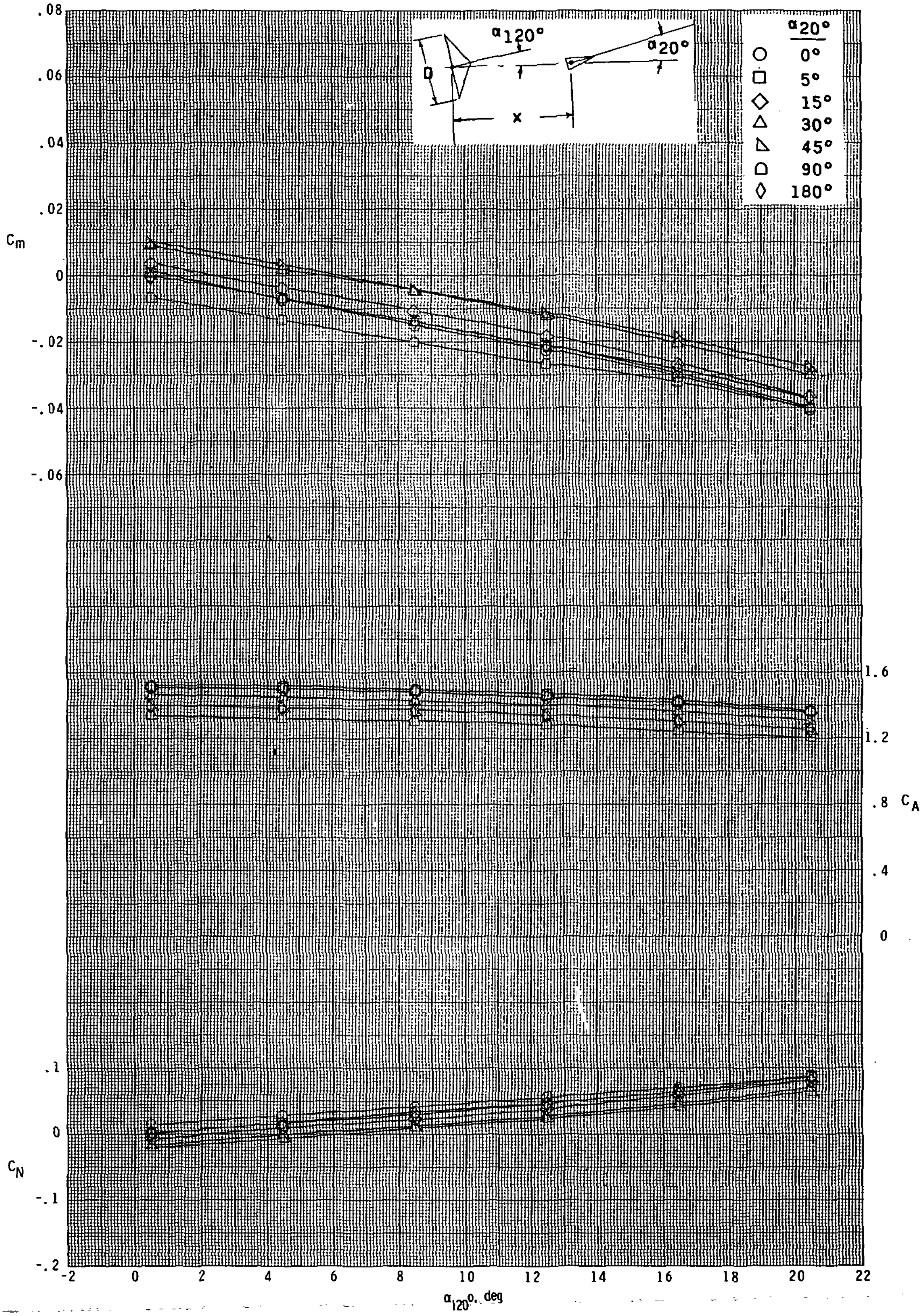

(i) x/D = 2.070; y/D = 0.50.

Figure 6.- Continued.

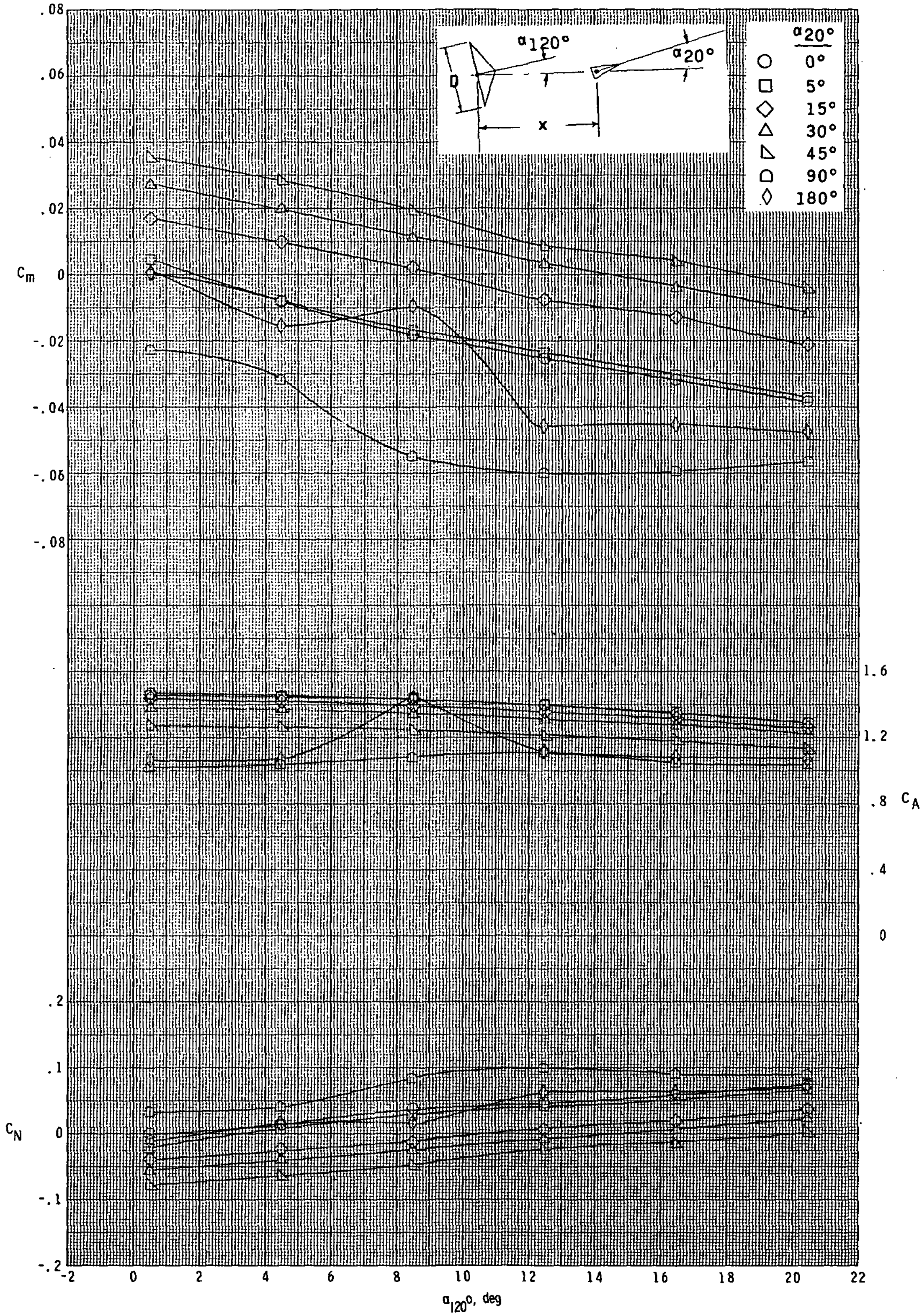

(j) x/D = 3.520; y/D = 0.

Figure 6.- Continued.

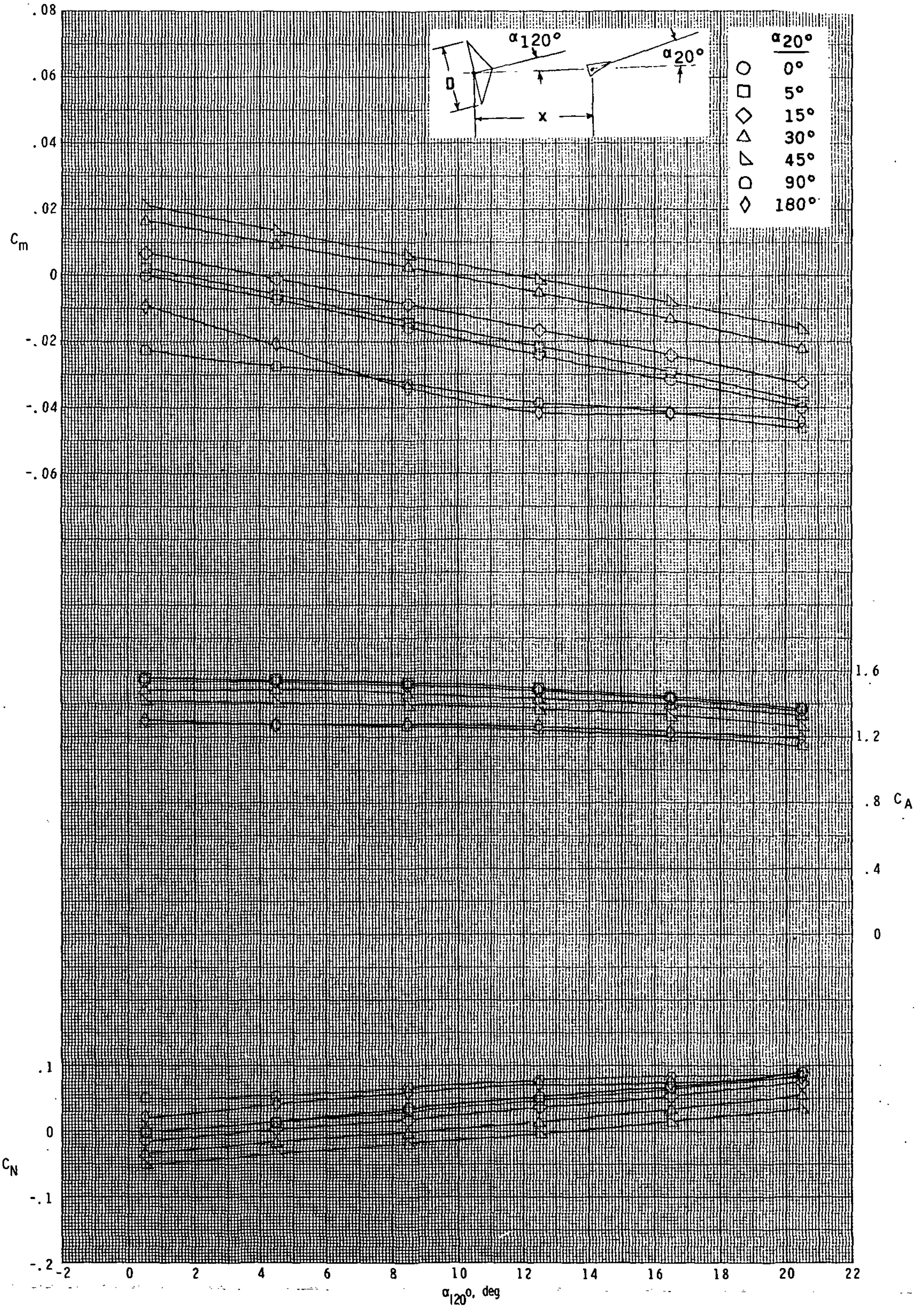

(k) $x/D = 3.520$; $y/D = 0.25$.

Figure 6.- Continued.

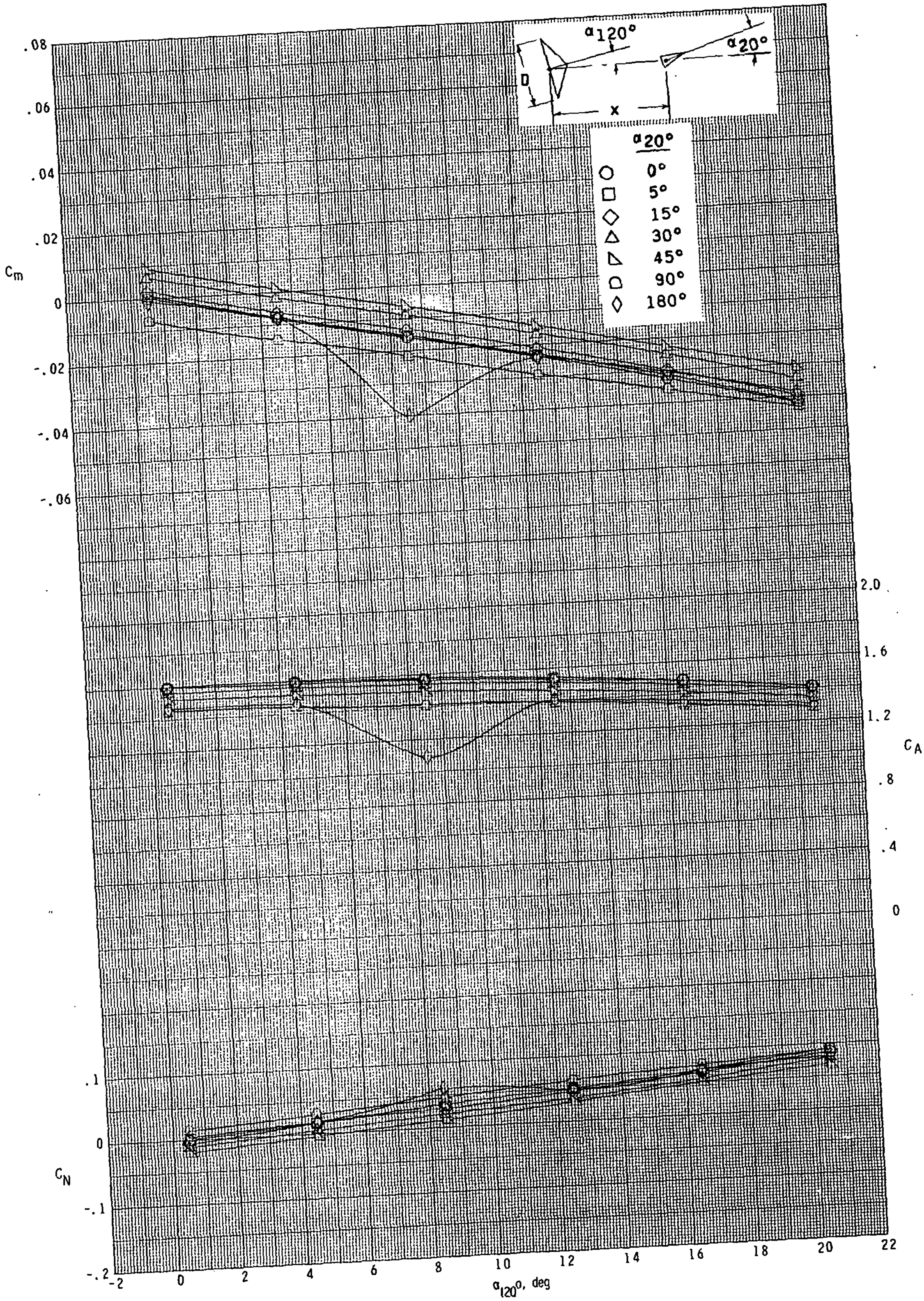

(l) x/D = 3.520; y/D = 0.50.

Figure 6.- Concluded.

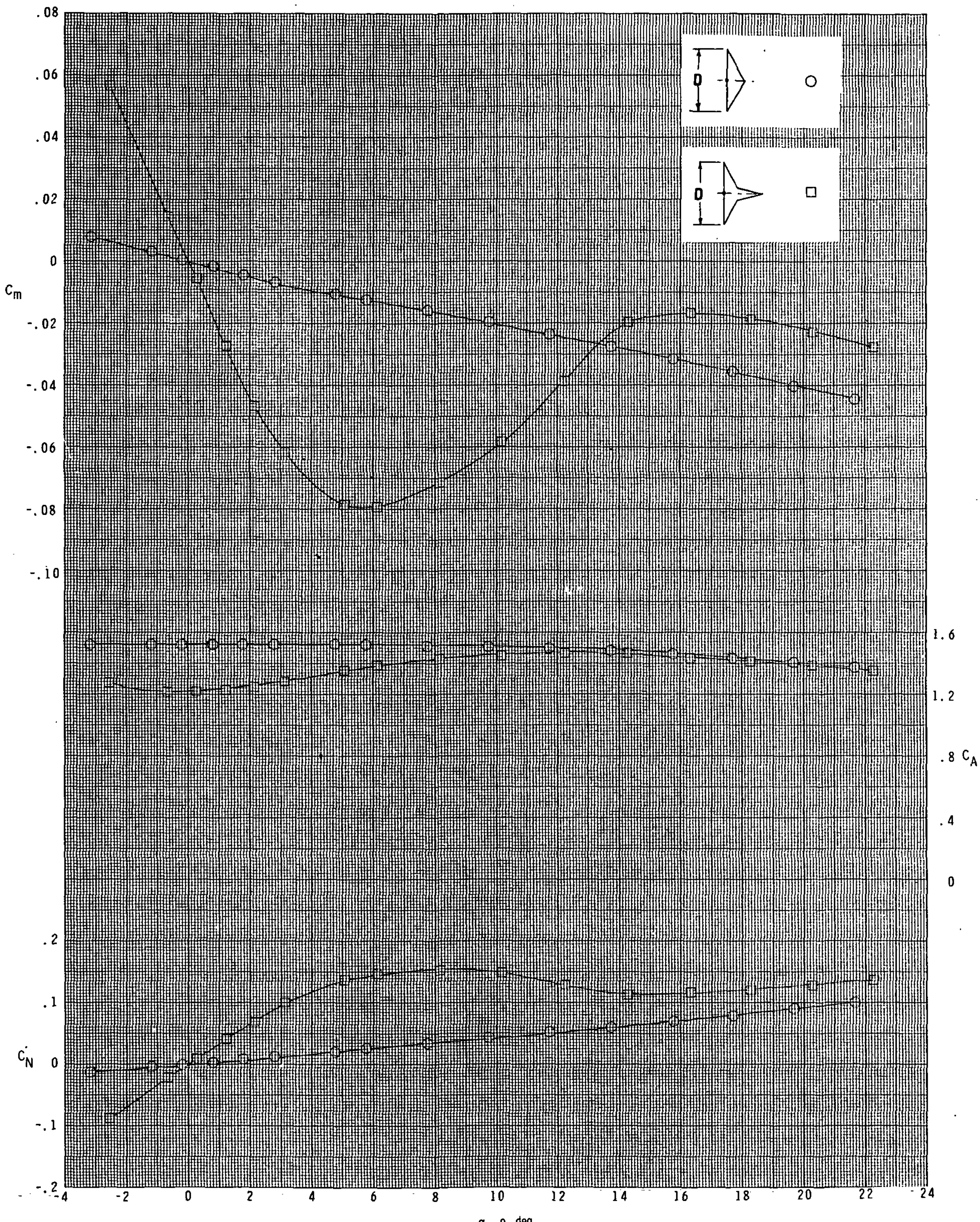

(a) $M_\infty = 2.36$.

Figure 7.- Variation of pitching-moment, axial-force, and normal-force coefficients with angle of attack for 16.002-cm-diameter (6.30 in.), 120°-included-angle cone with attached and separated 20°-included-angle cone.

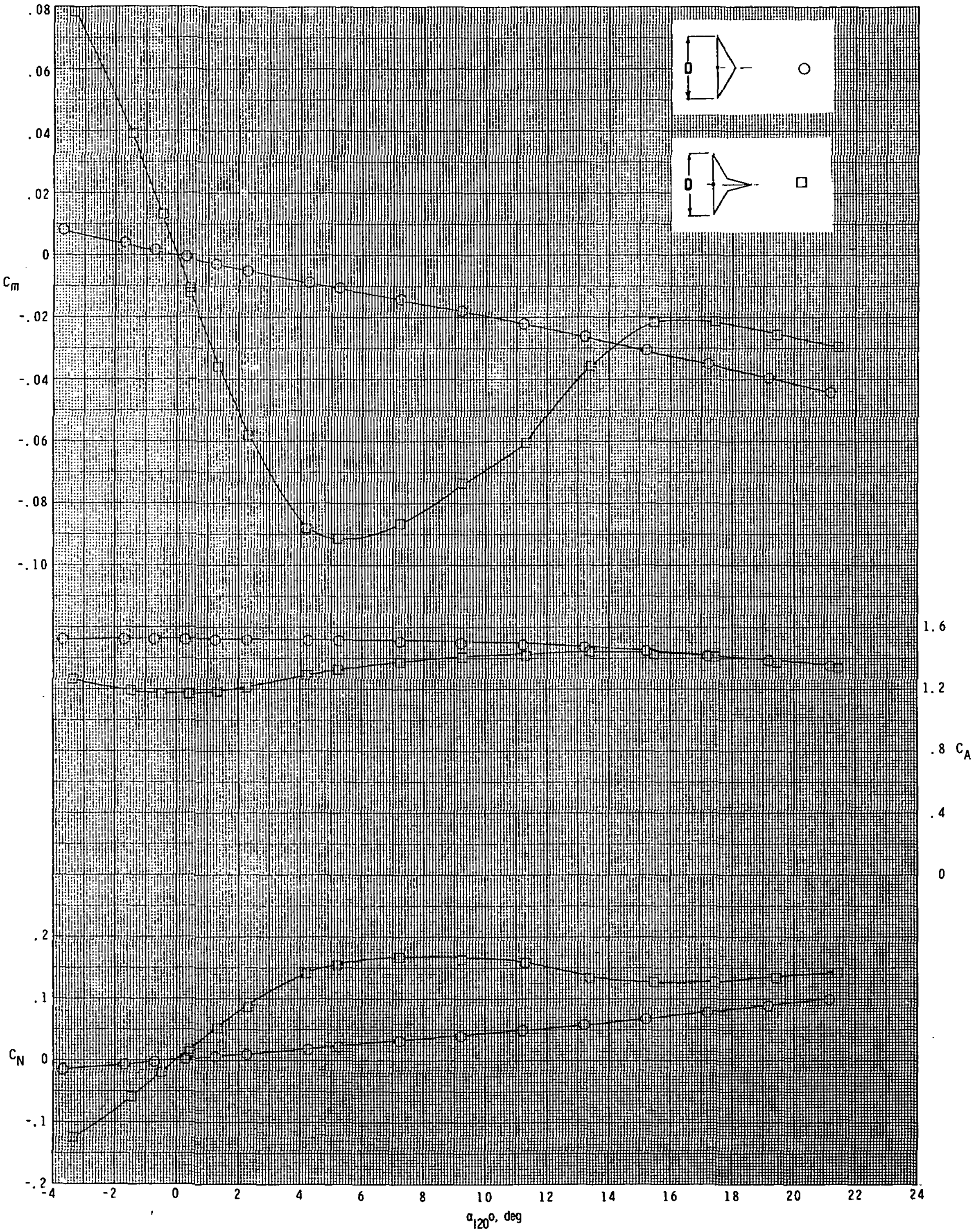

(b) $M_\infty = 2.70$.

Figure 7.- Concluded.

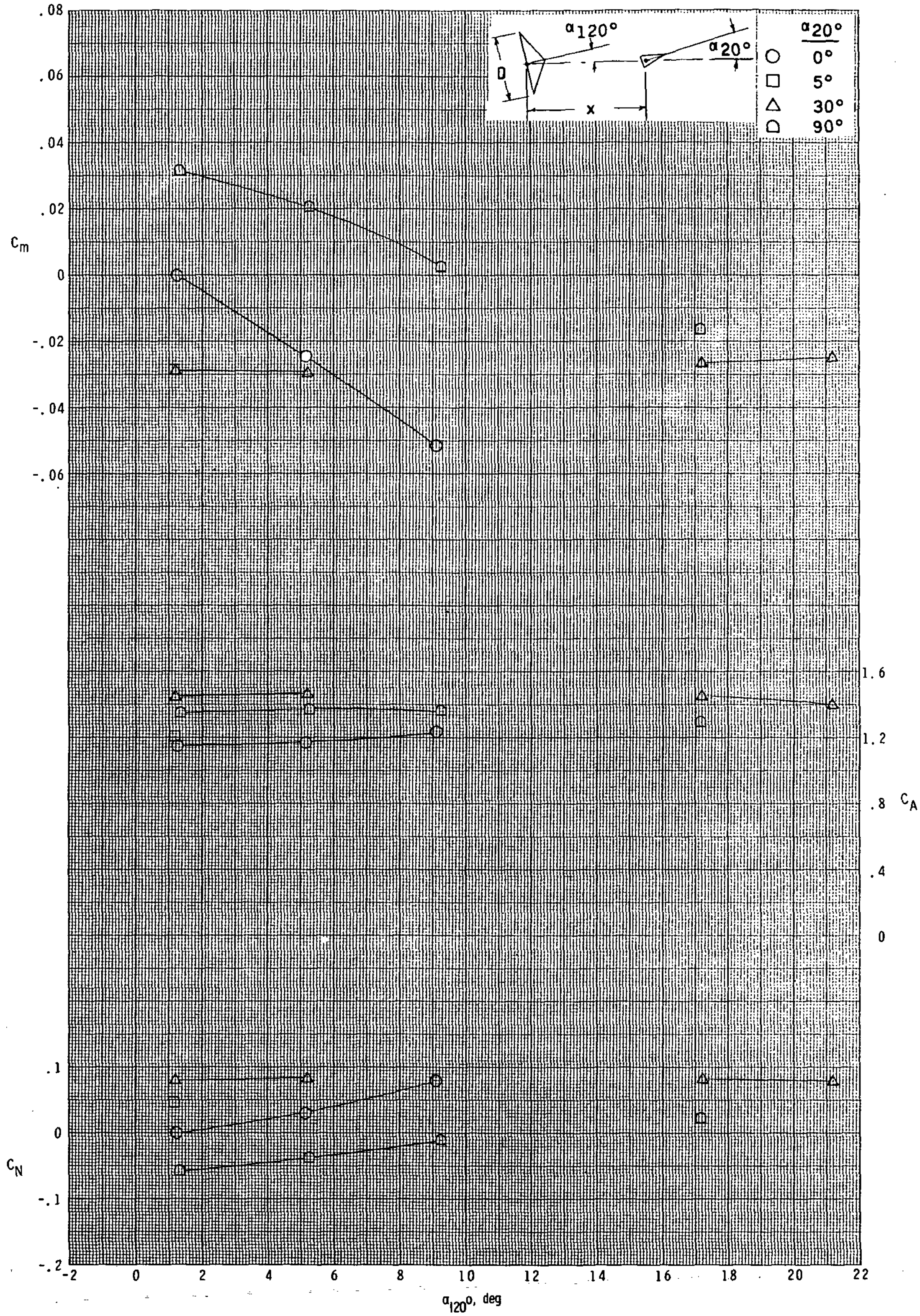

(a) x/D = 0.476; y/D = 0.

Figure 8.- Variation of pitching-moment, axial-force, and normal-force coefficients with angle of attack for 16.002-cm-diameter (6.30 in.), 120°-included-angle cone with attached and separated 20°-included-angle cone at $M_\infty = 2.36$.

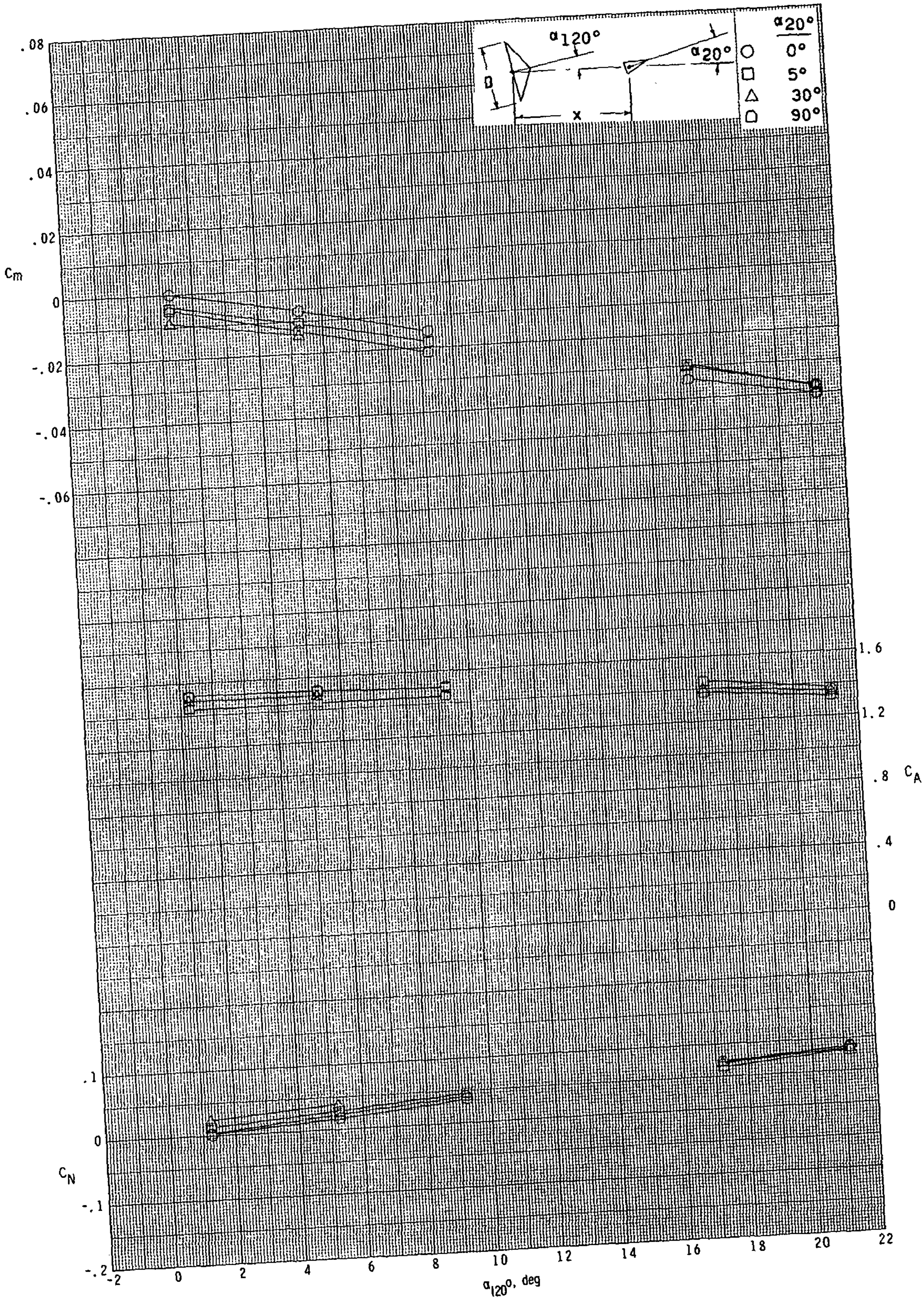

(b) $x/D = 0.476$; $y/D = 0.25$.

Figure 8.- Continued.

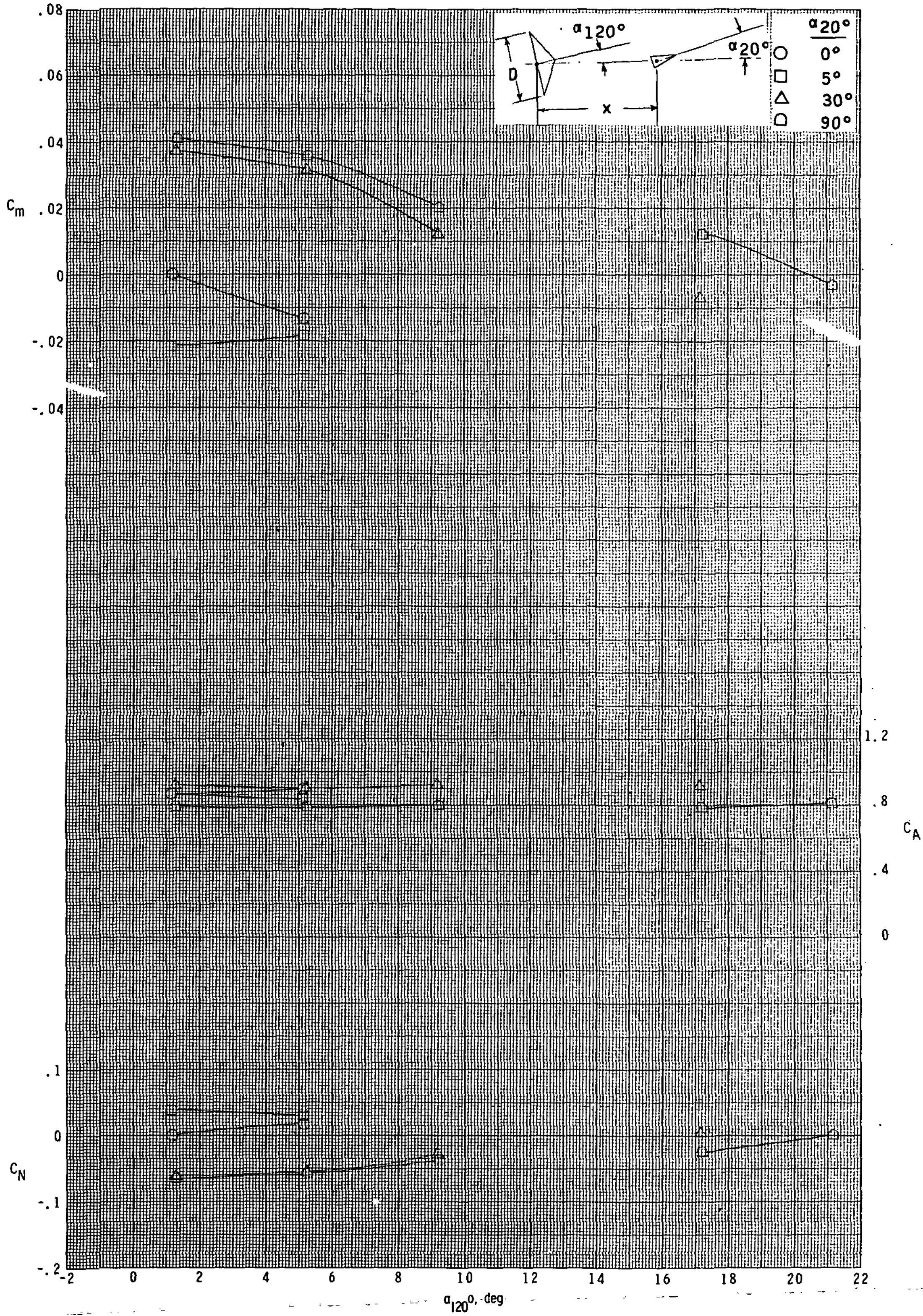

(c) x/D = 0.952; y/D = 0.

Figure 8.- Continued.

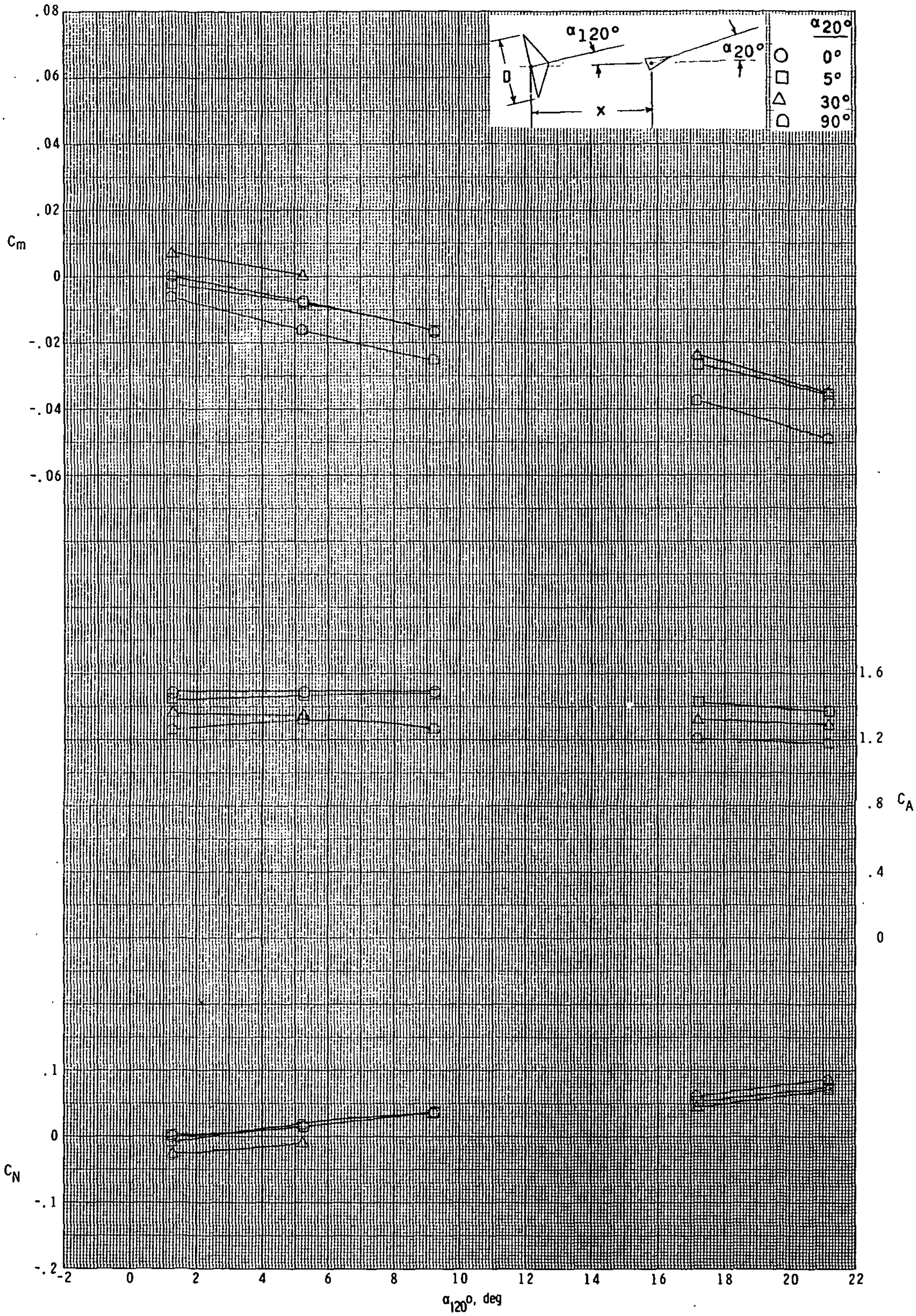

(d) x/D = 0.952; y/D = 0.25.

Figure 8.- Continued.

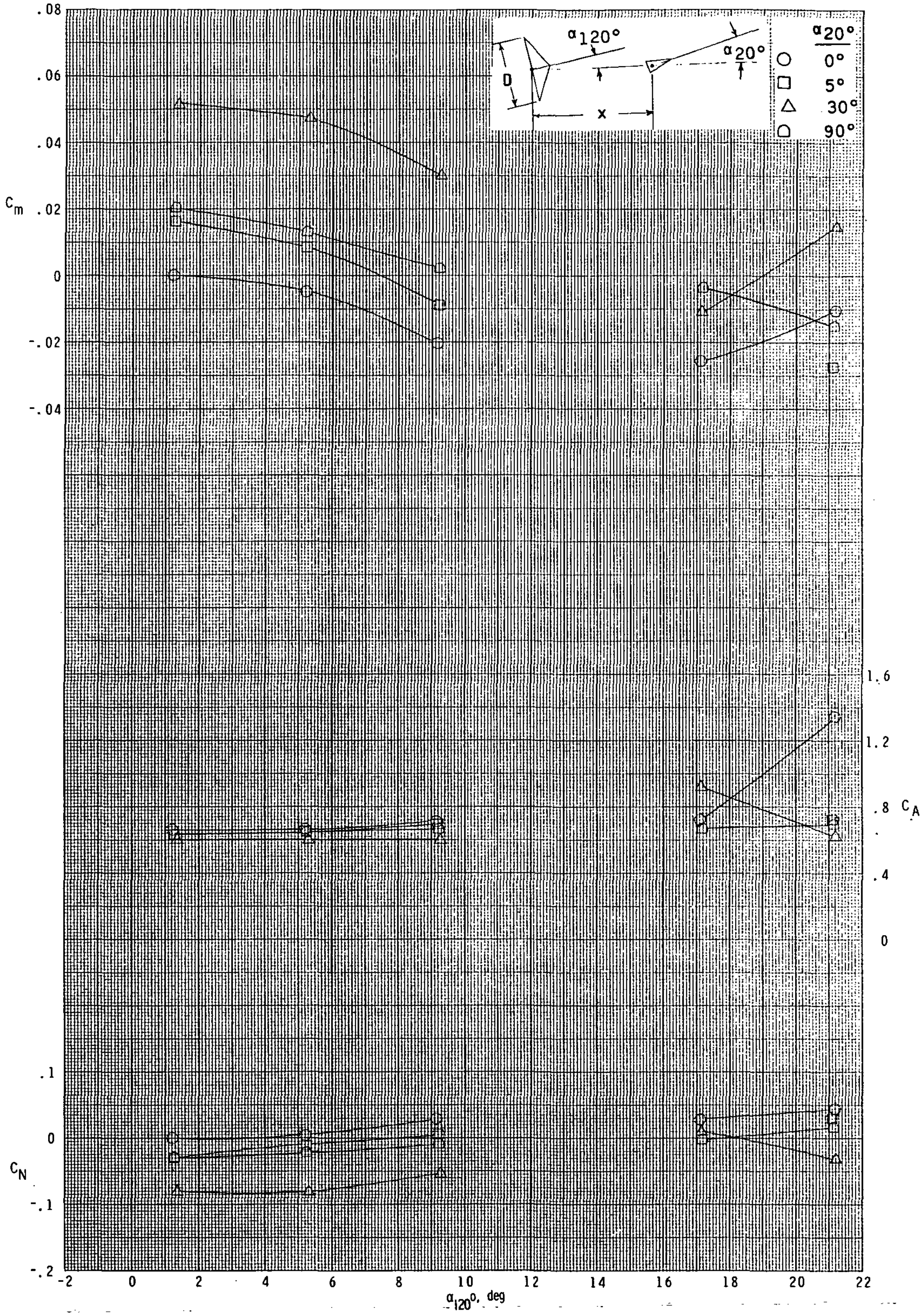

(e) x/D = 1.587; y/D = 0.
Figure 8.- Continued.

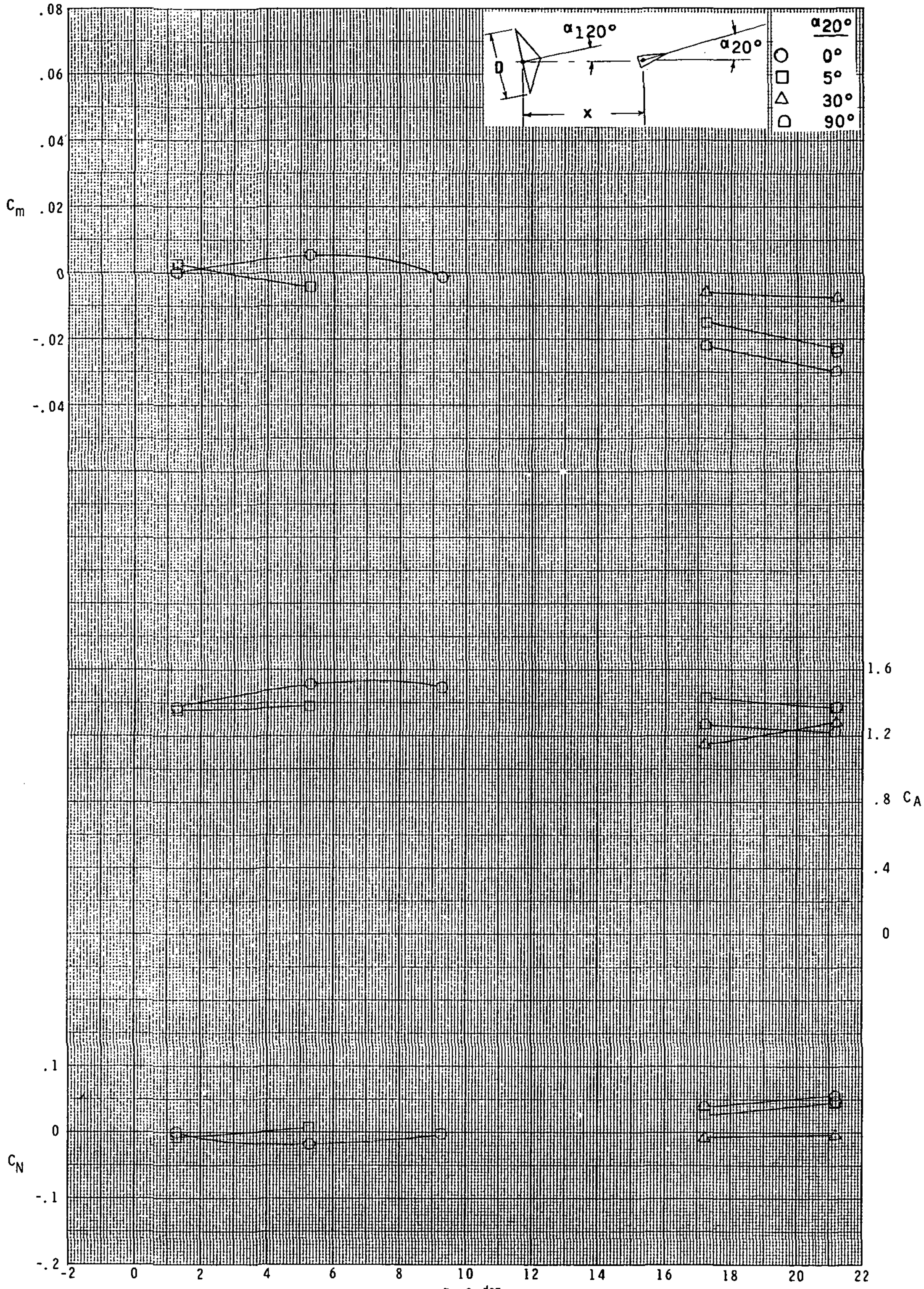

(f) x/D = 1.587; y/D = 0.25.

Figure 8.- Concluded.

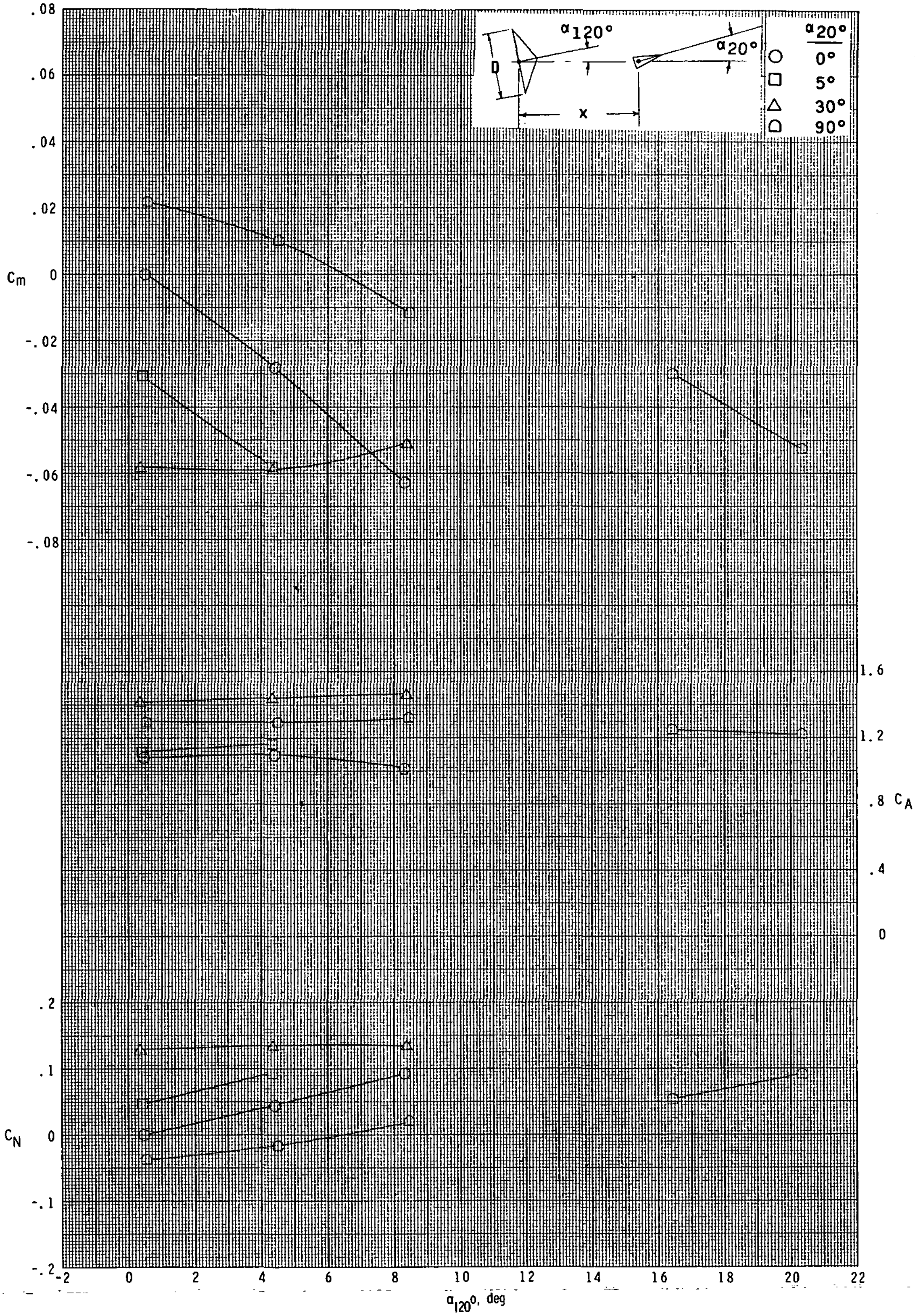

(a) $x/D = 0.476$; $y/D = 0$.

Figure 9.- Variation of pitching-moment, axial-force, and normal-force coefficients with angle of attack for 16.002-cm-diameter (6.30 in.), 120°-included-angle cone for various angles of attack of 20°-included-angle cone at $M_{\infty} = 2.70$.

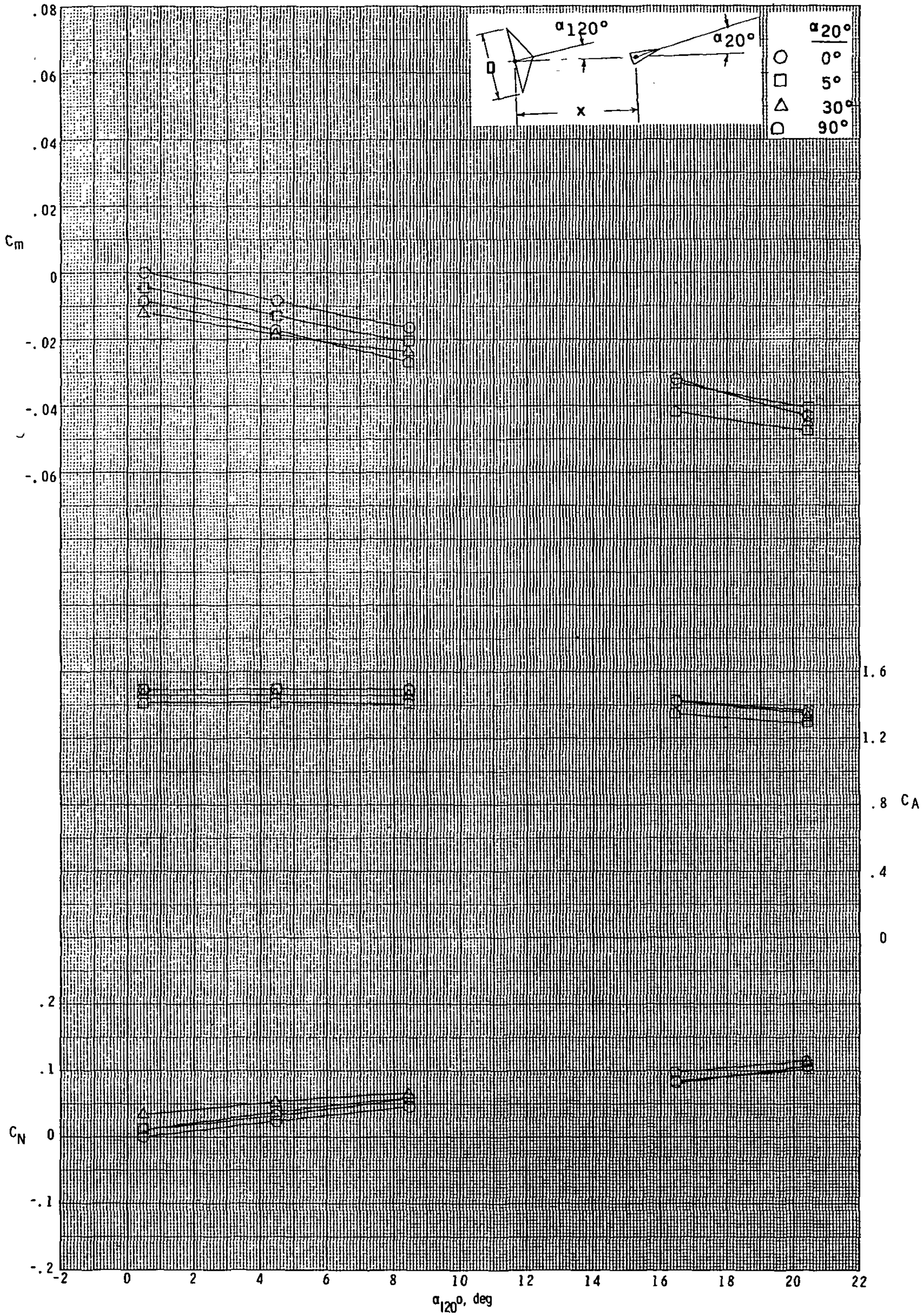

(b) x/D = 0.476; y/D = 0.25.

Figure 9.- Continued.

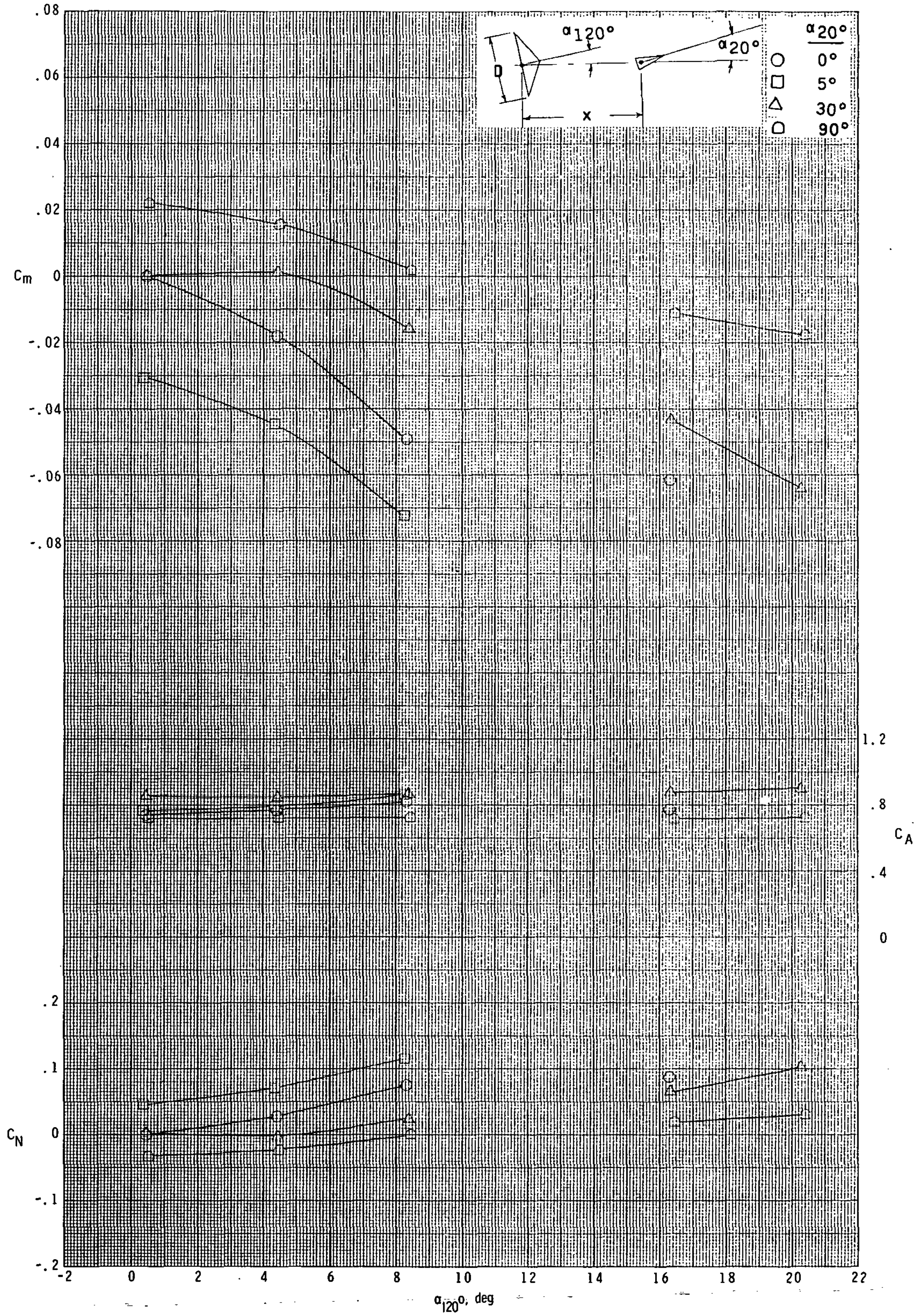

(c) x/D = 0.952; y/D = 0.

Figure 9.- Continued.

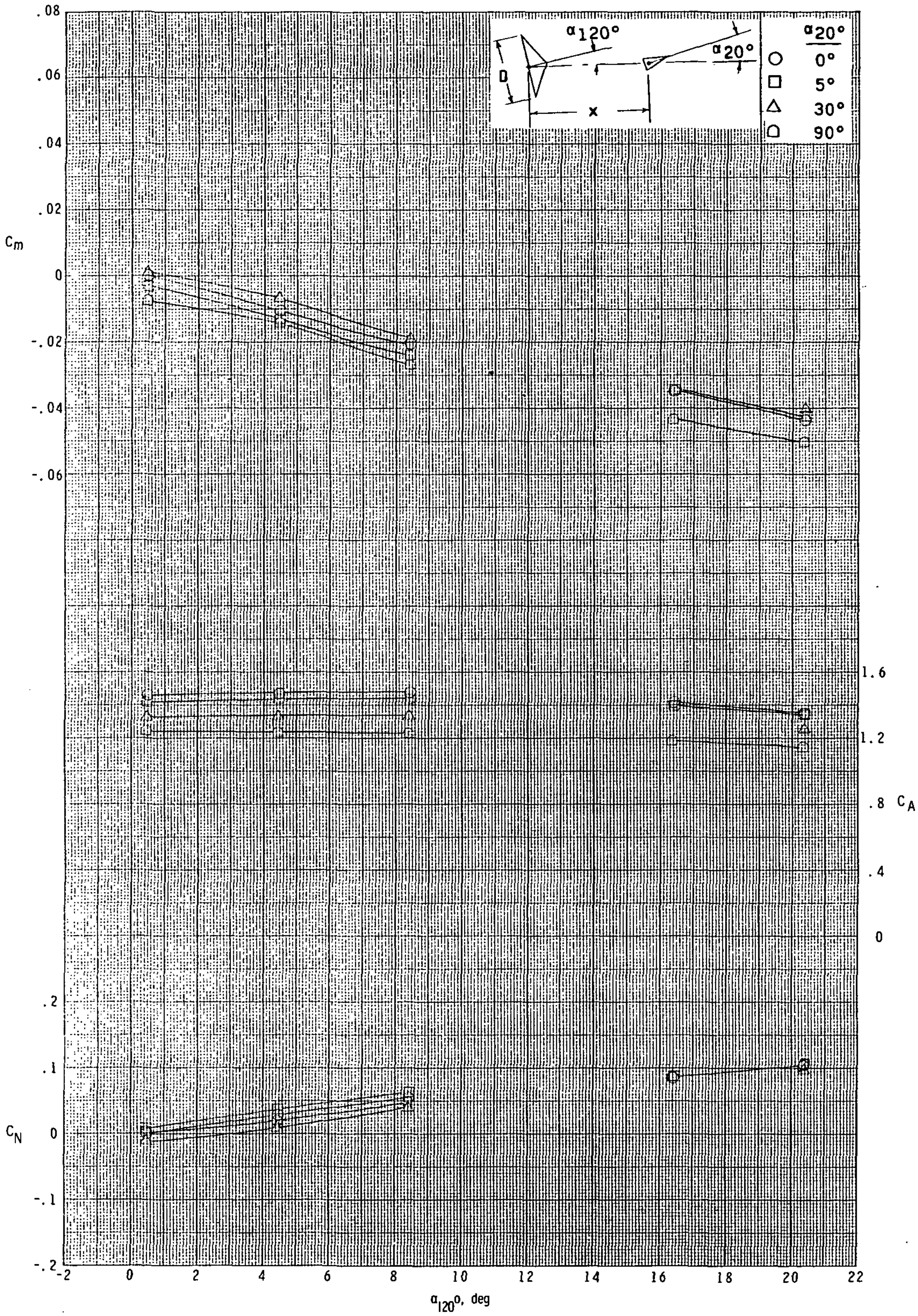

(d) x/D = 0.952; y/D = 0.25.

Figure 9.- Continued.

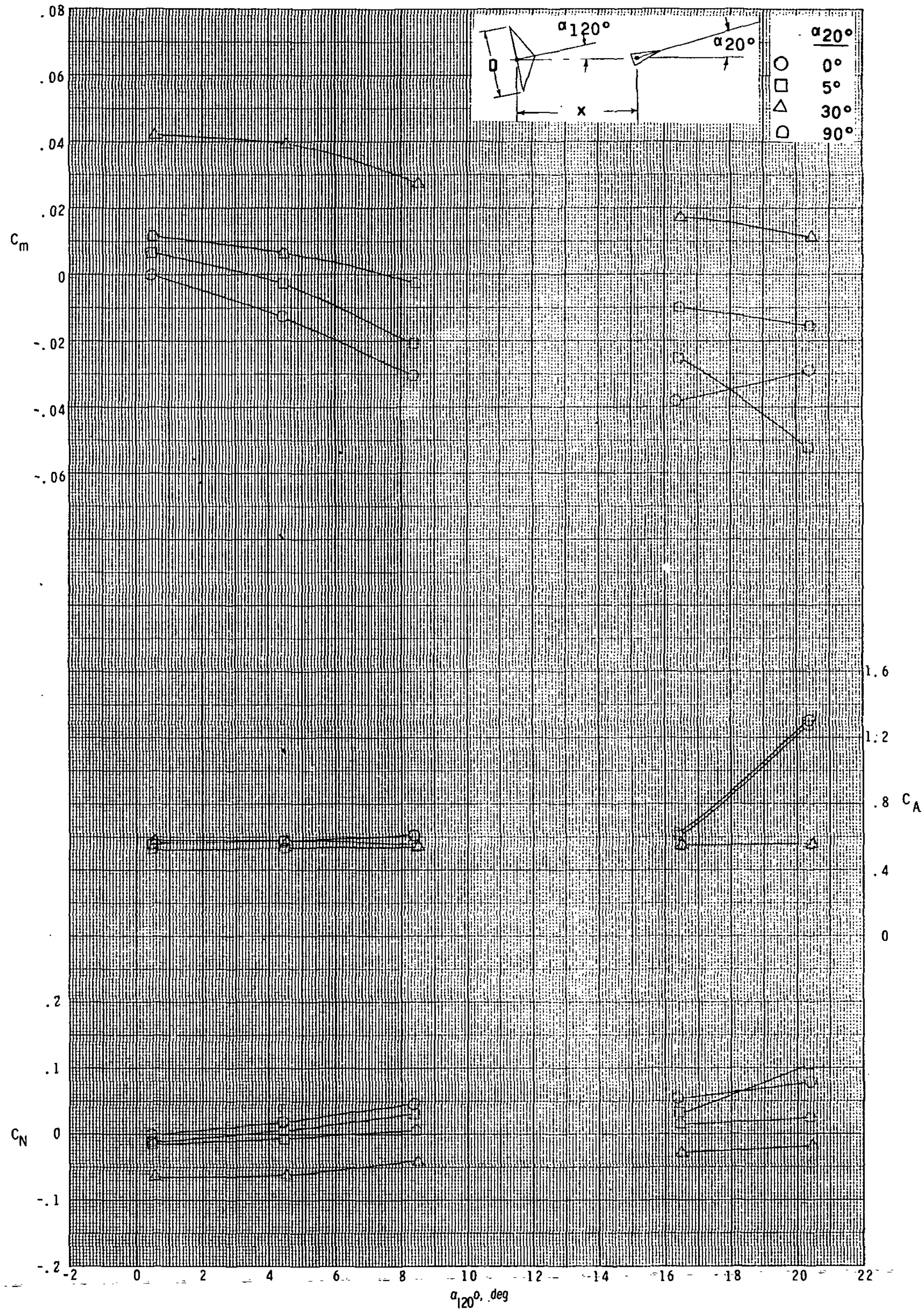

(e) x/D = 1.587; y/D = 0.

Figure 9.- Continued.

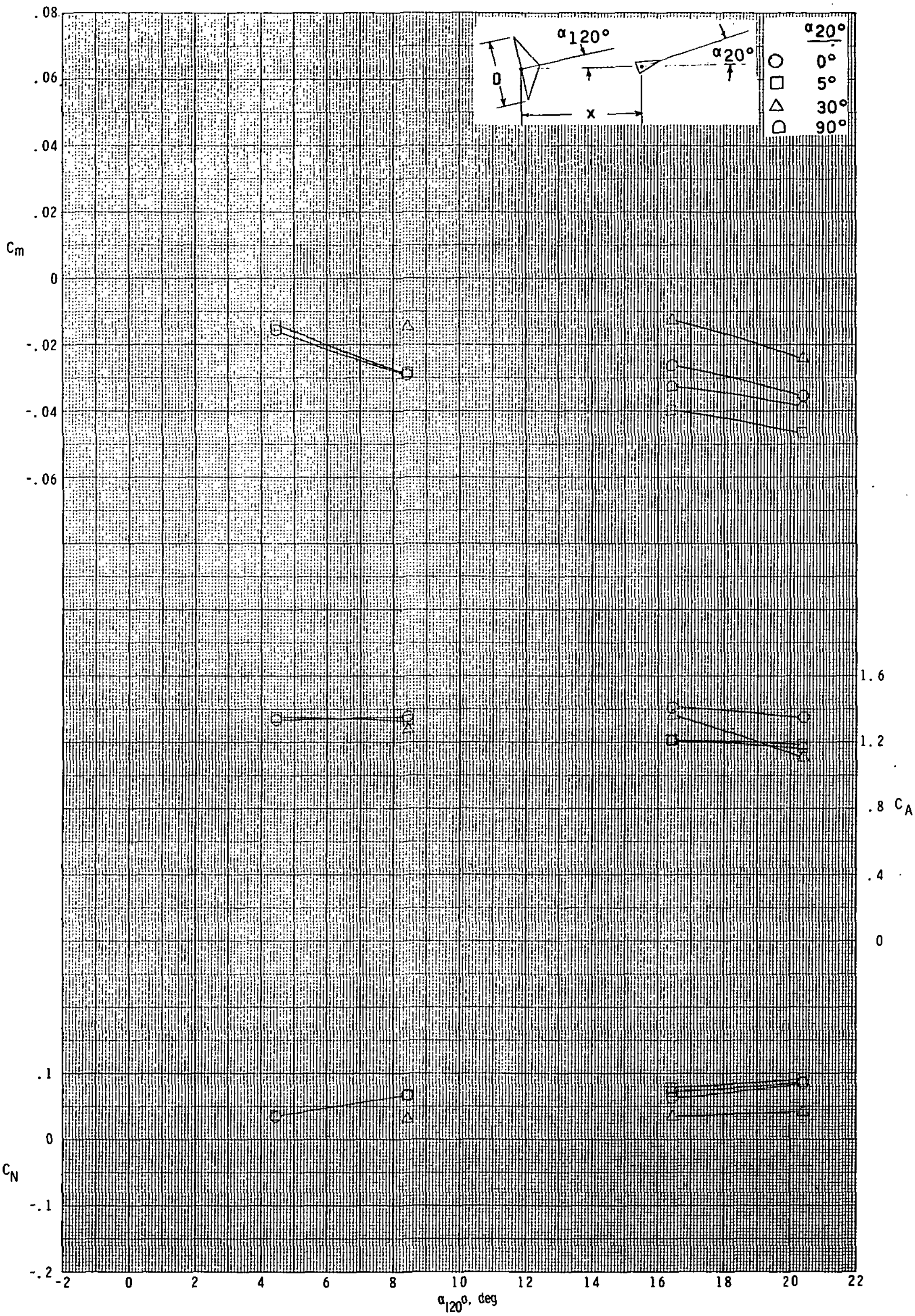

(f) x/D = 1.587; y/D = 0.25.

Figure 9.- Concluded.

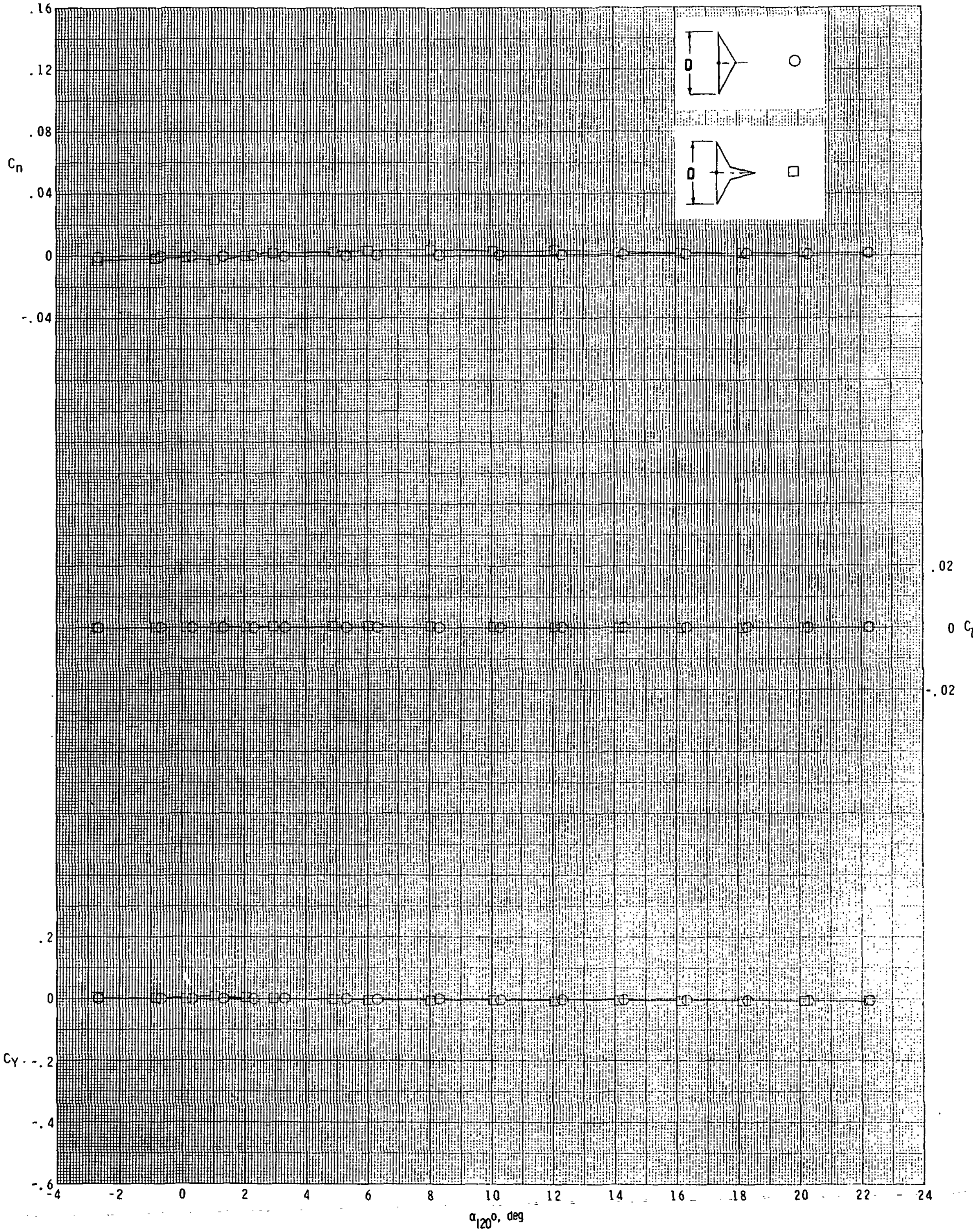

(a) $M_\infty = 2.36$.

Figure 10.- Variation of yawing-moment, rolling-moment, and side-force coefficients with angle of attack for 12.268-cm-diameter (4.83 in.), 120^o-included-angle cone with attached and separated 20^o-included-angle cone.

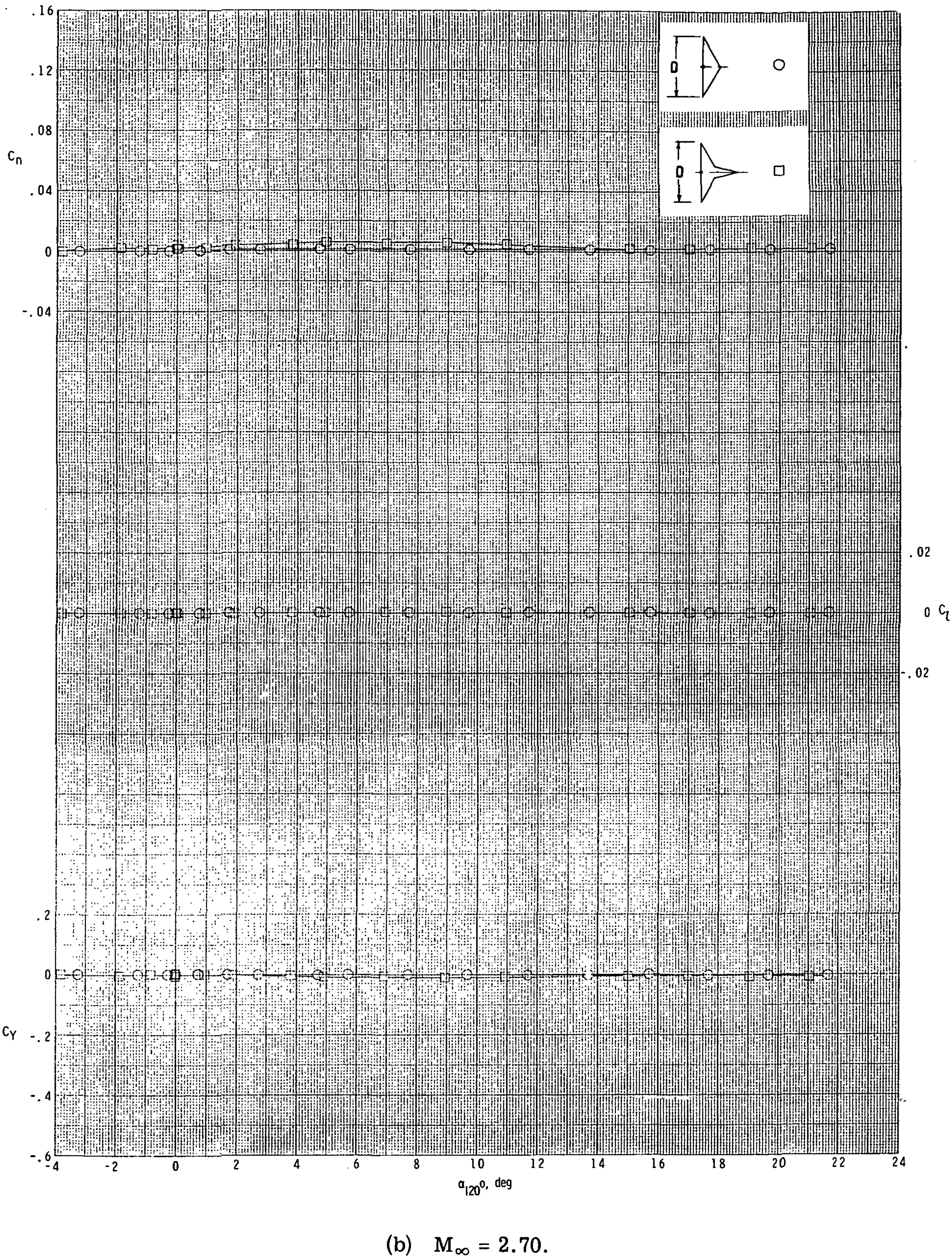

(b) $M_\infty = 2.70$.

Figure 10.- Concluded.

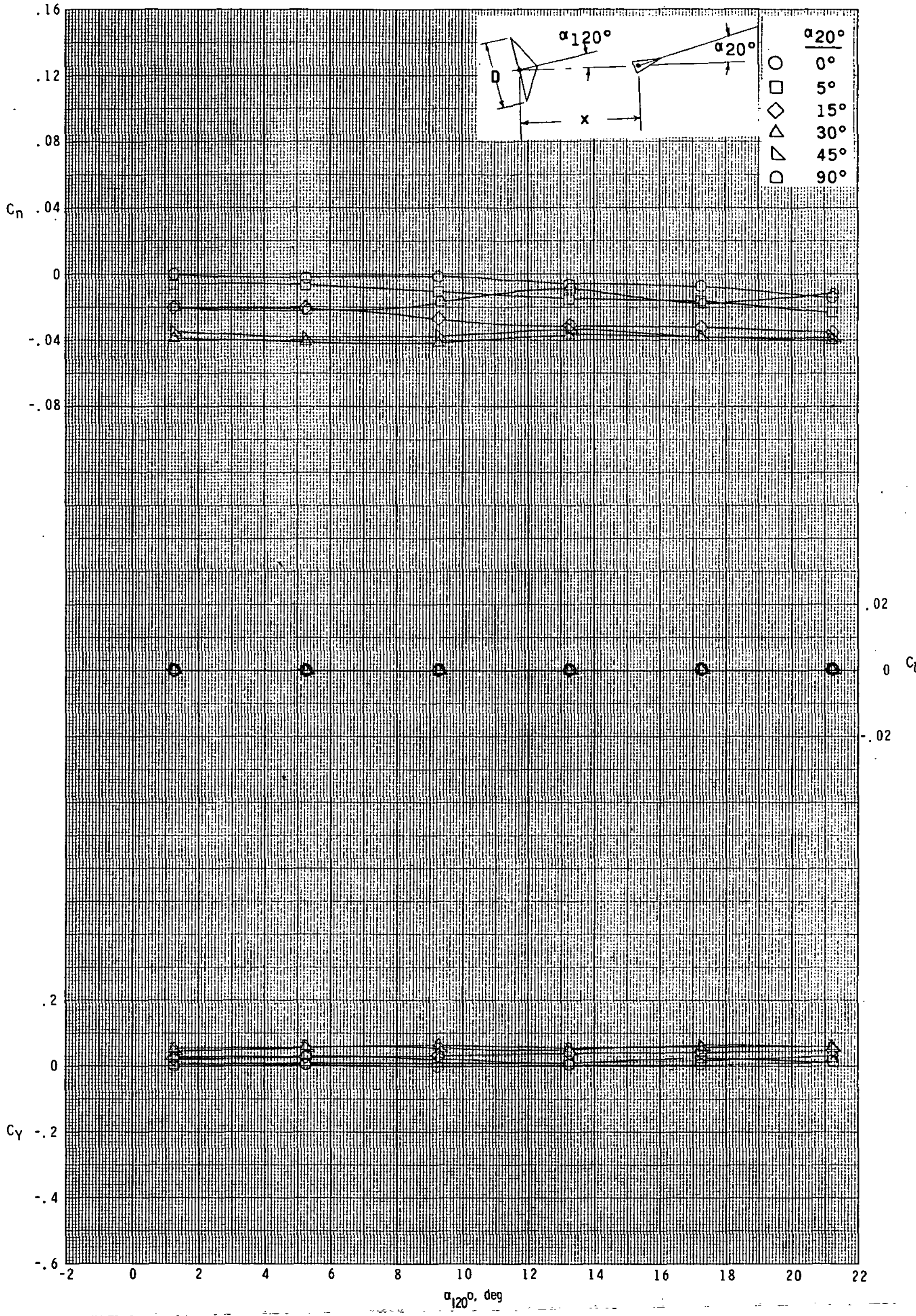

(a) x/D = 0.621; y/D = 0.

Figure 11.- Variation of yawing-moment, rolling-moment, and side-force coefficients with angle of attack for 12.268-cm-diameter (4.83 in.), 120°-included-angle cone for various angles of attack of 20°-included-angle cone at $M_\infty = 2.36$.

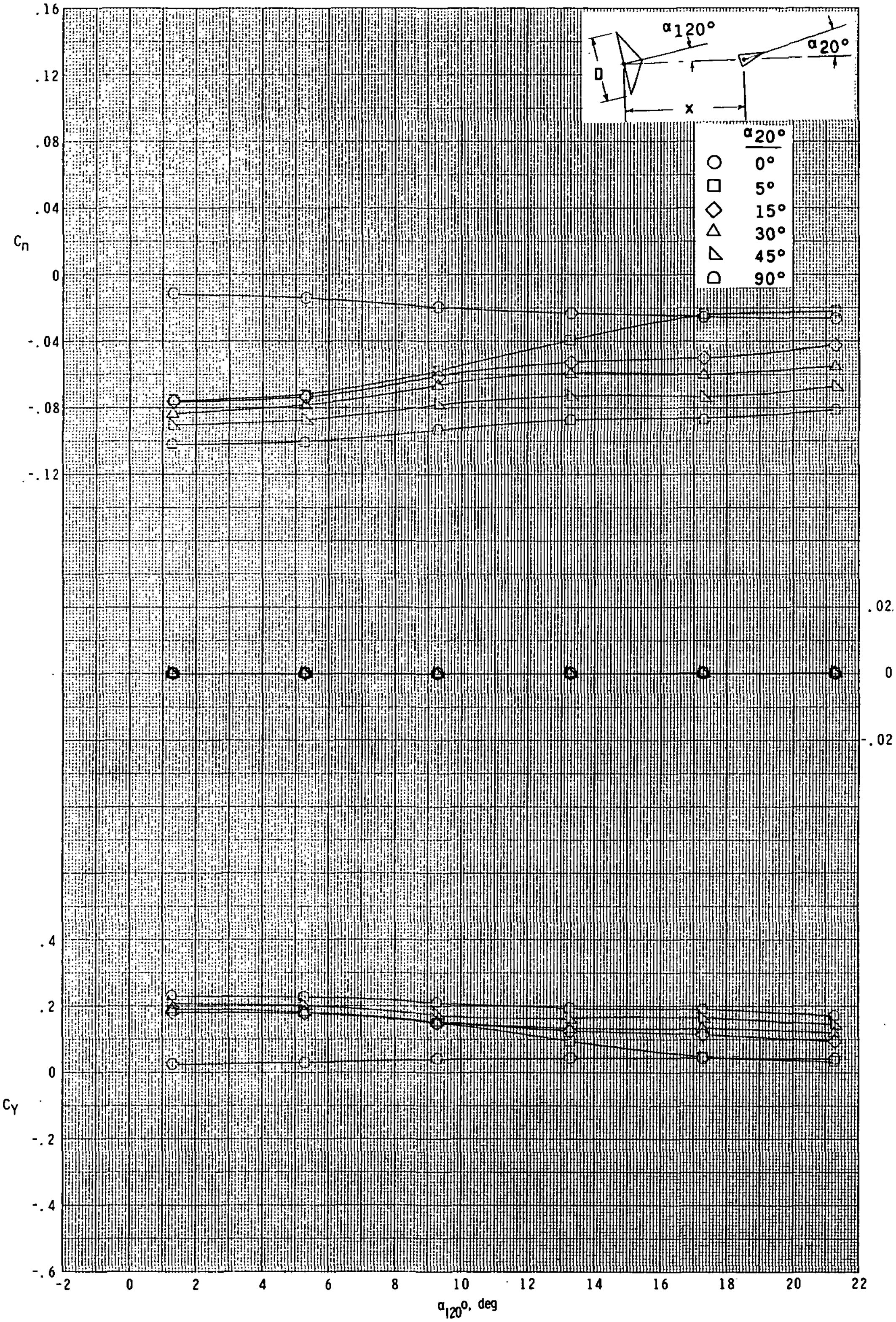

(b) x/D = 0.621; y/D = 0.25.

Figure 11.- Continued.

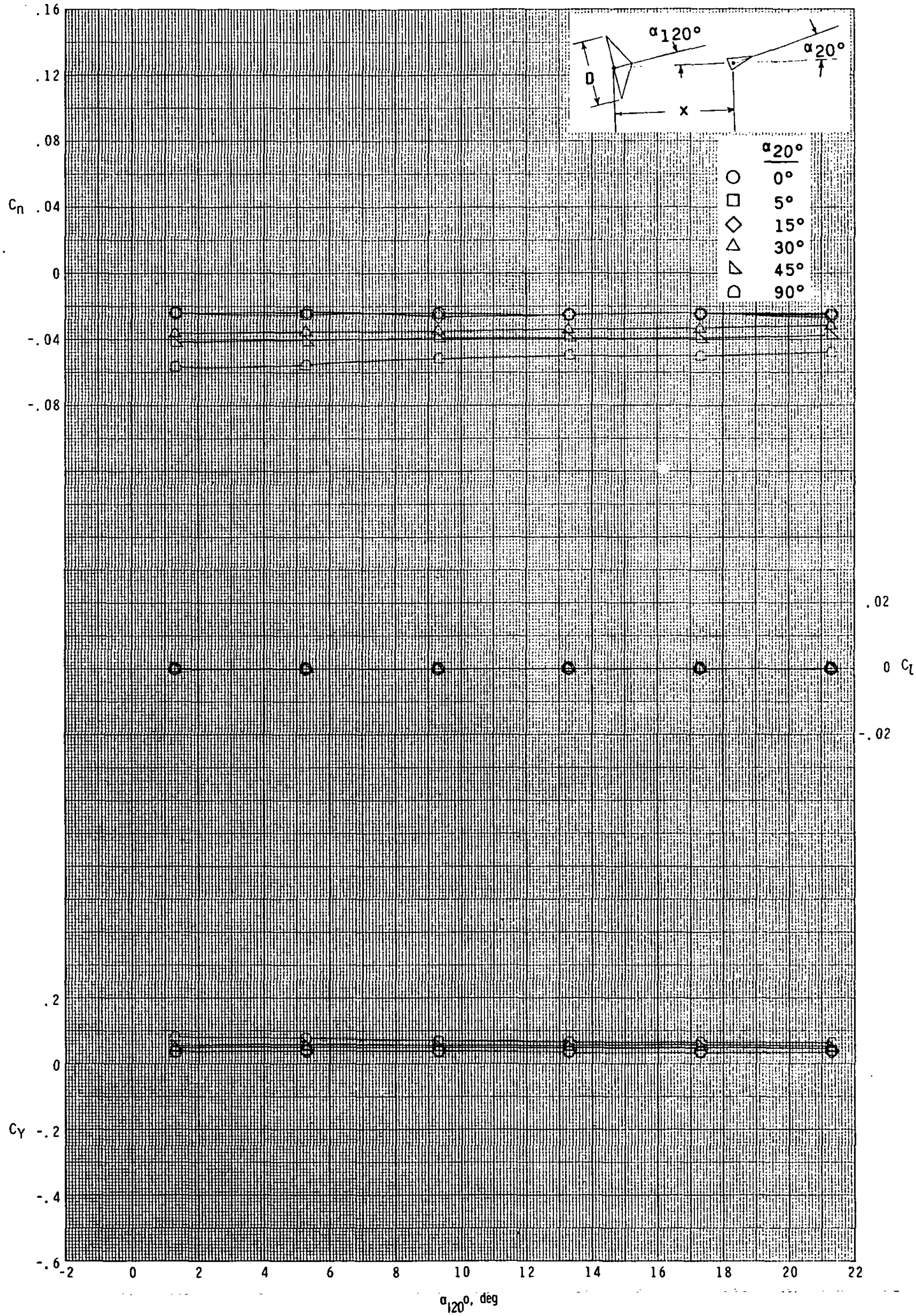

(c) $x/D = 0.621$; $y/D = 0.50$.

Figure 11.- Continued.

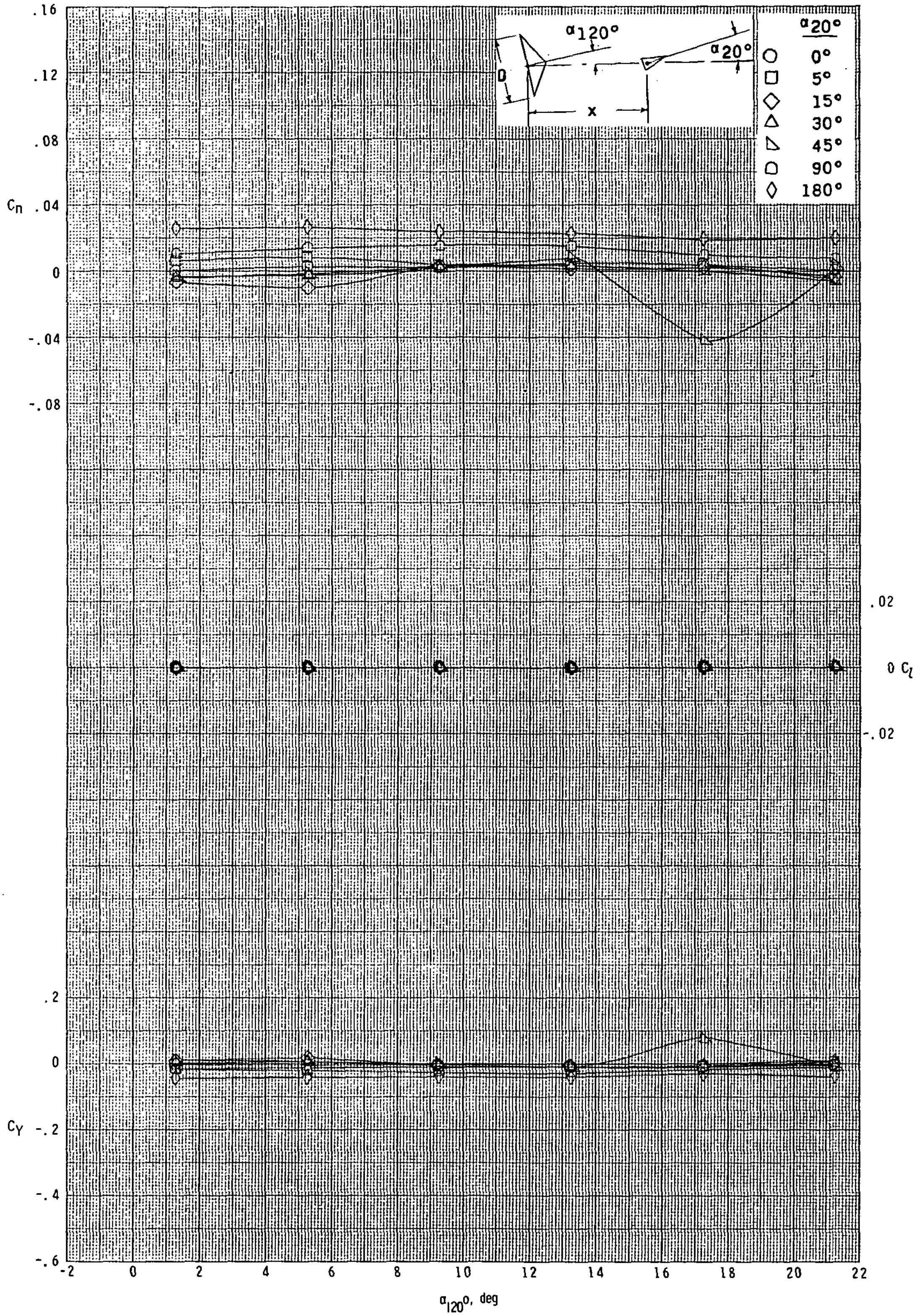

(d) x/D = 1.242; y/D = 0.

Figure 11.- Continued.

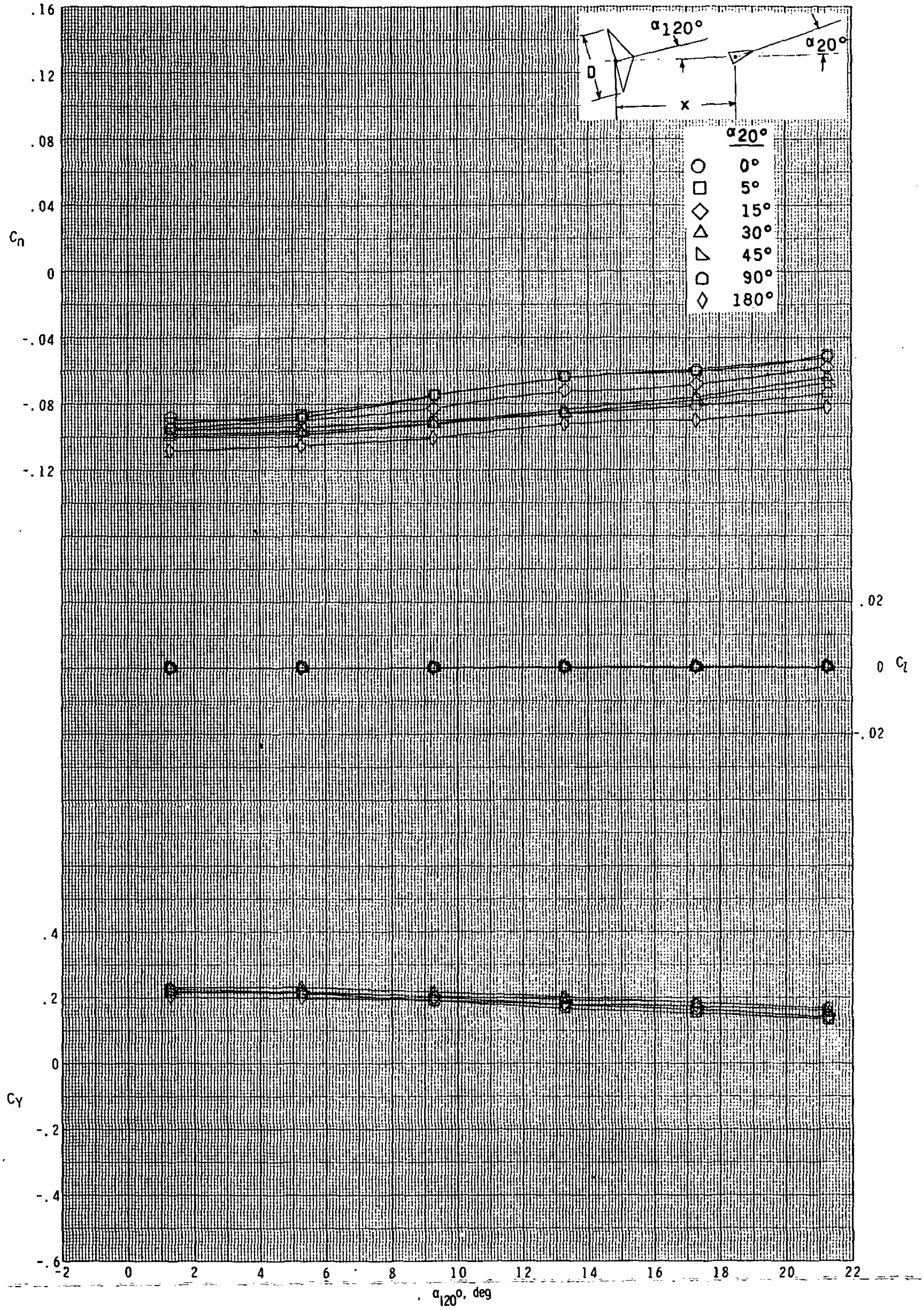

(e) $x/D = 1.242$; $y/D = 0.25$.

Figure 11.- Continued.

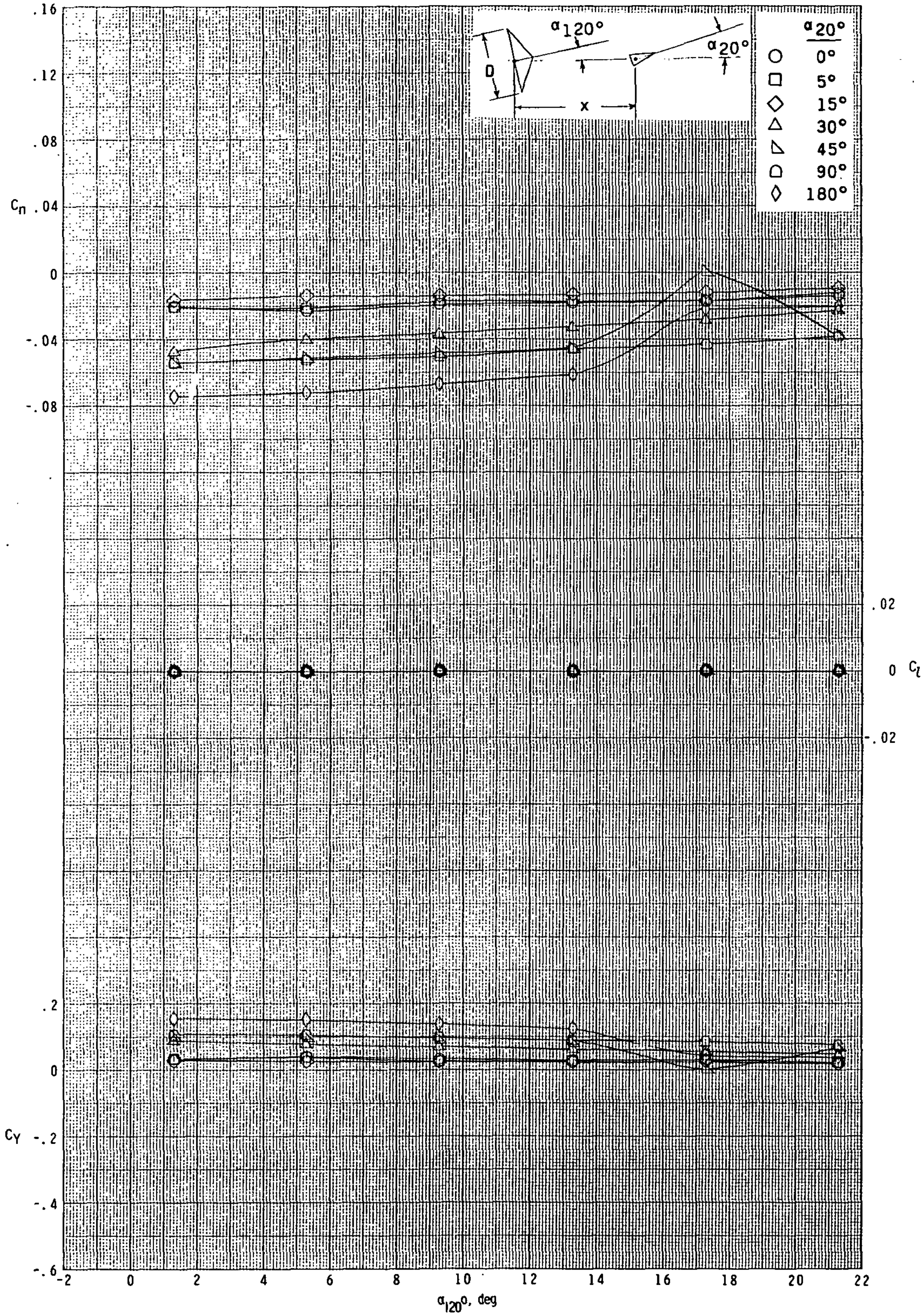

(f) x/D = 1.242; y/D = 0.50.

Figure 11.- Continued.

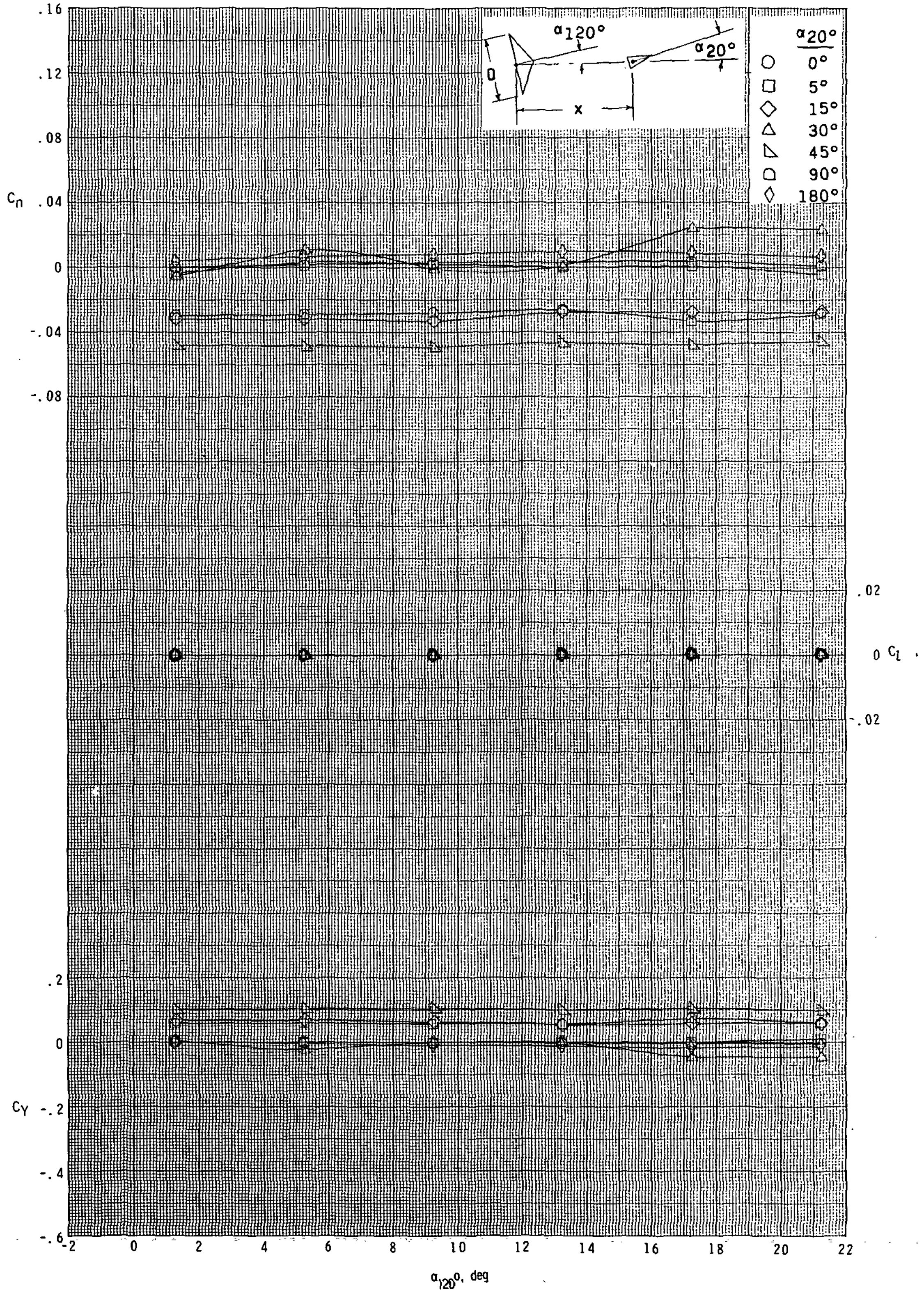

(g) x/D = 2.070; y/D = 0.
Figure 11.- Continued.

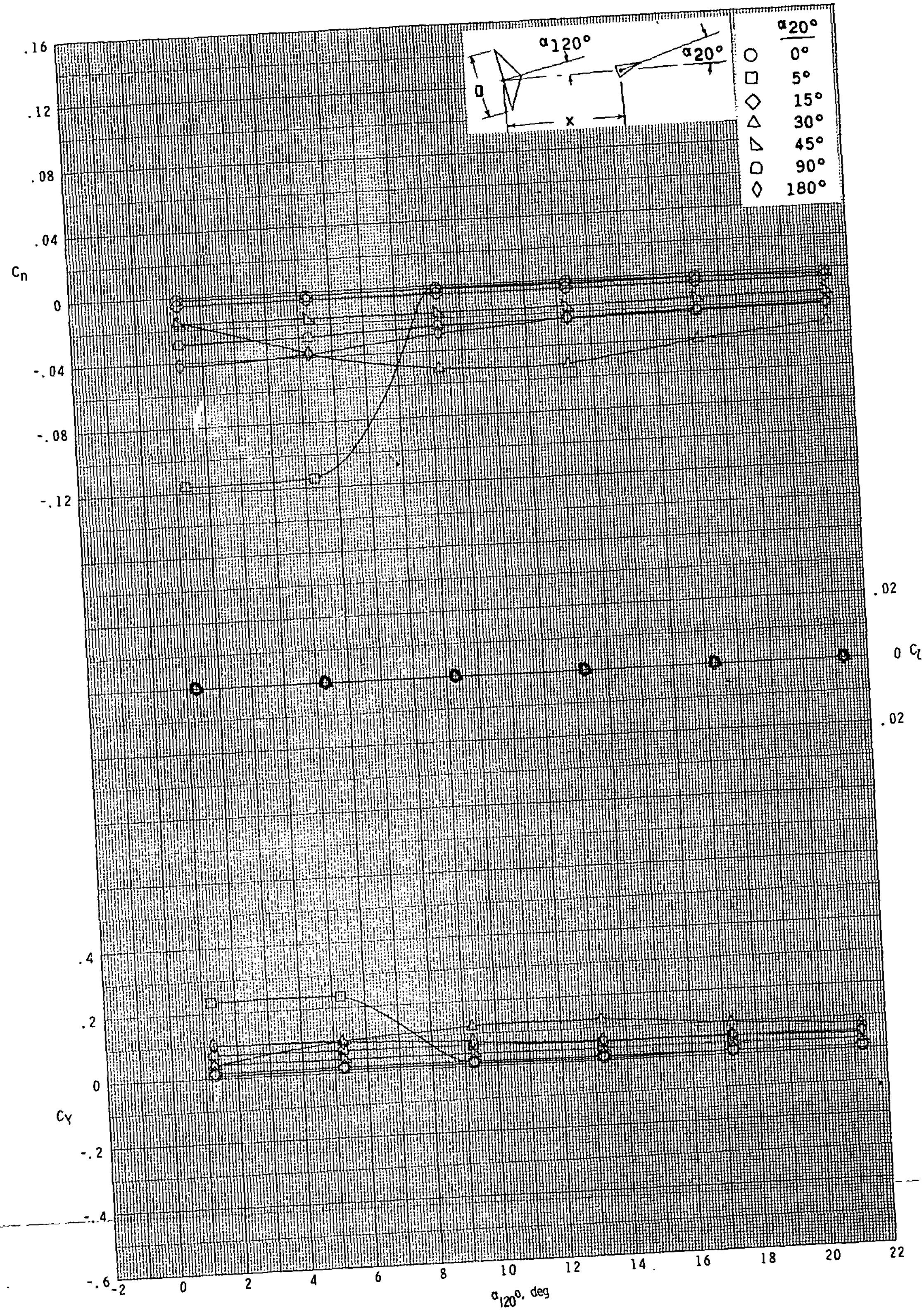

(h) x/D = 2.070; y/D = 0.25.

Figure 11.- Continued.

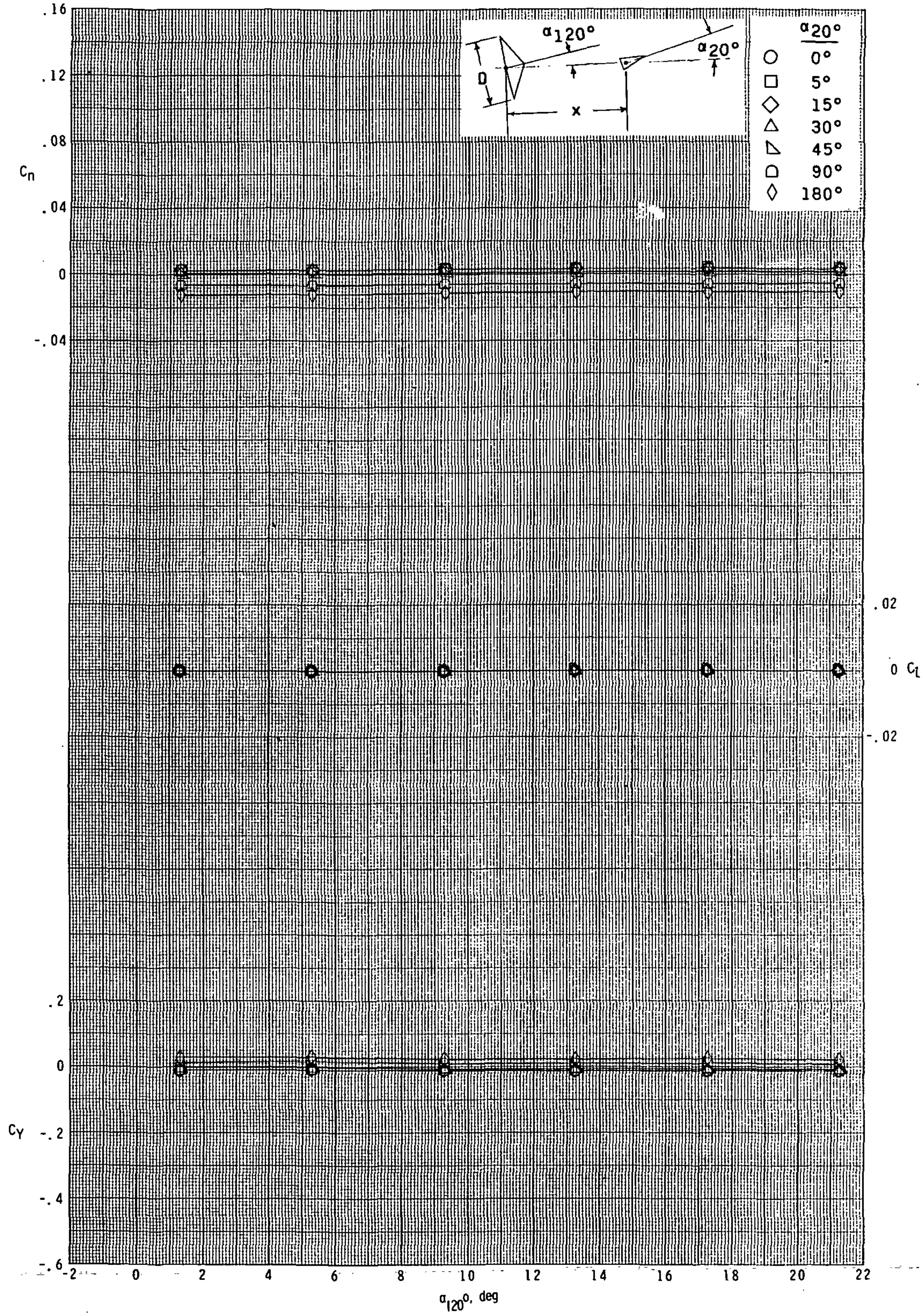

(i) $x/D = 2.070$; $y/D = 0.50$.

Figure 11.- Continued.

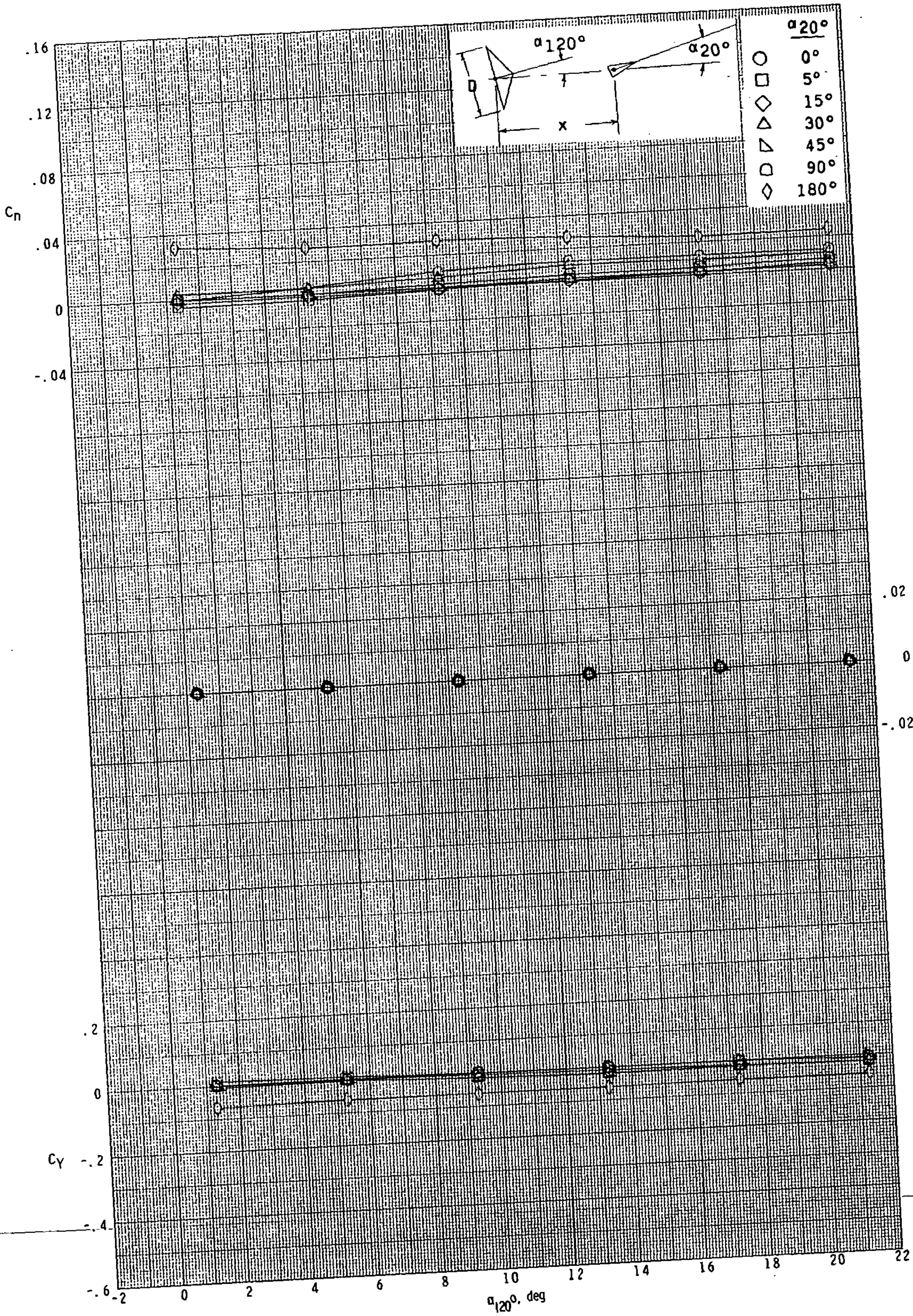

(j) x/D = 3.520; y/D = 0.

Figure 11.- Continued.

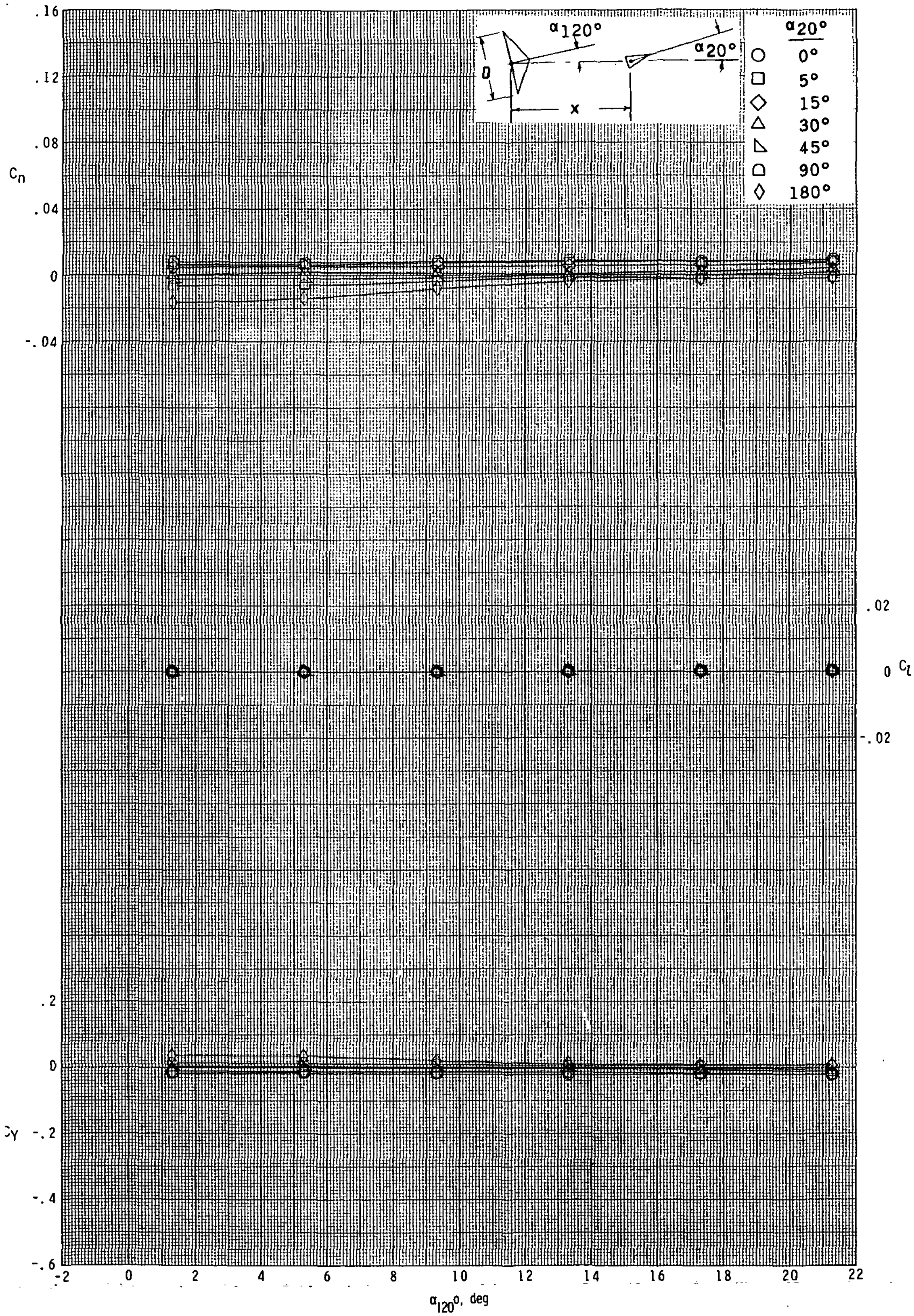

(k) x/D = 3.520; y/D = 0.25.

Figure 11.- Continued.

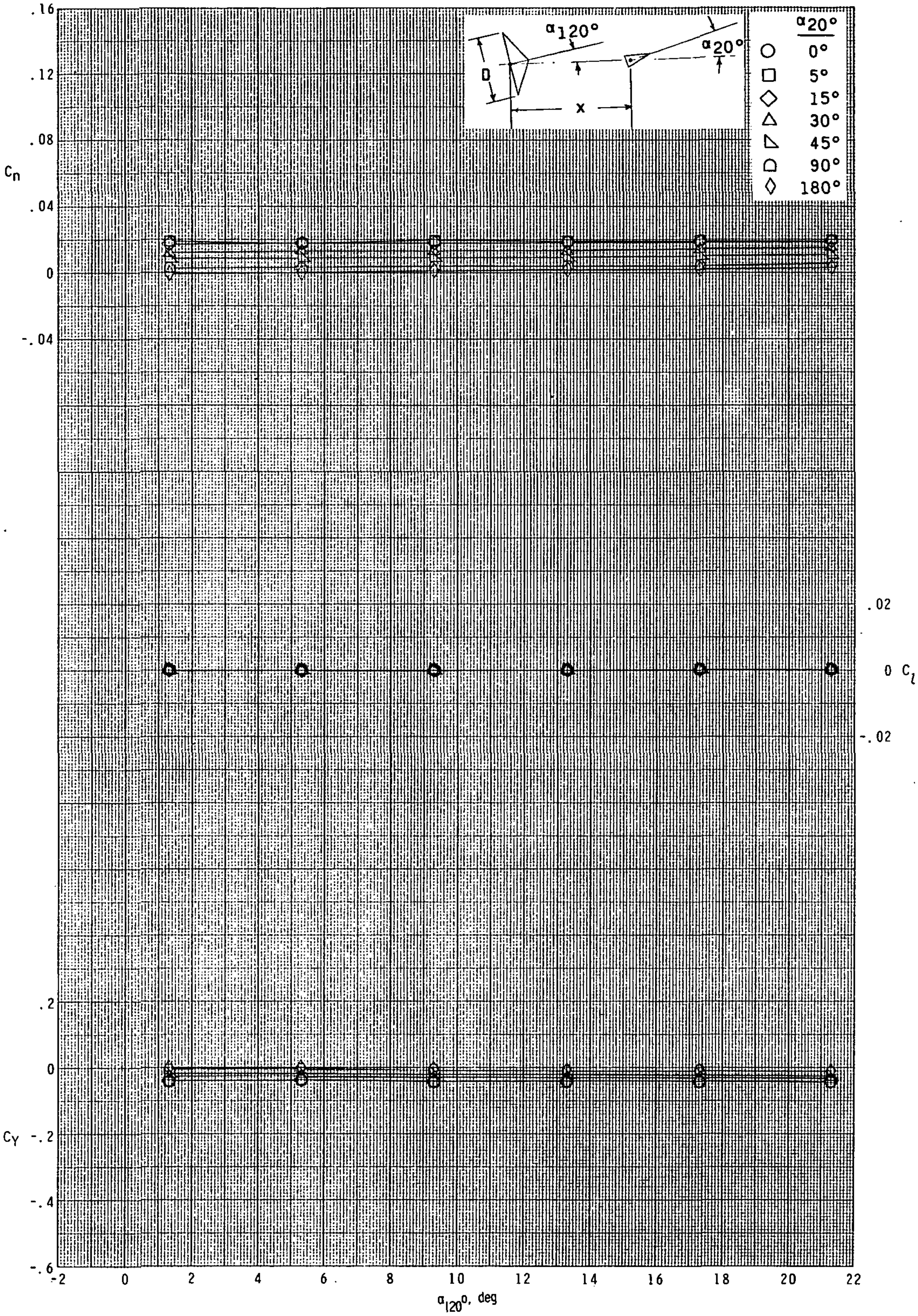

(l) x/D = 3.520; y/D = 0.50.
Figure 11.- Concluded.

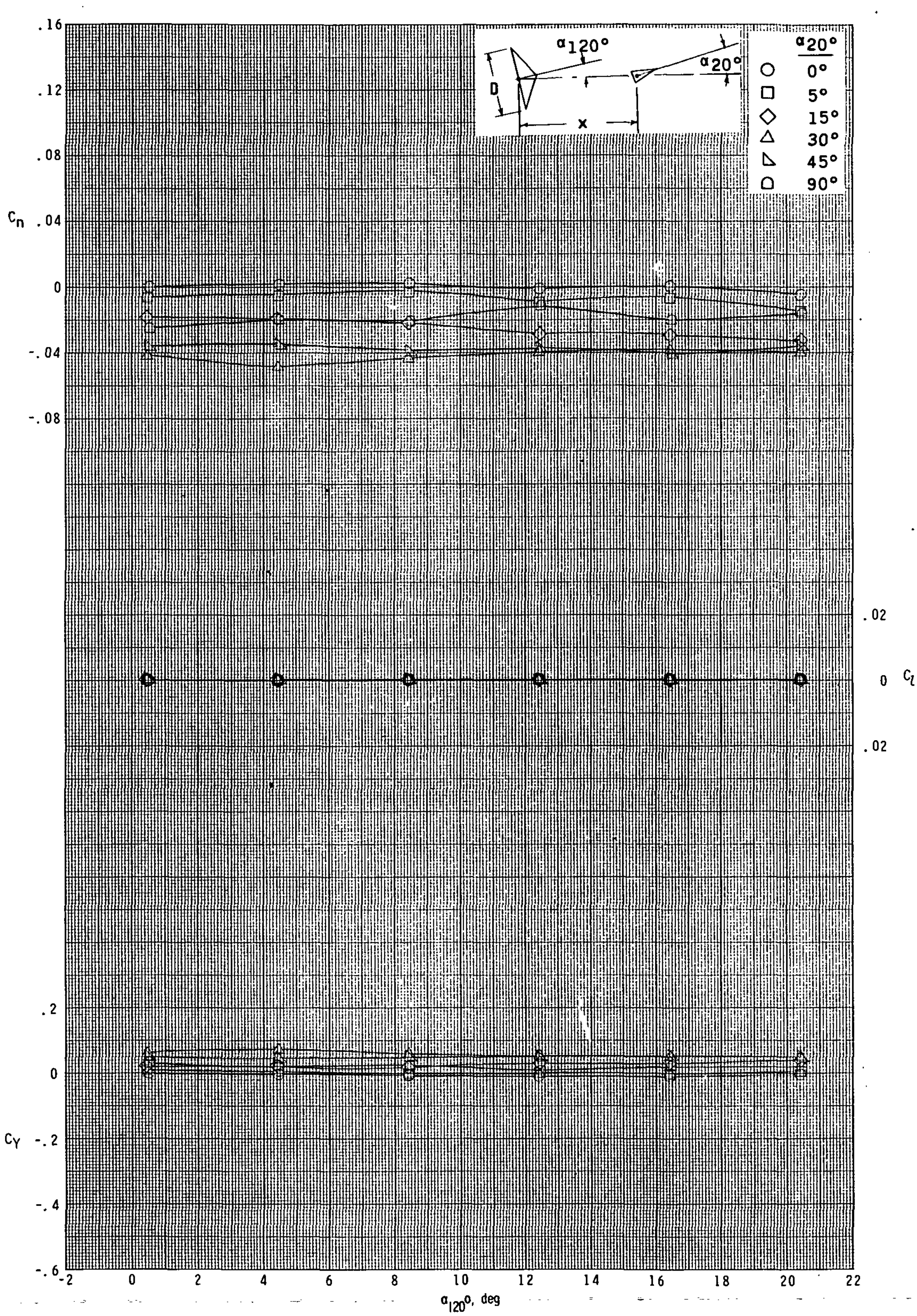

(a) $x/D = 0.621$; $y/D = 0$.

Figure 12.- Variation of yawing-moment, rolling-moment, and side-force coefficients with angle of attack for 12.268-cm-diameter (4.83 in.), 120°-included-angle cone for various angles of attack of 20°-included-angle cone at $M_\infty = 2.70$.

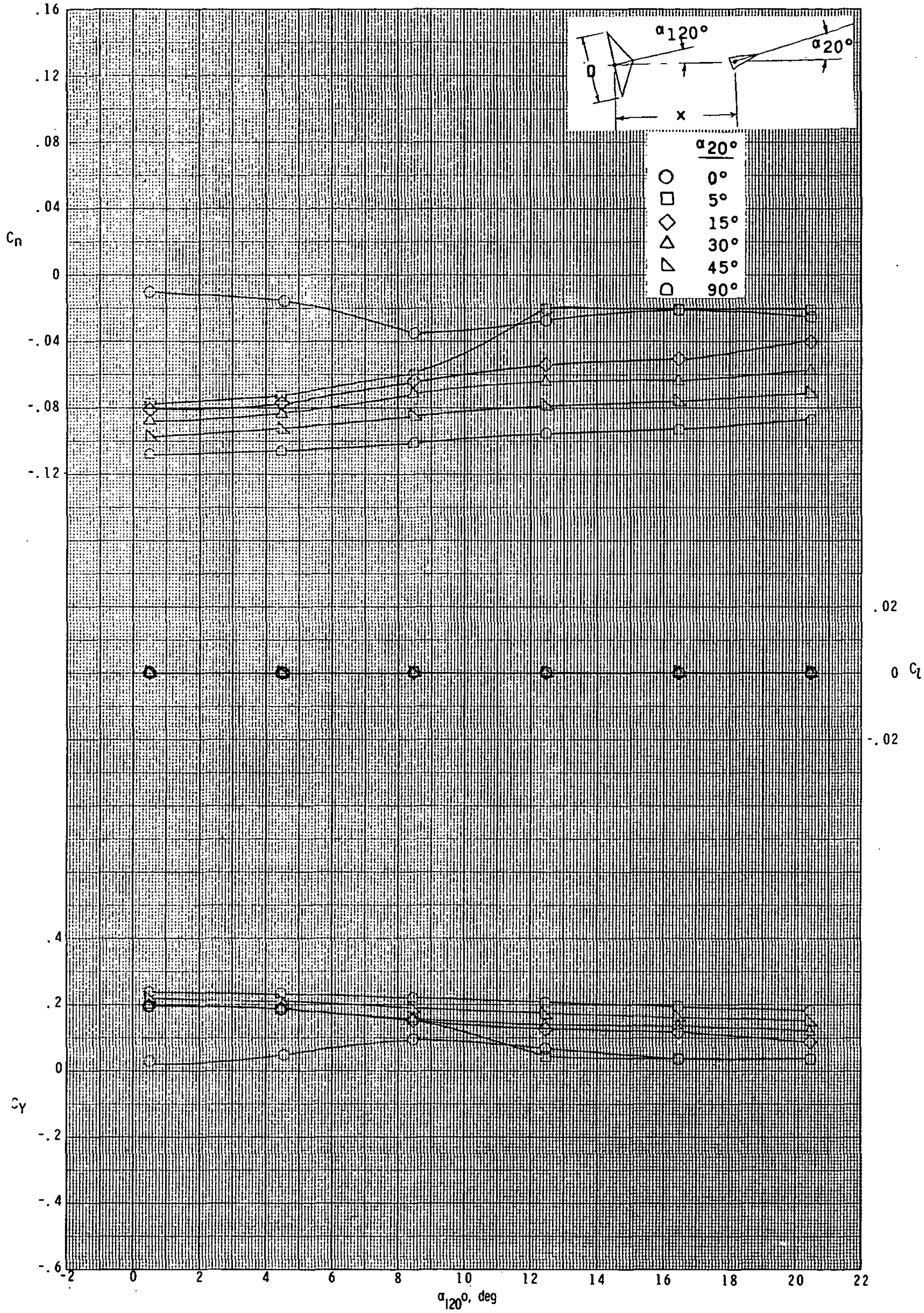

(b) x/D = 0.621; y/D = 0.25.

Figure 12.- Continued.

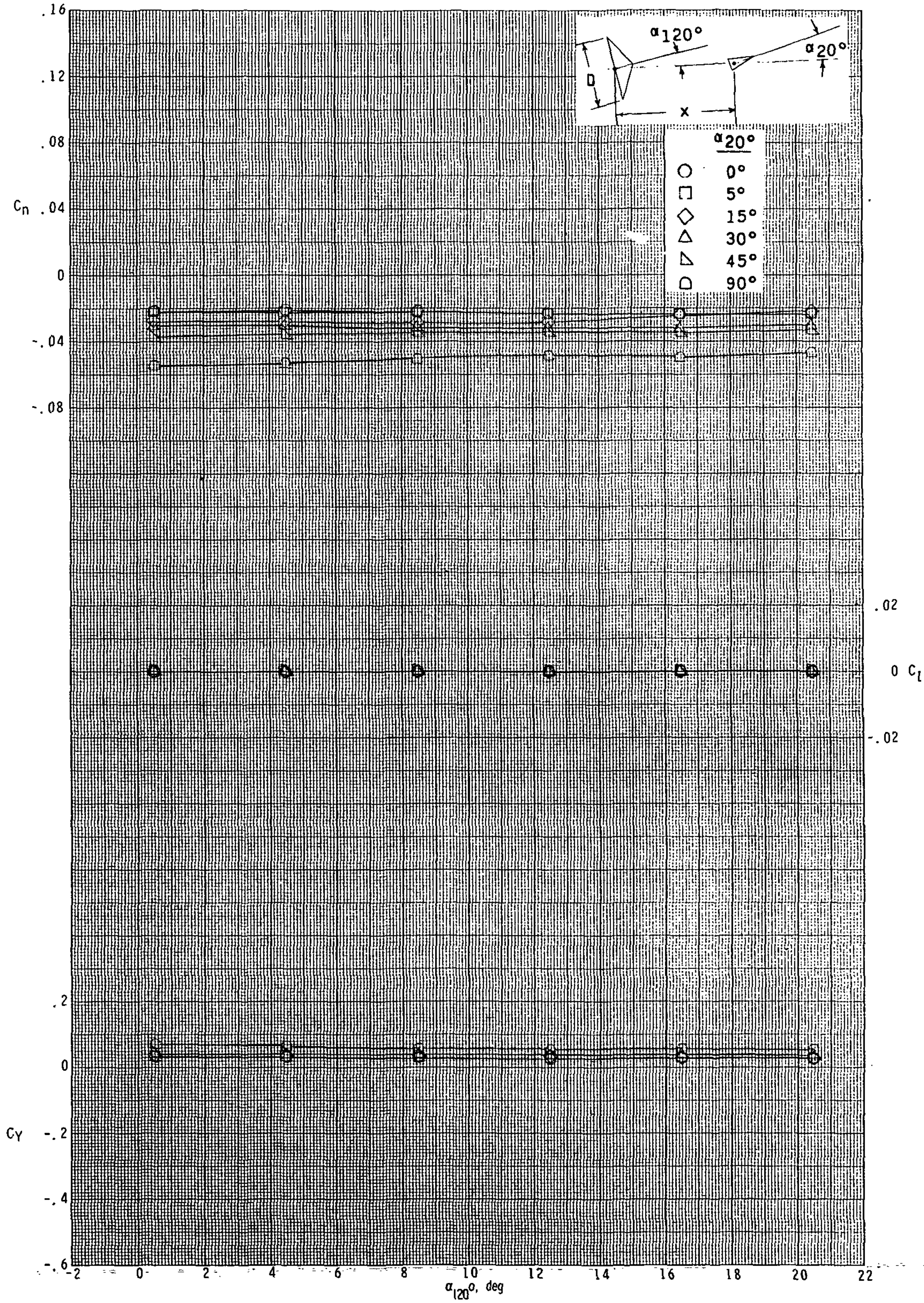

(c) x/D = 0.621; y/D = 0.50.

Figure 12.- Continued.

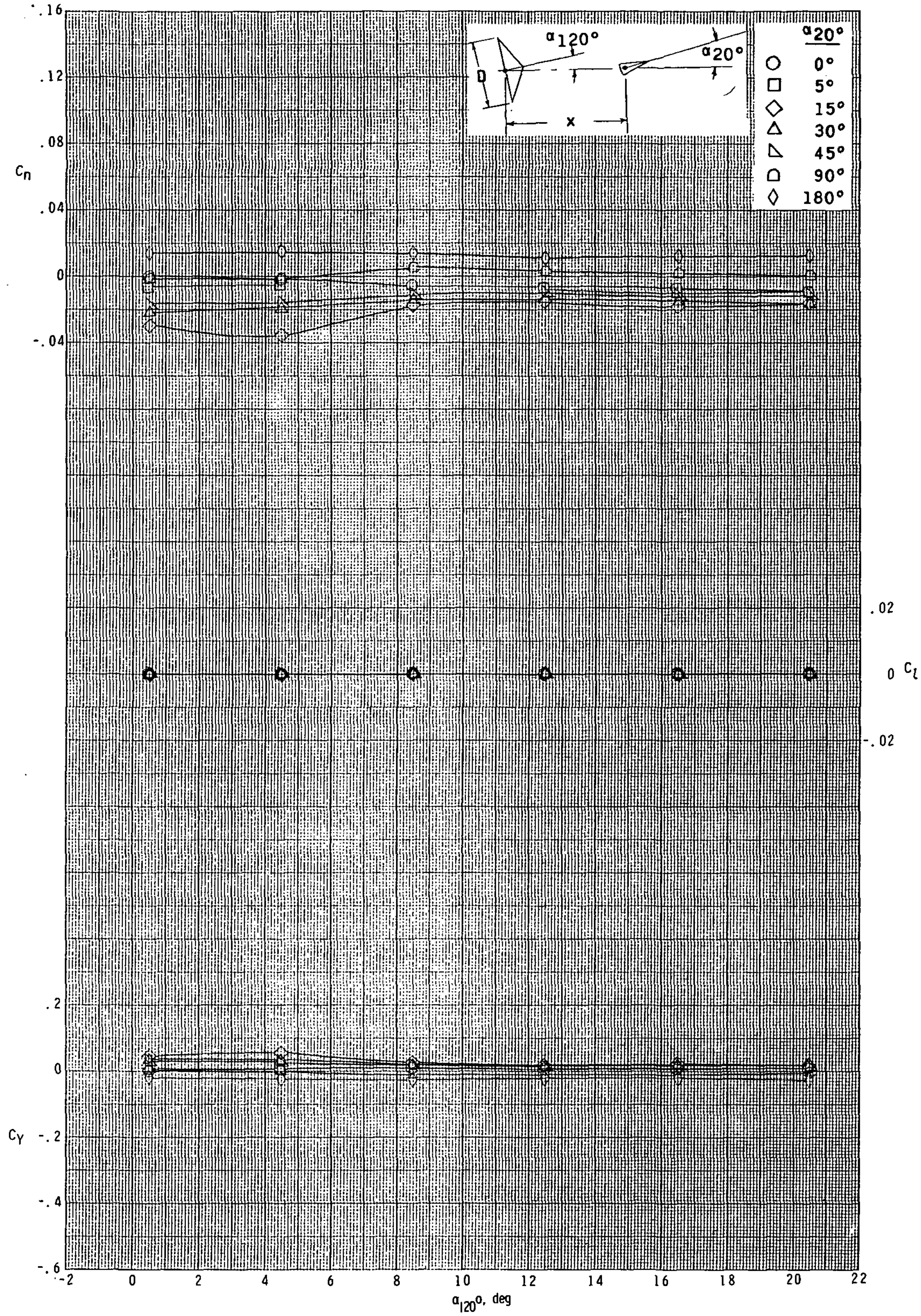

(d) x/D = 1.242; y/D = 0.

Figure 12.- Continued.

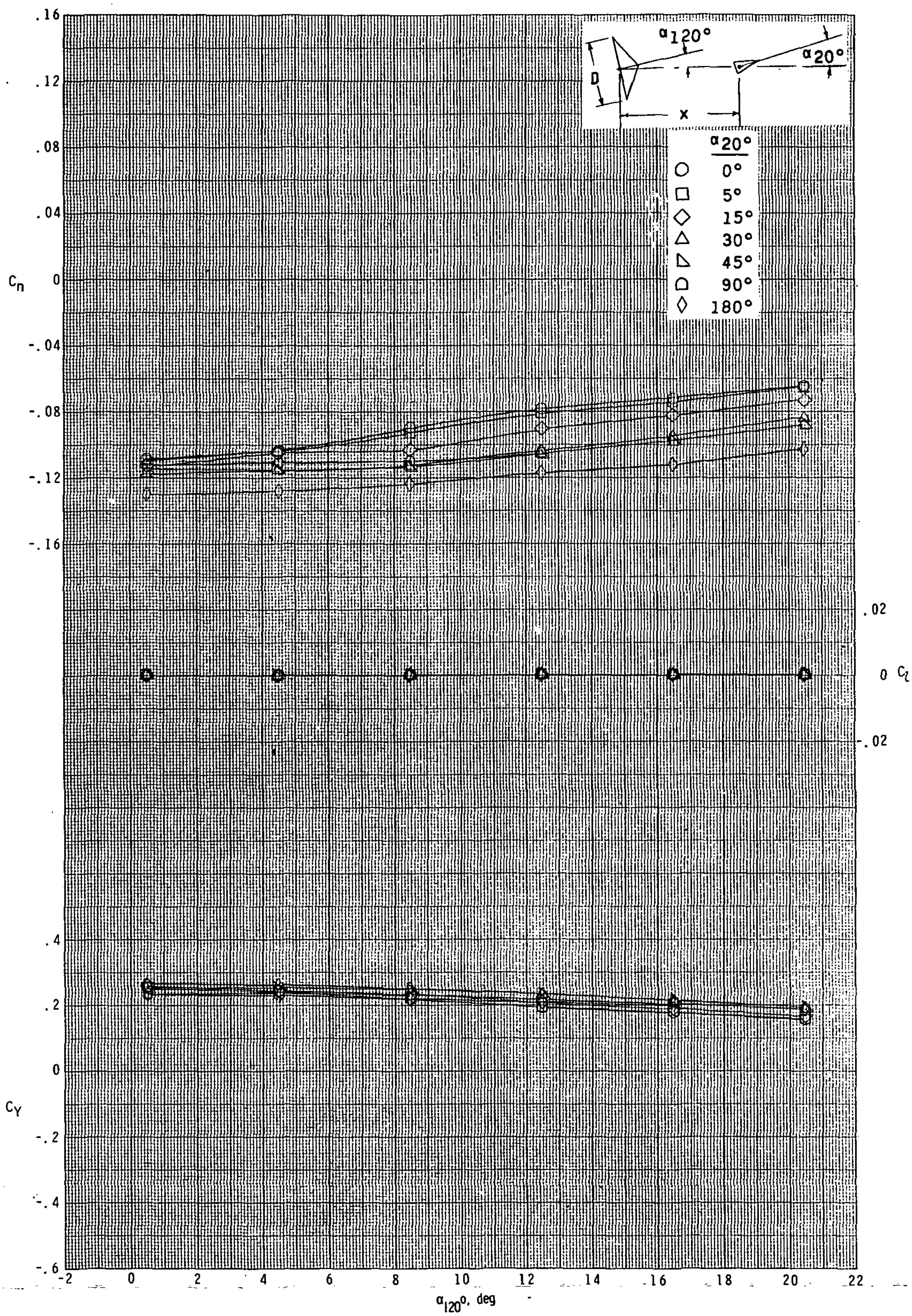

(e) x/D = 1.242; y/D = 0.25.

Figure 12.- Continued.

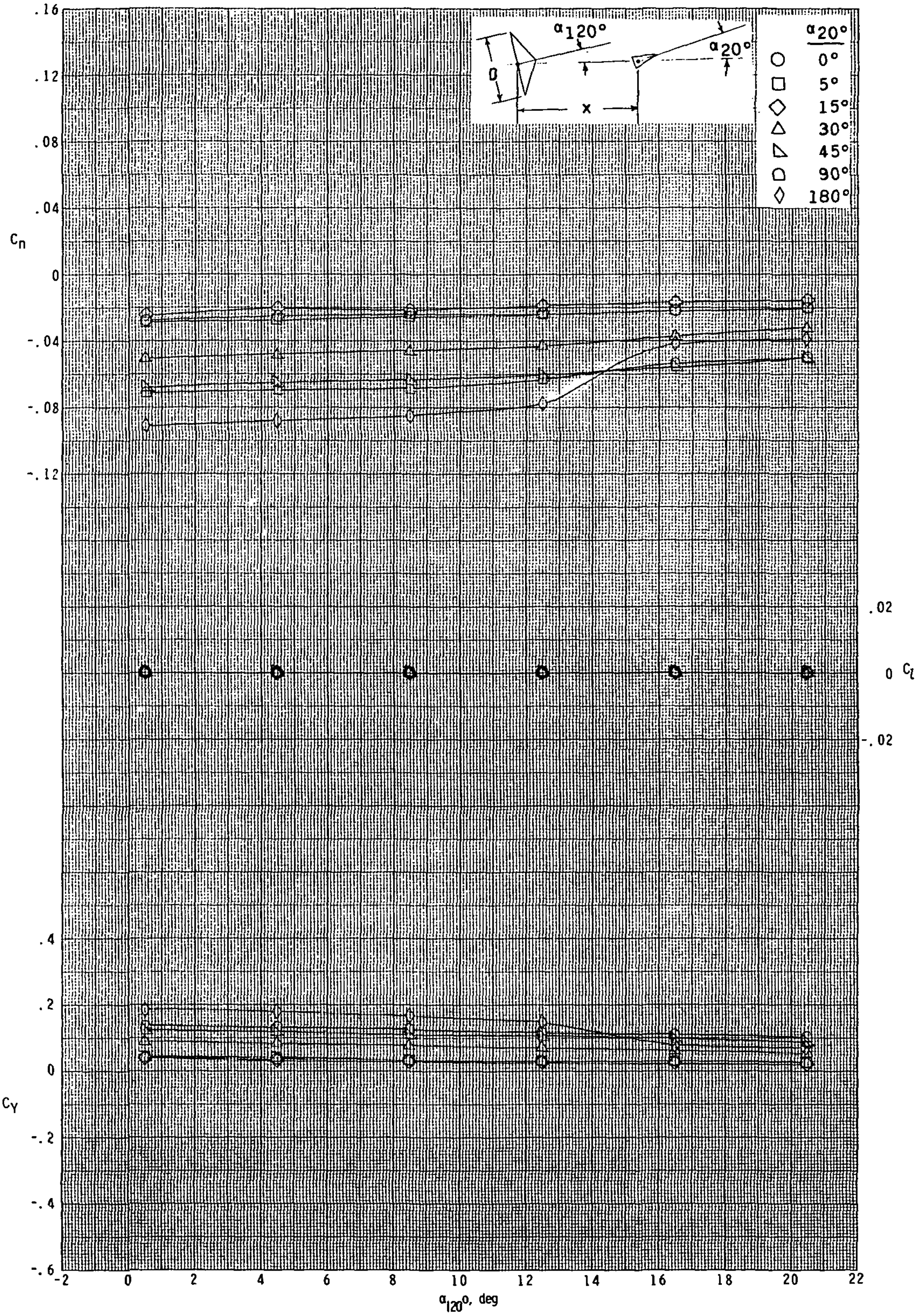

(f) x/D = 1.242; y/D = 0.50.

Figure 12.- Continued.

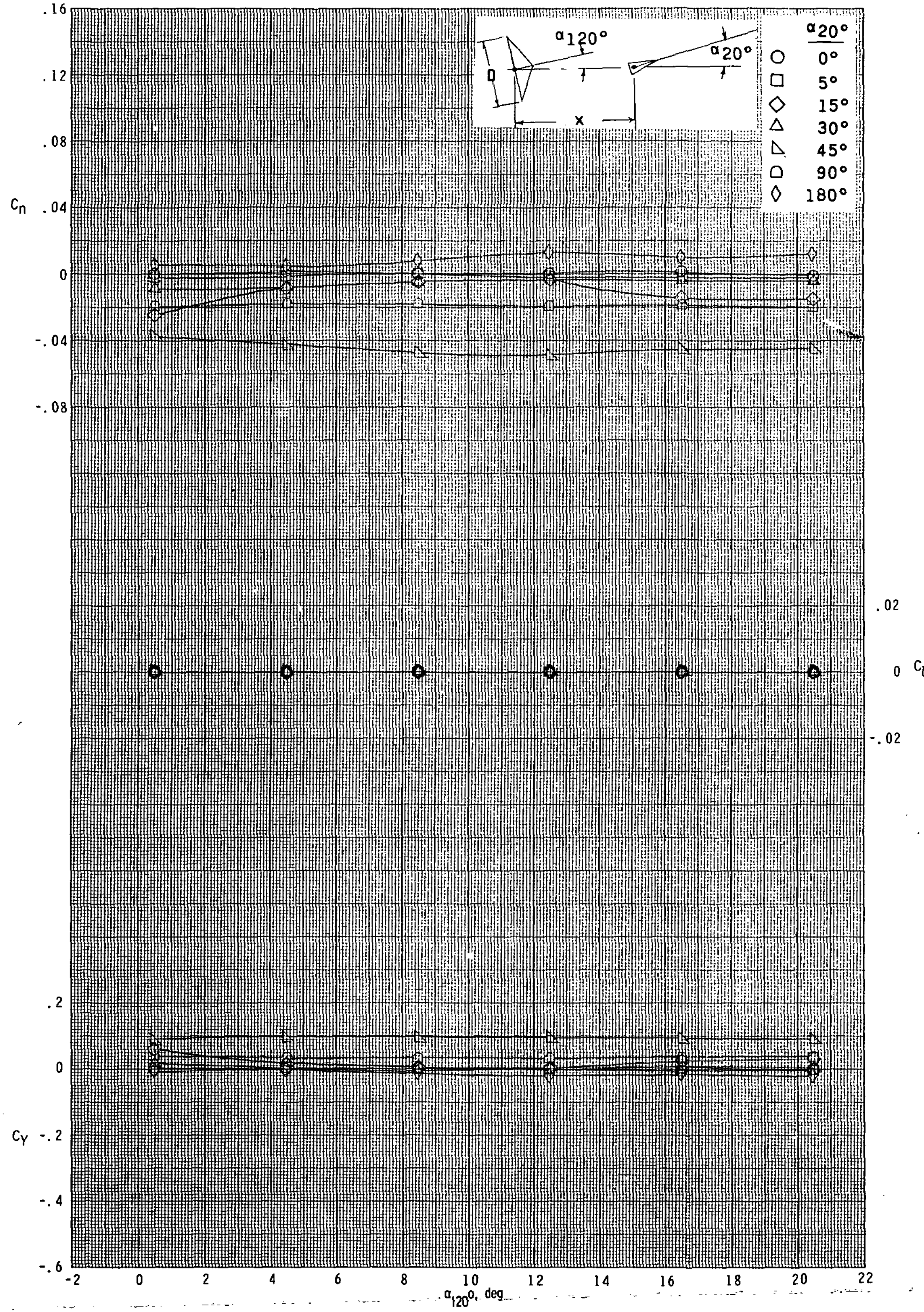

(g) x/D = 2.070; y/D = 0.

Figure 12.- Continued.

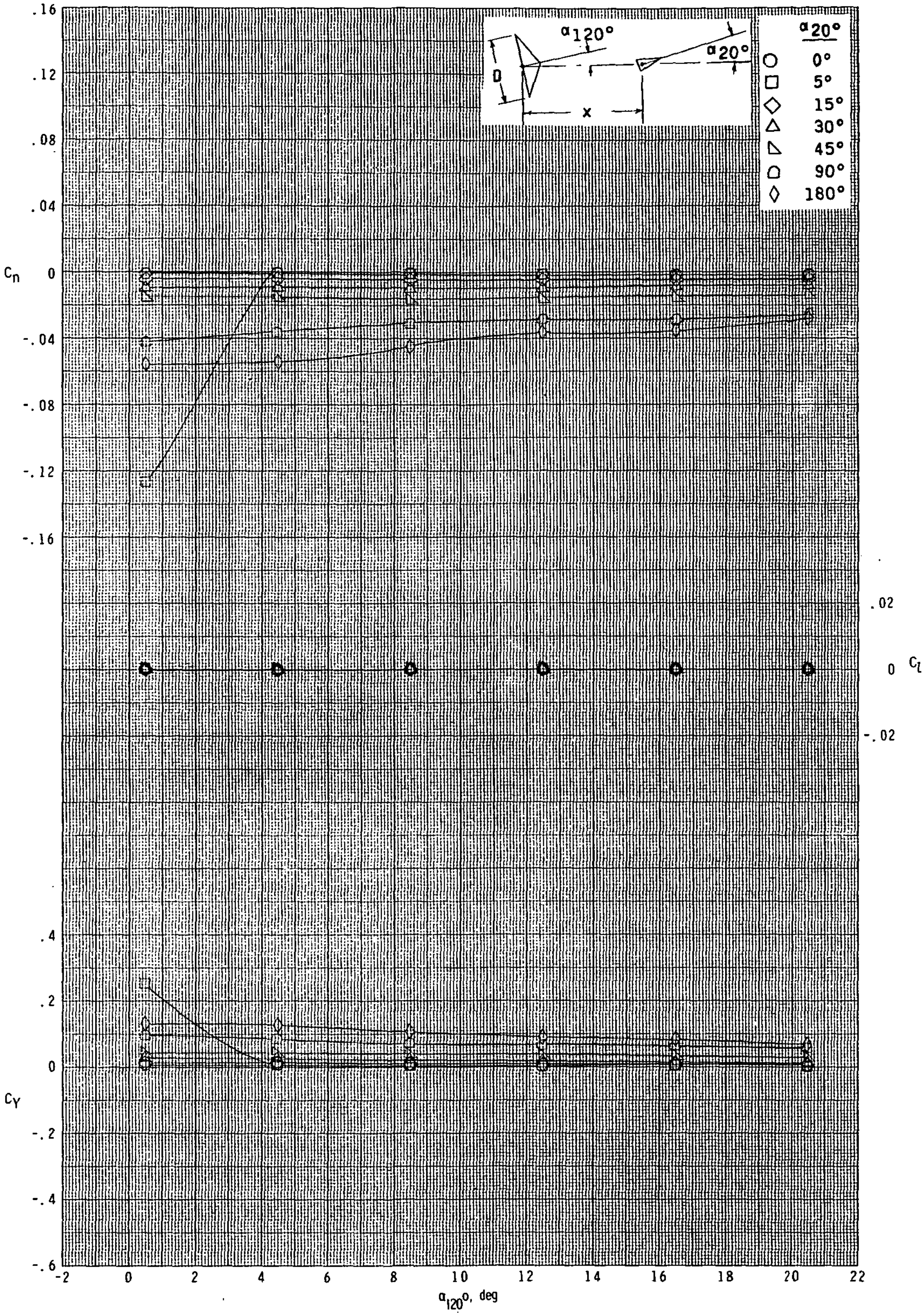

(h) x/D = 2.070; y/D = 0.25.

Figure 12.- Continued.

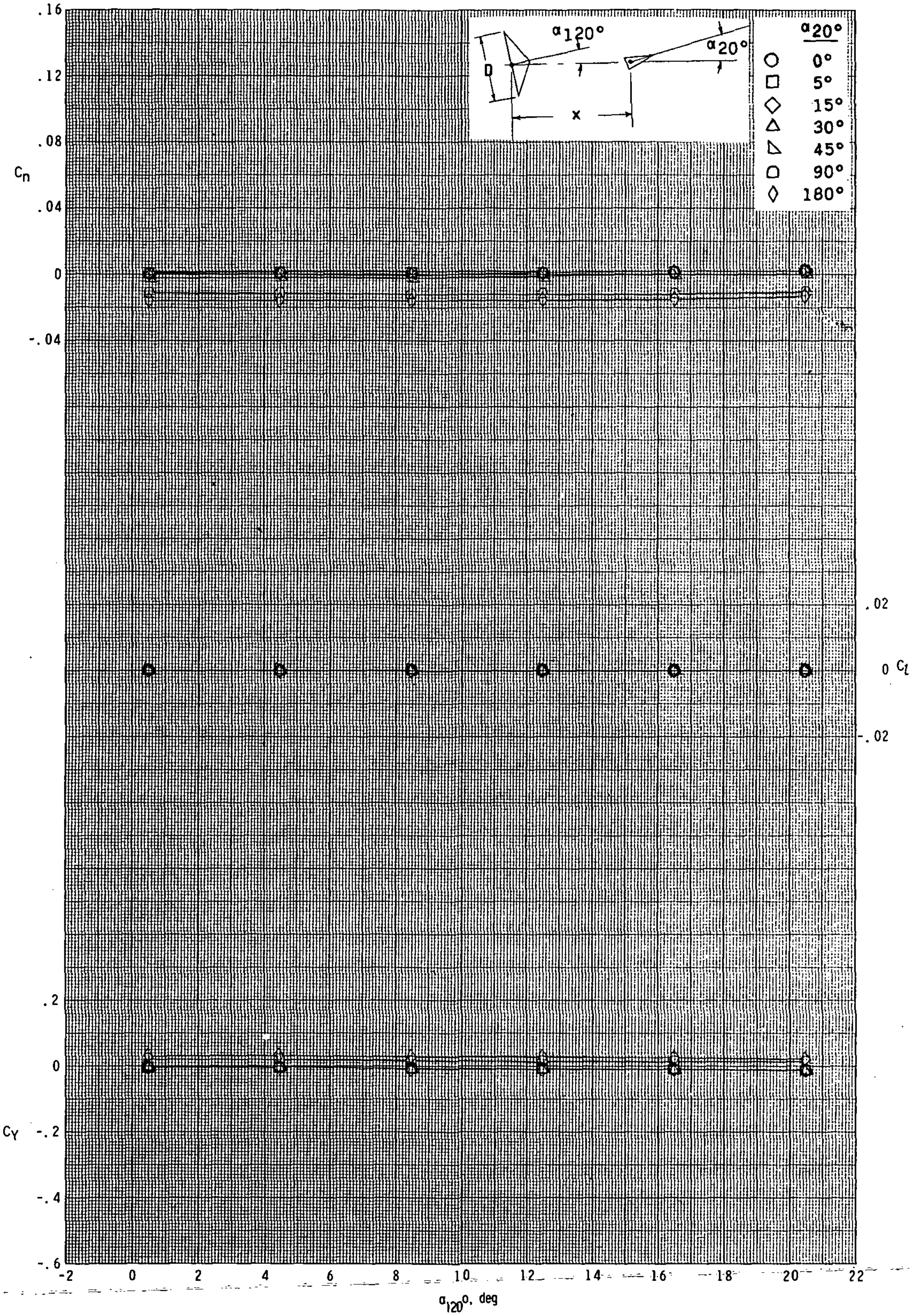

(i) x/D = 2.070; y/D = 0.50.

Figure 12.- Continued.

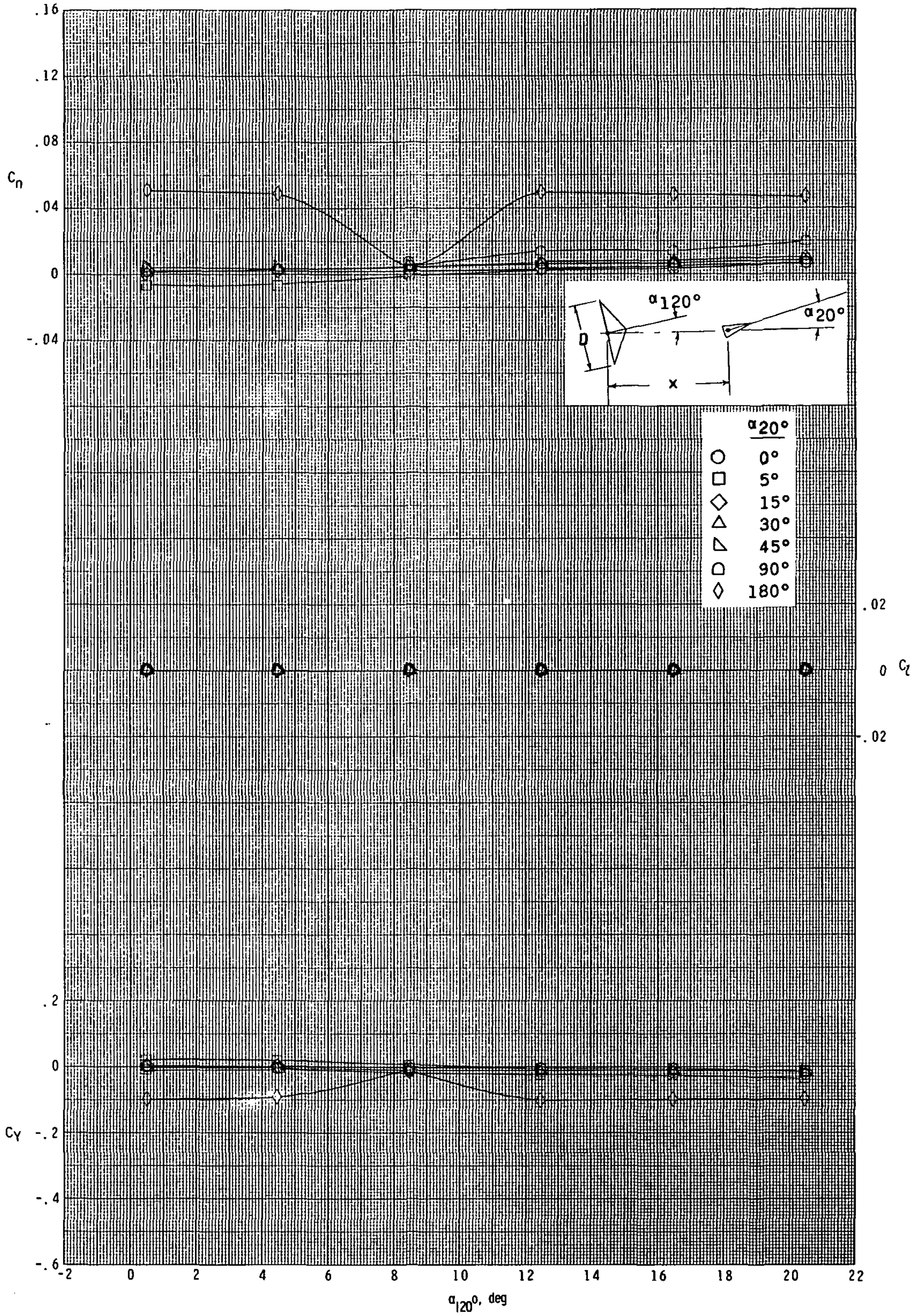

(j) x/D = 3.520; y/D = 0.
Figure 12.- Continued.

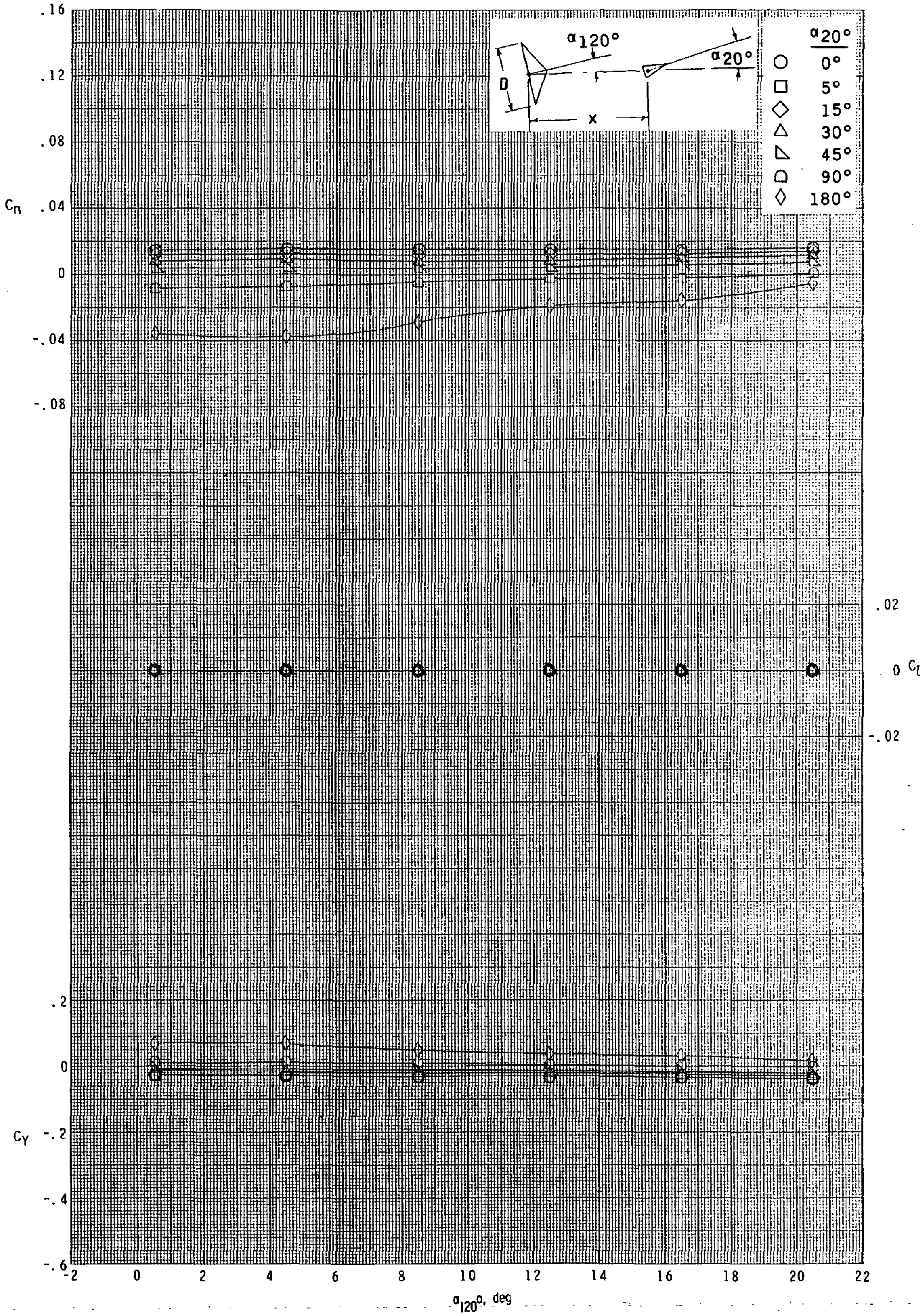

(k) x/D = 3.520; y/D = 0.25.

Figure 12.- Continued.

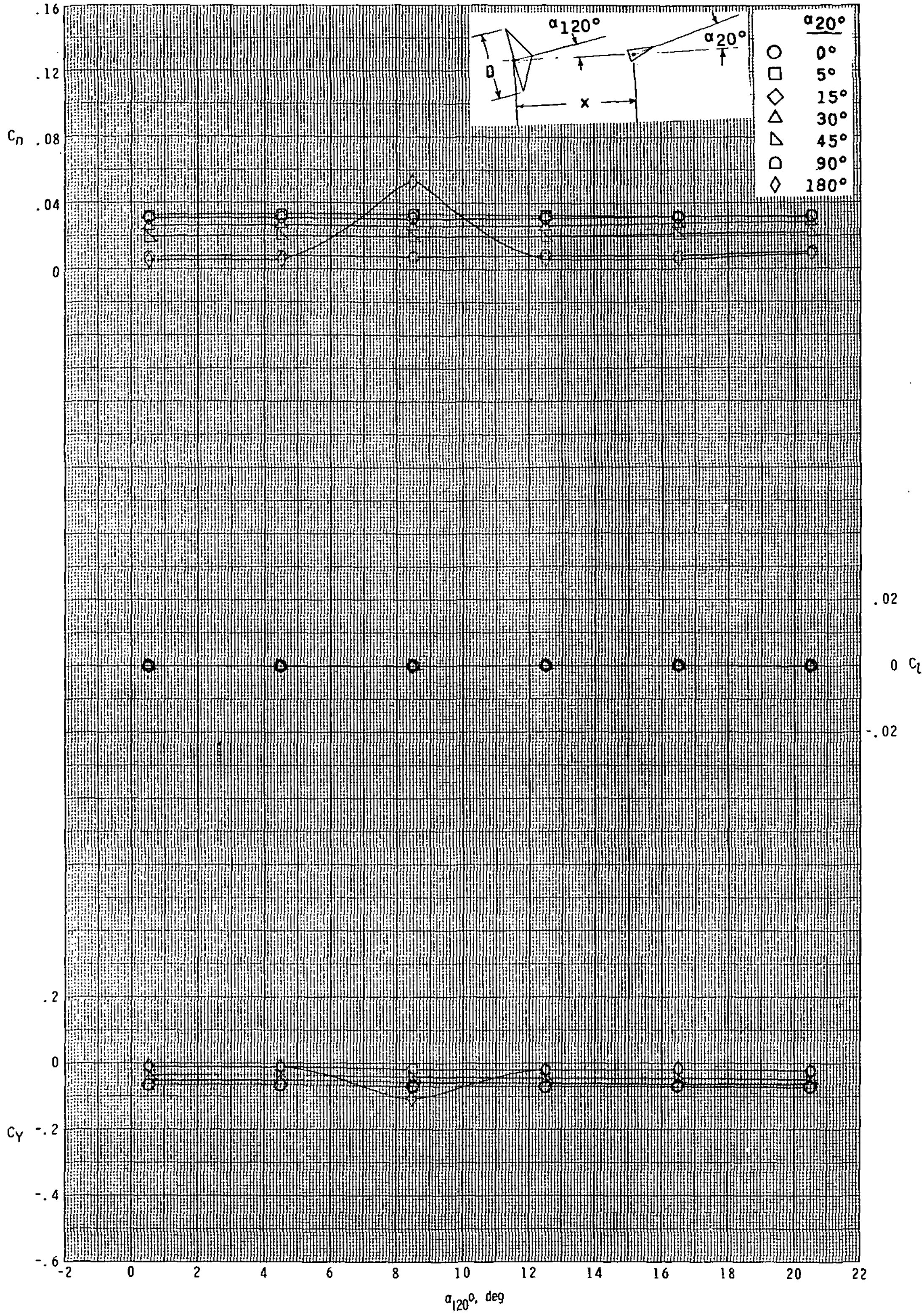

(l) x/D = 3.520; y/D = 0.50.

Figure 12.- Concluded.

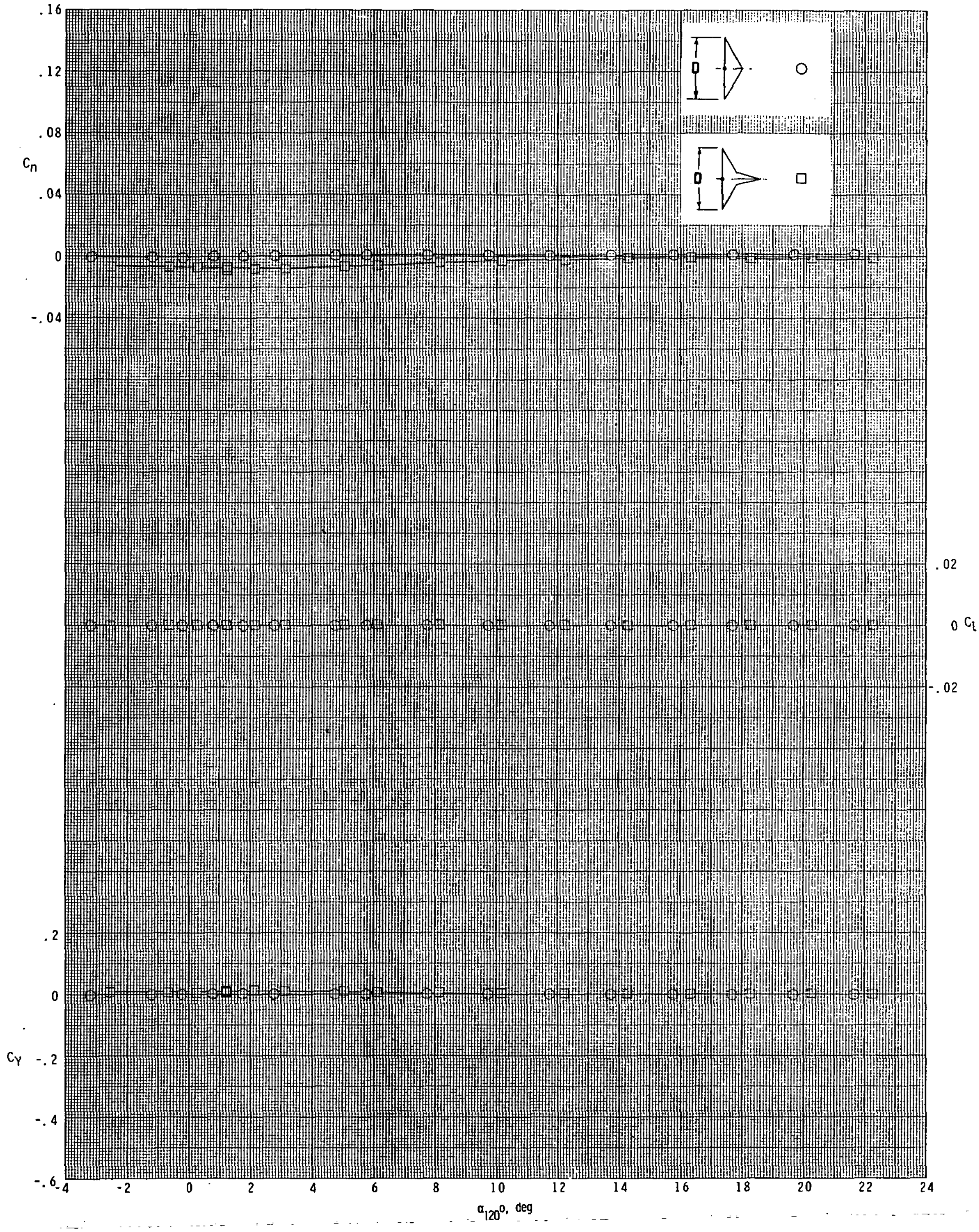

(a) $M_\infty = 2.36$.

Figure 13.- Variation of yawing-moment, rolling-moment, and side-force coefficients with angle of attack for 16.002-cm-diameter (6.30 in.), 120^o-included-angle cone with attached and separated 20^o-included-angle cone.

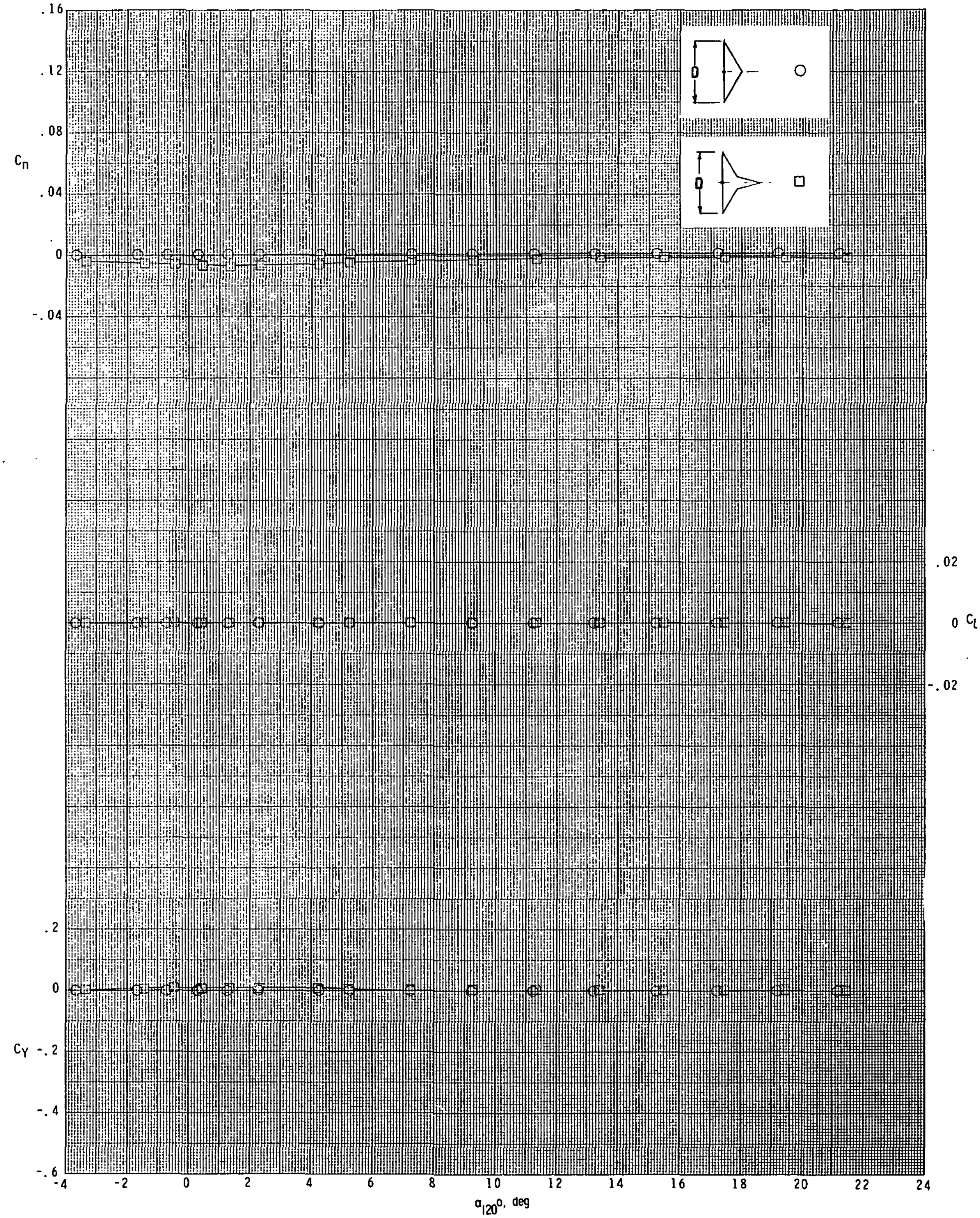

(b) $M_\infty = 2.70$.

Figure 13.- Concluded.

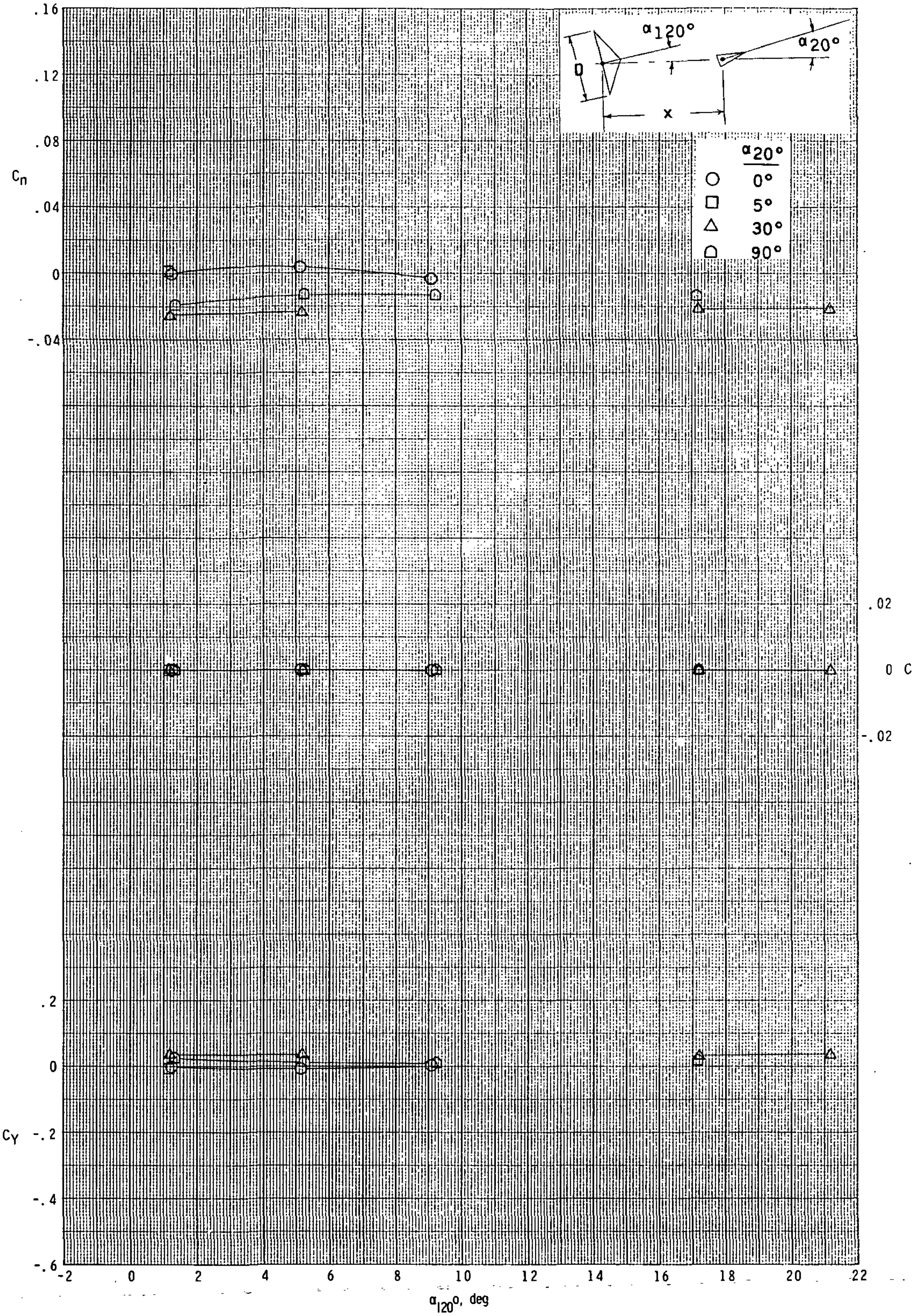

(a) x/D = 0.476; y/D = 0.

Figure 14.- Variation of yawing-moment, rolling-moment, and side-force coefficients with angle of attack for 16.002-cm-diameter (6.30 in.), 120°-included-angle cone for various angles of attack of 20°-included-angle cone at $M_\infty = 2.36$.

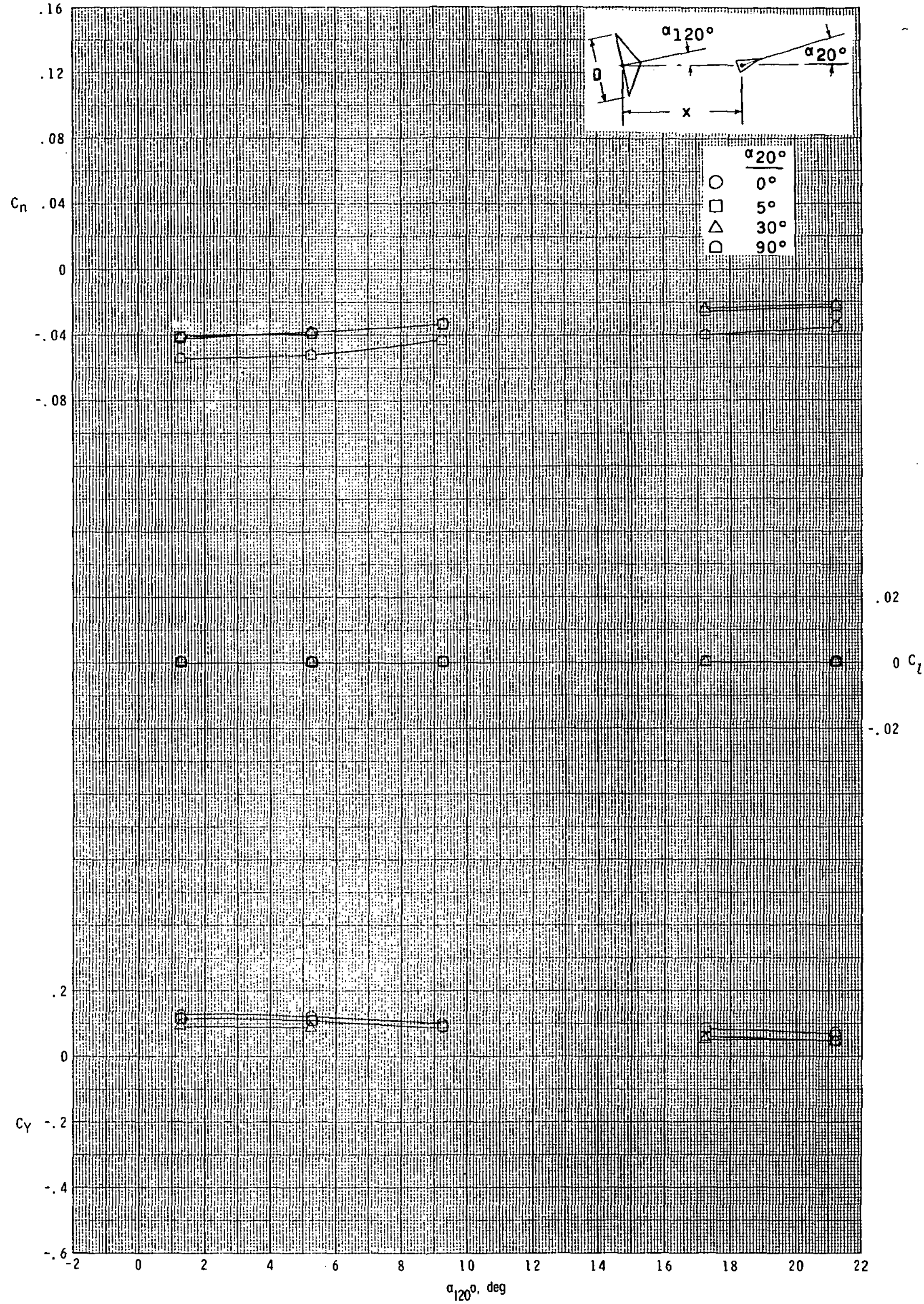

(b) x/D = 0.476; y/D = 0.25.

Figure 14.- Continued.

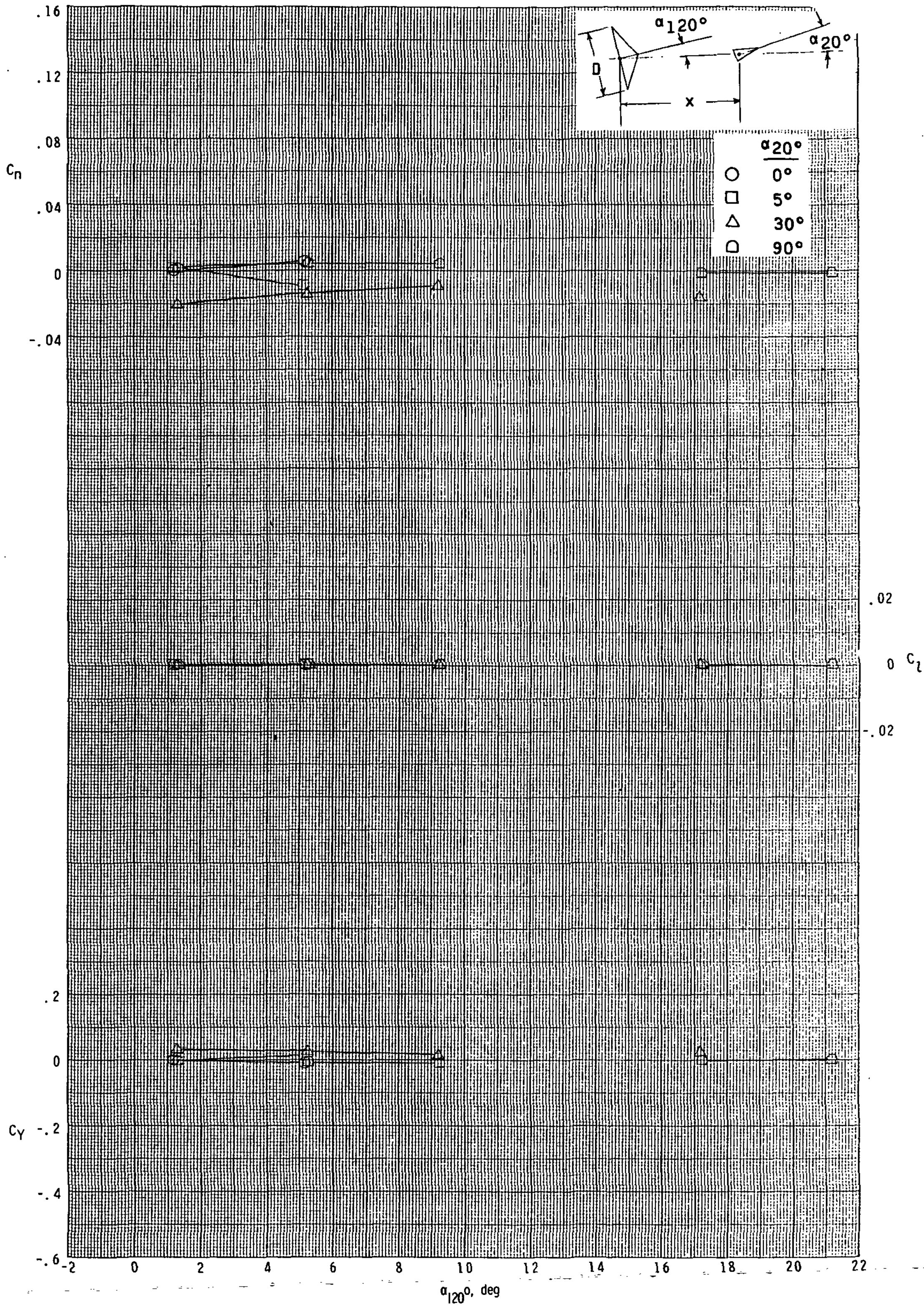

(c) x/D = 0.952; y/D = 0.

Figure 14.- Continued.

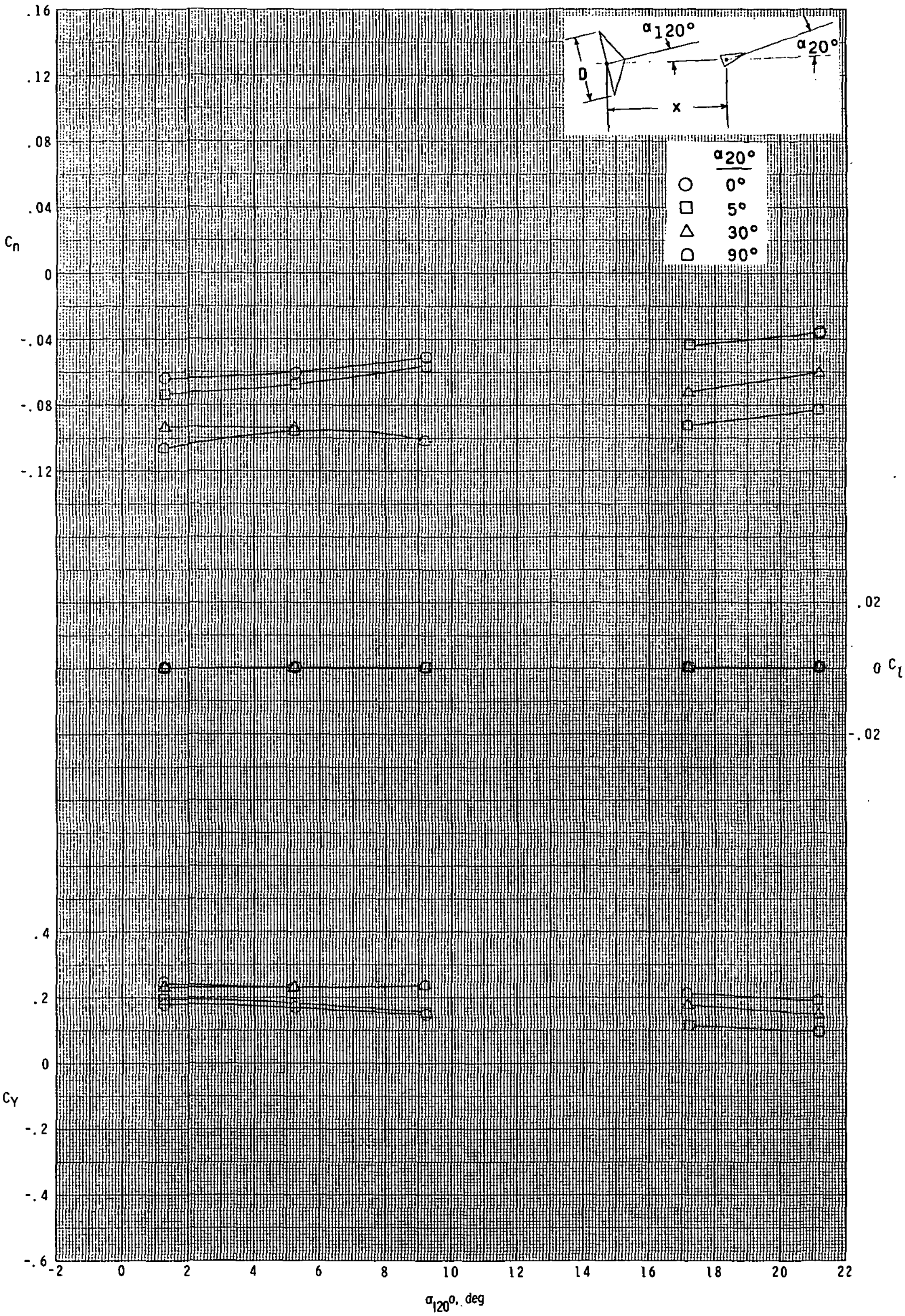

(d) x/D = 0.952; y/D = 0.25.

Figure 14.- Continued.

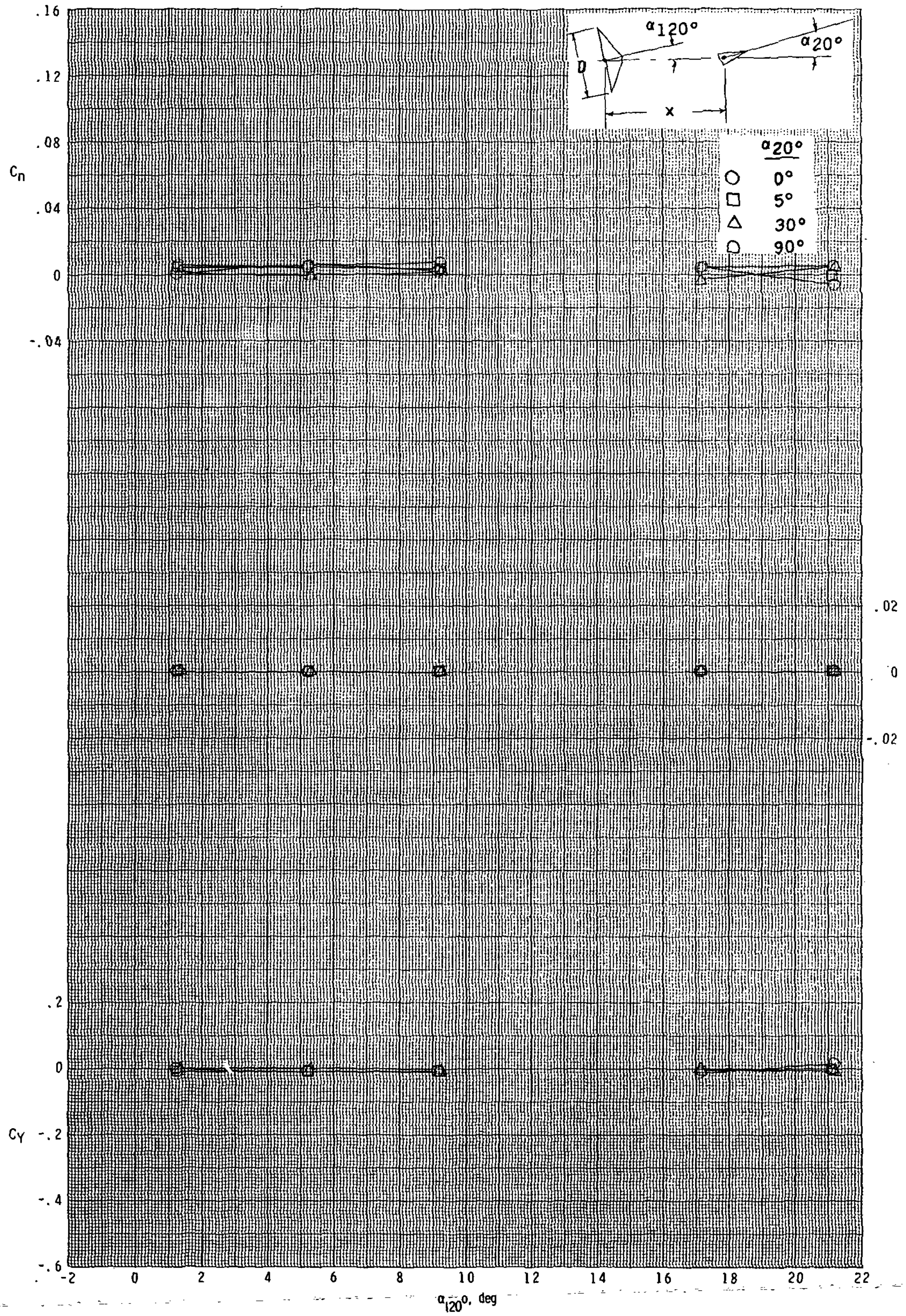

(e) x/D = 1.587; y/D = 0.
Figure 14.- Continued.

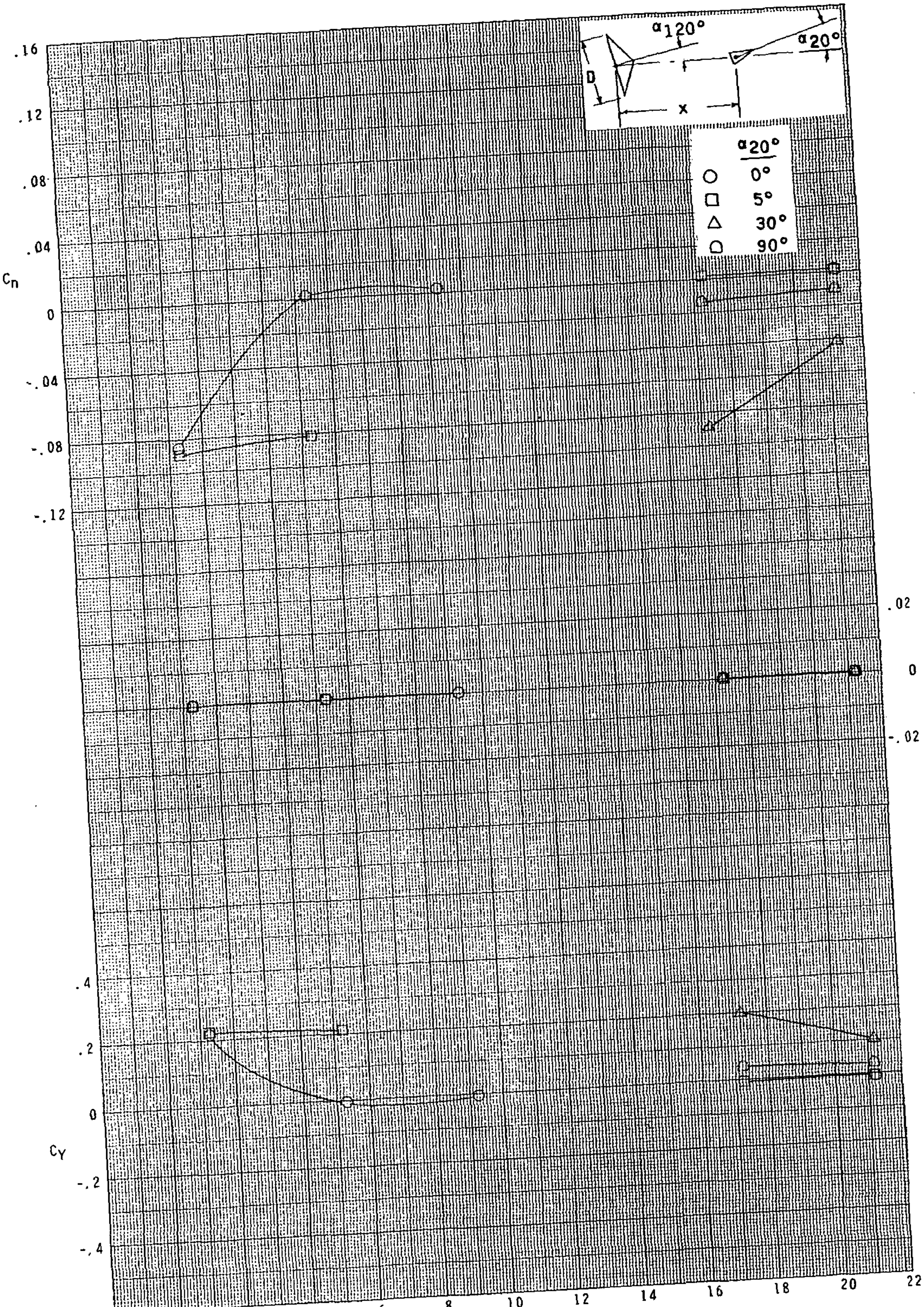

(f) x/D = 1.587; y/D = 0.25.

Figure 14.- Concluded.

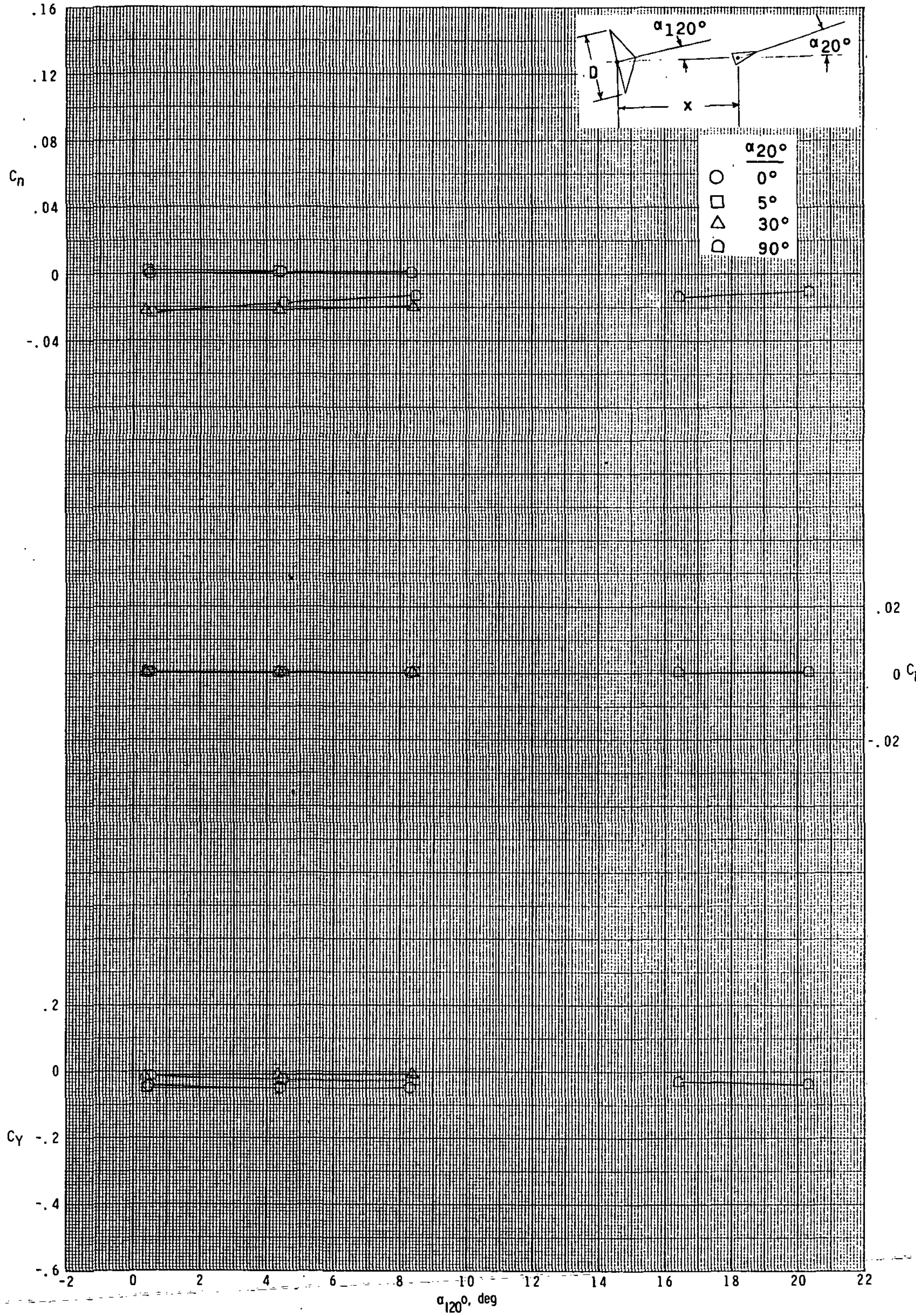

(a) $x/D = 0.476$; $y/D = 0$.

Figure 15.- Variation of yawing-moment, rolling-moment, and side-force coefficients with angle of attack for 16.002-cm-diameter (6.30 in.), 120°-included-angle cone for various angles of attack of 20°-included-angle cone at $M_{\infty} = 2.70$.

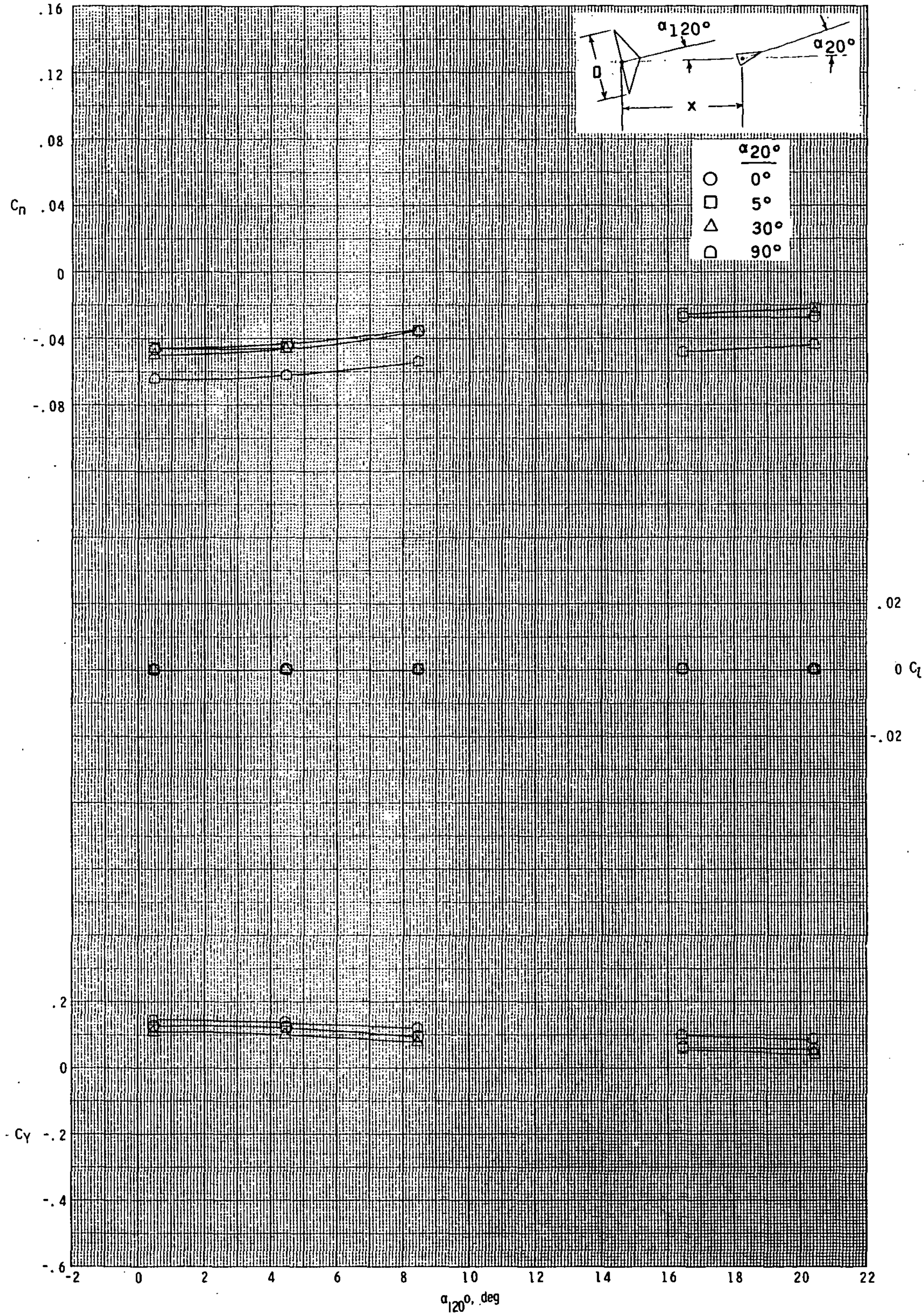

(b) x/D = 0.476; y/D = 0.25.

Figure 15.- Continued.

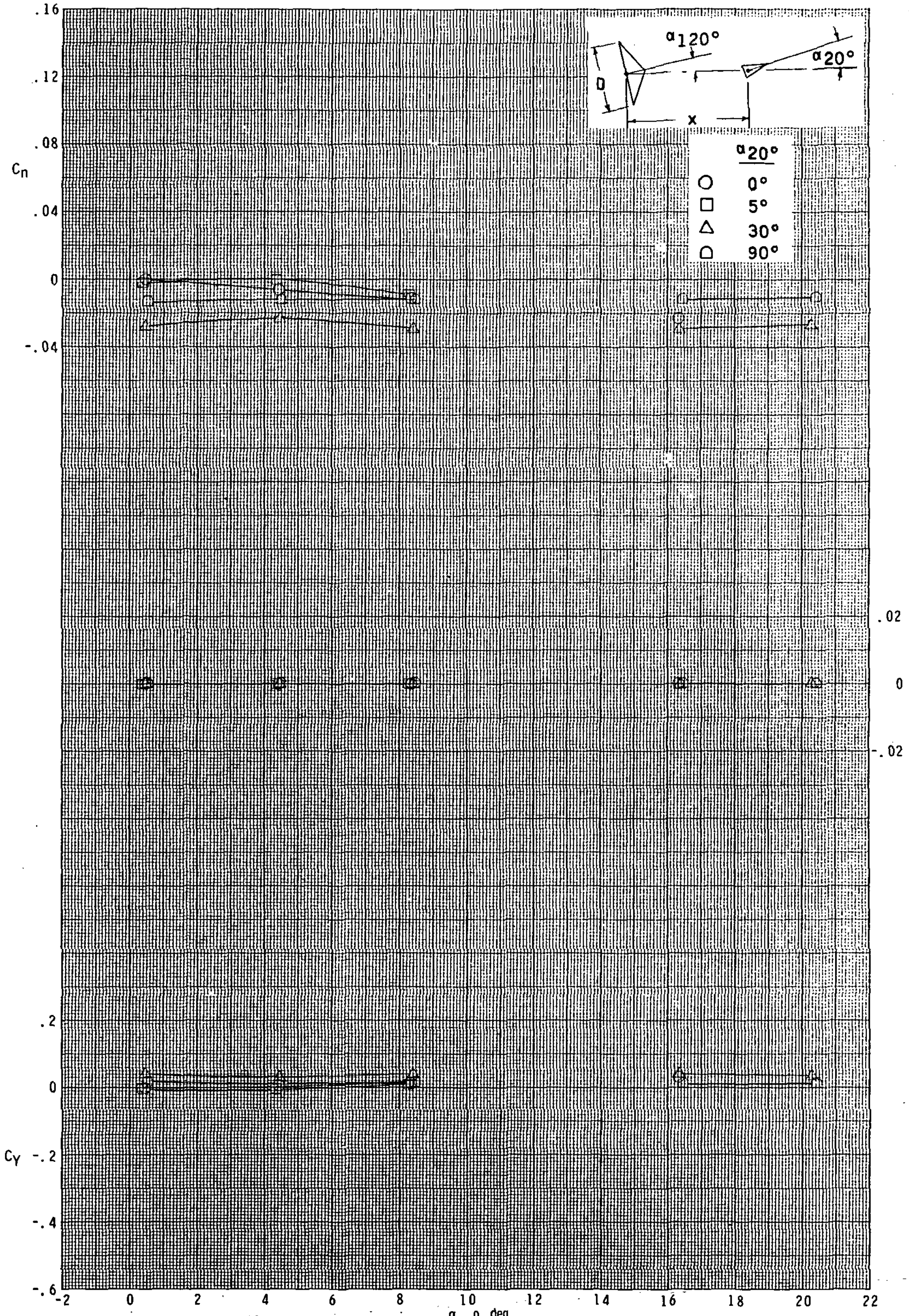

(c) x/D = 0.952; y/D = 0.

Figure 15.- Continued.

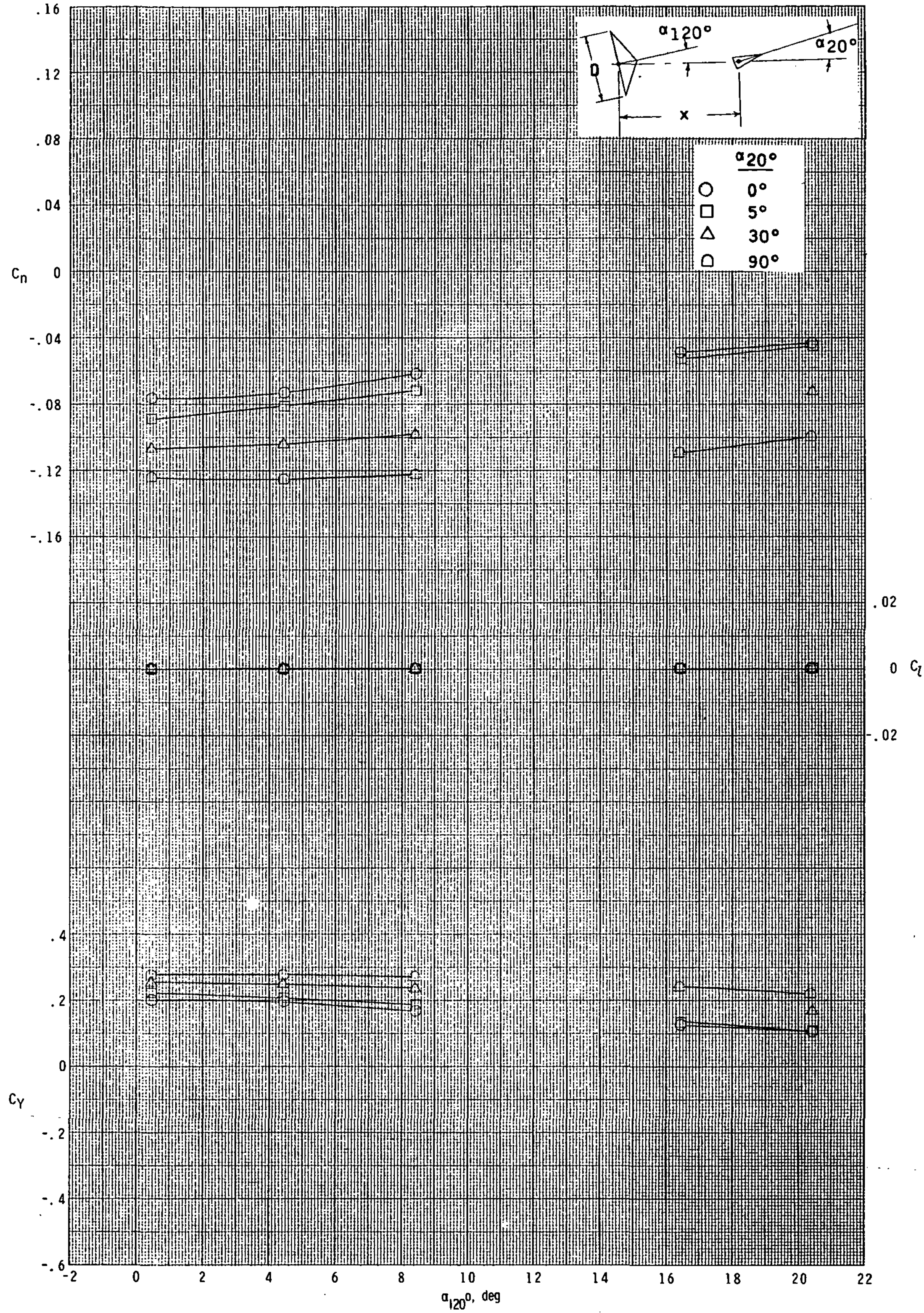

(d) x/D = 0.952; y/D = 0.25.

Figure 15.- Continued.

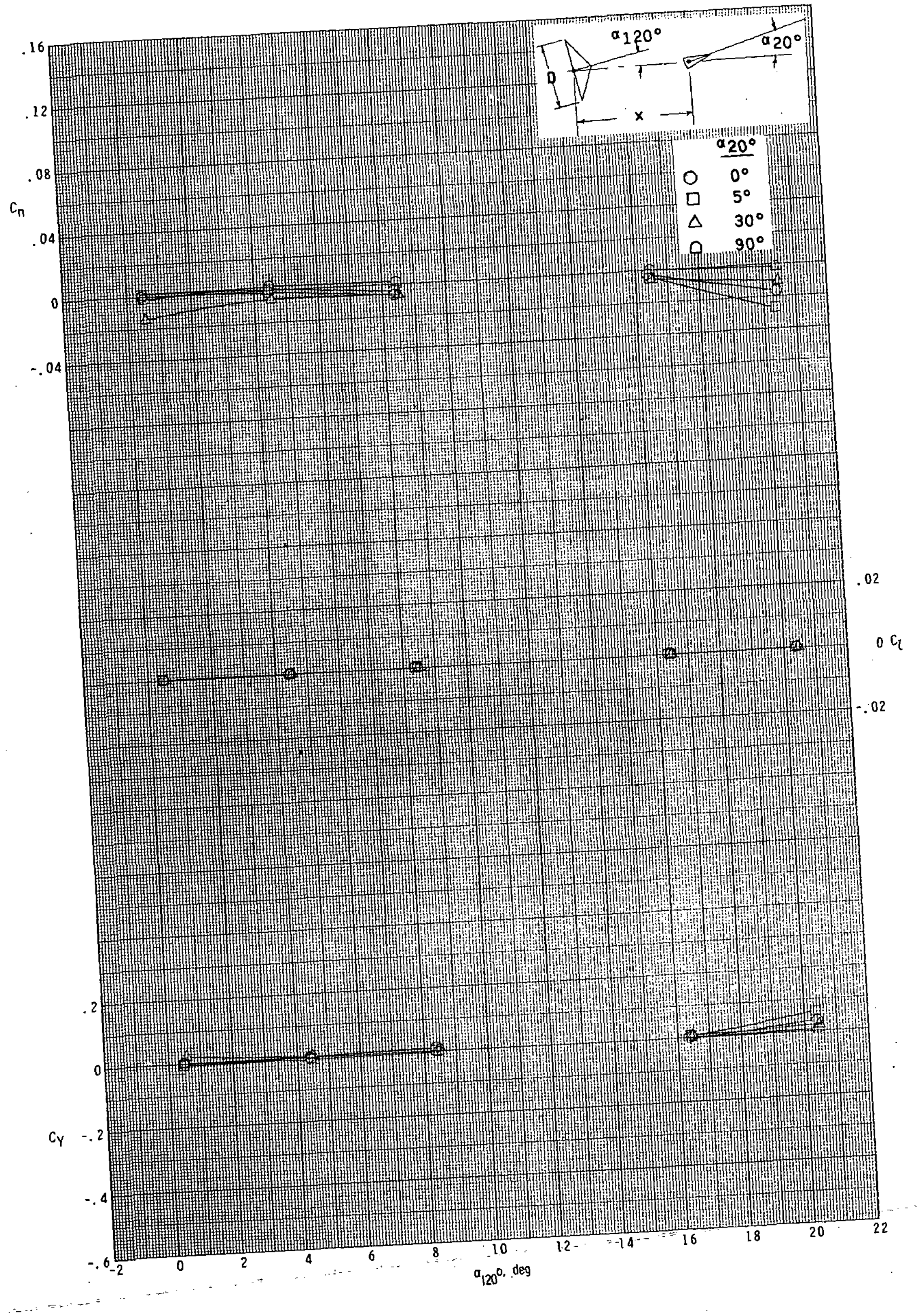

(e) x/D = 1.587; y/D = 0.
Figure 15.- Continued.

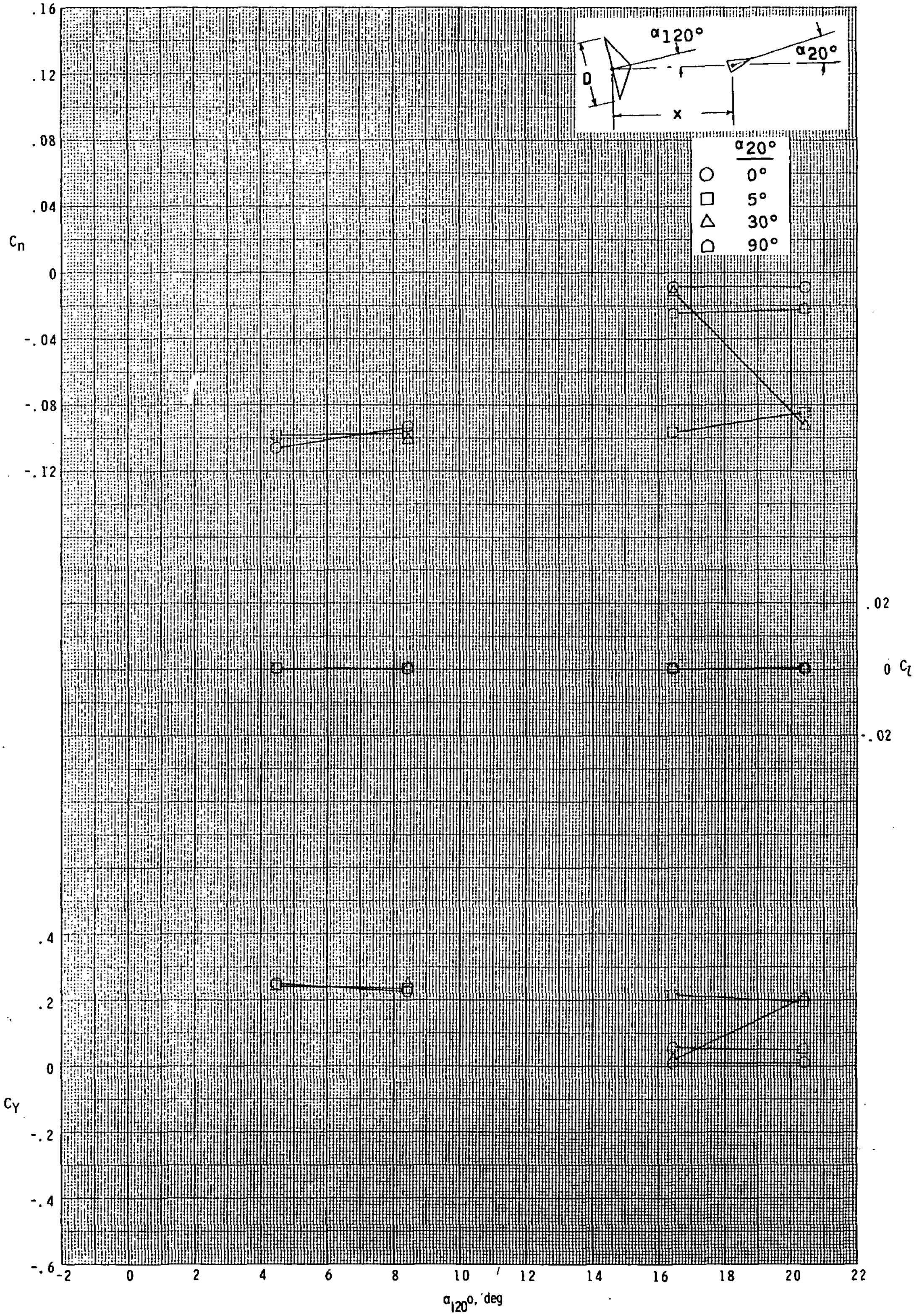

(f) x/D = 1.587; y/D = 0.25.

Figure 15.- Concluded.

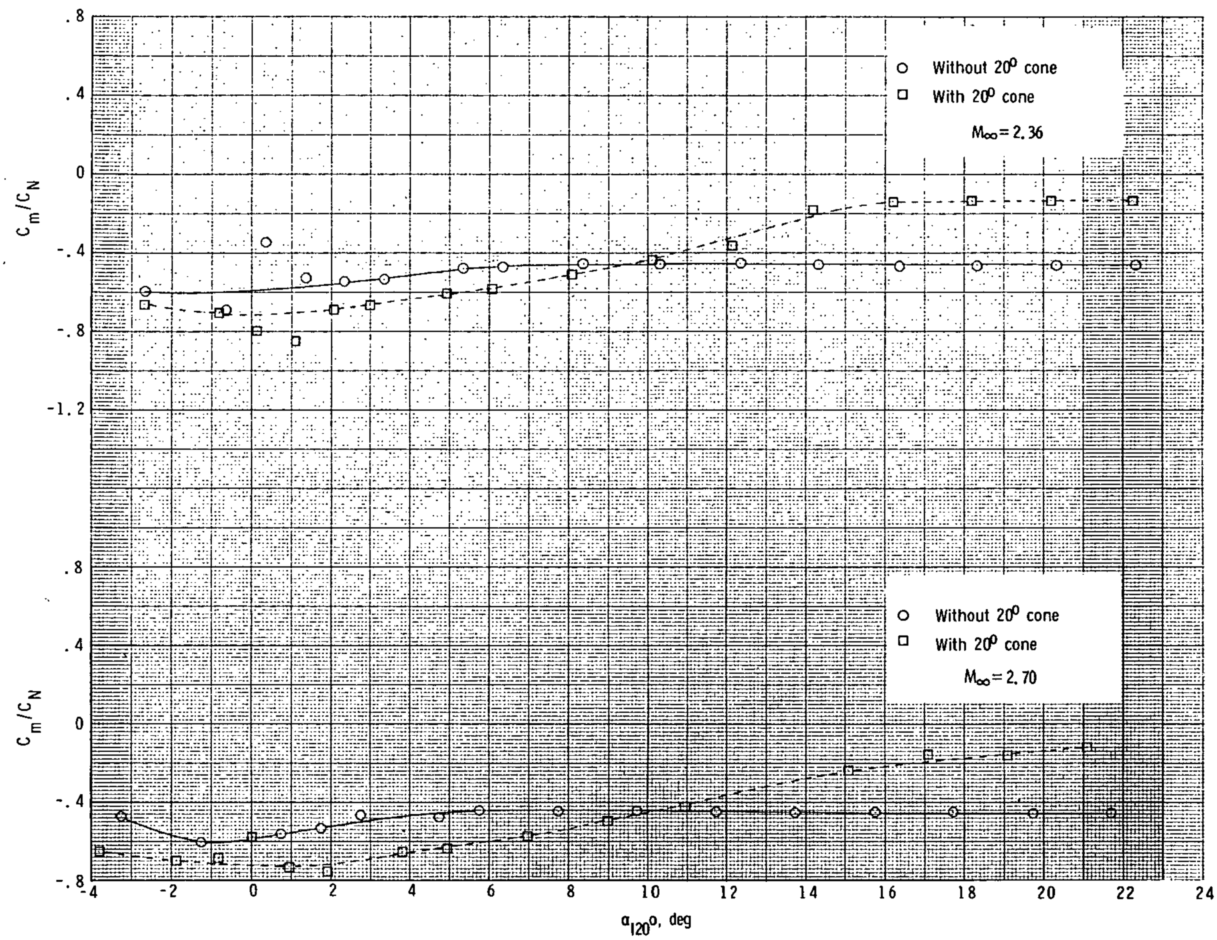

(a) 12.268-cm-diameter (4.83 in.), 120° cone.

Figure 16.- Variation of longitudinal center of pressure C_m/C_N with angle of attack for 120°-included-angle cones with attached and separated 20°-included-angle cone.

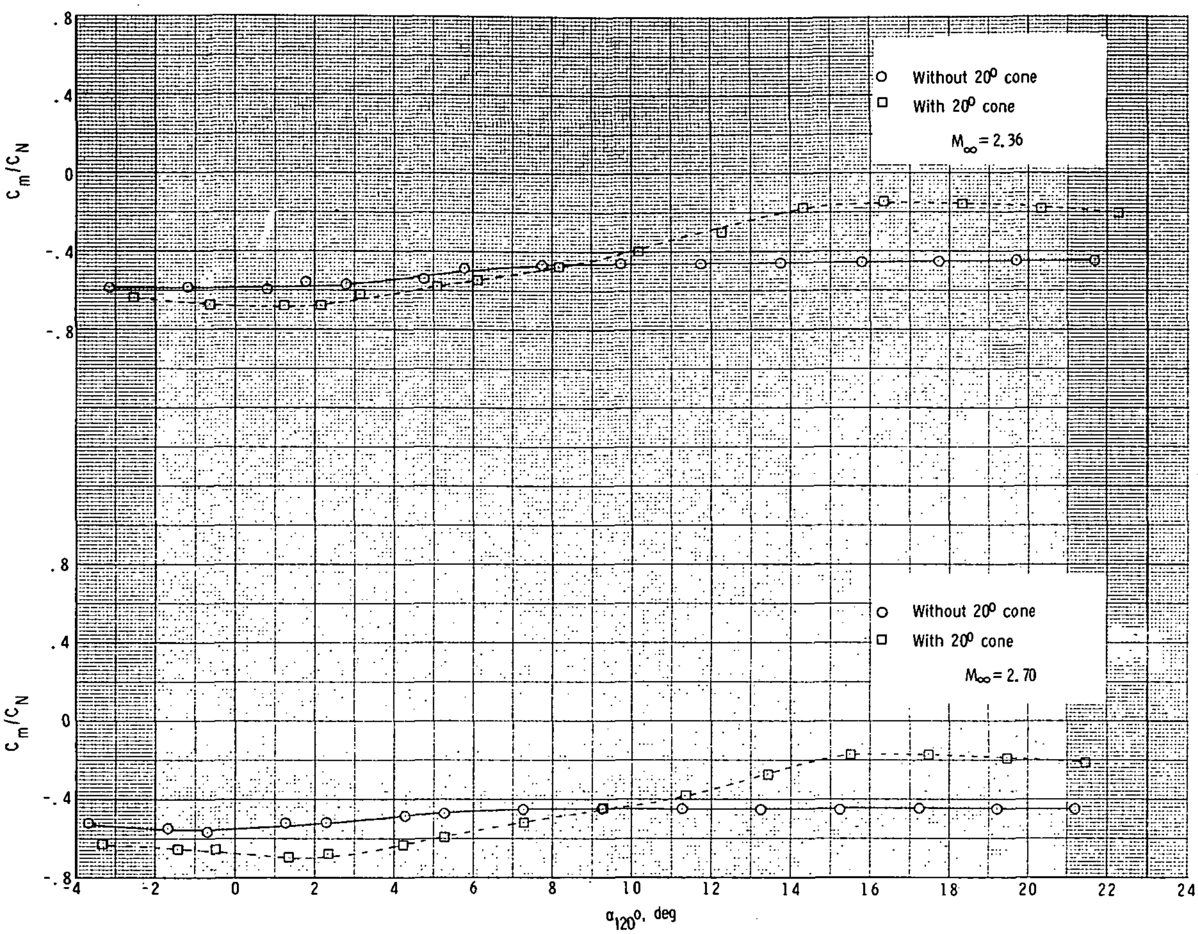

(b) 16.002-cm-diameter (6.30 in.), 120° cone.

Figure 16.- Concluded.

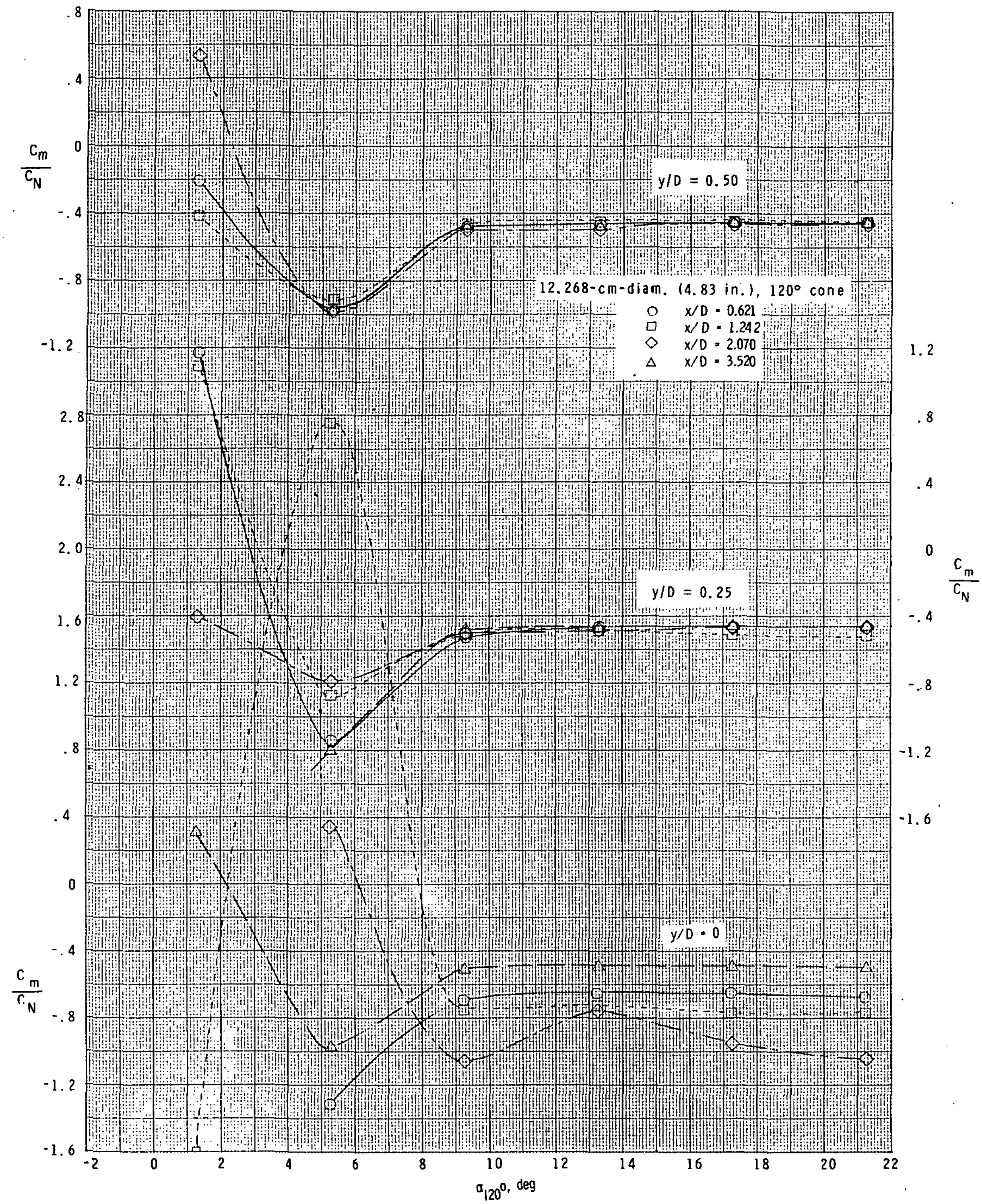

(a) $M_\infty = 2.36$; $\alpha_{20^o} = 0^o$.

Figure 17.- Variation of longitudinal center of pressure C_m/C_N with angle of attack for 12.268-cm-diameter (4.83 in.), 120^o-included-angle cone for various x/D locations, y/D locations, and angles of attack of 20^o-included-angle cone.

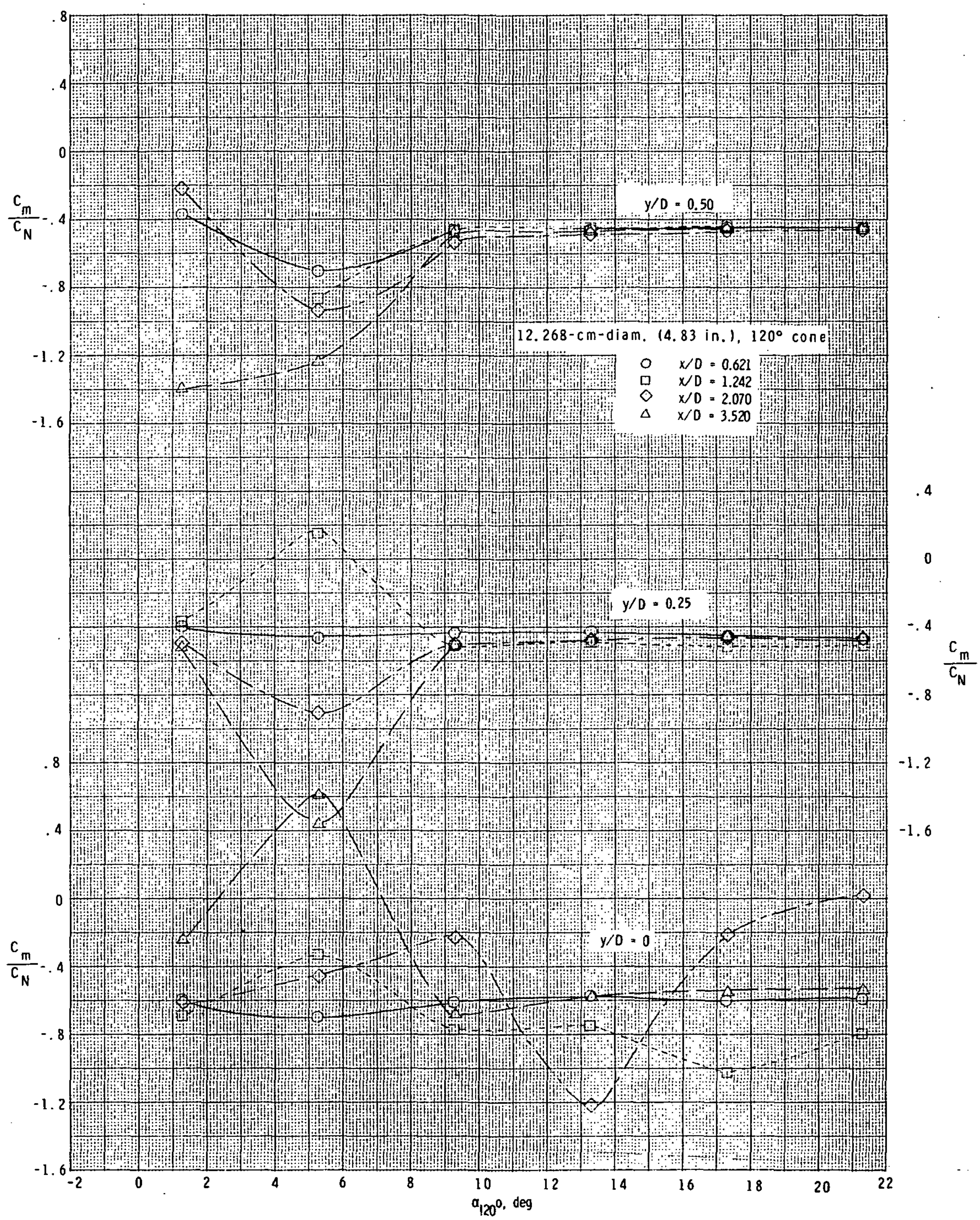

(b) $M_\infty = 2.36$; $\alpha_{20^o} = 5^o$.

Figure 17.- Continued.

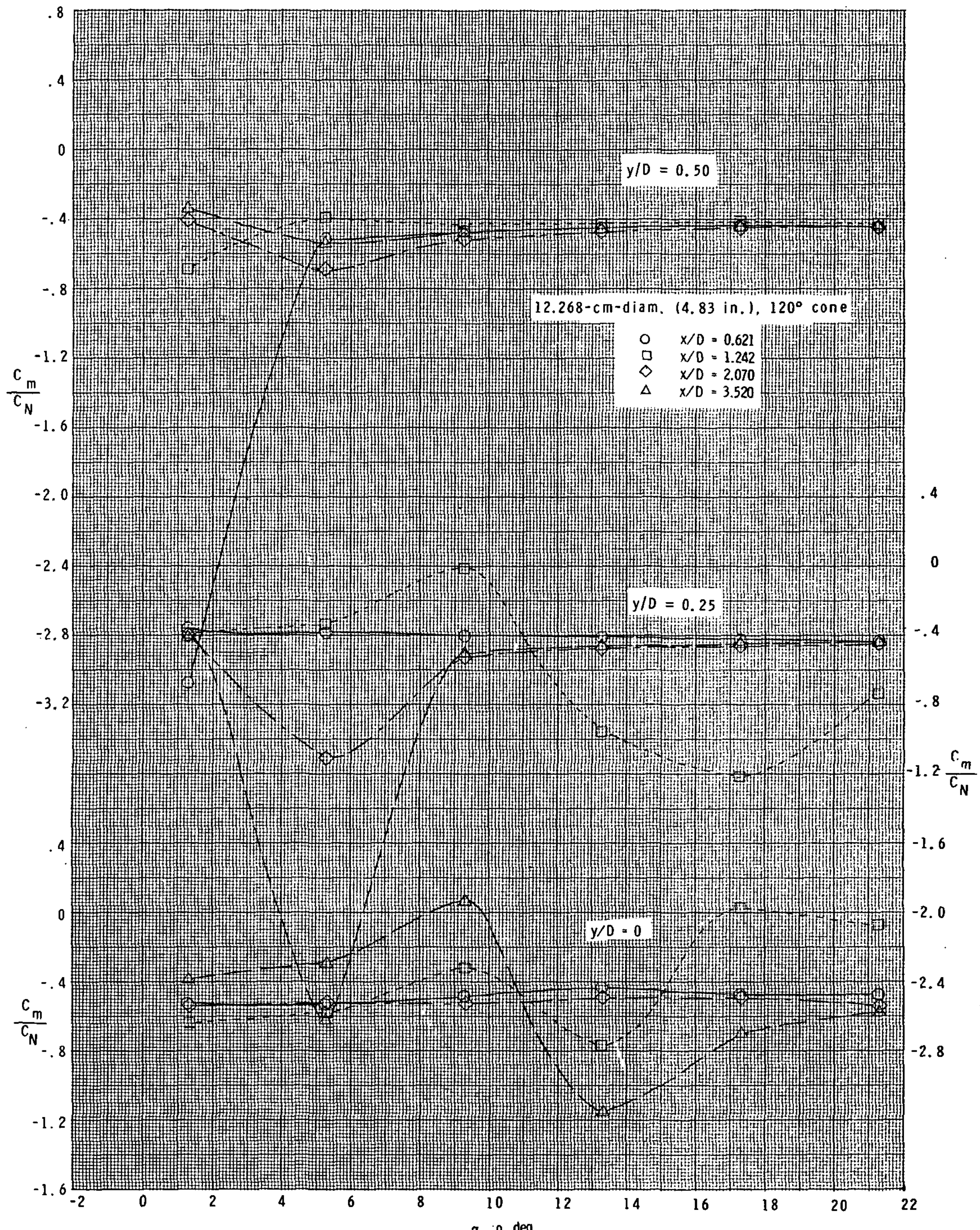

(c) $M_\infty = 2.36$; $\alpha_{20^o} = 15^o$.

Figure 17.- Continued.

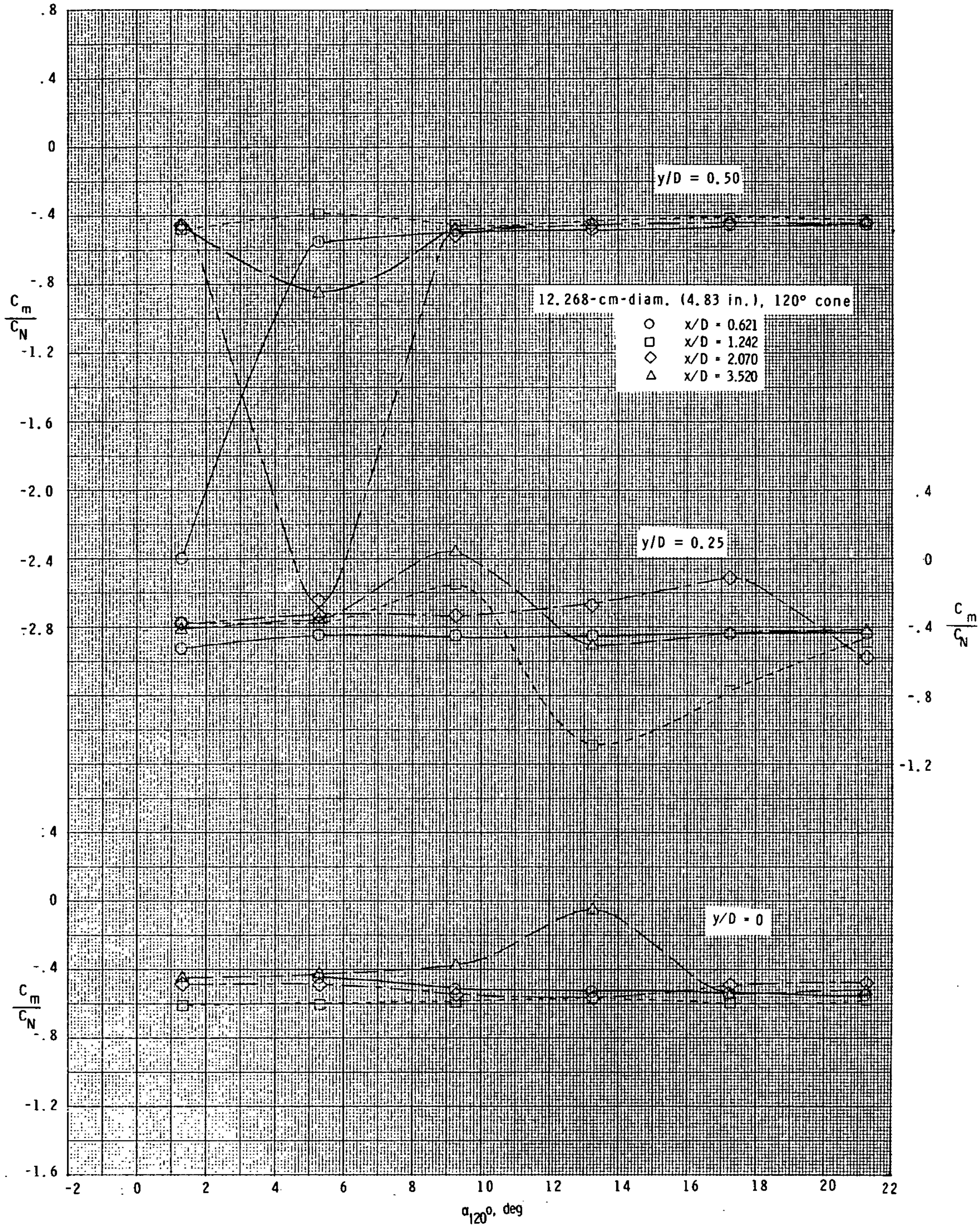

(d) $M_\infty = 2.36$; $\alpha_{20^o} = 30^o$.

Figure 17.- Continued.

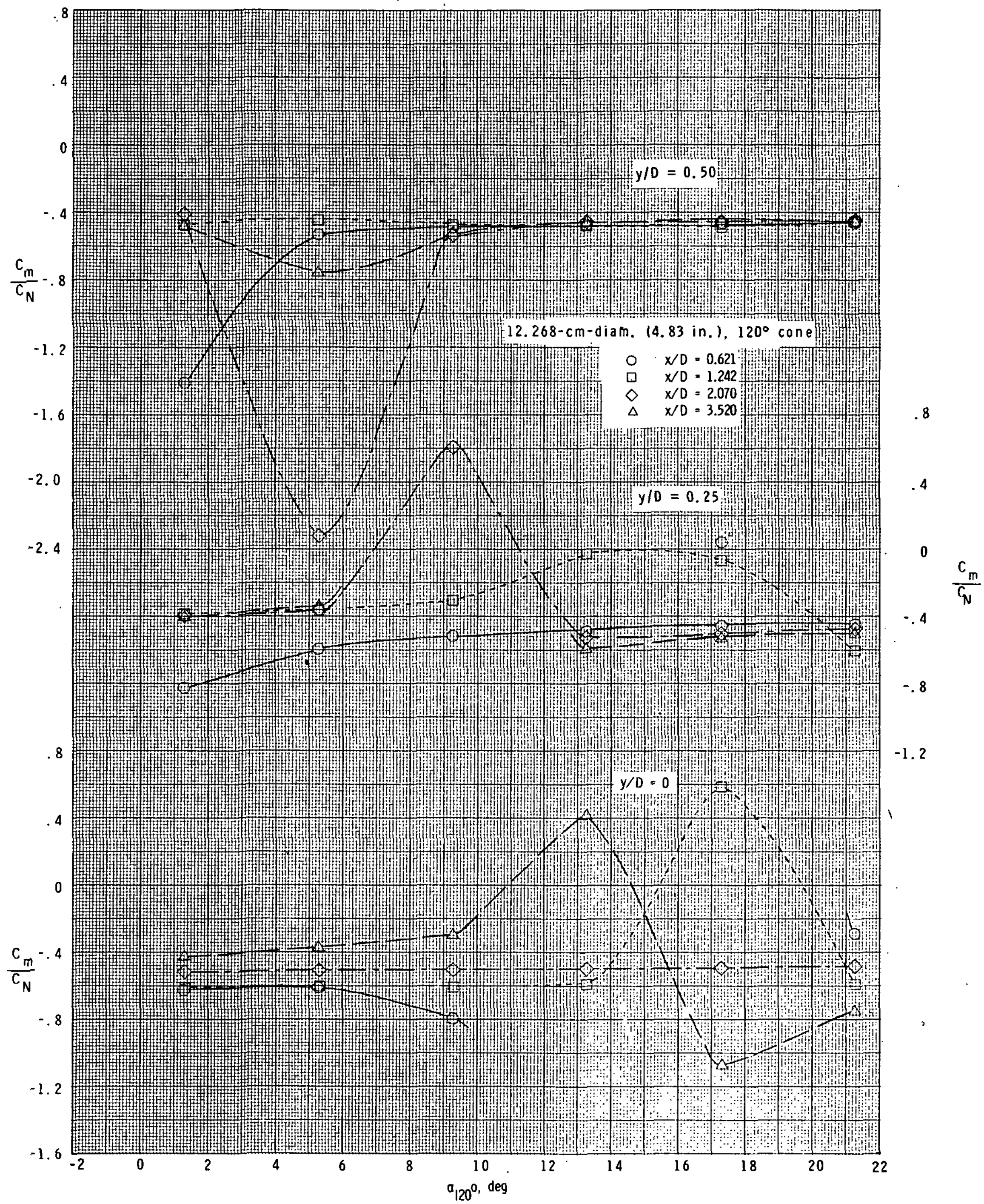

(e) $M_\infty = 2.36$; $\alpha_{20^o} = 45^o$.

Figure 17.- Continued.

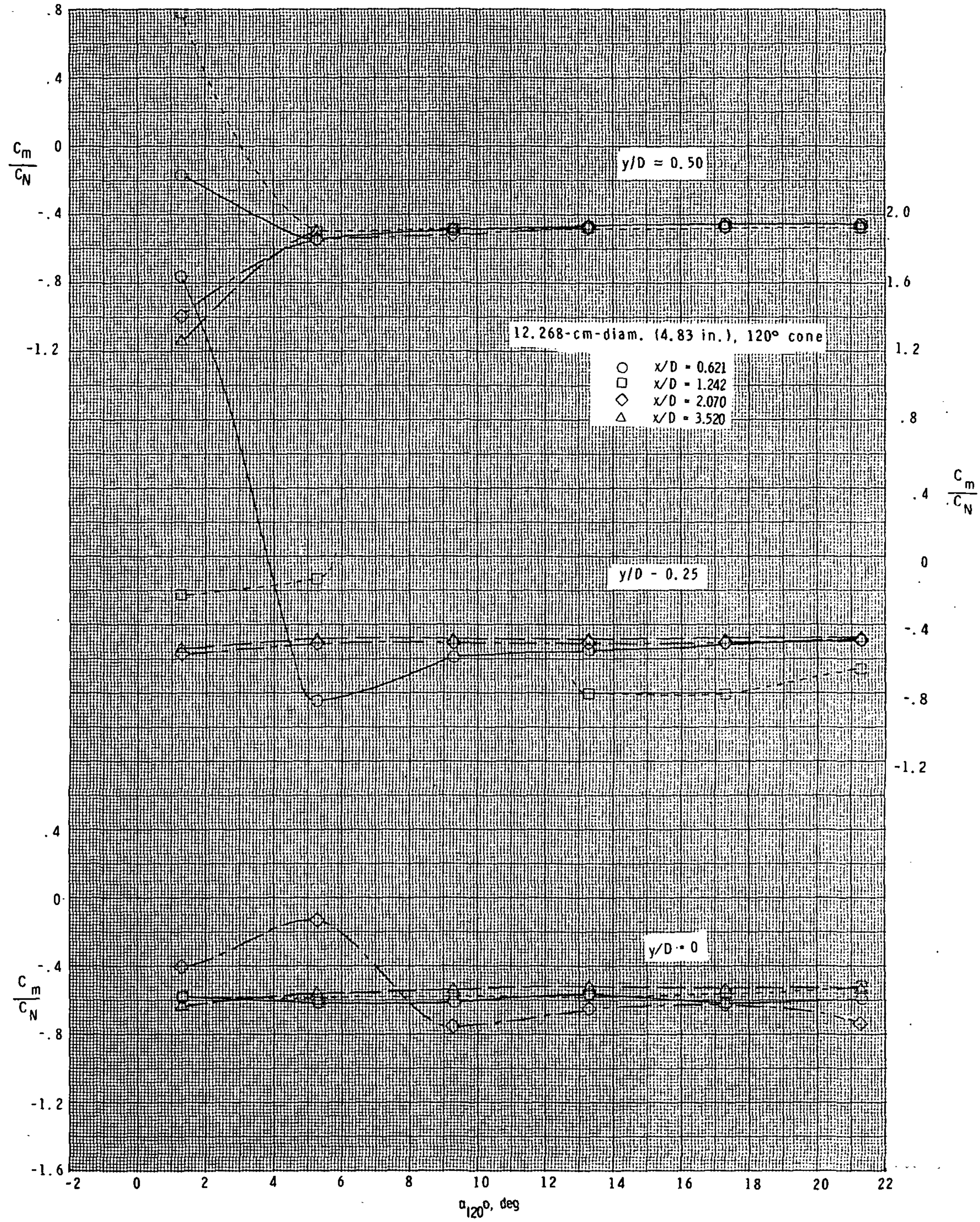

(f) $M_\infty = 2.36$; $\alpha_{20^o} = 90^o$.

Figure 17.- Continued.

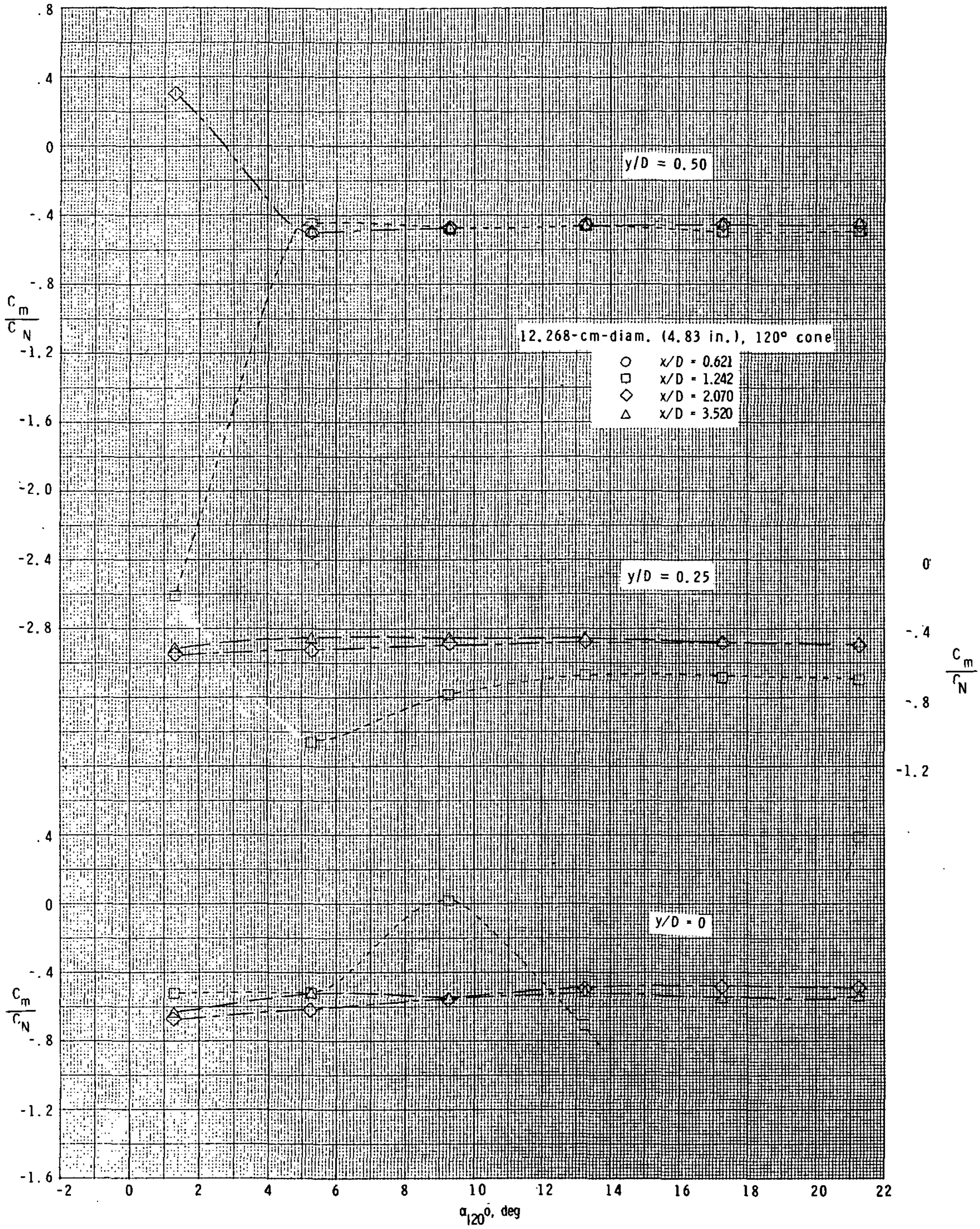

(g) $M_\infty = 2.36$; $\alpha_{20^\circ} = 180^\circ$.

Figure 17.- Continued.

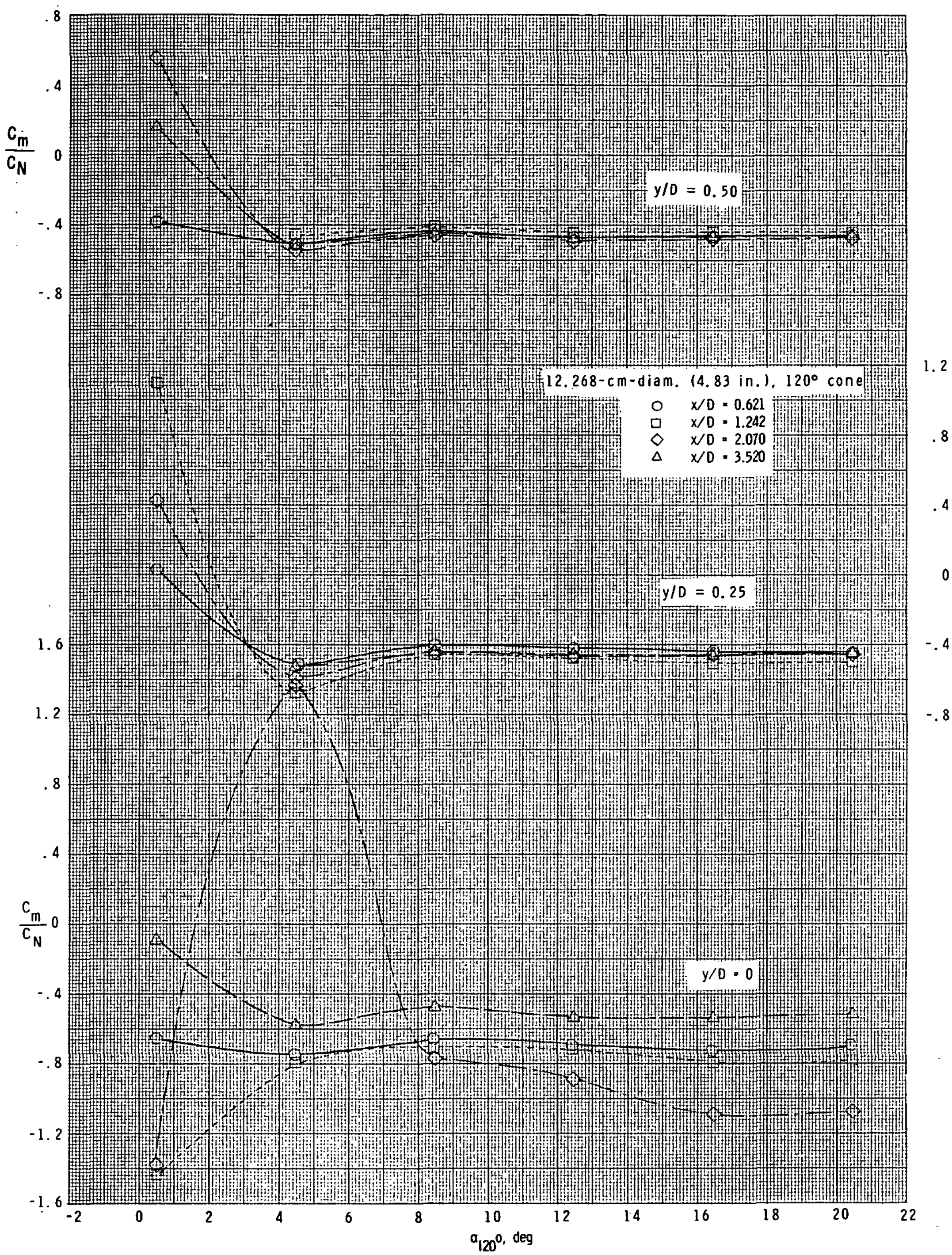

(h) $M_\infty = 2.70$; $\alpha_{20^o} = 0^o$.

Figure 17.- Continued.

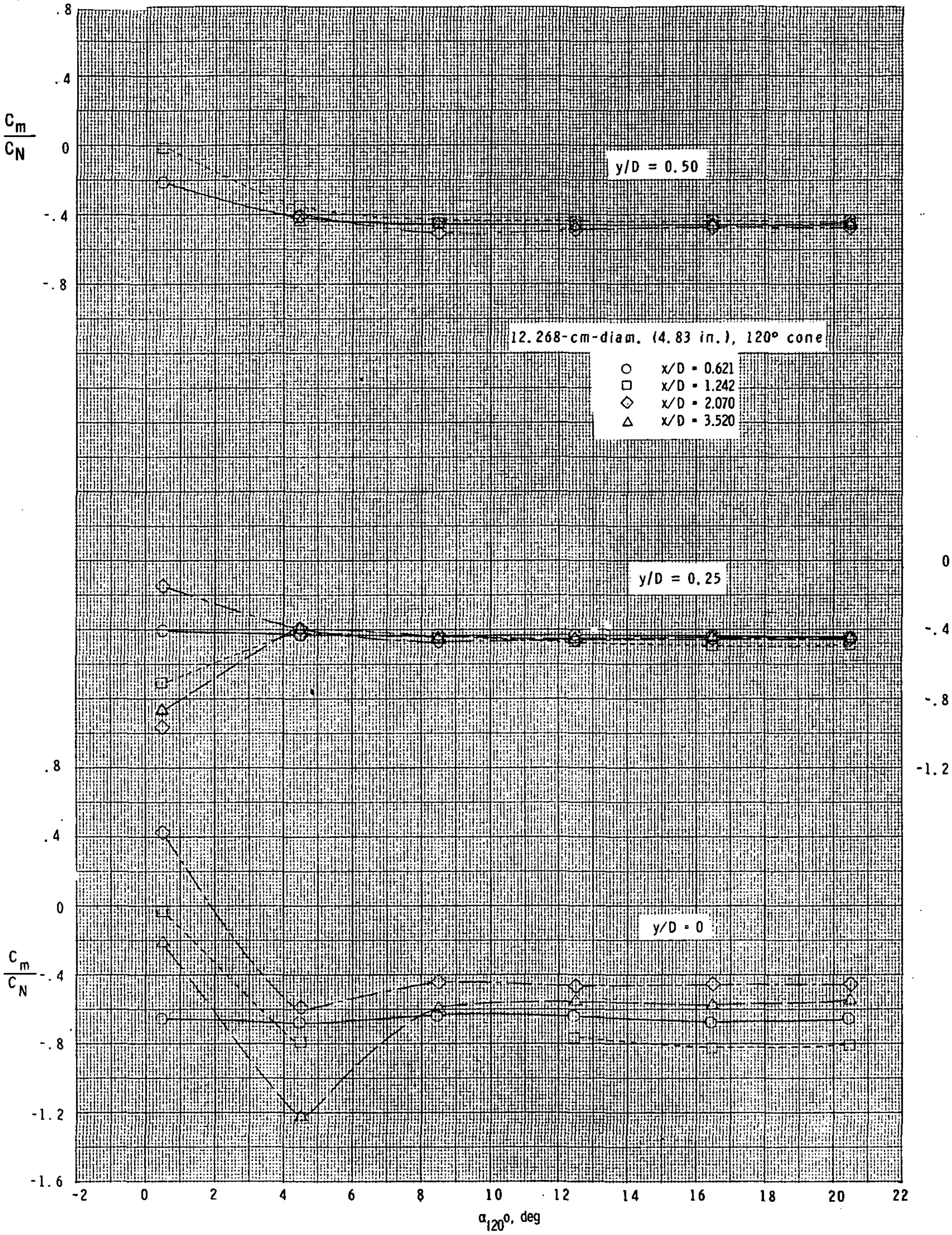

(i) $M_\infty = 2.70$; $\alpha_{20^o} = 5^o$.

Figure 17.- Continued.

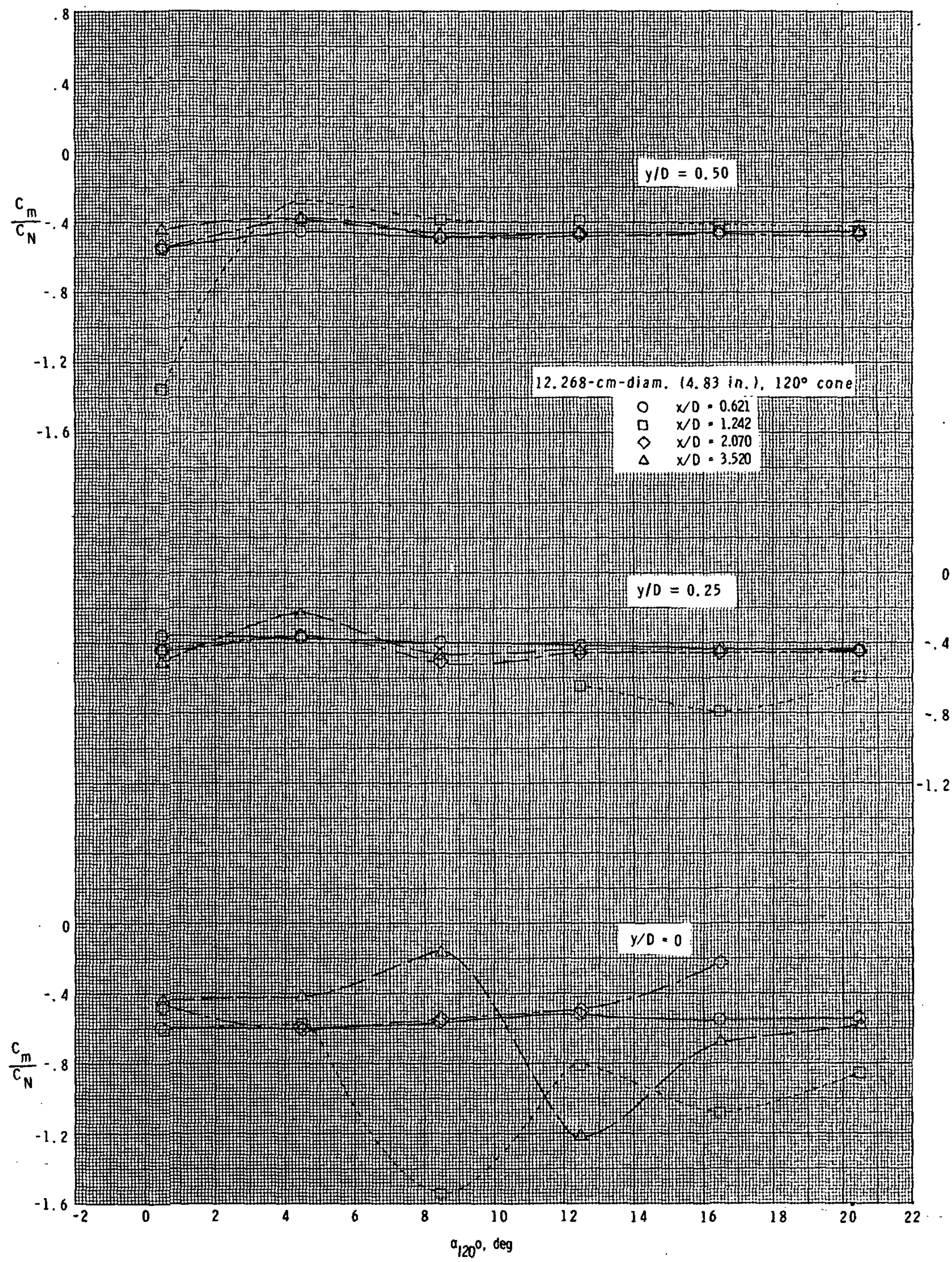

(j) $M_\infty = 2.70$; $\alpha_{20^o} = 15^o$.

Figure 17.- Continued.

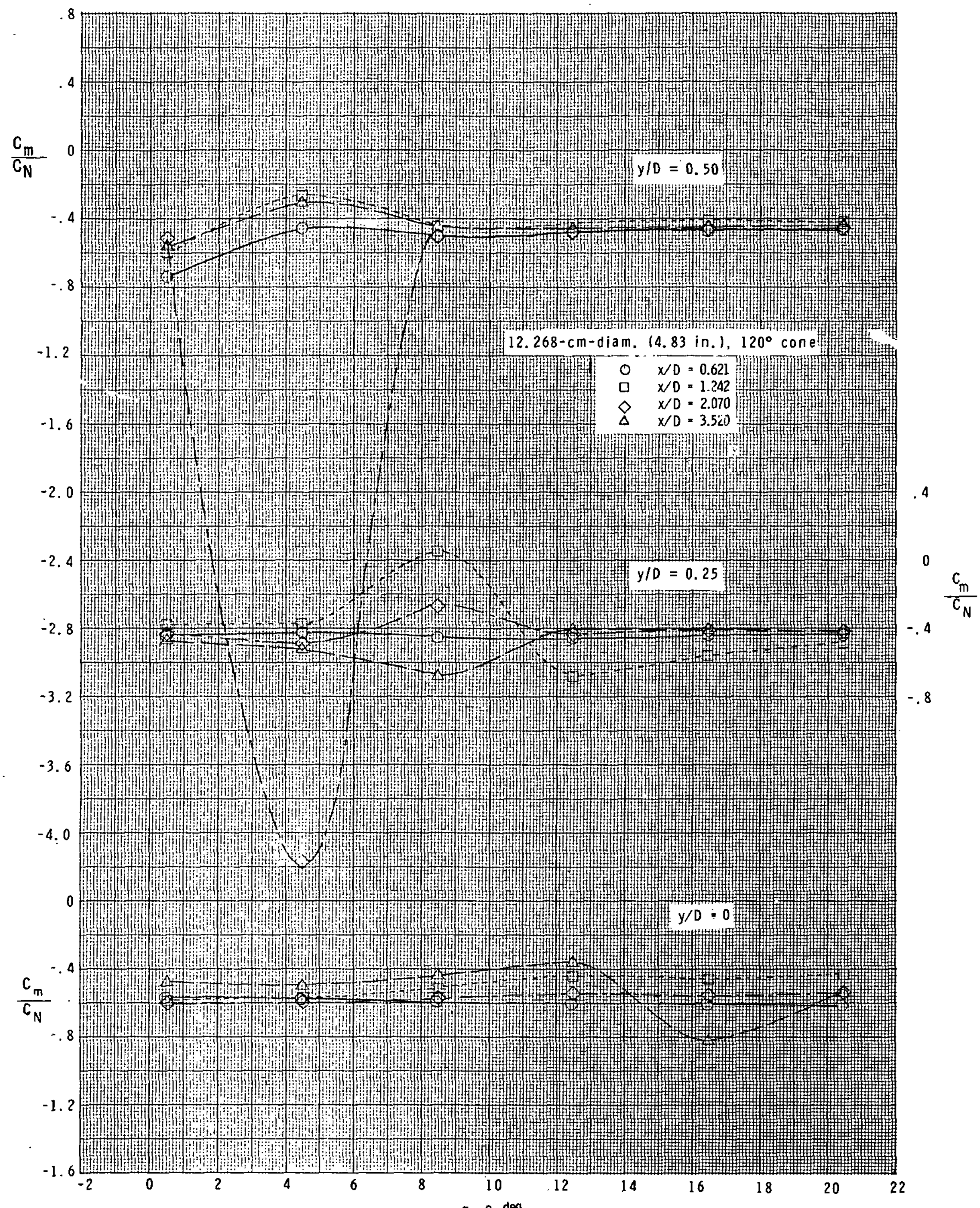

(k) $M_\infty = 2.70$; $\alpha_{20^\circ} = 30^\circ$.

Figure 17.- Continued.

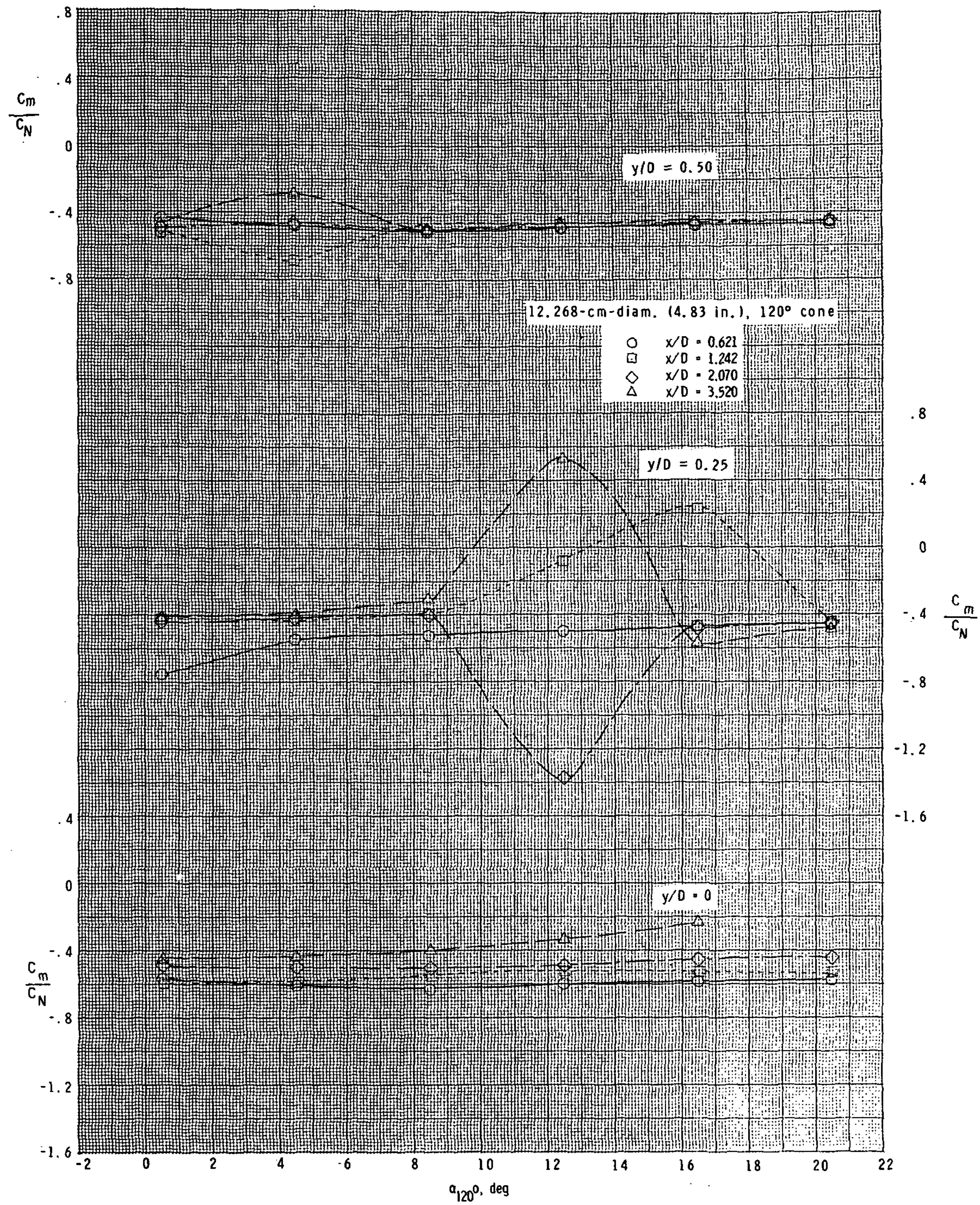

(l) $M_\infty = 2.70$; $\alpha_{20^o} = 45^o$.

Figure 17.- Continued.

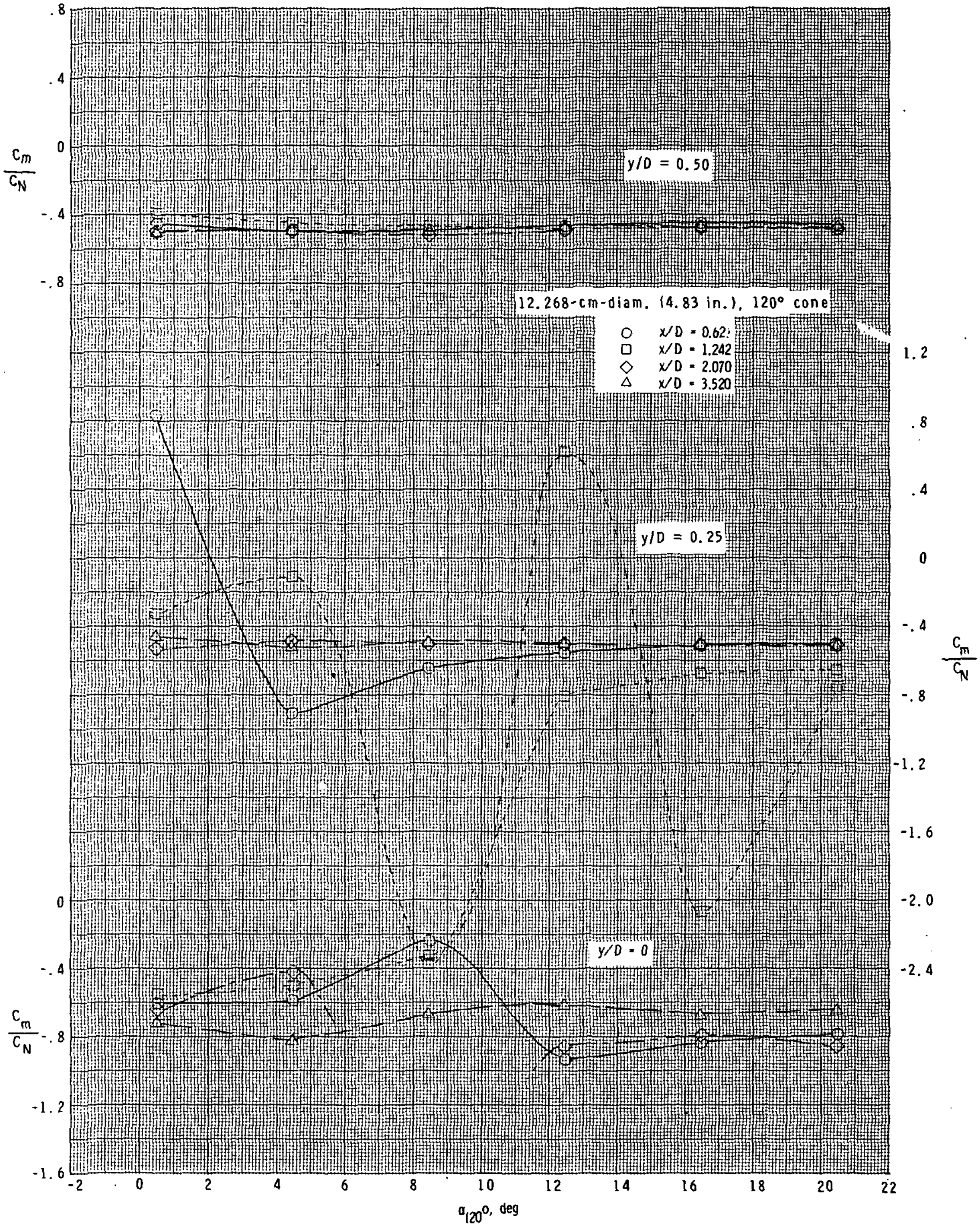

(m) $M_\infty = 2.70$; $\alpha_{20^o} = 90^o$.

Figure 17.- Continued.

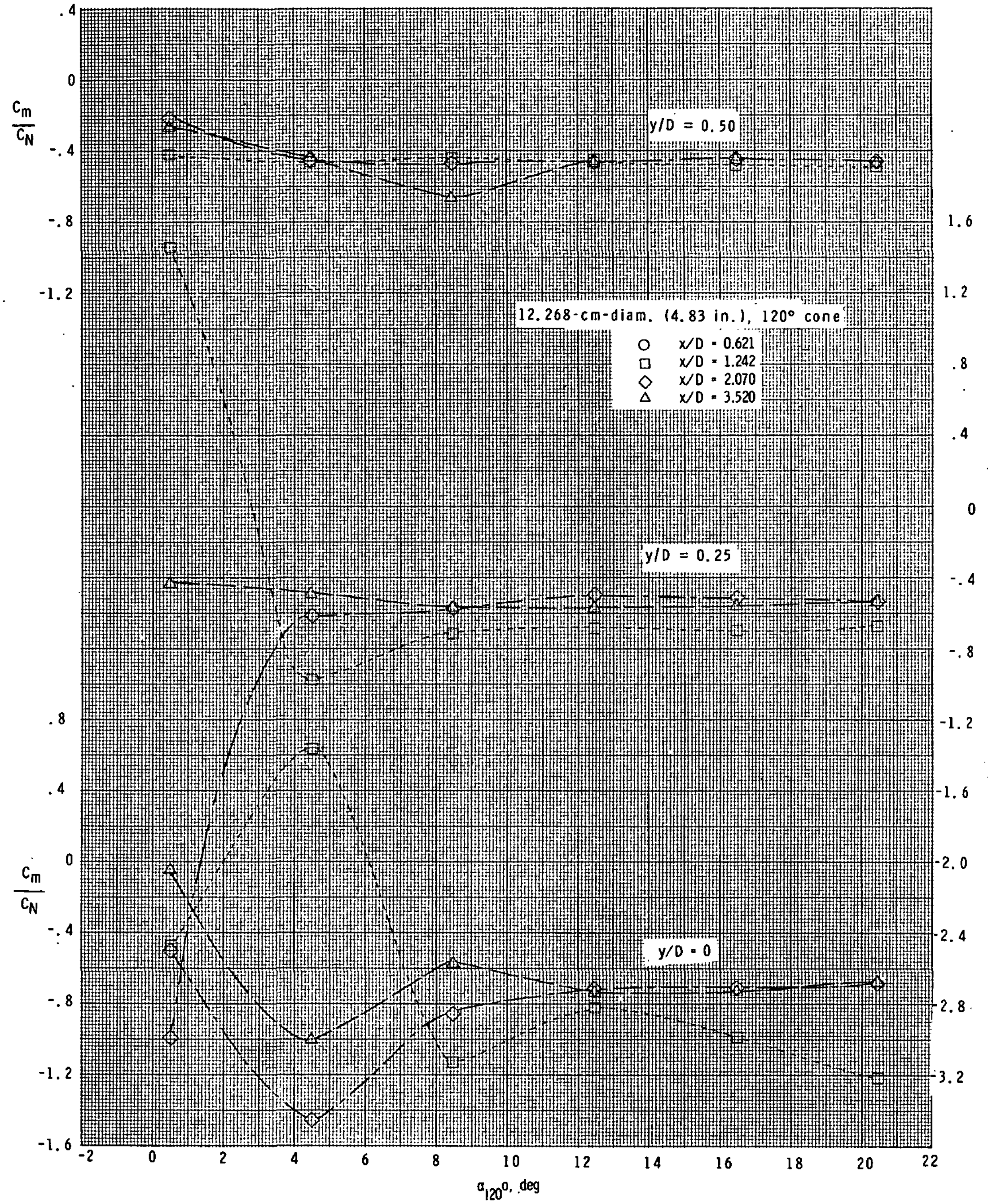

(n) $M_\infty = 2.70$; $\alpha_{20^o} = 180^o$.

Figure 17.- Concluded.

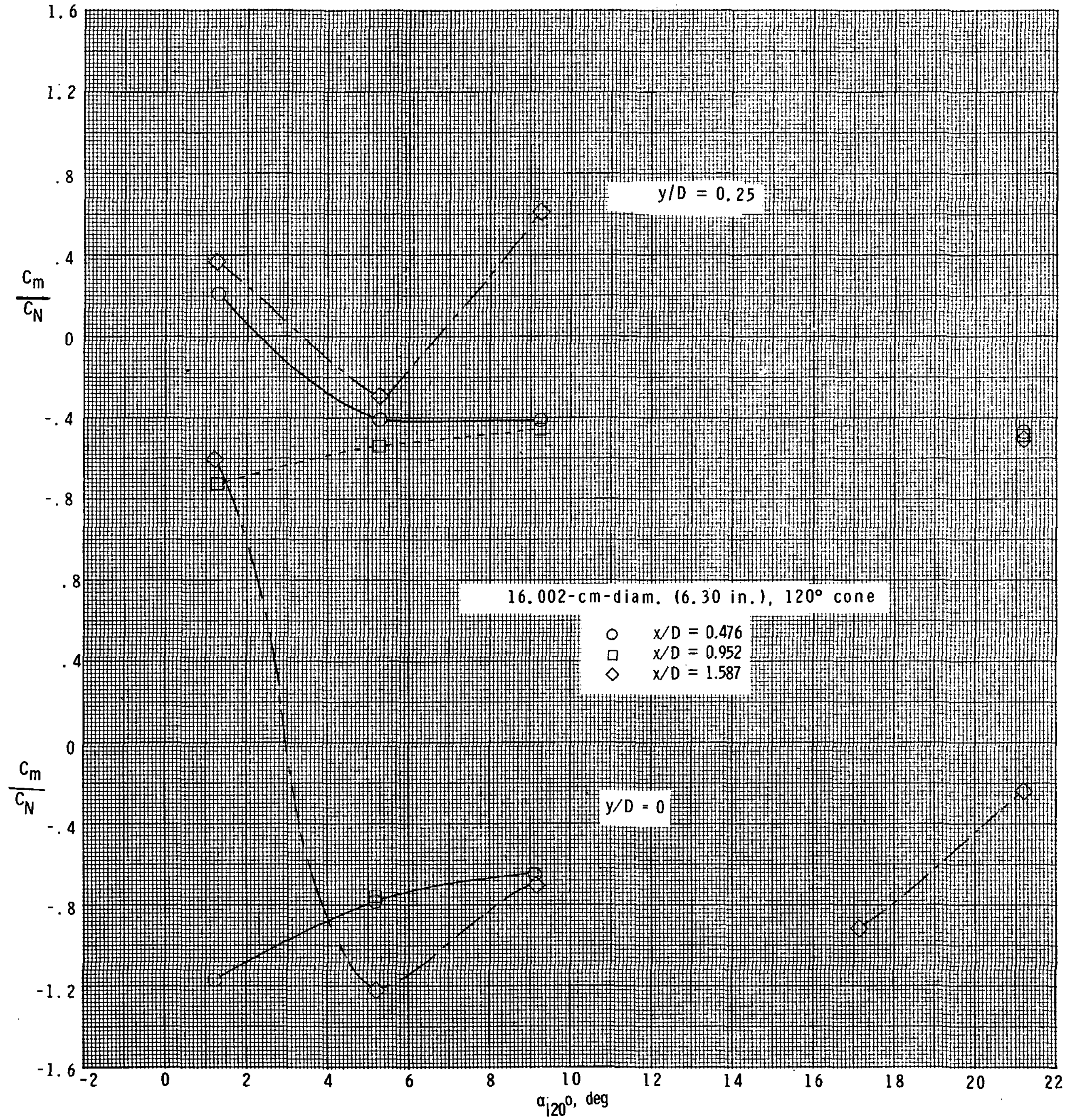

(a) $M_\infty = 2.36$; $\alpha_{20^o} = 0^o$.

Figure 18.- Variation of longitudinal center of pressure C_m/C_N with angle of attack for 16.002-cm-diameter (6.30 in.), 120°-included-angle cone for various x/D locations, y/D locations, and angles of attack of 20°-included-angle cone.

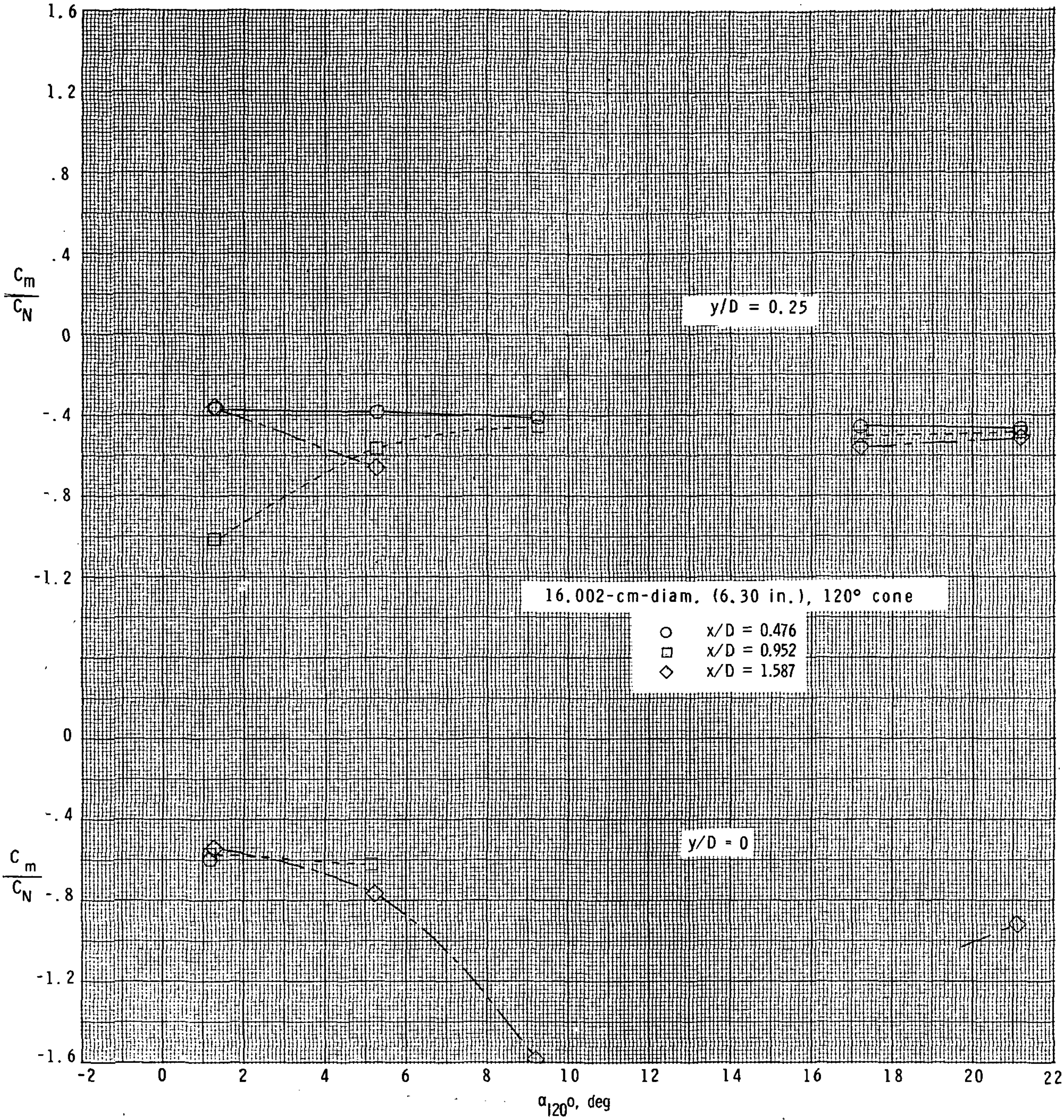

(b) $M_\infty = 2.36$; $\alpha_{20^o} = 5^o$.

Figure 18.- Continued.

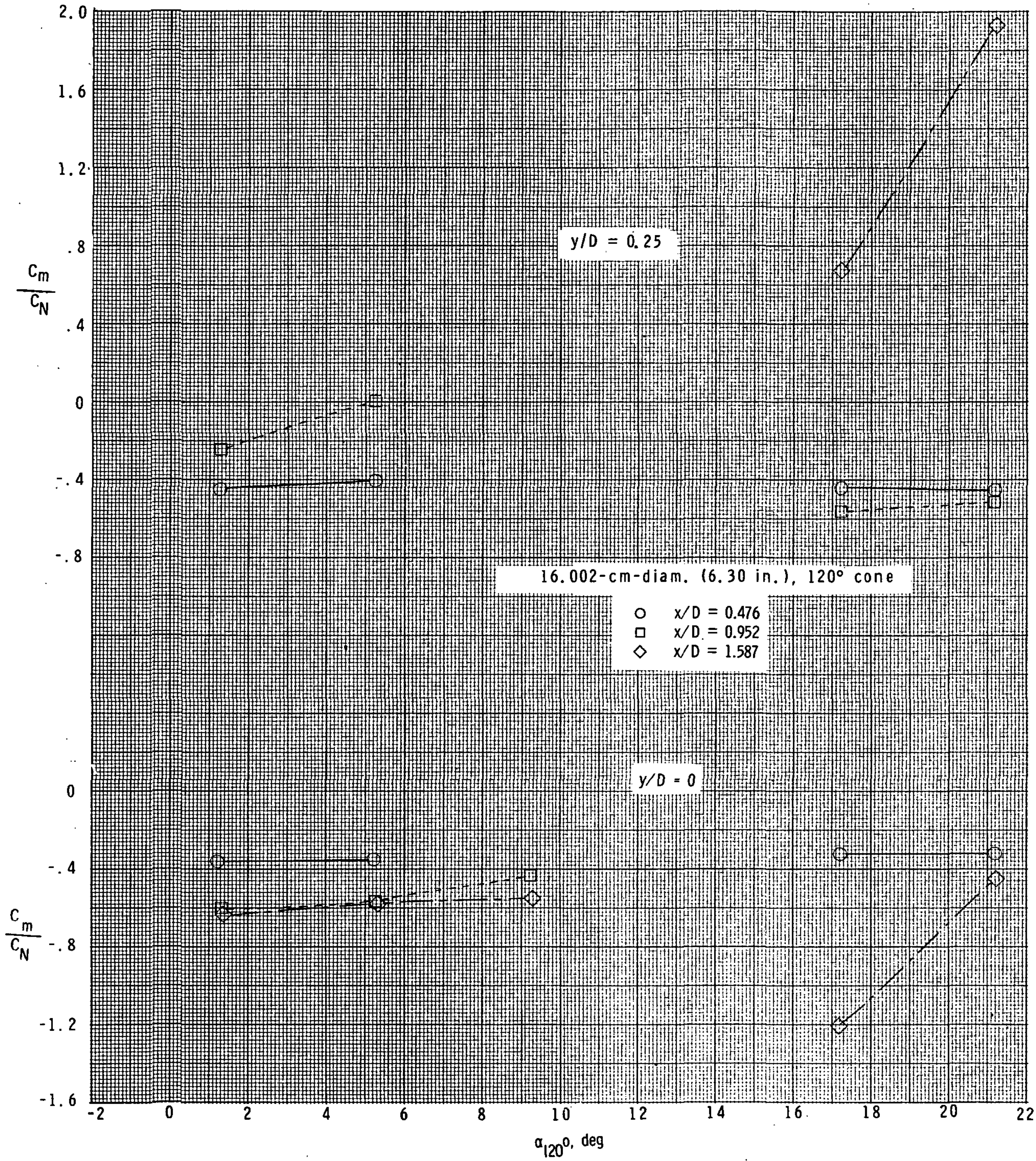

(c) $M_\infty = 2.36$; $\alpha_{20^o} = 30^o$.

Figure 18.- Continued.

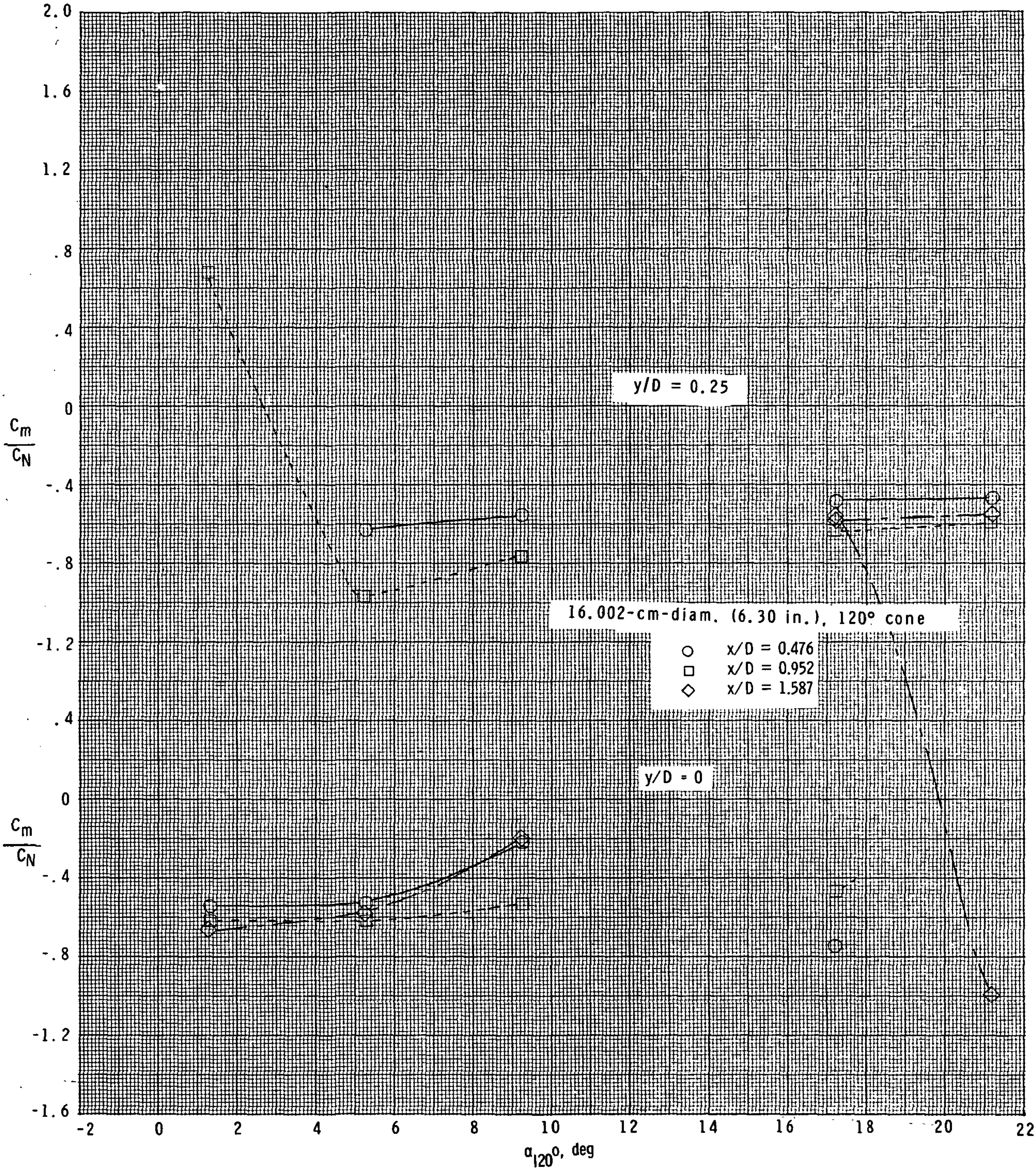

(d) $M_\infty = 2.36$; $\alpha_{20^o} = 90^o$.

Figure 18.- Continued.

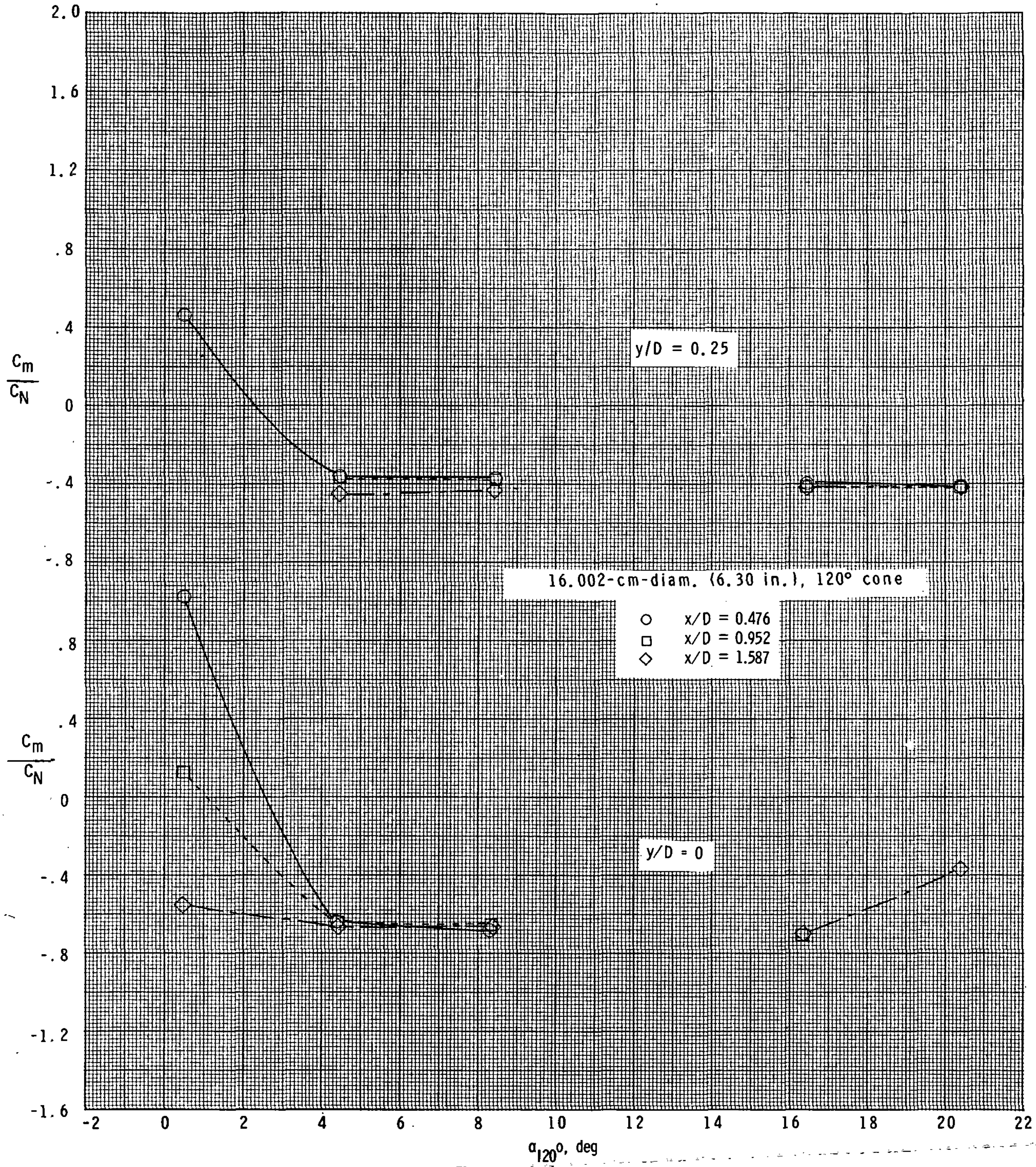

(e) $M_\infty = 2.70$; $\alpha_{20^o} = 0^o$.

Figure 18.- Continued.

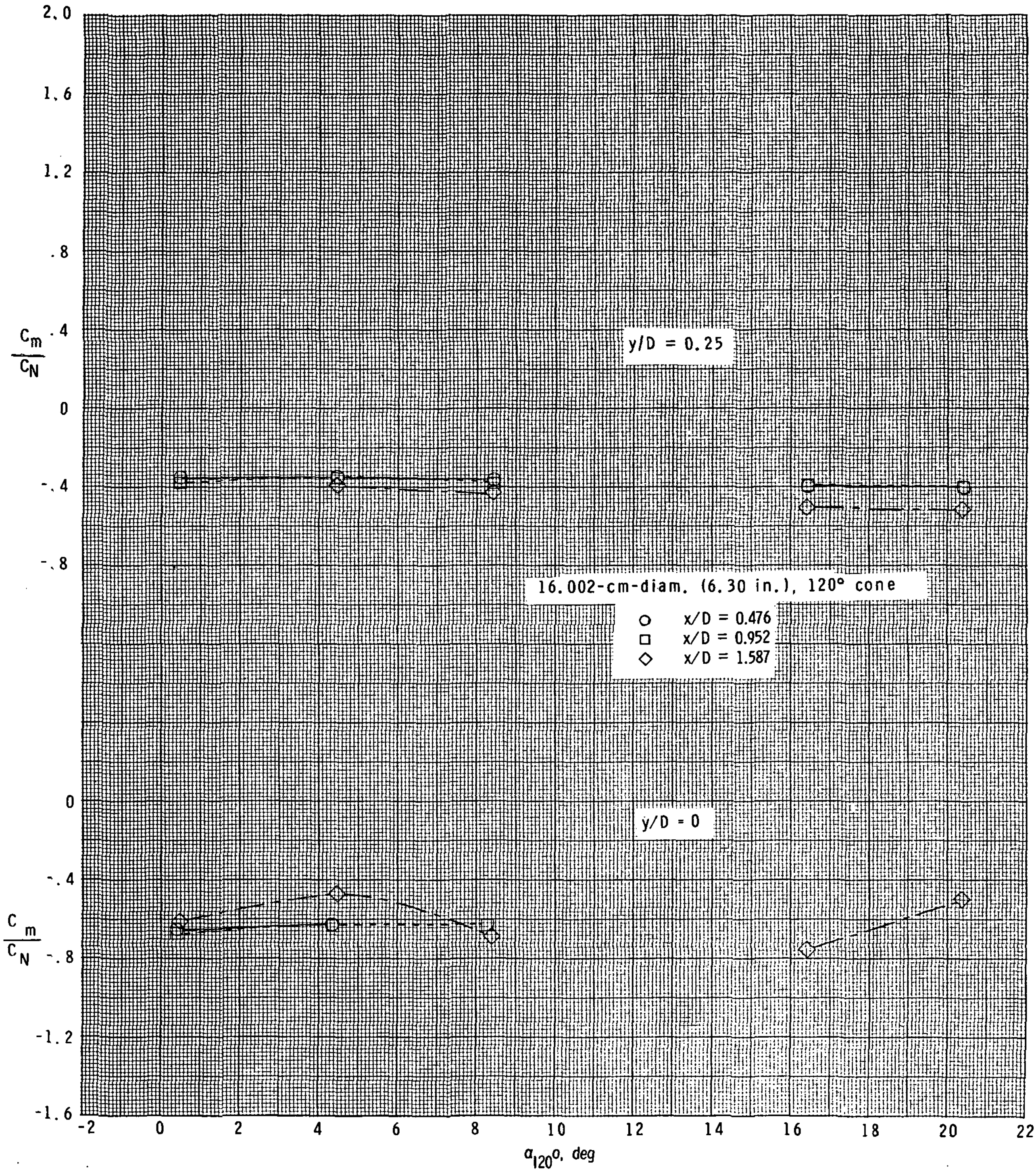

(f) $M_\infty = 2.70$; $\alpha_{20^o} = 5^o$.

Figure 18.- Continued.

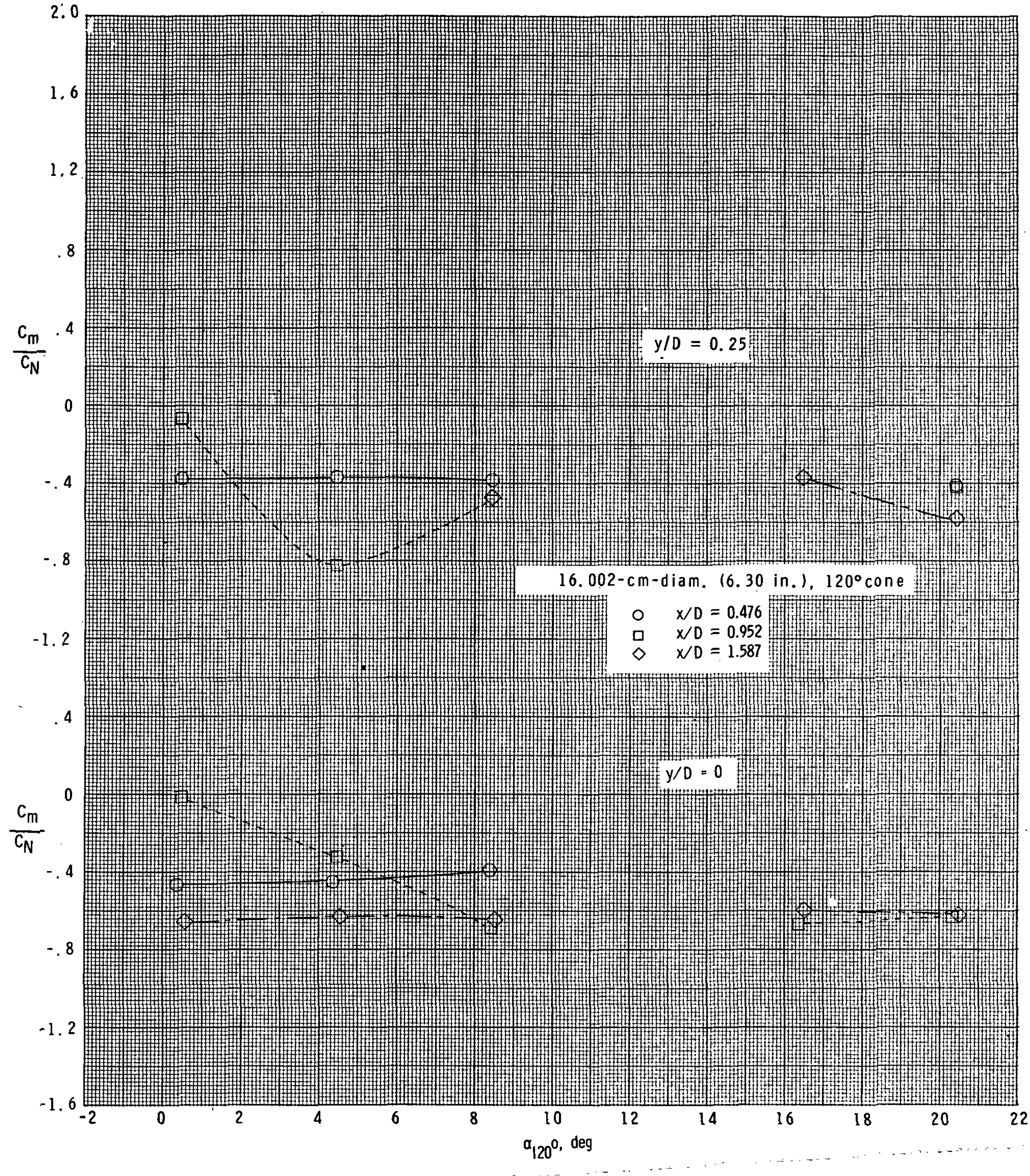

(g) $M_\infty = 2.70$; $\alpha_{20^o} = 30^o$.

Figure 18.- Continued.

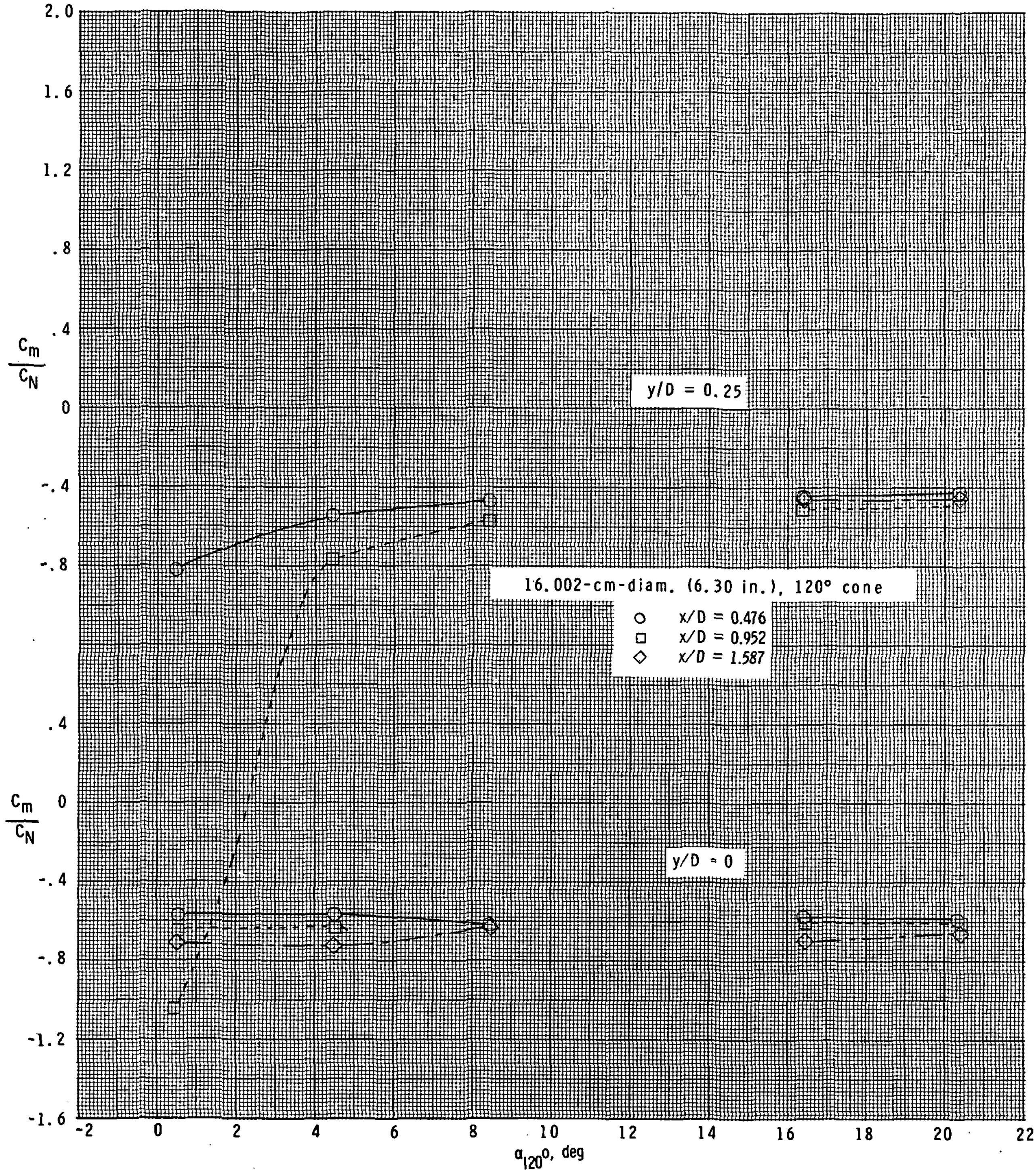

(h) $M_\infty = 2.70$; $\alpha_{20^o} = 90^o$.

Figure 18.- Concluded.

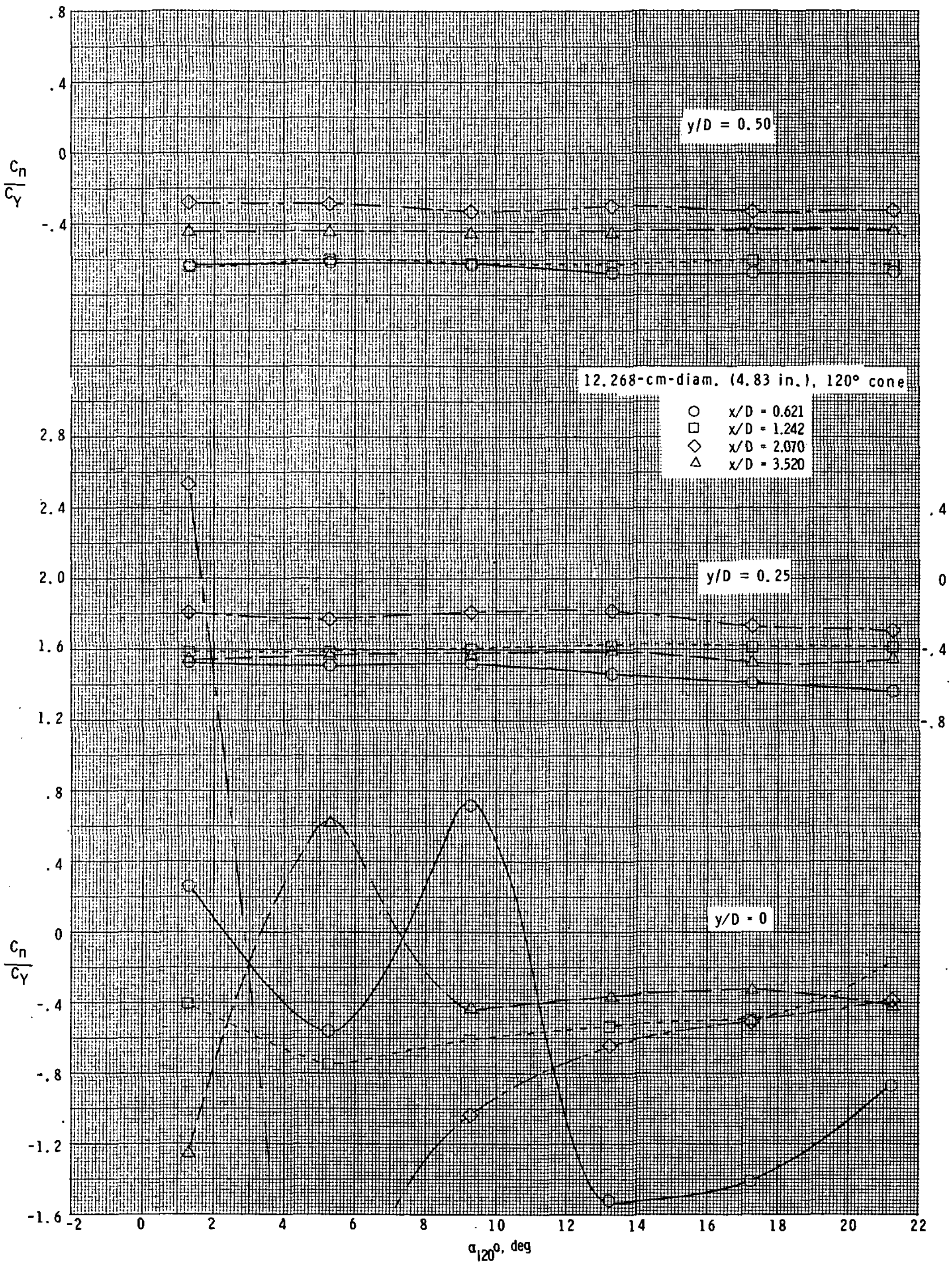

(a) $M_\infty = 2.36$; $\alpha_{20^o} = 0^o$.

Figure 19.- Variation of lateral center of pressure C_n/C_Y with angle of attack for 12.268-cm-diameter (4.83 in.), 120^o-included-angle cone for various x/D locations, y/D locations, and angles of attack of 20^o-included-angle cone.

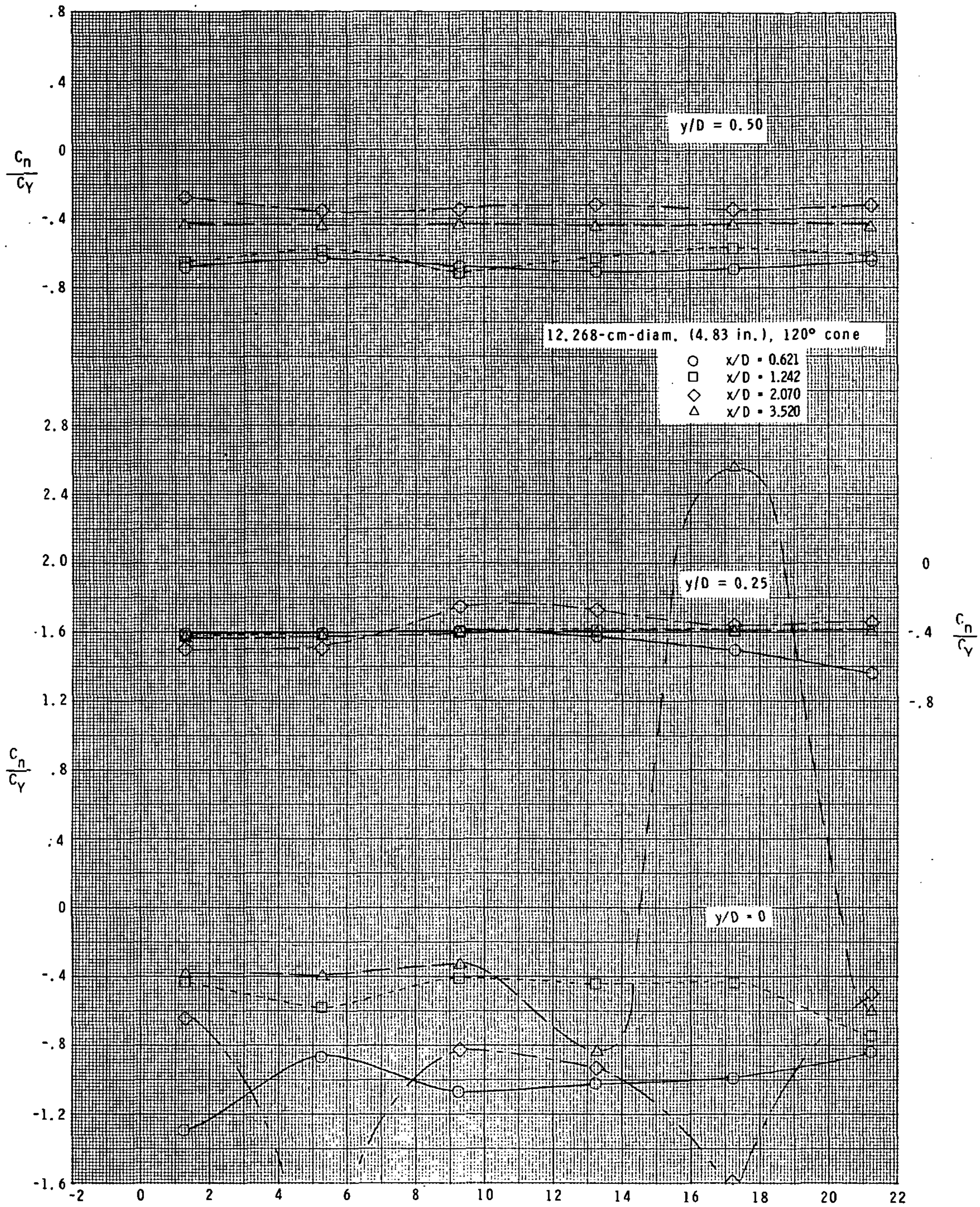

(b) $M_\infty = 2.36$; $\alpha_{20^o} = 5^o$.

Figure 19.- Continued.

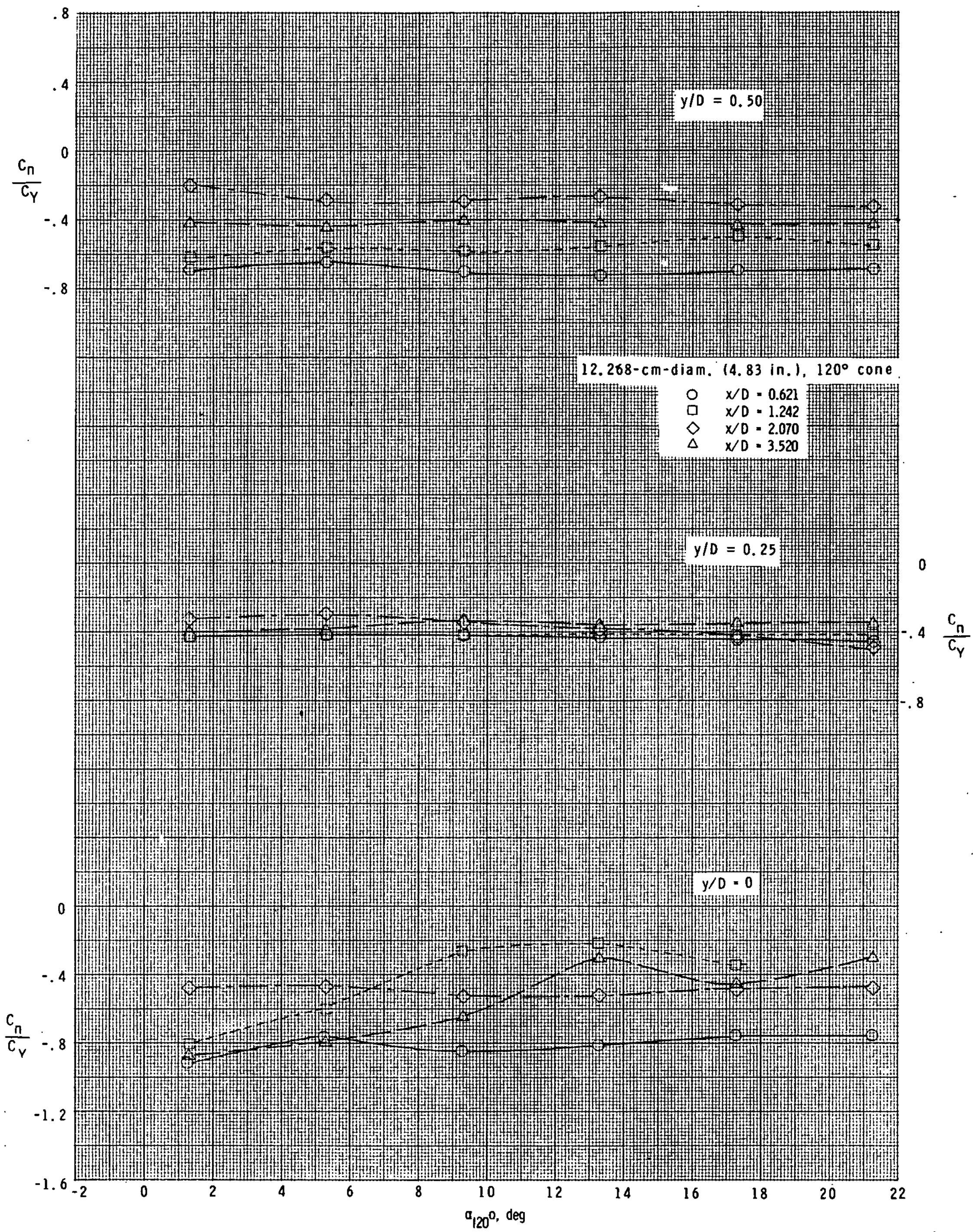

(c) $M_\infty = 2.36$; $\alpha_{20^o} = 15^o$.

Figure 19.- Continued.

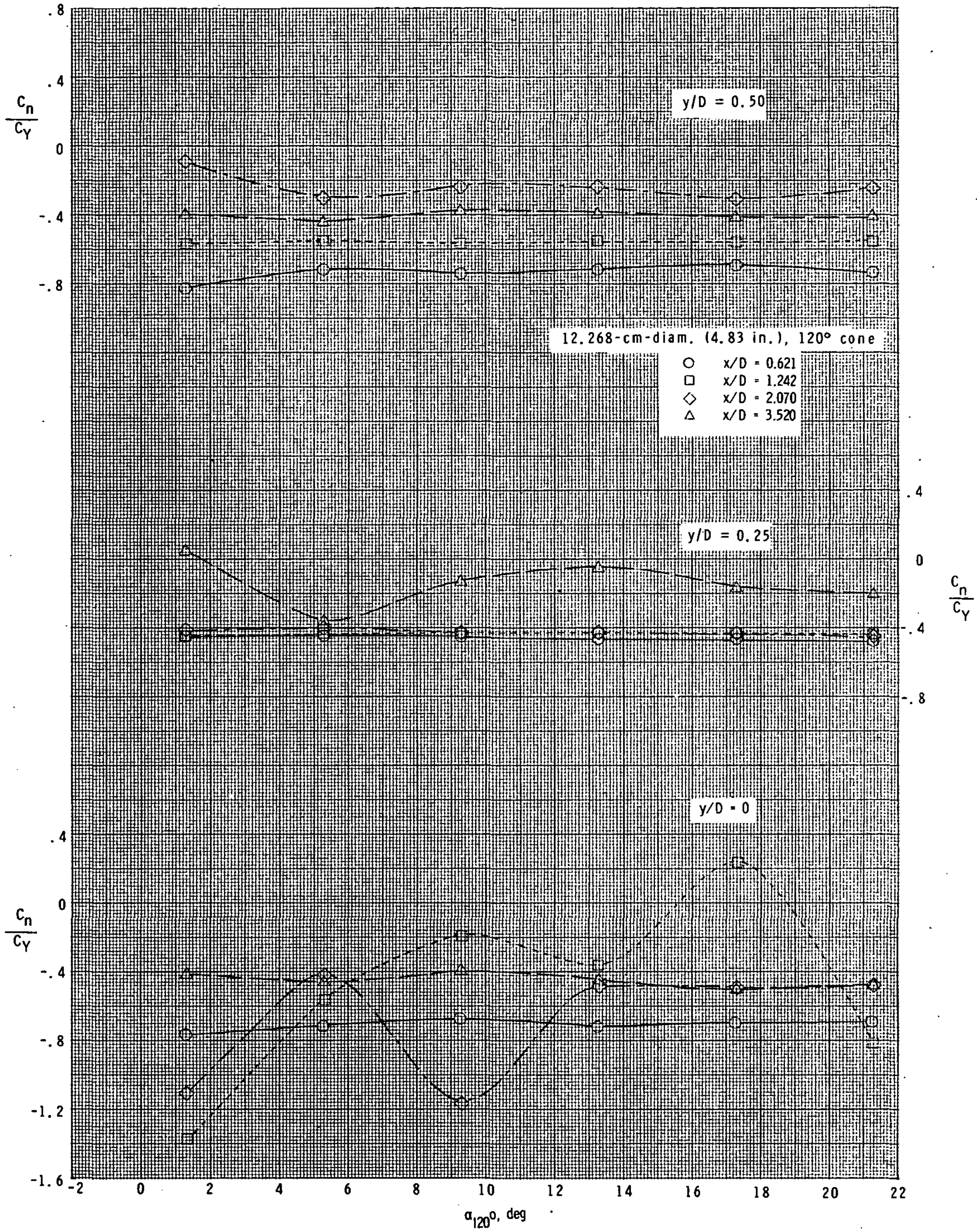

(d) $M_\infty = 2.36$; $\alpha_{20^o} = 30^o$.

Figure 19.- Continued.

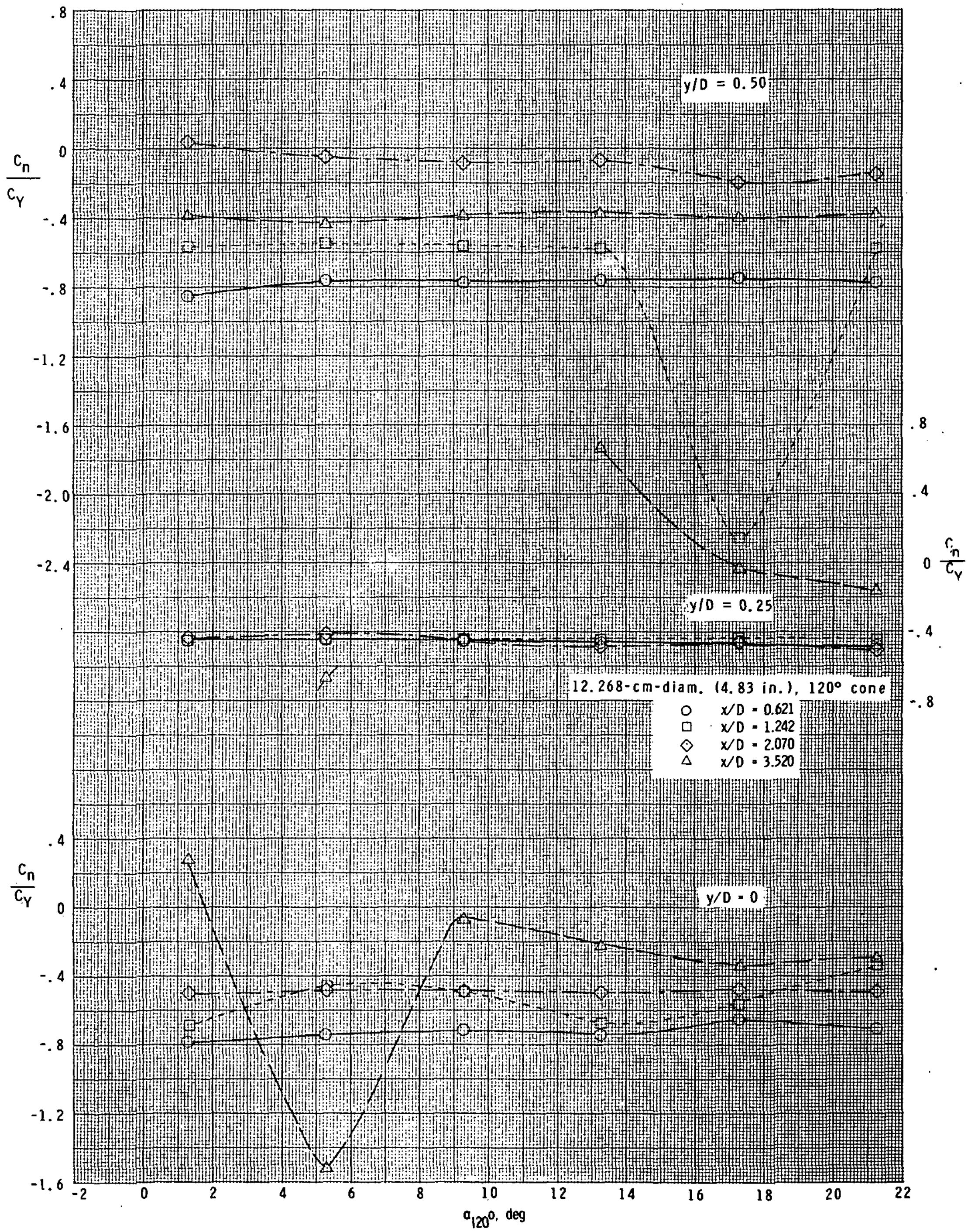

(e) $M_\infty = 2.36$; $\alpha_{20^o} = 45^o$.

Figure 19.- Continued.

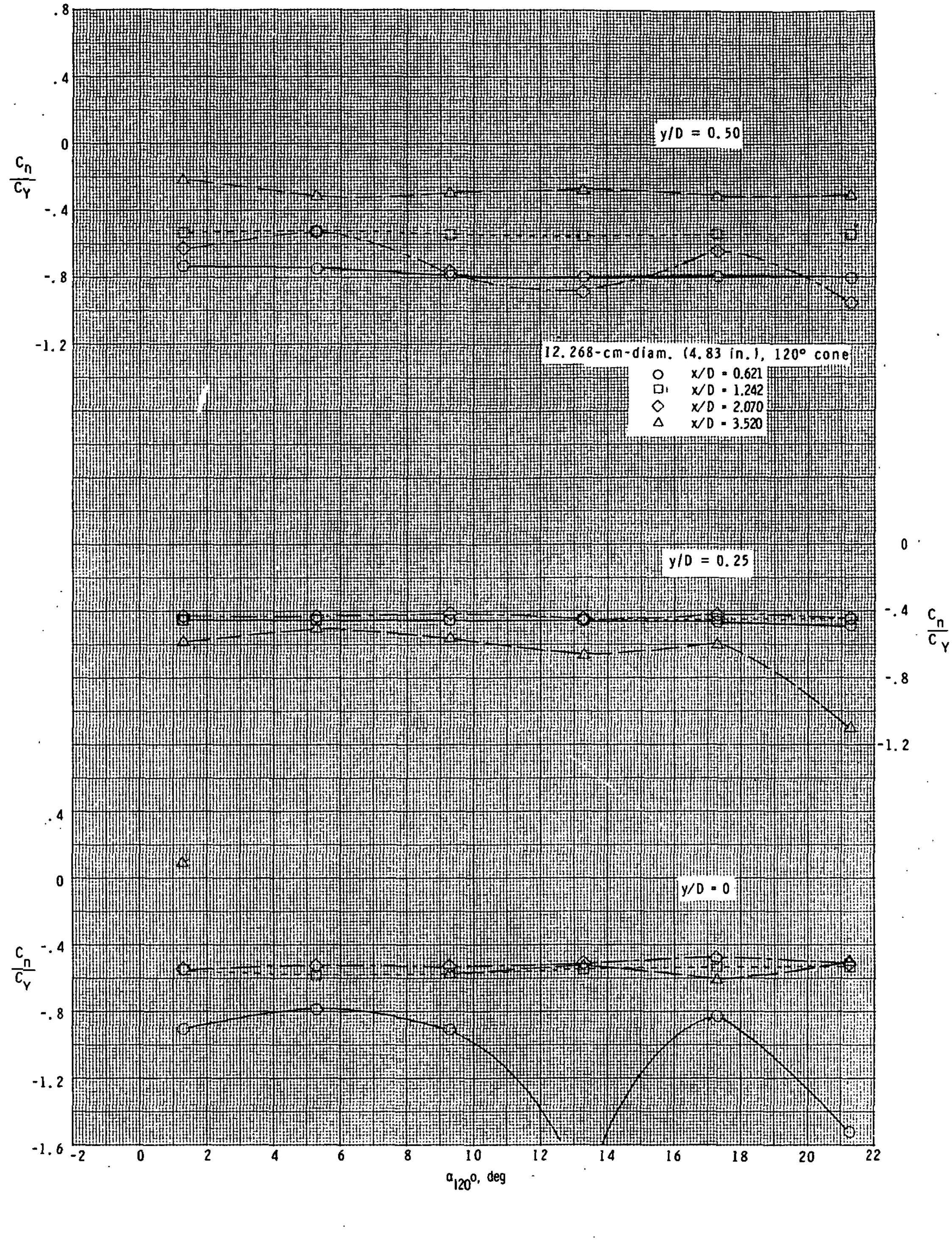

(f) $M_\infty = 2.36$; $\alpha_{20^o} = 90^o$.

Figure 19.- Continued.

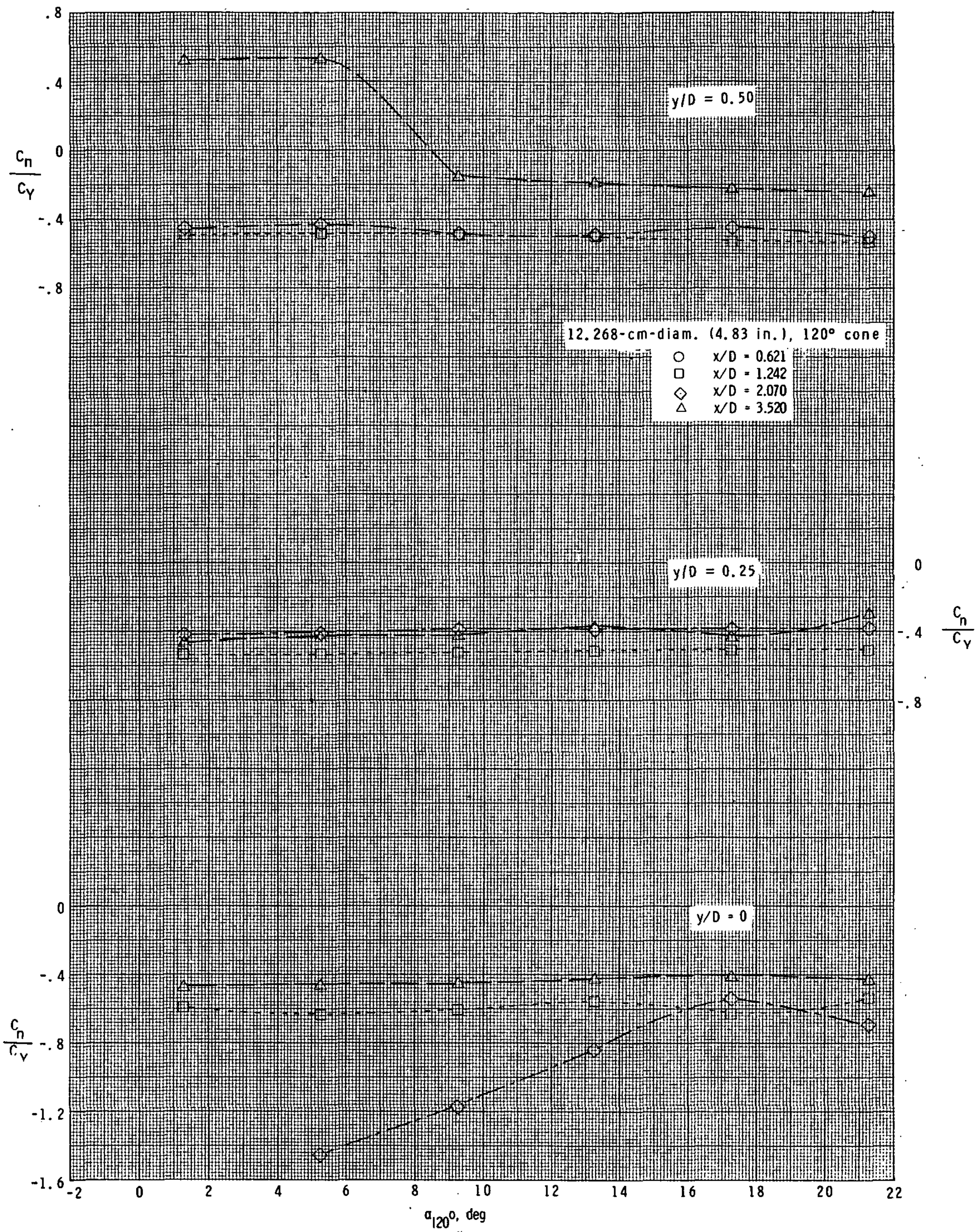

(g) $M_\infty = 2.36$; $\alpha_{20^o} = 180^o$.

Figure 19.- Continued.

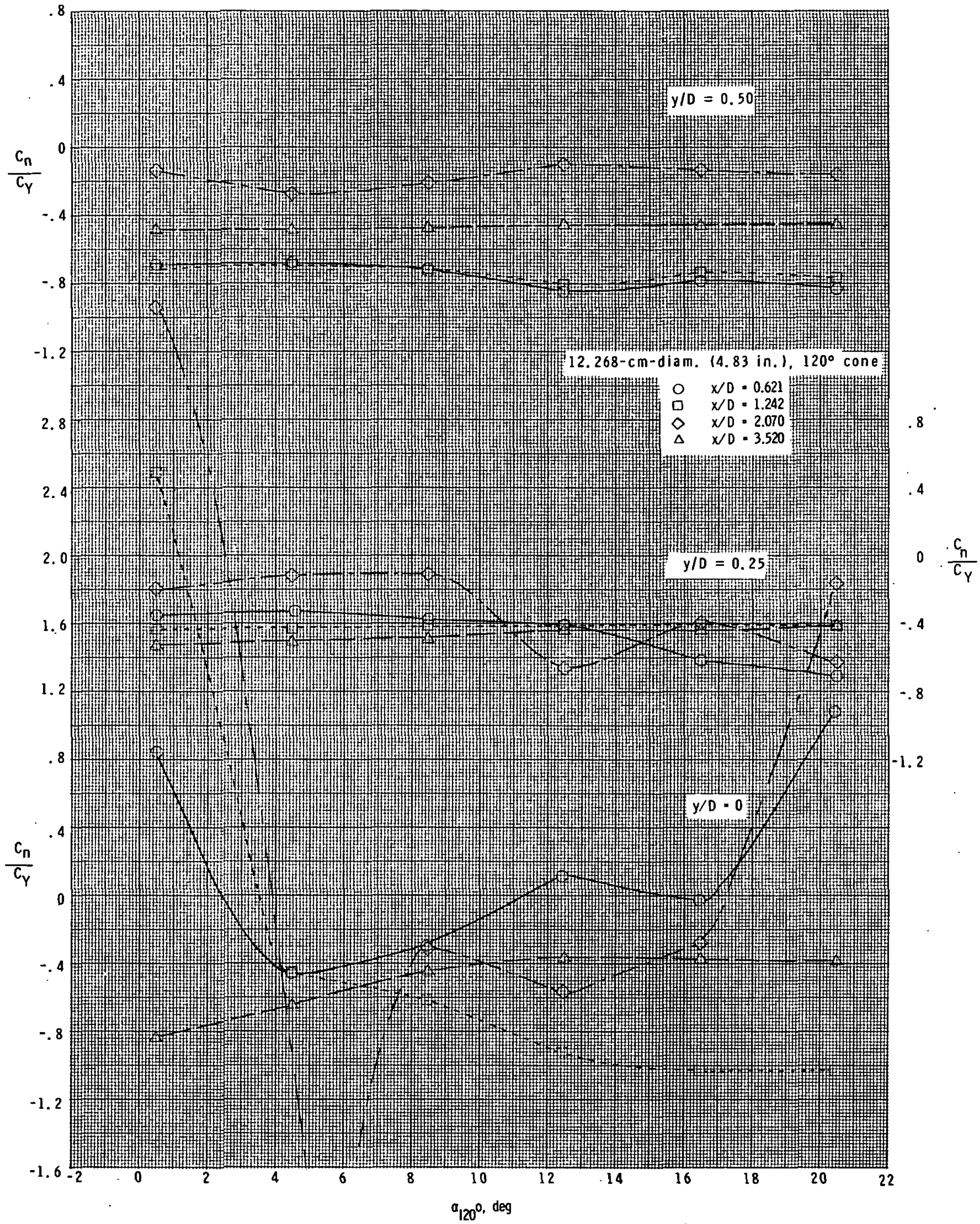

(h) $M_\infty = 2.70$; $\alpha_{20^o} = 0^o$.

Figure 19.- Continued.

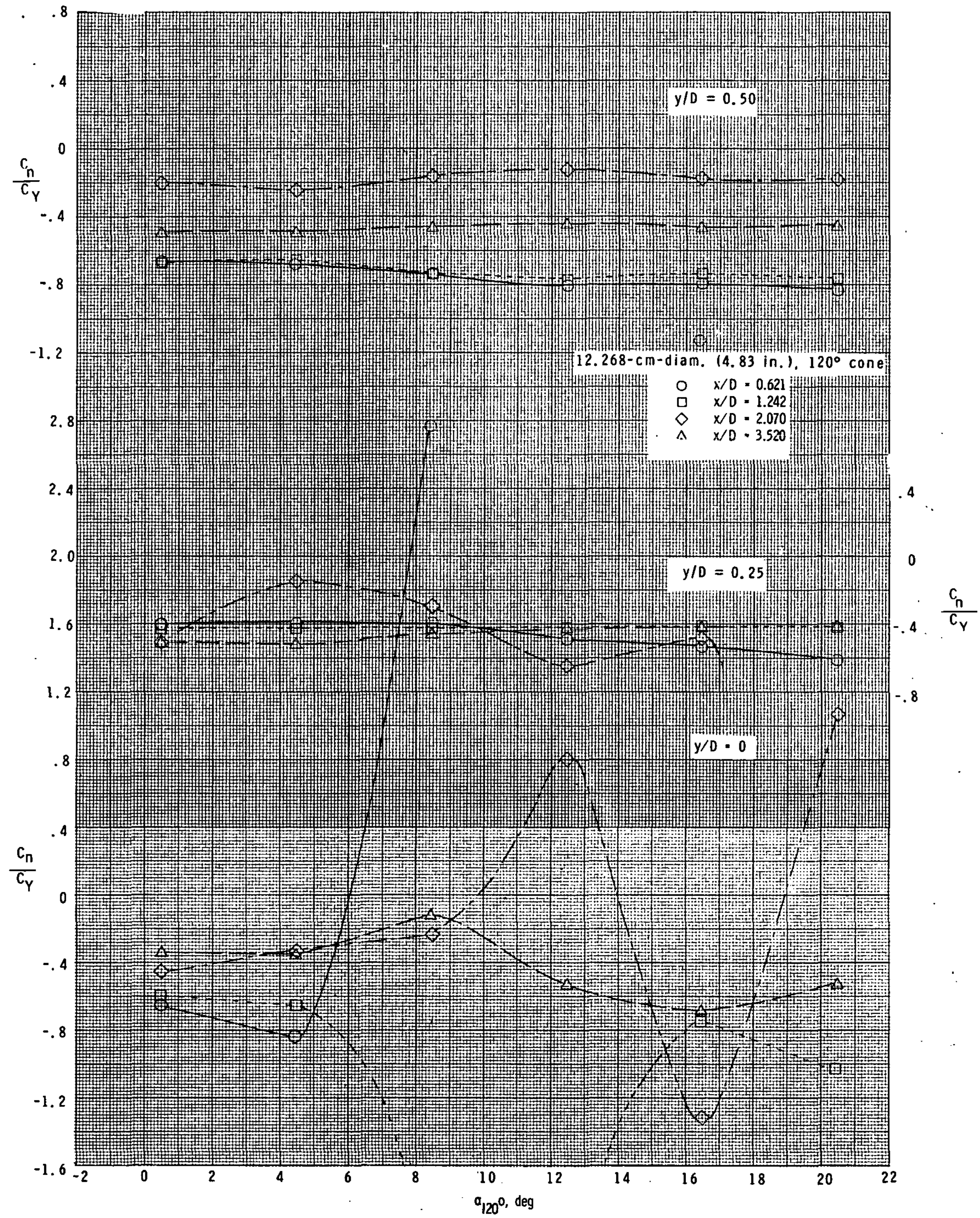

(i) $M_\infty = 2.70$; $\alpha_{20^o} = 5^o$.

Figure 19.- Continued.

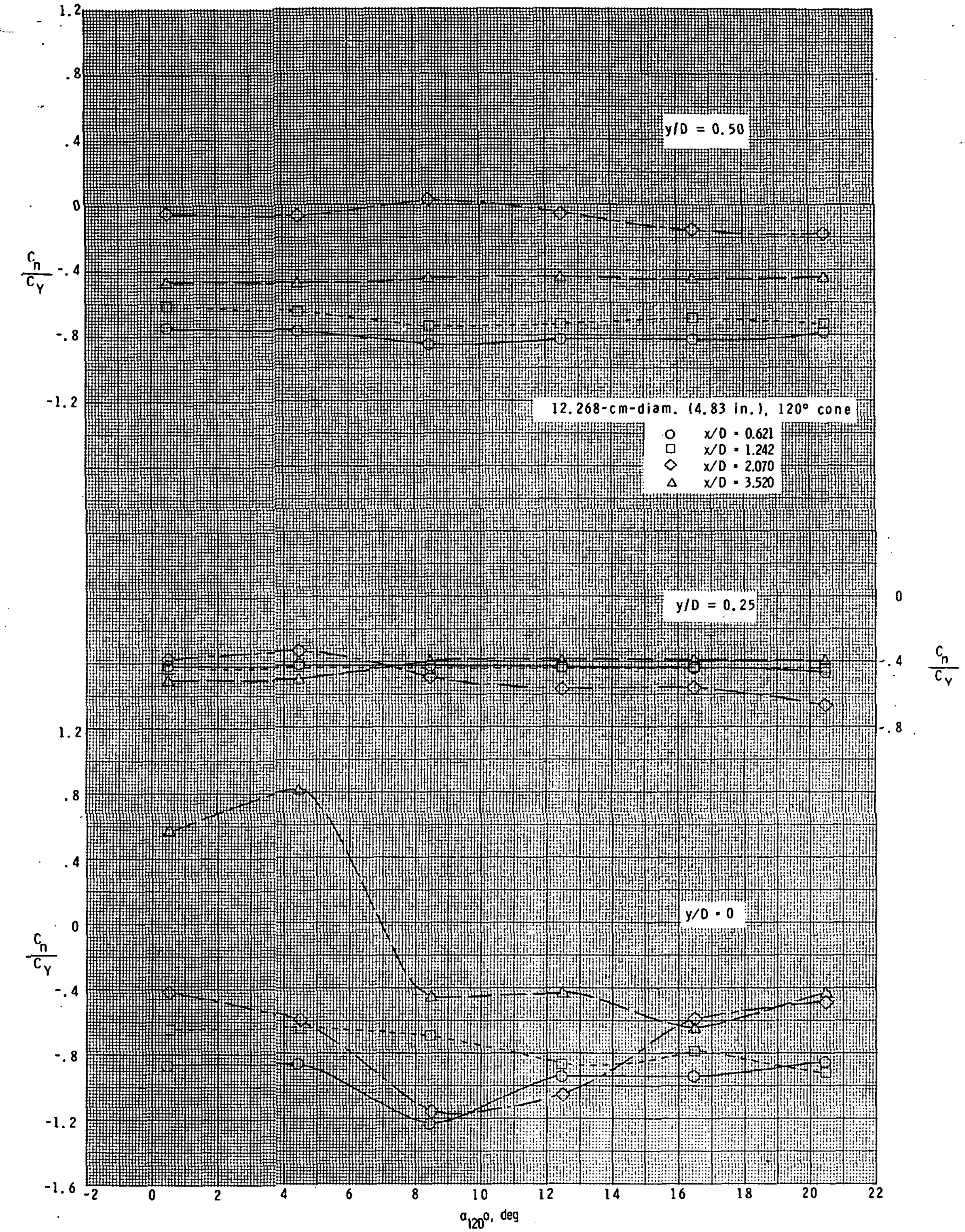

(j) $M_\infty = 2.70$; $\alpha_{20^o} = 15^o$.

Figure 19.- Continued.

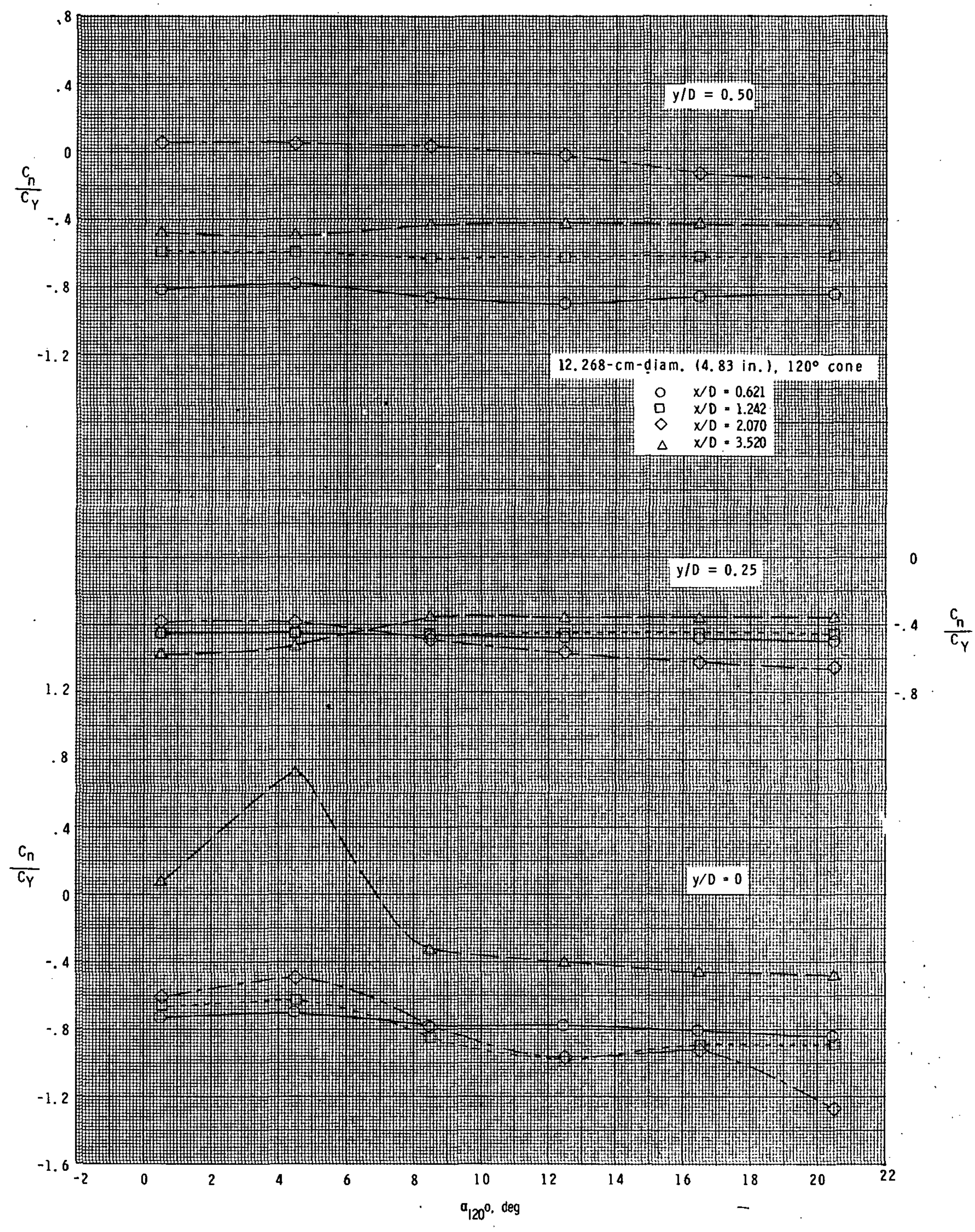

(k) $M_\infty = 2.70$; $\alpha_{20^o} = 30^o$.

Figure 19.- Continued.

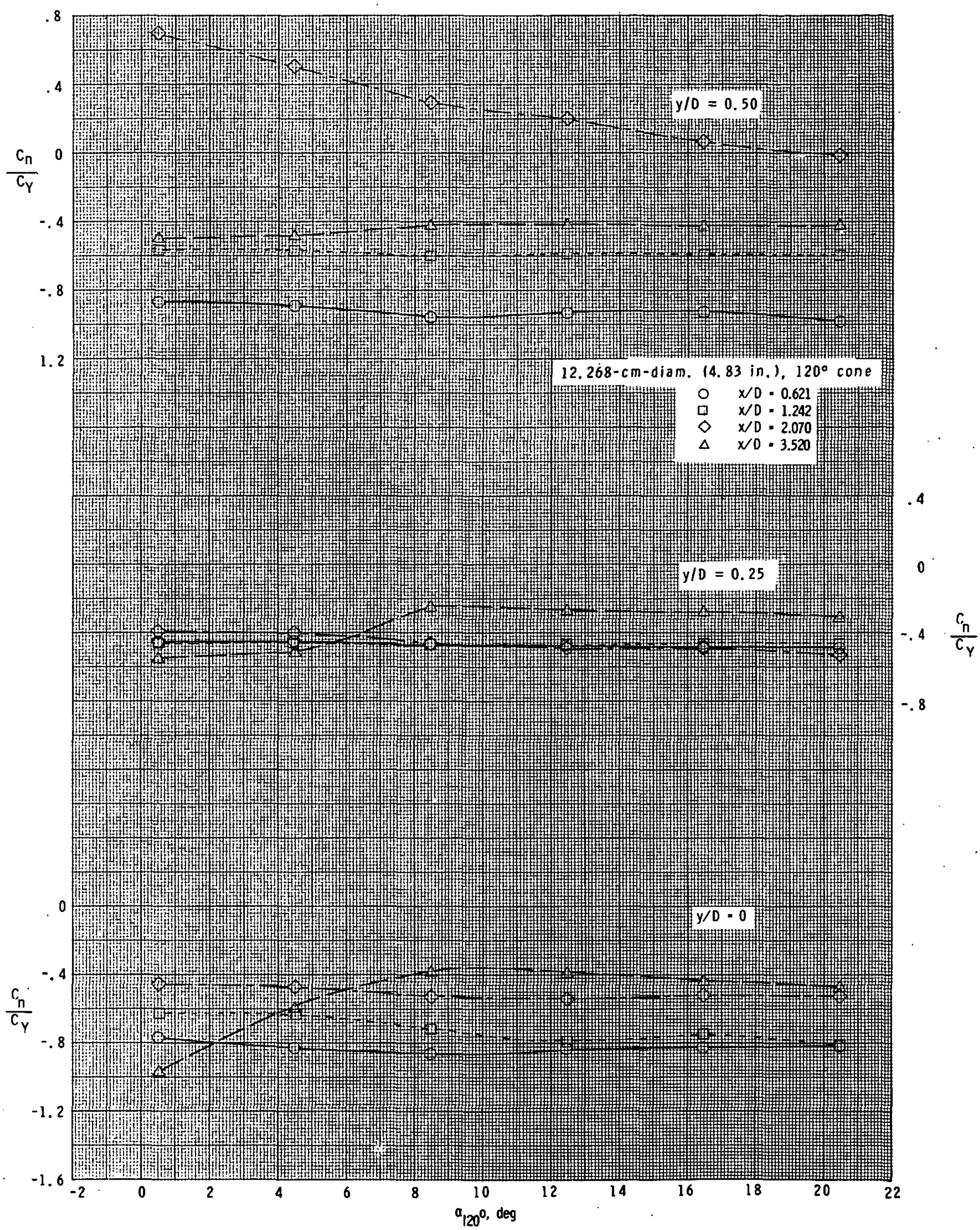

(l) $M_\infty = 2.70$; $\alpha_{20^\circ} = 45^\circ$.

Figure 19.- Continued.

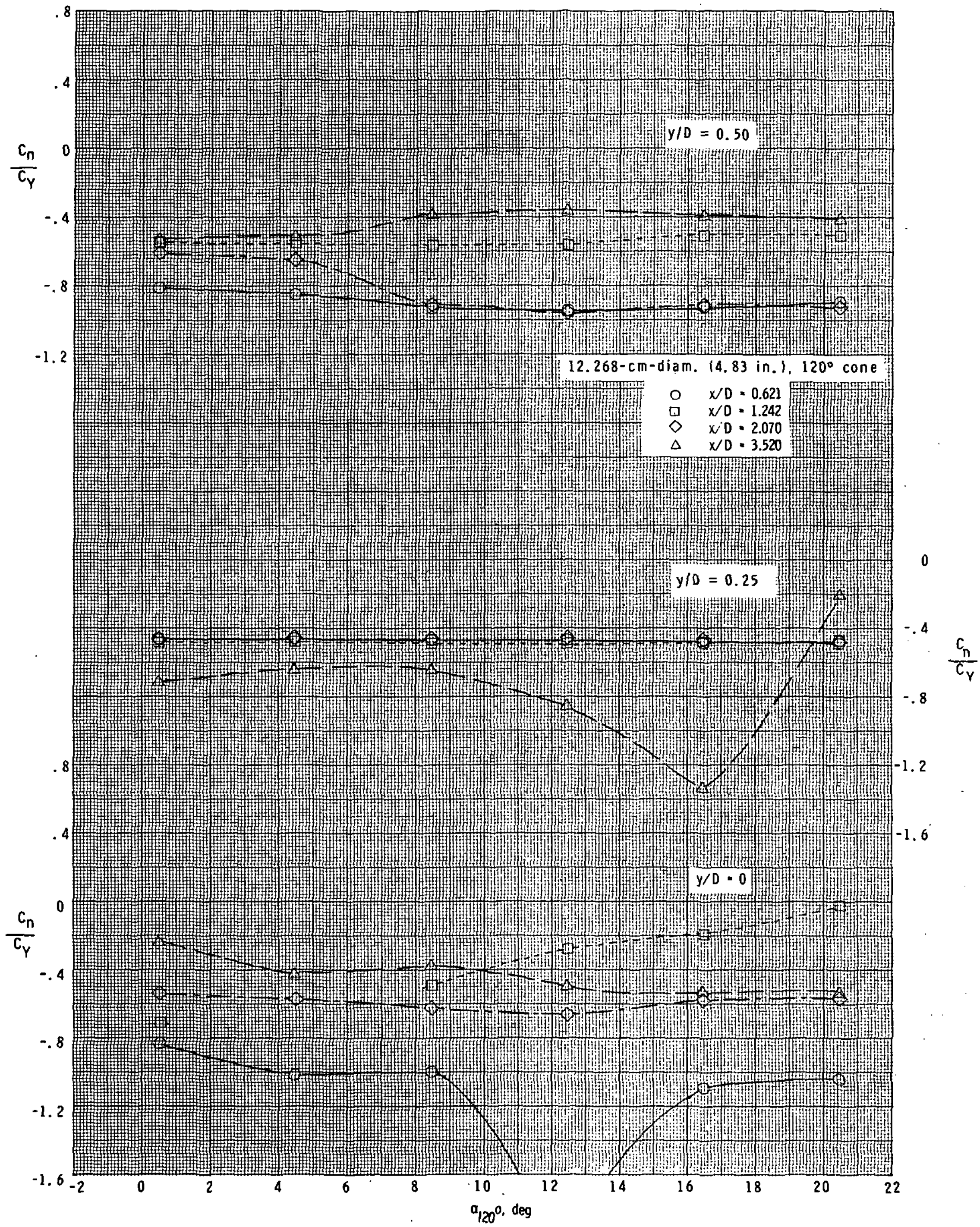

(m) $M_\infty = 2.70$; $\alpha_{20^o} = 90^o$.

Figure 19.- Continued.

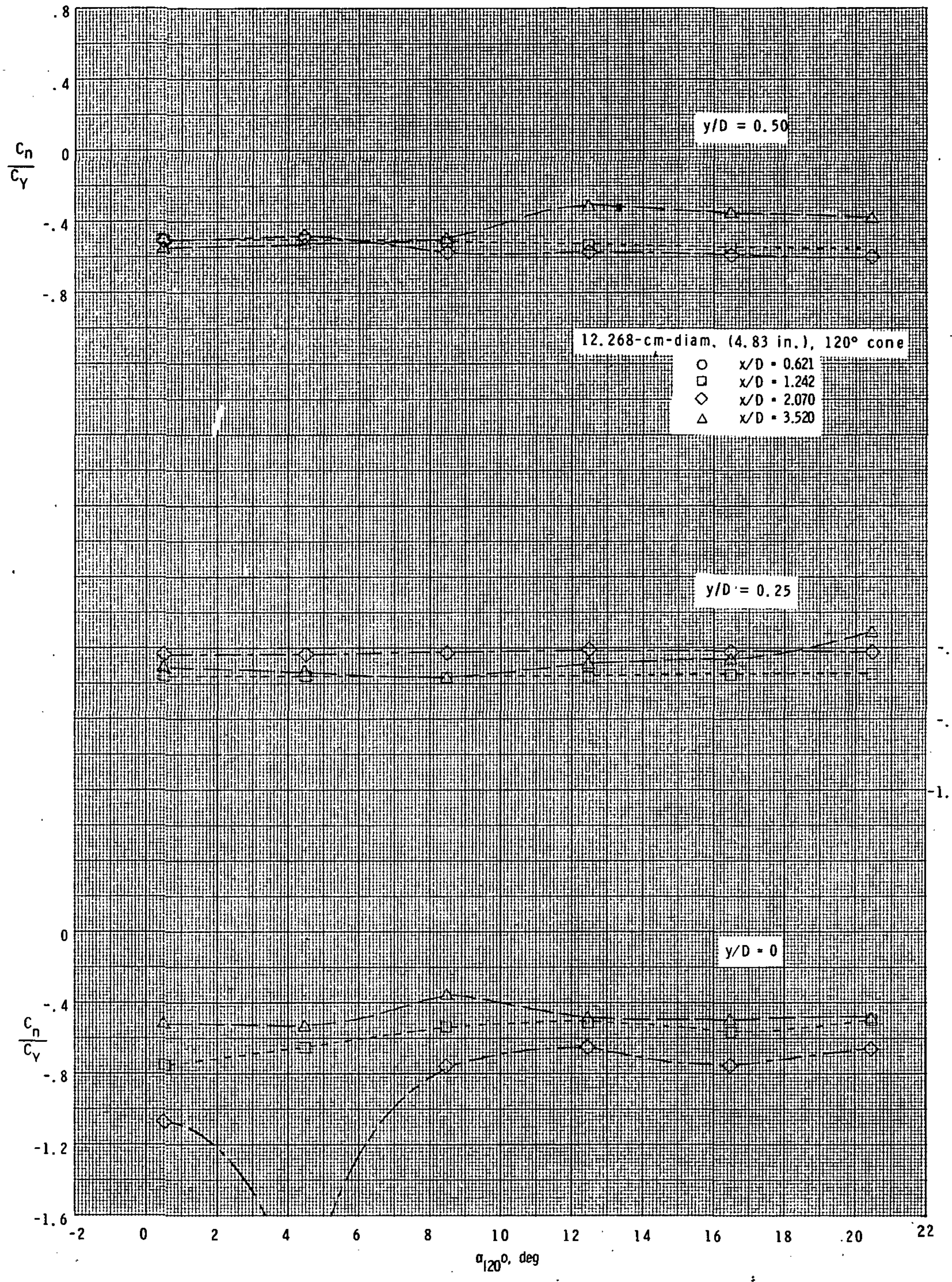

(n) $M_\infty = 2.70$; $\alpha_{20^o} = 180^o$.

Figure 19.- Concluded.

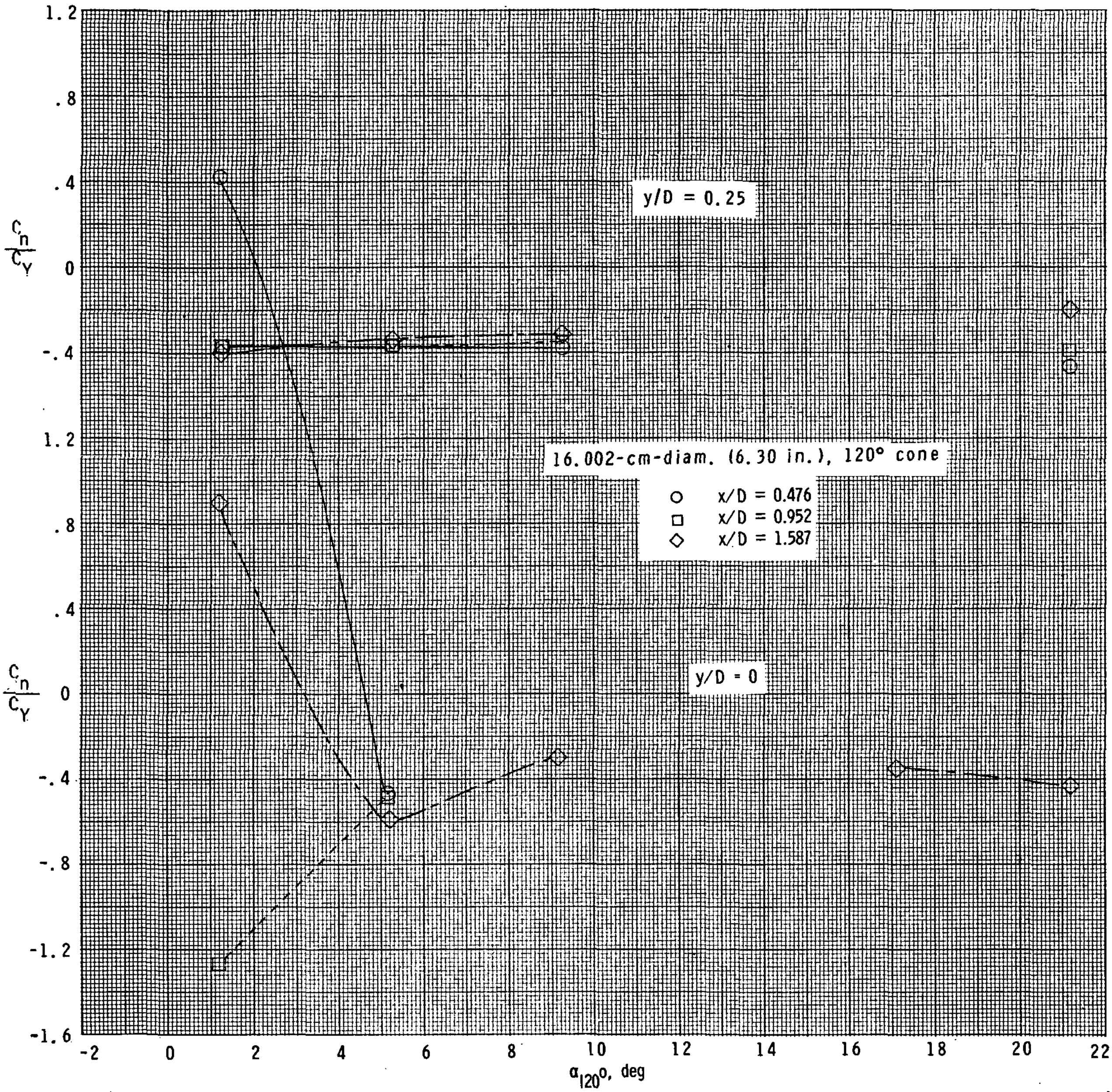

(a) $M_\infty = 2.36$; $\alpha_{20^o} = 0^o$.

Figure 20.- Variation of lateral center of pressure C_n/C_Y with angle of attack for 16.002-cm-diameter (6.30 in.), 120°-included-angle cone for various x/D locations, y/D locations, and angles of attack of 20°-included-angle cone.

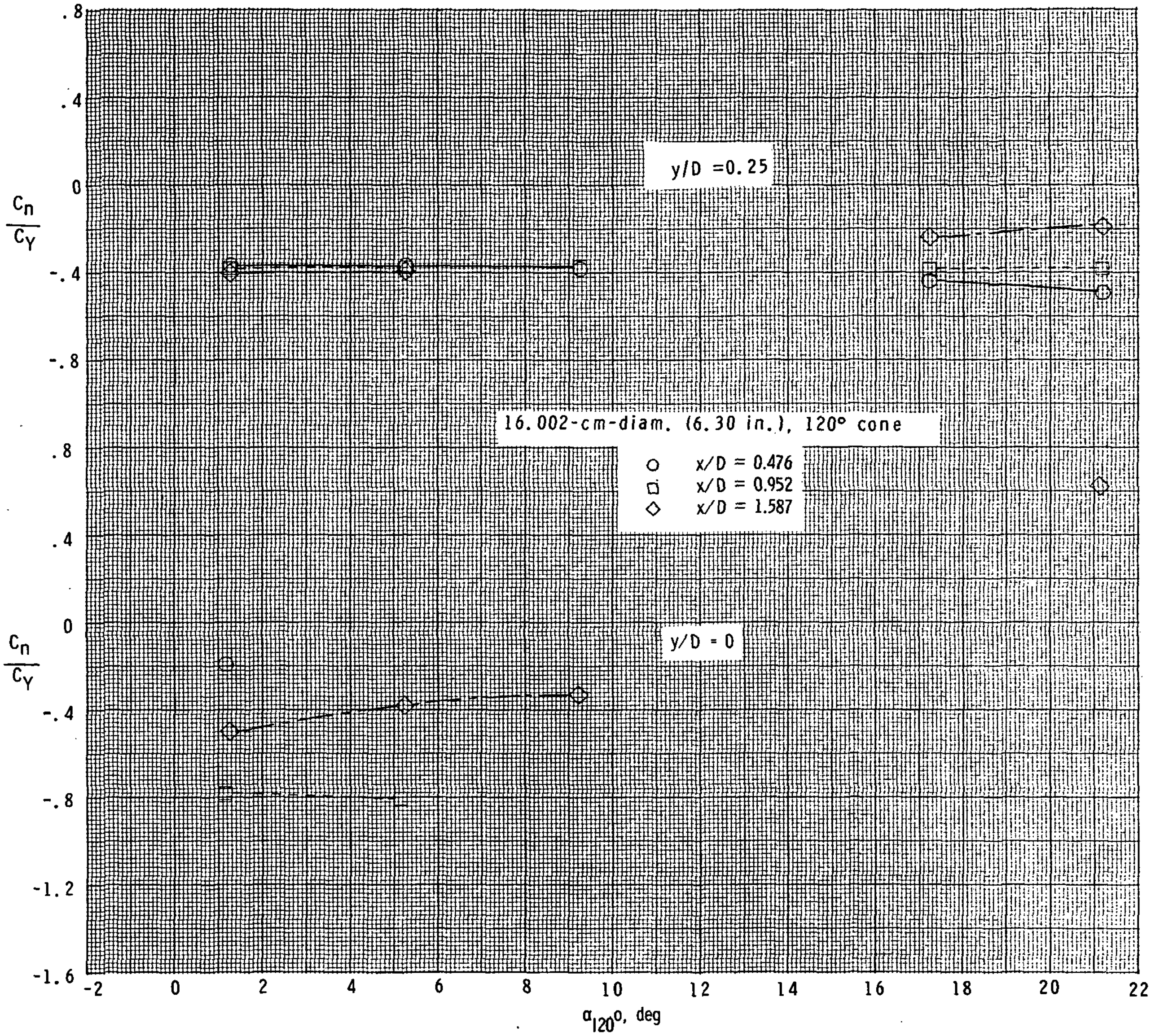

(b) $M_\infty = 2.36$; $\alpha_{20^o} = 5^o$.

Figure 20.- Continued.

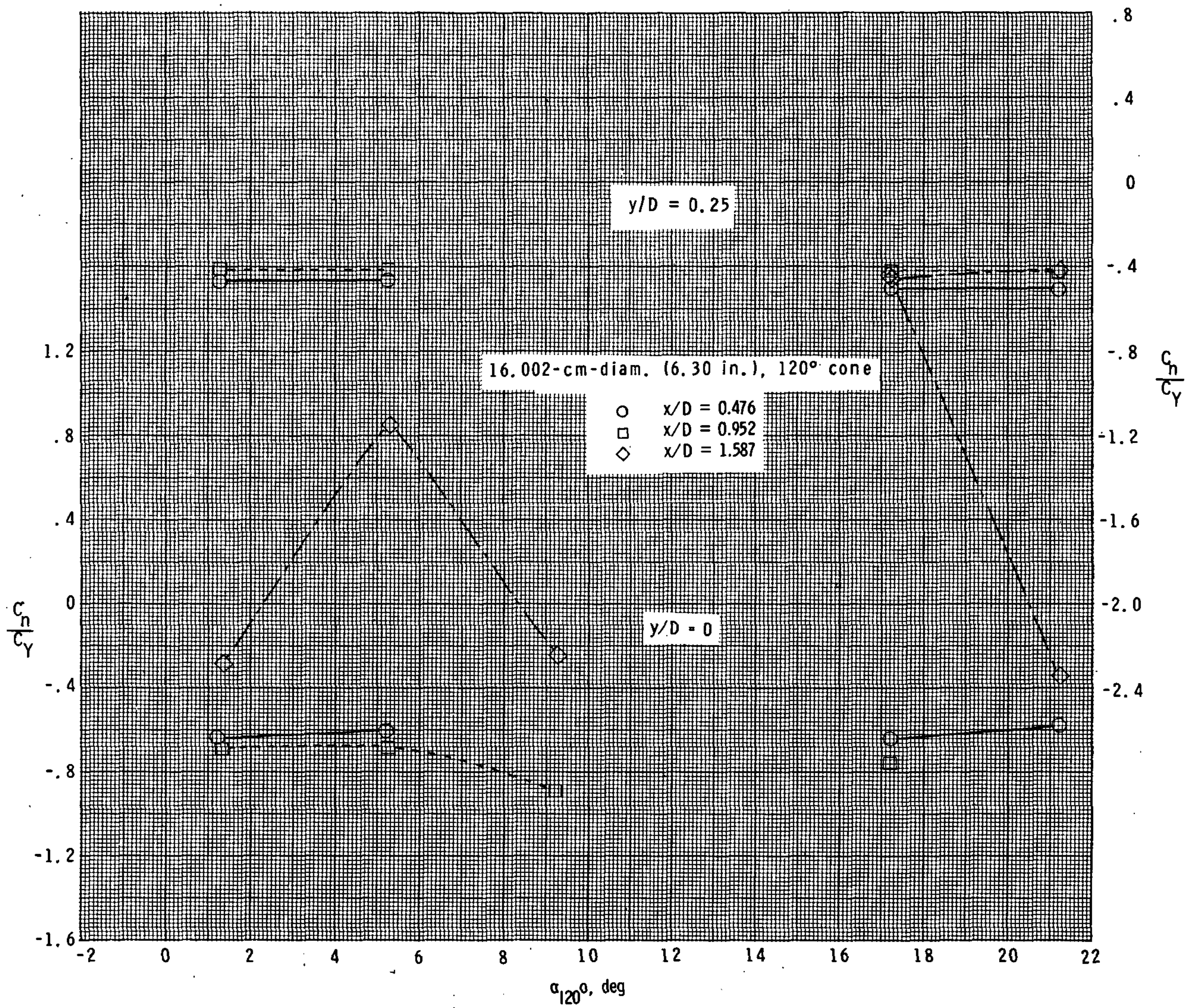

(c) $M_\infty = 2.36$; $\alpha_{20^o} = 30^o$.

Figure 20.- Continued.

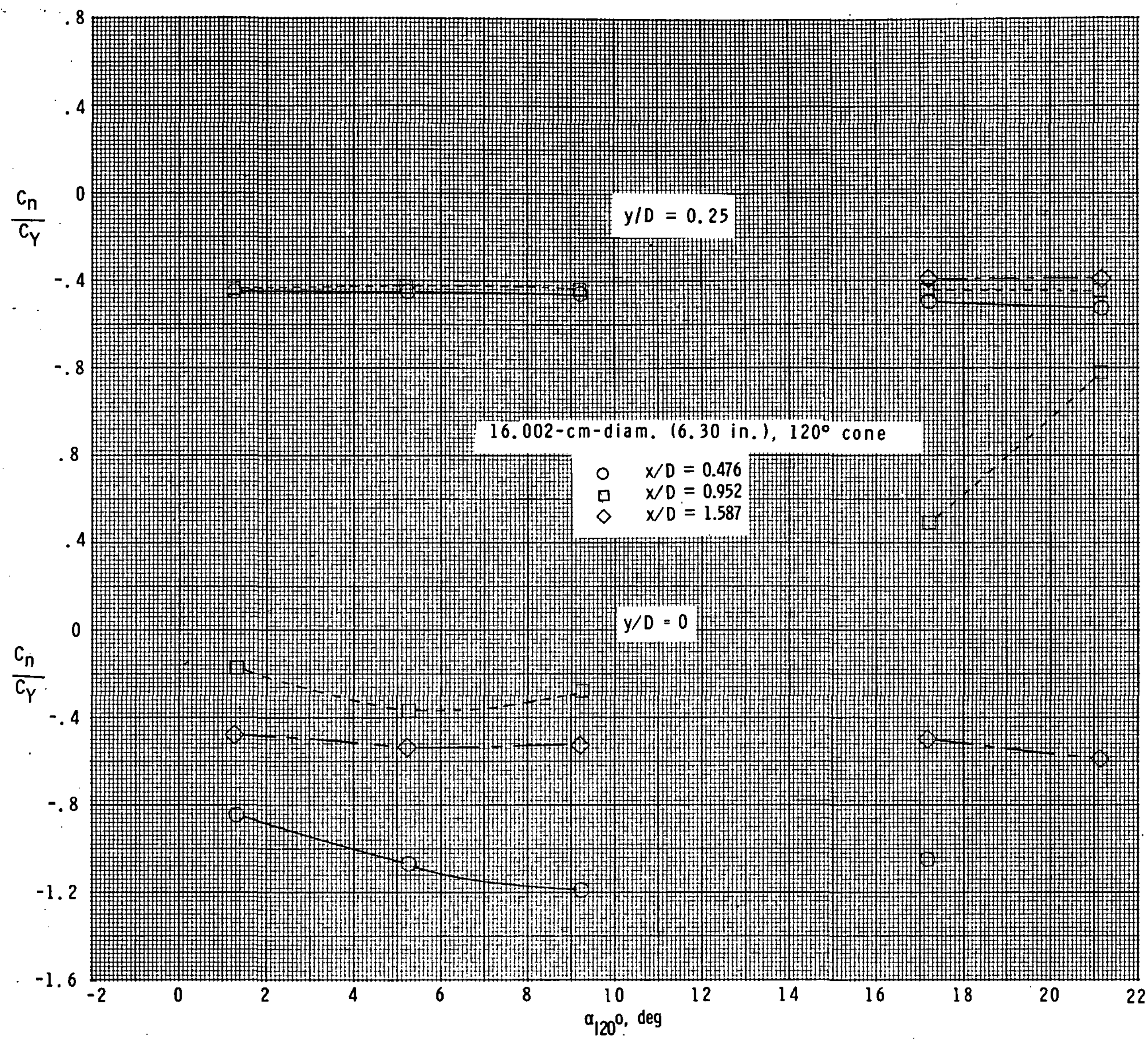

(d) $M_\infty = 2.36$; $\alpha_{20^\circ} = 90^\circ$.

Figure 20.- Continued.

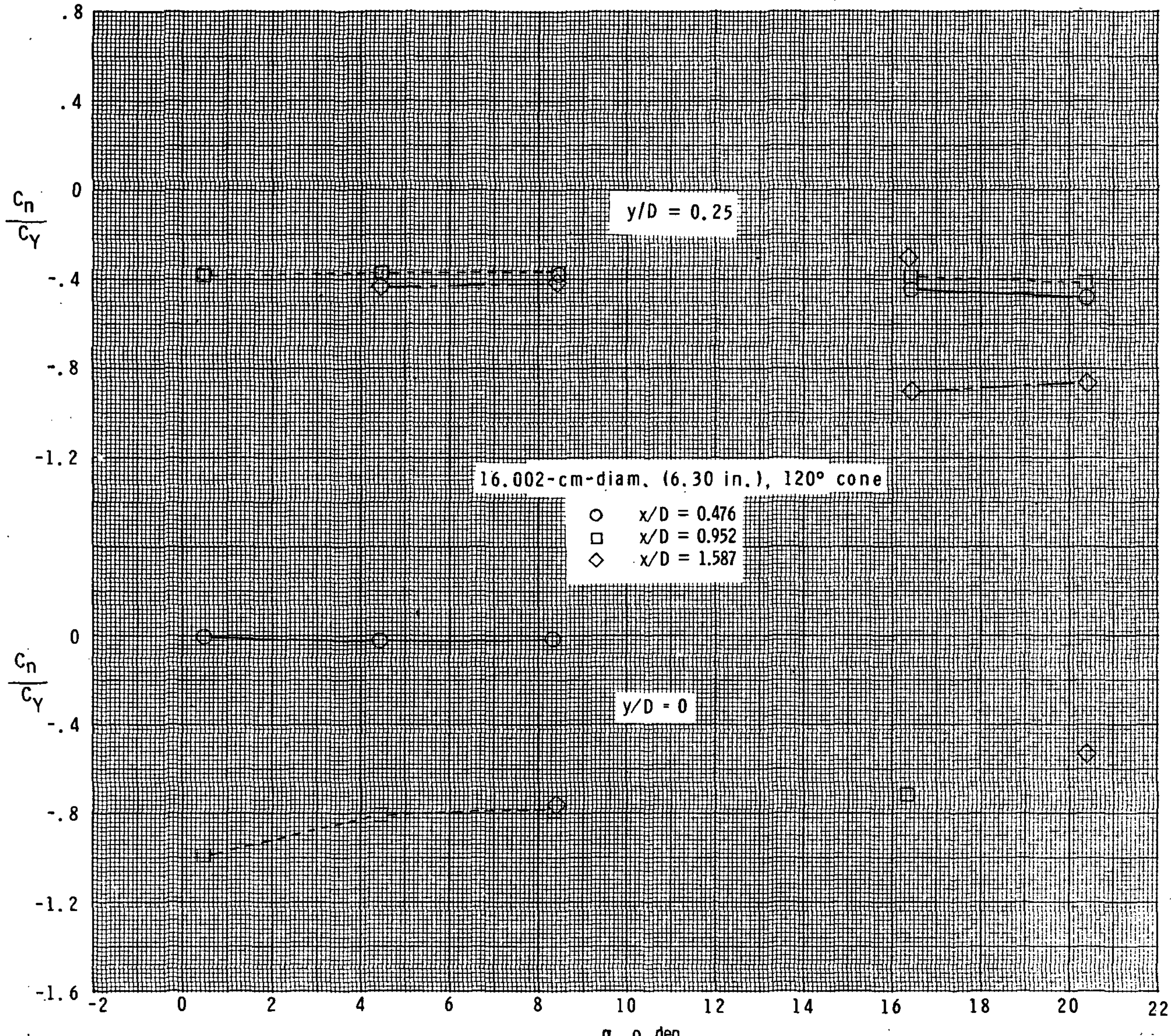

(e) $M_\infty = 2.70$; $\alpha_{20^o} = 0^o$.

Figure 20.- Continued.

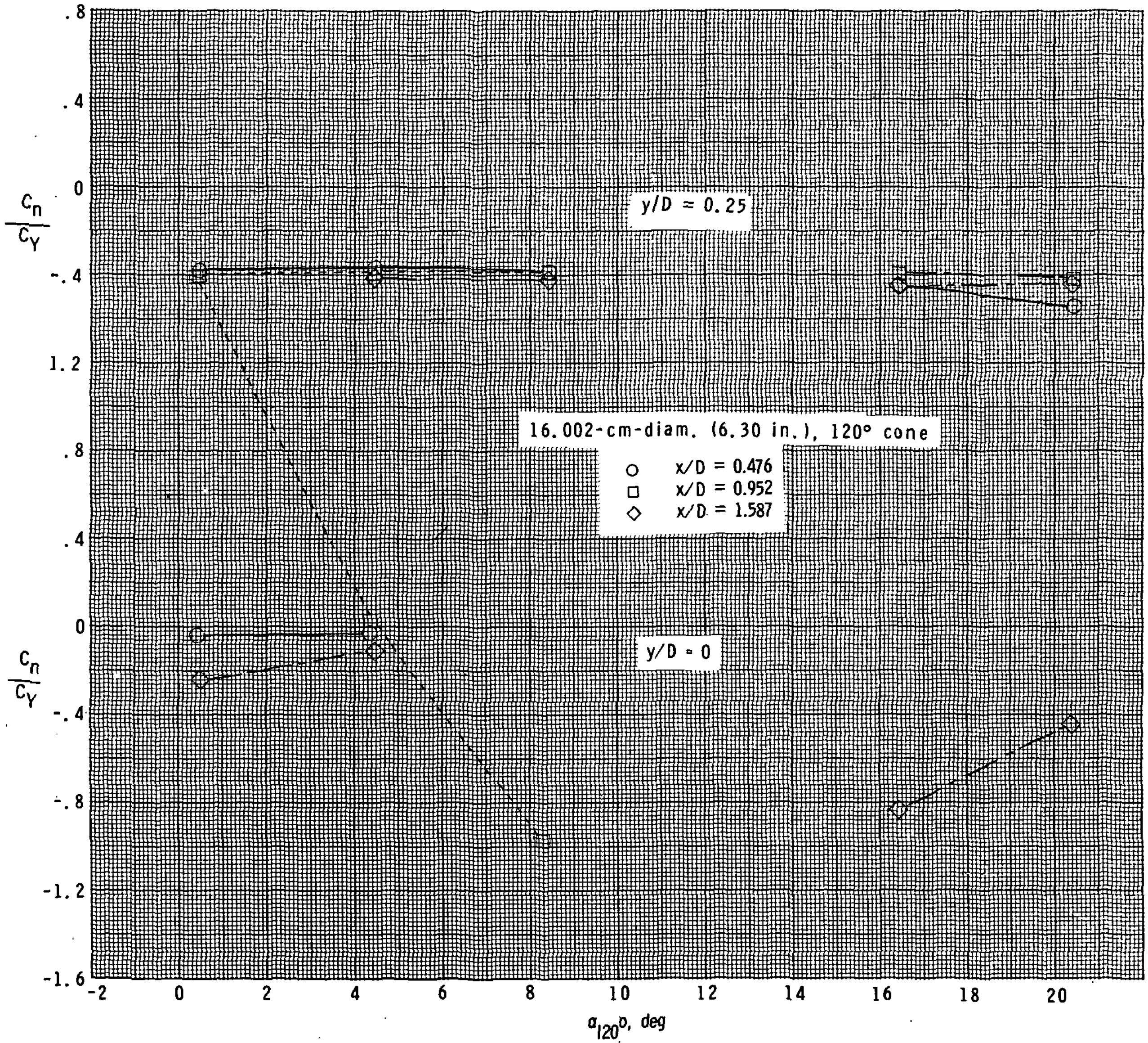

(f) $M_\infty = 2.70$; $\alpha_{20^o} = 5^o$.

Figure 20.- Continued.

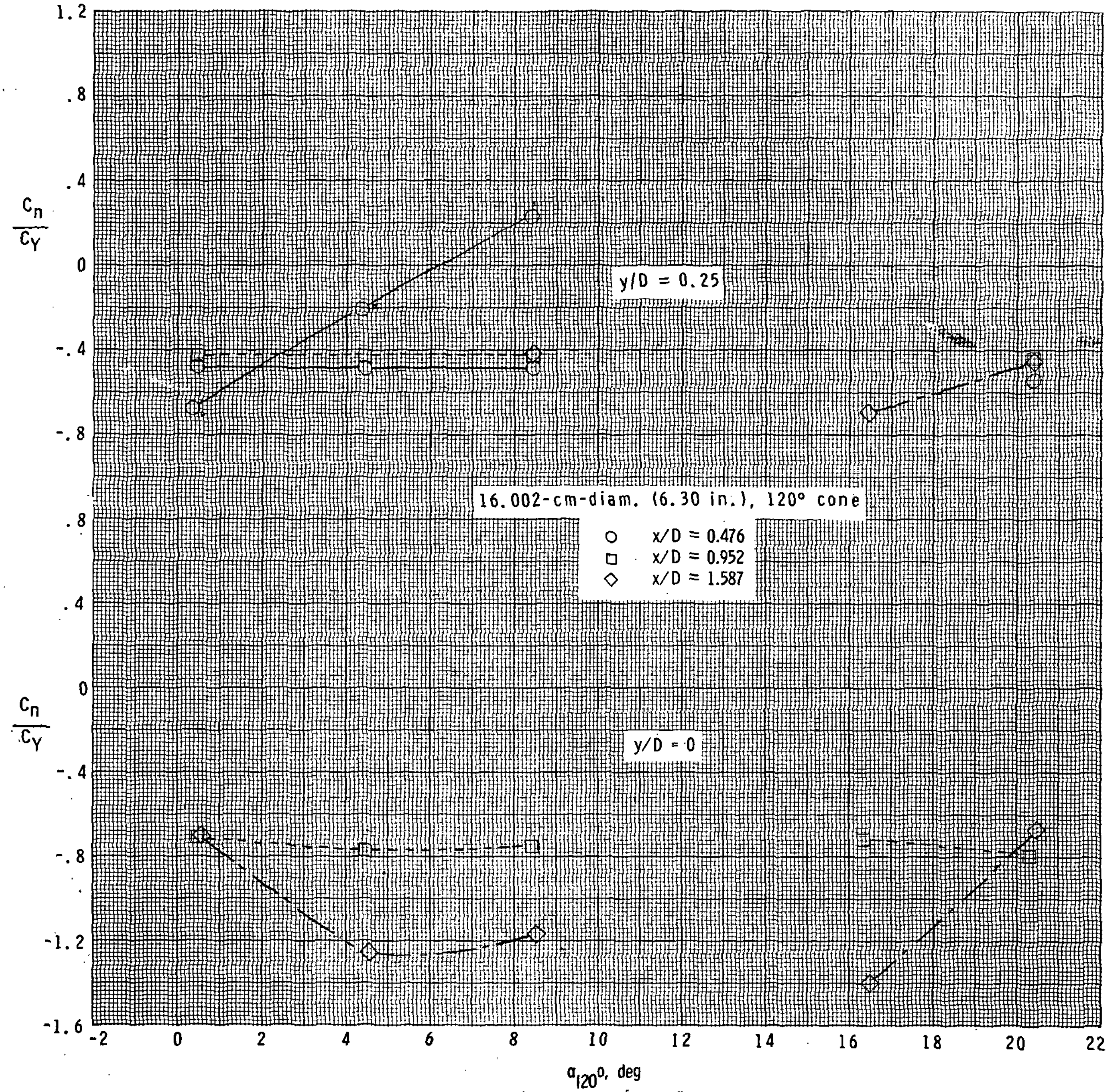

(g) $M_\infty = 2.70$; $\alpha_{20^o} = 30^o$.

Figure 20.- Continued.

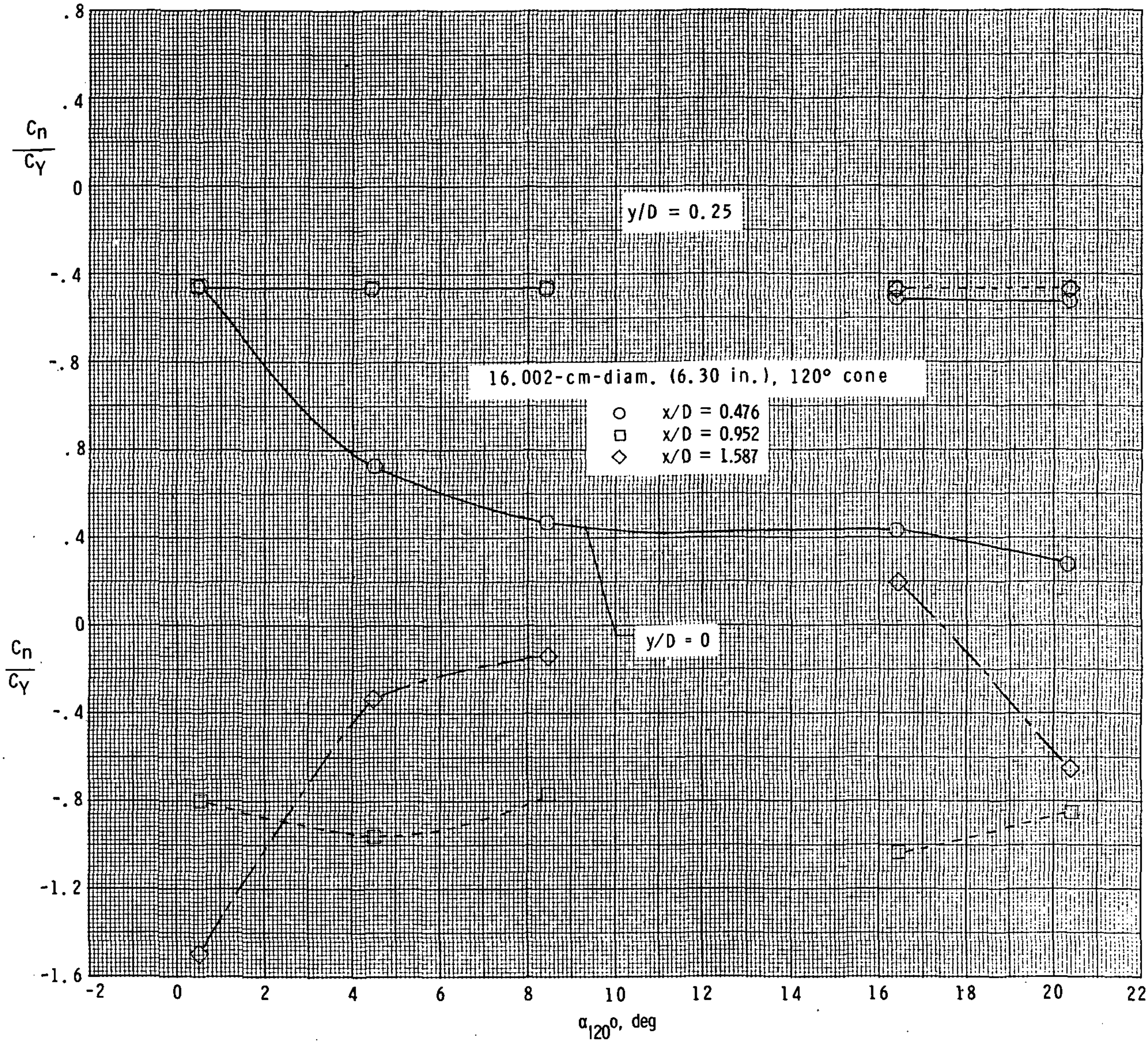

(h) $M_\infty = 2.70$; $\alpha_{20^o} = 90^o$.

Figure 20.- Concluded.

NATIONAL AERONAUTICS AND SPACE ADMINISTRATION
WASHINGTON, D.C. 20546

OFFICIAL BUSINESS
PENALTY FOR PRIVATE USE $300

FIRST CLASS MAIL

POSTAGE AND FEES PAID
NATIONAL AERONAUTICS AND
SPACE ADMINISTRATION
451

U.S.MAIL

POSTMASTER: If Undeliverable (Section 158 Postal Manual) Do Not Return

"The aeronautical and space activities of the United States shall be conducted so as to contribute . . . to the expansion of human knowledge of phenomena in the atmosphere and space. The Administration shall provide for the widest practicable and appropriate dissemination of information concerning its activities and the results thereof."

—NATIONAL AERONAUTICS AND SPACE ACT OF 1958

NASA SCIENTIFIC AND TECHNICAL PUBLICATIONS

TECHNICAL REPORTS: Scientific and technical information considered important, complete, and a lasting contribution to existing knowledge.

TECHNICAL NOTES: Information less broad in scope but nevertheless of importance as a contribution to existing knowledge.

TECHNICAL MEMORANDUMS: Information receiving limited distribution because of preliminary data, security classification, or other reasons. Also includes conference proceedings with either limited or unlimited distribution.

CONTRACTOR REPORTS: Scientific and technical information generated under a NASA contract or grant and considered an important contribution to existing knowledge.

TECHNICAL TRANSLATIONS: Information published in a foreign language considered to merit NASA distribution in English.

SPECIAL PUBLICATIONS: Information derived from or of value to NASA activities. Publications include final reports of major projects, monographs, data compilations, handbooks, sourcebooks, and special bibliographies.

TECHNOLOGY UTILIZATION PUBLICATIONS: Information on technology used by NASA that may be of particular interest in commercial and other non-aerospace applications. Publications include Tech Briefs, Technology Utilization Reports and Technology Surveys.

Details on the availability of these publications may be obtained from:

SCIENTIFIC AND TECHNICAL INFORMATION OFFICE

NATIONAL AERONAUTICS AND SPACE ADMINISTRATION

Washington, D.C. 20546